



HAL
open science

Functional implications of the nucleoporin Nup358/RanBP2 and transport receptors in adenoviral genome delivery

Irene Carlón-Andrés

► **To cite this version:**

Irene Carlón-Andrés. Functional implications of the nucleoporin Nup358/RanBP2 and transport receptors in adenoviral genome delivery. Human health and pathology. Université de Bordeaux, 2017. English. NNT : 2017BORD0807 . tel-02444535v2

HAL Id: tel-02444535

<https://theses.hal.science/tel-02444535v2>

Submitted on 20 Jan 2020

HAL is a multi-disciplinary open access archive for the deposit and dissemination of scientific research documents, whether they are published or not. The documents may come from teaching and research institutions in France or abroad, or from public or private research centers.

L'archive ouverte pluridisciplinaire **HAL**, est destinée au dépôt et à la diffusion de documents scientifiques de niveau recherche, publiés ou non, émanant des établissements d'enseignement et de recherche français ou étrangers, des laboratoires publics ou privés.

THÈSE PRÉSENTÉE POUR OBTENIR LE GRADE DE

DOCTEUR DE

L'UNIVERSITÉ DE BORDEAUX

ÉCOLE DOCTORALE des Sciences de la Vie et de la Santé

Spécialité: MICROBIOLOGIE et IMMUNOLOGIE

Par Irene CARLÓN-ANDRÉS

**Implication fonctionnelle de la nucléoporine Nup358/RanBP2 et
des récepteurs de transport dans l'entrée du génome adénoviral**

Sous la direction de Marie-Edith LAFON

Soutenue le 7 Décembre 2017

Membres du jury:

Pr Thierry NOËL	Université de Bordeaux	Président
Dr Carmen SAN MARTÍN	Consejo Superior de Investigaciones Científicas (CSIC)	Rapporteur
Pr Ralph KEHLENBACH	Universität Göttingen	Rapporteur
Dr Anne ROYOU	Université de Bordeaux	Examineur
Dr Harald WODRICH	Université de Bordeaux	Invité
Pr Marie-Edith LAFON	Université de Bordeaux	Invité

DISSERTATION FOR THE AWARD OF THE DEGREE:

**DOCTORATE OF THE
UNIVERSITY OF BORDEAUX**

Doctoral school of health and life sciences

Speciality: MICROBIOLOGY - IMMUNOLOGY

Irene CARLÓN-ANDRÉS

**Functional implications of the nucleoporin Nup358/RanBP2
and transport receptors in adenoviral genome delivery**

Thesis director: Marie-Edith LAFON

Presented the 7th December 2017

Members of the committee:

Pr Thierry NOËL	Université de Bordeaux	President
Dr Carmen SAN MARTÍN	Consejo Superior de Investigaciones Científicas (CSIC)	Reporter
Pr Ralph KEHLENBACH	Universität Göttingen	Reporter
Dr Anne ROYOU	Université de Bordeaux	Examiner
Dr Harald WODRICH	Université de Bordeaux	Guest
Pr Marie-Edith LAFON	Université de Bordeaux	Guest

Implication fonctionnelle de la nucléoporine Nup358/RanBP2 et des récepteurs de transport dans l'entrée du génome adénoviral

Les adénovirus (AdV), comme d'autres virus à réplication nucléaire, ont besoin d'arriver jusqu'au noyau cellulaire afin de libérer leur génome. Pour ce faire, les particules des AdV contenant l'ADN viral sont transportées jusqu'au complexe du pore nucléaire (NPC), via le centre d'organisation des microtubules, par un mécanisme encore mal compris qui implique l'exportine cellulaire CRM1. La capsid des AdV dépasse la taille limite d'entrée dans le noyau, et par conséquent, elle doit être désassemblée au niveau du NPC. Le mécanisme d'import de molécules d'ADN n'est pas un processus physiologique. Pour cela, les AdV doivent détourner la machinerie cellulaire afin d'importer leur génome dans le noyau. Le NPC est un complexe de protéines appelées nucléoporines. La Nup358/RanBP2, principal composant des filaments cytoplasmiques, sert de plateforme de liaison à des karyopherines (e.g Importin- β , CRM1) et à la protéine GTPase Ran. Les karyopherines reconnaissent des signaux spécifiques présents dans les *cargos* et facilitent leur transport d'une manière très régulée dépendante de RanGTP. Nous avons constaté que l'import du génome AdV est moins efficace en l'absence de Nup358. Dans ces conditions, nous avons observé que certaines karyopherines deviennent limitantes pour l'import du génome viral, et identifié la région minimale de Nup358 requise pour compenser ce défaut. D'autre part, nous avons confirmé l'implication de CRM1 dans l'arrivé des particules virales au noyau et identifié un nouveau rôle de CRM1 dans le désassemblage de la capsid des AdV. Ces travaux contribuent à mieux connaître le mécanisme d'entrée du génome AdV dans le noyau et donnent une idée de la façon dont les virus peuvent contourner la machinerie de transport cellulaire pour leur propre bénéfice.

Mots clés : Adénovirus, Nup358, CRM1, transport nucléo-cytoplasmique

Functional implications of the nucleoporin Nup358/RanBP2 and transport receptors in adenoviral genome delivery

Nuclear delivery of viral genomes is an essential step for nuclear replicating DNA viruses such as Adenovirus (AdV). AdV particles reach the nuclear pore complex (NPC) in the form of genome containing, partially disassembled capsids, through a poorly understood CRM1-dependent mechanism. These capsids exceed the NPC size limit and therefore, they must disassemble at the NPC to release the viral genome. Nuclear import of DNA cargos is not a physiological process. Consequently, AdV need to divert the cellular transport machinery for nuclear genome delivery. The NPC is a multi-protein complex consisting of nucleoporins (Nups). The Nup358/RanBP2 is the major component of the cytoplasmic filaments of the NPC and serves as binding platform for factors including karyopherins (i.e Importin- β , CRM1) and the small GTPase Ran. Selective transport of cargo through the NPC is mediated by karyopherins, which recognize specific signals within the cargos and facilitate their transport in a RanGTP-dependent regulated manner. We identified that Nup358-depleted cells reduce nuclear import efficiency of the AdV genome. Indeed, we observed that karyopherins are rate-limiting for AdV genome import under these conditions and we mapped the minimal region of Nup358 necessary to compensate the import defect. On the other hand, we could confirm the requirement of CRM1 in nuclear targeting of AdV capsids and identified an additional role in mediating AdV capsid disassembly. This work helps to understand the strategy used by AdV to deliver their genome and gives insight about how viruses hijack the cellular transport machinery for their own benefit.

Key words: Adenovirus, Nup358, CRM1, nucleo-cytoplasmic transport

Laboratoire MFP CNRS UMR-5234

146 rue Léo Saignat Batiment 3A

33076 BORDEAUX – France

Les adénovirus (AdV), comme d'autres virus à réplication nucléaire, ont besoin d'arriver jusqu'au noyau cellulaire pour y libérer leur génome. Pour ce faire, les AdV reconnaissent des récepteurs présents sur la surface de la cellule qui vont ensuite faciliter l'internalisation du virus par endocytose. Une fois libérée dans le cytosol, la particule virale partiellement désassemblée est ensuite transportée le long des microtubules vers le noyau où elle sera finalement transférée par un mécanisme encore mal compris, qui implique l'exportine cellulaire CRM1. La capsidie icosaédrique des AdV (~ 90 nm de diamètre) contient un génome à ADN double brin linéaire de ~36 kb, lié à ~800 copies de la protéine virale VII (pVII). Cette protéine est responsable de l'organisation du génome viral en chromatine et fait partie du core adénoviral pendant l'import au noyau. La capsidie AdV est trop grande pour passer à travers du pore nucléaire, et par conséquent, la libération du génome viral requiert le désassemblage complet de la capsidie au niveau du complexe du pore nucléaire (NPC). Le mécanisme d'import de molécules d'ADN n'est pas un processus physiologique que le virus peut directement utiliser pour libérer son génome dans le noyau. Par conséquent, pour y parvenir, le virus doit détourner la machinerie cellulaire existante pour ses propres fonctions d'import.

Le NPC est un très gros complexe protéique qui forme des tunnels à travers l'enveloppe nucléaire permettant le passage sélectif de molécules. Pour les molécules de taille comprise entre ~5.3 et 39 nm de diamètre, ce transport est facilité par des récepteurs de transport nucléaire, appartenant à la famille des karyopherines. Ces récepteurs sont connus sous le nom d'importines et d'exportines et reconnaissent respectivement des signaux de localisation nucléaire (NLS) ou des signaux d'export nucléaire (NES) présents dans les *cargos*. La directionnalité du transport à travers du NPC est déterminée par le gradient de RanGTP/GDP. Les importines lient RanGTP et leur cargo de manière exclusive (soit l'un, soit l'autre). Les importines ont plus d'affinité pour RanGTP que pour leur cargo et par conséquent, le complexe d'import nucléaire ne peut être constitué que dans le cytosol, où la concentration de RanGTP est basse. Une fois dans le noyau, les importines se lient au RanGTP et ceci induit la dissociation du complexe d'import conduisant à la libération du cargo dans le noyau. À l'inverse, le complexe d'export nucléaire est constitué d'une exportine, du cargo et de RanGTP, et par conséquent, la formation du complexe a lieu dans le noyau, où la concentration de RanGTP est élevée. Une fois dans le cytosol, l'hydrolyse de GTP induit la dissociation du complexe d'export permettant la libération du cargo dans le cytoplasme. Le gradient de RanGTP entre le cytosol et le noyau est maintenu grâce au facteur d'échange de nucléotides RCC1, qui génère RanGTP. Du côté cytoplasmique, le facteur RanGAP (soit soluble ou associé à la protéine Nup358 au niveau du NPC), et les protéines d'union à

RanGTP (RanBP) facilitent l'hydrolyse de GTP et donc, induisent la production de RanGDP dans le cytosol.

Le NPC est constitué de protéines appelées nucléoporines. La nucléoporine 358 (Nup358 ou RanBP2) est le principal composant des filaments cytoplasmiques du NPC. La Nup358 joue de préférence un rôle dans l'import de certains *cargos* cellulaires, car elle contient des domaines riches en acides-aminés phenylalanine-glycine (FG-repeats en anglais) qui permettent la liaison transitoire à différents récepteurs d'import. De même, elle possède quatre domaines de liaison à la protéine GTPase Ran (RanBD, acronyme de *Ran binding domains* en anglais) qui facilitent le recyclage des récepteurs d'import. De cette façon, Nup358 aide à maintenir une concentration optimale de récepteurs d'import autour du NPC, garantissant ainsi l'import efficace des *cargos* vers le noyau. Bien que Nup358 puisse aussi interagir avec l'exportine CRM1 et faciliter le désassemblage de complexes d'export via ses RanBD et l'association avec la protéine RanGAP, l'absence de Nup358 a peu d'impact sur l'export dépendant de CRM1. En effet, les facteurs qui facilitent l'hydrolyse de GTP (RanGAP et RanBP) sont aussi présents de manière soluble dans le cytosol et donc, peuvent également faciliter l'export de protéines.

Des études précédentes ont montré que l'exportine CRM1 est un facteur nécessaire au mécanisme de transfert de la particule de l'AdV des microtubules vers le NPC. En effet, un inhibiteur spécifique de cette protéine, la Leptomycine B (LMB), induit l'accumulation des particules virales au niveau du MTOC en bloquant l'import nucléaire du génome viral. Cependant, les détails moléculaires du rôle de CRM1 ne sont pas clairs. Dans le modèle proposé pour le désassemblage de la capsid au niveau du NPC, la coopération entre la protéine motrice kinésine-1 et Nup358 serait nécessaire. En effet, la capsid virale interagirait avec la kinésine-1 via la protéine de capsid IX. La fixation de la particule virale au NPC permettrait cette interaction entre les deux protéines kinésine-1 et Nup358. Cette liaison activerait la kinésine-1. Elle produirait ensuite une force antérograde qui faciliterait le désassemblage de la capsid libérant le génome viral et entraînerait le déplacement des protéines Nup358 et Nup214 du NPC. Cette délocalisation des nucléoporines augmenterait la perméabilité du NPC, facilitant ainsi l'entrée du génome viral dans le noyau. L'import de la pVII adénovirale peut être effectué par l'intermédiaire de plusieurs importines différentes. De ce fait, cette protéine virale a été proposée comme adaptateur pour l'import nucléaire du génome viral. En effet, le récepteur d'import transportin-1 est capable de faciliter le transport du génome viral lié à la protéine VII dans des systèmes *in vitro*. Cette protéine VII serait le récepteur majeur d'import du génome de l'adénovirus.

Dans ce travail, nous nous sommes intéressés aux mécanismes d'entrée du génome adénoviral dans le noyau. L'entrée du génome comprend quatre étapes distinctes, dont le mécanisme est encore peu connu : i) la translocation des microtubules au NPC, ii) l'attachement du virus au NPC, iii) le désassemblage de la capsid qui implique l'exposition du génome viral au niveau du NPC et iv) l'import du génome viral dans le noyau. L'objectif de ce travail a été d'étudier le rôle de Nup358 pour essayer de mieux comprendre quel est son implication pendant l'entrée du génome viral dans le noyau, au vu des apparentes divergences de la littérature. Nous avons analysé la contribution des différents récepteurs d'import dans l'import du génome adénoviral dans le noyau. Finalement, nous avons étudié l'implication de l'exportine CRM1 dans le mécanisme de translocation des particules virales des microtubules au NPC, ainsi que son implication en aval de cette étape, pendant le désassemblage de la capsid adénovirale.

Pour l'étude de l'entrée du génome viral dans le noyau, nous avons suivi l'apparition du signal d'immunofluorescence spécifique pour la pVII. Comme décrit précédemment, la pVII est la principale protéine liée à l'ADN viral. Elle contient des NLS et reste associée à l'ADN viral pendant l'import du génome au noyau. La pVII est uniquement détectable lors du désassemblage complet de la capsid et elle est observée sous forme de points, en raison d'un point par génome viral. De cette manière, nous avons pu distinguer entre capsides « intactes » (son marquage est négatif pour la pVII), capsides désassemblées (elles co-localisent avec la pVII) et des génomes importés dans le noyau (signal de pVII dans le noyau).

Pour étudier le rôle de Nup358 dans l'import du génome adénoviral, nous avons inhibé l'expression de cette protéine par ARN interférence. La détection de la capsid virale et de la pVII a permis d'étudier l'efficacité d'import du génome viral dans le noyau au cours du temps, en présence ou absence de Nup358. Nous avons observé que l'import du génome AdV dans le noyau est retardé lors de l'infection des cellules dépourvues de Nup358, ce qui suggère que l'import du génome est moins efficace dans ces conditions mais pas restreint. En absence de Nup358 endogène, ce délai peut être restauré avec l'expression de Nup358 entière ou avec un fragment contenant seulement la moitié N-terminale de la protéine. De la même façon ce défaut est corrigé par un excès de récepteurs de transport, notamment du récepteur d'import transportin-1. En effet, nous avons constaté que la partie N-terminale de Nup358 recrute des récepteurs de transport nécessaires pour l'import du génome AdV, ce qui suggère que la Nup358 est nécessaire à l'import du génome adénoviral pour assurer la présence d'une quantité suffisante de récepteurs d'import, notamment de la transportin-1, au niveau du NPC.

D'autre part, nous avons étudié le rôle du transporteur CRM1 pendant l'entrée du génome AdV dans le noyau. Nous avons confirmé son implication dans l'arrivée des particules virales au noyau après inhibition spécifique de CRM1 par le traitement des cellules avec LMB. Nous avons également observé que la surexpression de fragments des nucléoporines Nup214 et Nup358 capables de interagir avec CRM1, induit la rétention de CRM1 dans le noyau. Par conséquent, la fonction d'export de protéines dépendante de CRM1 et le mécanisme de transfert de particules adénovirales au NPC étaient bloqués. Cependant, l'inhibition de CRM1 ou sa rétention dans le noyau implique également la rétention des cargos dépendants de CRM1 dans ce compartiment.

Afin d'étudier l'implication de CRM1 dans la libération du génome adénoviral en dehors de sa fonction de transport nucléo-cytoplasmique, nous avons établi un protocole d'infection des cellules mitotiques. En effet, cette étape du cycle cellulaire, la membrane nucléaire est désintégrée et les NPC substantiellement désassemblés. Cela nous a permis dans un premier temps de constater que le désassemblage de la capsid de l'AdV ne requiert pas de NPC assemblés, ni le transport nucléo-cytoplasmique. Étonnamment, nous avons observé une forte réduction de l'efficacité du désassemblage de la capsid virale après inhibition de CRM1 par la LMB dans ces cellules mitotiques. Ce blocage est non seulement restauré en surexprimant un mutant de CRM1 résistant à LMB, mais aussi augmenté par rapport aux cellules contrôle. Nous avons observé également une augmentation de l'efficacité du désassemblage de la capsid dans des cellules mitotiques non-traitées à la LMB qui surexpriment un fragment C-terminal de Nup358. Ce fragment lie CRM1 et facilite le désassemblage de complexes d'export en interphase. Finalement, nous avons identifié un mutant de CRM1 qui est incapable de restaurer un désassemblage efficace de la capsid dans des cellules mitotiques traitées à la LMB. Ce mutant est résistant à la LMB mais il contient des mutations additionnelles dans le domaine de liaison à RanGTP. L'ensemble de ces résultats montrent l'implication de CRM1 non seulement dans la translocation de particules adénovirales au NPC, mais aussi dans le désassemblage de la capsid virale. En plus, les résultats suggèrent l'implication directe de CRM1 dans le désassemblage de la capsid virale en complexe avec RanGTP.

Ces travaux contribuent à mieux connaître l'implication de la machinerie de transport nucléo-cytoplasmique dans la libération et import du génome AdV dans le noyau. Ainsi, ce travail propose des mécanismes de contournement de la machinerie de transport cellulaire qui pourraient être partagés par des autres virus afin d'accéder au noyau pour se multiplier.

Acknowledgement

First, I would like to thank the members of my thesis dissertation committee, Ralph Kehlenbach and Carmen San Martín who accepted to be reporters of this thesis manuscript, as well as Anne Royou who kindly accepted to evaluate my manuscript. Likewise, I wish to thank Thierry Noel for having accepted to be the president of the dissertation committee, and looking back, for allowing me to be part of the Master “MiMu”.

I would like to thank also Marie-Edith for having accepted me as her PhD student. I really appreciate your availability and help, and also your cheerfulness and professionalism.

I specially thank Harald Wodrich for the immense support and commitment from the beginning of times, since I arrived “unexpectedly” to the lab. I appreciate your humanity and nice discussions. Thank you for transmitting your passion and curiosity for science.

I would like to thank Ralph Kehlenbach for the nice advices and discussions that helped me a lot during my thesis. Also for having welcomed me in Goettingen for few weeks.

I want to thank all members of our team. Fabienne, for your help specially preparing the *concours*, thank you for your very didactic explanations and your patience. Also to Benoît, for your availability answering the infinite questions that we have, as well as for the not always scientific but funny discussions during lunch time. I also thank Muriel, Jessica and Cathy for your professionalism and help, also for the contribution to those discussions at lunch time. I thank also the HBV team, Michael, Marie-Lise and Christian, as well as the past members of the lab, for the discussions in and out of the lab meetings. I would like to thank all members of the UMR5234 for their help using different apparatus and specially people from the *parasito*-lab for their kindness and invitations to “celebrate Fridays”.

I thank, of course, “*aux filles*”, because we learnt together “*qu’est-ce que c’est la réalité de notre métier*”. You are the greatest labmates one could ever imagine.

A las personas que me han apoyado y ayudado a relativizar y disfrutar de estos años en Burdeos fuera del laboratorio.

Finalmente a mis padres, a quienes estoy eternamente agradecida y dedico el esfuerzo de este trabajo.

*“Caminante, no hay camino,
se hace camino al andar”*

Antonio Machado

TABLE OF CONTENTS

I_INTRODUCTION

1. OVERVIEW OF ADENOVIRUSES (ADV)	1
1.1 Discovery and clinical relevance	1
1.2 Treatment.....	1
1.3 Classification and associated diseases	3
1.4 AdV as a tool in research and gene therapy	3
2. STRUCTURE OF THE ADENOVIRAL PARTICLE	4
2.1 Capsid proteins	6
2.2 Core proteins.....	6
2.3 Genome organization.....	7
3. ADENOVIRAL INFECTION CYCLE	9
3.1 Binding	9
3.2 Entry	11
3.3 Trafficking	11
3.4 Genome delivery.....	12
3.5 Genome transcription and replication.....	12
3.6 Late phases	13
4. BASIC MECHANISMS OF NUCLEOCYTOPLASMIC TRANSPORT	14
4.1 The RanGTP gradient.....	16
4.2 Nuclear import.....	17
4.2.1 Importin- α/β complex pathway	19
4.2.2 Transportin-1 pathway.....	19
4.3 Nuclear export	20
4.3.1 CRM1-dependent export	20
5. THE NUCLEAR PORE COMPLEX.....	21
5.1 FG-Nups involved in transport.....	22
5.1.1 Nup214.....	23
5.1.2 Nup358.....	25
5.1.2.1 Nup358 domains	25
5.1.2.2 Interactions involved in import.....	27

5.1.2.3	<i>Interactions involved in export</i>	27
5.1.2.4	<i>Non-transport functions of Nup358</i>	29
6.	REGULATION OF NUCLEOCYTOPLASMIC TRANSPORT.....	29
6.1	Modulation of localization signals	29
6.2	Regulation of transport factors	30
6.3	Cytoskeleton-facilitated nuclear transport.....	30
6.4	Regulatory mechanisms at the NPC	31
7.	ROLE OF THE TRANSPORT MACHINERY IN MITOSIS	32
7.1	Nuclear envelope breakdown (NEBD).....	32
7.2	Mitotic spindle formation	33
7.3	NPC post-mitotic assembly	35
8.	NUCLEAR IMPORT OF VIRAL DNA.....	35
9.	ADENOVIRAL GENOME DELIVERY	36
9.1	Docking of the capsid at the NPC	37
9.2	Capsid disassembly and genome release	38
9.3	Genome import.....	38
9.4	Controversy	39
10.	AIM OF THE WORK.....	40

II_MATERIALS AND METHODS

1.	MOLECULAR BIOLOGY METHODS	41
1.1.	Bacterial culture.....	41
1.2.	Bacterial transformation	41
1.3.	Polymerase chain reaction (PCR).....	41
1.4.	Cloning	43
1.5.	List of plasmids	43
2.	CELL BIOLOGY METHODS	46
2.1.	Cell lines	46
2.2.	Cell maintenance	46
2.3.	Transient transfection of DNA	46
2.4.	RNA interference-mediated depletion.....	47

2.4.1. <i>siRNA</i>	47
2.4.2. <i>shRNA</i>	48
2.5. Coating of coverslips with poly-L-lysine	49
2.6. Cell-cycle synchronization	49
2.7. Leptomycin b (LMB) treatment	49
3. VIRAL PRODUCTION.....	50
3.1. Viral amplification.....	50
3.2. Virus purification.....	50
3.3. Virus labelling	51
3.4. Virus quantification	51
4. VIRAL INFECTION	52
4.1. Time course infection in interphase cells	52
4.2. Infection of mitotic cells.....	53
5. IMMUNOFLUORESCENCE (IF) ANALYSIS.....	53
5.1. IF staining.....	53
5.2. Image acquisition	55
5.3. Image quantification	55
5.3.1. <i>Quantification of fluorescence intensity</i>	56
5.3.2. <i>Quantification of single signal</i>	57
5.3.3. <i>Quantification of co-localization</i>	58
5.4. Statistical analysis.....	59
6. BIOCHEMICAL METHODS	59
6.1. Cell extracts preparation.....	59
6.2. Co-immunoprecipitation (Co-IP)	60
6.3. Pull-down (PD).....	60
6.4. SDS-page electrophoresis.....	60
6.5. Western blot (WB).....	61

II_RESULTS

1. THE ROLE OF NUP358 IN ADV GENOME DELIVERY	62
1.1. Nup358 depletion leads to inefficient AdV genome import.....	62

1.1.1.	Nup358 depletion delays AdV genome import.....	63
1.1.2.	Nup358 depletion affects AdV genome release but not capsid disassembly	65
1.1.3.	Nup358 depletion does not affect virion entry into the cytoplasm	67
1.2.	The N-terminal half of Nup358 is sufficient for promoting efficient AdV genome import.....	69
1.3.	Transport receptors compensate for the lack of Nup358.....	71
1.3.1.	AdV genome import is not exclusively mediated by transportin-1	74
1.4.	The N-terminal FG-cluster of Nup358 recruits transport receptors	76
1.4.1.	The FG-repeat patch- and RanBD1-containing fragment of Nup358 recruits endogenous transportin-1	76
1.4.2.	The N-terminal FG-repeat cluster of Nup358 recruits endogenous transportin-1 and importin β	78
1.4.3.	The N-terminal half of Nup358 is not sufficient to tether CRM1 to the NPC... ..	82
2.	THE ROLE OF CRM1 IN ADV GENOME DELIVERY	84
2.1.	Soluble fragments of cytoplasmic Nups impair AdV genome delivery in interphase	84
2.1.1.	The C-terminal CRM1-binding fragment of Nup214 disrupts nuclear targeting of AdV capsids	85
2.1.2.	Soluble fragments of Nup358 impair AdV genome delivery	87
2.1.3.	CRM1-binding fragments of Nup358 induce accumulation of AdV capsids at the MTOC	90
2.1.4.	CRM1-binding fragments of Nup358 disrupt CRM1 export function necessary for nuclear targeting of AdV.	92
2.1.5.	The C-terminal fragment of Nup358 impairs AdV genome delivery in a CRM1-dependent and -independent manner.....	94
2.2.	Infection of mitotic cells as a model system to study AdV genome delivery	97
2.2.1.	Establishment of an infection protocol for mitotic cells	97
2.2.2.	Mitotic spindles are reconstituted upon release from colcemid-treatment.....	99
2.2.3.	AdV are able to deliver their genome in mitotic cells.....	100

2.3.	The role of CRM1 in promoting AdV capsid disassembly	101
2.3.1.	Functional inactivation of CRM1 does not impair AdV entry in mitosis	101
2.3.2.	Inhibition of CRM1 prevents the disassembly of AdV capsids	103
2.3.3.	Exposure of AdV core accelerates AdV capsid targeting to the chromatin.....	105
2.3.4.	Separation of AdV cores from disassembled capsids is accelerated by overexpression of CRM1	107
2.3.5.	Disassembled capsids are targeted to the mitotic chromatin.....	108
2.3.6.	Soluble fragments of Nups affect AdV genome delivery differently in mitosis.....	111
2.4.	Specific point mutations at the N-terminus of CRM1 impair AdV genome delivery	115
2.4.1.	Mutations in CRM1 prevent AdV genome delivery in mitotic cells	115
2.4.2.	Mutations in CRM1 affect AdV genome delivery in interphase cells	118
2.4.3.	The CRM1 mutant W142A P143A conserves the protein export function	120
2.4.4.	The CRM1 W142A P143A mutant is able to bind Nup214 and Nup358.....	122
2.5.	Viral components involved in CRM1-dependent AdV genome delivery	124
2.5.1.	CRM1 does not interact with purified Ad5 particles	124
2.5.2.	The Δ pIX AdV mutant shows premature disassembly of the capsid.....	126
2.5.3.	CRM1-dependent nuclear targeting of AdV capsids does not depend on viral pIX.....	128

III_DISCUSSION

1.	THE ROLE OF NUP358 IN ADENOVIRUS GENOME IMPORT	131
1.1.	Depletion of Nup358 delays AdV genome import.....	131
1.2.	The N-terminal half of Nup358 is required for efficient genome import.....	134
1.3.	Transport receptors are rate-limiting for AdV genome delivery.....	136
1.4.	The N-terminal half of Nup358 recruits import receptors.....	139
1.5.	Conclusion.....	141
2.	THE ROLE OF CRM1 IN ADENOVIRAL GENOME DELIVERY	142
2.1.	A novel role for CRM1 in promoting AdV capsid disassembly	142

2.2.	Effect of soluble C-terminal fragments of Nup214	144
2.3.	Effect of soluble C-terminal fragments of Nup358	145
2.3.1.	Additional Nup358-associated factors may be implicated in AdV genome delivery	146
2.3.2.	<i>C-terminal CRM1-binding region of Nup358 potentiates CRM1-dependent disassembly of AdV capsids</i>	148
2.4.	Effect of soluble N-terminal and central fragments of Nup358	149
2.5.	Specific point mutations at the N-terminus of CRM1 impair AdV genome delivery...	150
2.6.	Viral components involved in CRM1-dependent AdV genome delivery	153
2.6.1.	<i>Potential interaction of CRM1 with the AdV capsid</i>	153
2.6.2.	<i>CRM1-dependent AdV genome delivery does not involve AdV protein pIX</i>	155
2.7.	Conclusion	156
3.	GENERAL CONCLUSIONS.....	157
IV_REFERENCES.....		158
ABBREVIATIONS.....		177
LIST OF FIGURES.....		180
LIST OF TABLES		182

INTRODUCTION

1. OVERVIEW OF ADENOVIRUSES (ADV)

1.1 Discovery and clinical relevance

Human adenoviruses (HAdV) were first isolated from adenoid tissue cell culture by Rowe and colleagues in 1953 (Rowe et al., 1953). Initially referred as “cytopathogenic agent”, some years later, Enders and co-workers proposed “Adenovirus” as group name (Enders et al., 1956). Few years after their discovery, Trentin and his colleagues showed for the first time, that human adenovirus type 12 has the capacity to cause tumors in hamsters (Trentin et al., 1962; Yabe et al., 1962). Since then, AdV have been suspected to induce cancer in humans but not clear link has been established (Mackey et al., 1976; Green et al., 1979; Wold et al., 1979). Instead, some AdV types have been amply shown to cause acute respiratory disease in military trainees (Hilleman and Werner, 1954; Top, 1975; Clemmons et al., 2017).

In general, the vast majority of cases of infection are mild and self-limited. However, there are groups of patients with higher risk: children (Singh-Naz and Rodriguez, 1996) and immunocompromised hosts (mainly recipients of allogeneic haematopoietic stem cell transplants) (Lion, 2014) are the most affected. AdV may cause epidemics of febrile respiratory illness, pharyngoconjunctival fever, keratoconjunctivitis, or gastroenteritis and diarrheal illness (Lynch and Kajon, 2016).

1.2 Treatment

AdV still entail a therapeutic challenge, in spite of the extensive research performed on the molecular level over the last sixty years. The lack of standardized clinical trials has not facilitated targeted treatment for this virus, so that there is an absence of specific treatment. The drug most commonly used at the moment is Cidofovir, a monophosphate nucleotide, analogue of cytosine, that can inhibit viral DNA polymerase and thus viral replication (Lenaerts and Naesens, 2006). However, its administration causes a considerable nephrotoxicity (Symeonidis et al., 2007). An oral vaccine preventing diseases from HAdV-E4 and HAdV-B7 is approved for military personnel in the US, but it is not available for civilians (Lynch and Kajon, 2016).

Table 1. Classification of human AdV¹

Species	Type	Primary receptor	Site of infection
A	12,18,31	CAR	Gastrointestinal tract
B	16,21,50, 11,34,35	CD46	Respiratory tract, eye Respiratory and/or urinary tract, eye
	3,7,11,14	DSG-2	Respiratory and/or urinary tract, eye
C	1,2, 5 ,6	CAR	Respiratory tract
D	8-10,13,15,17,19,20,22-30, 32,33,36,38,39,42-49,51	CAR	Eye, gastrointestinal tract
	8,19,37	GD1a, Sialic acid	Eye
	53,54	?	Eye
E	4	CAR	Respiratory tract, eye
F	40,41	CAR	Gastrointestinal tract
G	52	CAR, Sialic acid	Gastrointestinal tract

¹Modified from Cupelli and Stehle, 2011, and updated from “The Online (10th) Report of the ICTV” website: <http://www.ictvonline.org>. Features of the species HAdV-C5 used in this study are outlined in red. HAdV-G52 receptor has been recently characterized by Lenman et al., 2015.

1.3 Classification and associated diseases

Two different classifications schemes have served to organize the diversity of viruses. The Baltimore method, initially proposed by David Baltimore (Baltimore, 1971), divides viruses into 7 groups considering their own strategy of transmitting its genetic information. HAdV are included in the first group, since the nature of their genome consists of a double stranded DNA molecule. The second classification has been developed by the International Committee on Taxonomy of Viruses (ICTV, <http://www.ictvonline.org/>, Accessed August 1, 2017). The agreed hierarchy of viral taxa, from the lower to the higher level, is: Species, Genus, Order and Family. HAdV are thus distributed in 7 different species, from A to G, all of them included in the genus *Mastadenovirus*, which in turn, belongs to the *Adenoviridae* family. Today, there have been reported 84 genotypes of HAdV according to the genebank (<http://hadv.wg.gmu.edu/>; May, 2017 update). Among them, the ICTV has recognized 54 types, traditionally discriminated serologically (**Table 1**). Nowadays, the criteria are wider, and similar to those used for species classification: host range, cellular tropism, oncogenicity in rodents or genome characteristics (% GC content, organization of the E3 region). HAdV species display different tissue tropisms which correlate with clinical manifestations of infection. In the case of HAdV-A species, there is usually an association with gastrointestinal tract diseases, while species B and C tend to cause respiratory tract illness. HAdV-D species is related to cases of conjunctivitis, and in the case of species E, it is usually associated with respiratory and ocular infections. Finally, species F and G are responsible for common cases of gastroenteritis (see for review Ghebremedhin, 2014)

1.4 AdV as a tool in research and gene therapy

HAdV have become a very useful tool to learn about fundamental cellular processes. During the seventies, many researchers chose HAdV-C2 and the closely related HAdV-C5 as model systems for studying mRNA synthesis in animal cells (Berget et al., 1977; Chow et al., 1977 see for review Berk, 2016). These studies served to detect mRNA splicing. This discovery was recognized with the Nobel Prize in 1993.

Investigation of the adenoviral infections has also provided new insight about strategies of infecting cells that are shared by many other different viruses. As an example, AdV research contributed with the first known case of disruption of antigen presentation by major histocompatibility proteins (MHC). In this case, AdV make use of a glycoprotein coded by the E3 gene (E3 gp19k) to retain MHC class I proteins inside the endoplasmic reticulum (Andersson et al., 1985; Burgert and Kvist, 1985; Flint and Nemerow, 2016).

AdV are widely used as therapeutic agents as well, in gene therapy and oncolytic virotherapy. The first approach takes advantage of the high nuclear transfer efficiency of AdV, with the aim to deliver therapeutic genes to the target cell in substitution of the E1 gene region, necessary for viral replication. In contrast, oncolytic AdV are replication-competent and engineered to preferentially replicate in cancer cells, inducing specific tumour cell lysis. The adenoviral vector system possesses several advantages that make them suitable for gene therapy applications: they have the ability to infect both dividing and quiescent cells, recombinant vectors are stable, they have a large insert capacity, they are not oncogenic, can be produced in large amounts and transgenes are expressed episomally (Ghosh et al., 2006). However, some aspects regarding organ toxicity or inflammatory response need to be improved in order to make them safer (Yamamoto et al., 2017).

2. STRUCTURE OF THE ADENOVIRAL PARTICLE

AdV are relatively complex viruses with a total molecular weight of 150 MDa. The adenoviral particle consists of a protein capsid surrounding a double-stranded linear DNA genome. The capsid is icosahedral in shape presenting a *pseudo* T=25 symmetry with a diameter of about 90 nm. The viral DNA is a linear molecule of about 36 kbp, encoding 45 proteins of which only 13 are structural components of the incoming virion (see below; **Figure 1**) while the rest constitutes regulatory and/or scaffolding proteins expressed during the viral replication cycle (Cusack, 2005; Reddy and Nemerow, 2014). The adenoviral capsid itself is composed of 7 different proteins considered as major or minor proteins. In addition, 6 other proteins are packaged with the viral DNA conforming what is termed viral core. Historically, these proteins were numbered (II–IX) depending on their electrophoretic mobility on SDS–polyacrylamide gels for HAdV-C5 (Maizel et al., 1968).

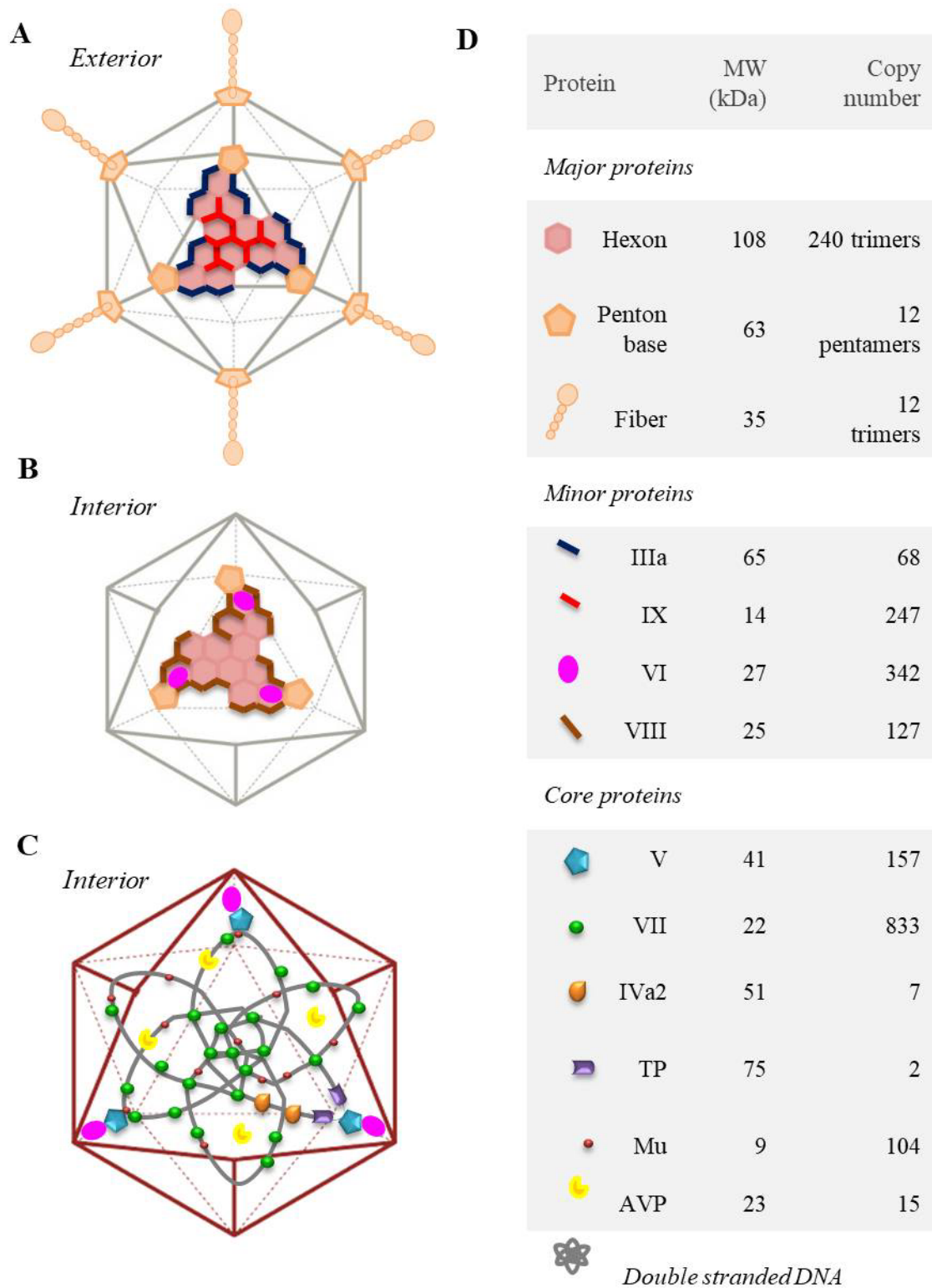


Figure 1. Capsid structure and composition of HAdV. (A) Schematic representation of the external capsid proteins in HAdV. Proteins are represented with a colored symbol and the corresponding names, size in kDa and copy number per virion are shown in (D). (B) Schematic illustration of the triangular facet of the icosahedral capsid shown as inside-out view. (C) Schematic organization of HAdV core proteins in association with the viral genome. (D) Features of the HAdV-C5 proteins (Benevento et al. 2014) including the molecular weight (MW) and the copy number per virion. Structural data used as reference to represent the capsid taken from Reddy and Nemerow, 2014.

2.1 Capsid proteins

The hexon (pII) is the major structural protein of the capsid. Each triangular facet of the icosahedral capsid comprises 12 hexon trimers. The vertices of the virion are formed by a penton base (protein III) with the attached fiber (protein IV). The capsid structure formed by major proteins hexon, penton base and fiber is stabilized by a number of minor components. Their exact localization is still under debate. Some authors suggest that the proteins IX and IIIa are found at the external side of the capsid, intercalated between central hexons at each triangular facet and connecting them to the penton structure, respectively. From the inner side of the capsid, the protein VIII cements the interphase between two facets. Finally, the protein VI is localized underneath each peripentonal hexons helping to link the viral core to the capsid (Reddy and Nemerow, 2014) (**Figure 1A** and **1B**). In contrast, an alternative structure was proposed by Liu et al. (Liu et al., 2010) in which the protein IIIa is sitting on the inner surface underneath the penton base. The protein IIIa together with the inner minor protein VIII link the vertex hexons with the facets, and the external capsid protein IX is in charge of connecting individual hexons and facets together. The protein VI is also found located in a cavity on the inner surface of each hexon, but not exclusively at the vertex region.

2.2 Core proteins

The core is composed of the viral genome compacted with several viral proteins. The most abundant DNA-associated component is the protein VII. It is a basic protein with a structure similar to cellular histones. Protein VII has the ability to condense the viral DNA into chromatin-like structures and neutralize the charge for packaging into the capsid (Sung et al., 1983). It remains bound to the viral DNA (Brown and Weber, 1980) during at least the early phases of infection (P K Chatterjee et al., 1986; Karen and Hearing, 2011; Komatsu et al., 2011). It is present in about 800 copies per DNA molecule (**Figure 1C** and **1D**), making its detection by immunofluorescence a suitable system to study the adenoviral genome delivery (Komatsu et al., 2015). The protein VII interacts with protein IVa2, which in turn, is bound to the specific packaging sequences (Ψ) on the virus DNA (Zhang and Arcos, 2005). Protein IVa2 is believed to be present in a few copies at a single vertex in the mature virion (Christensen et al., 2008).

Protein V bridges capsid-DNA connection by binding protein VI and DNA, in a sequence-independent manner (Pérez-Vargas et al., 2014). In addition, it is associated with core proteins VII and Mu (Chatterjee et al., 1985). Its function has been related to the assistance in capsid assembly (Ugai et al., 2012); however, it is possible that there is some functional

redundancy with protein Mu (Ugai et al., 2007), since protein V is only present in the genera of *Mastadenovirus* (Gorman et al., 2005).

Protein Mu (also known as pX) is synthesized as a precursor (preMu) that needs to be cleaved at the N- and C-terminal regions by the viral encoded protease (Anderson et al., 1989). PreMu has been proposed to participate in viral DNA condensation during viral assembly, since it was shown to precipitate double-stranded DNA in solution (Anderson et al., 1989). Viral protease-driven maturation of PreMu would help to relax the compact DNA core to facilitate AdV genome delivery of incoming virions (Pérez-Berná et al., 2009). PreMu, but not Mu, has been suggested to play a role in modulating expression of E2 early proteins (Lee et al., 2004).

The viral DNA is bound at each end by two copies of the terminal protein (TP). TP protects the viral DNA from degradation and serves as the primer for the initiation of DNA replication by forming a dimer with the encoded viral DNA polymerase (pol) (de Jong et al., 2003).

Incoming virions also contain about 20 copies of the adenoviral protease (AVP). The AVP is in charge of processing virion precursor proteins: IIIa, VII, VIII, IX, TP and preMu, during virus maturation. It is catalytically activated by two steps: it first binds non-specifically to viral DNA, which allows cleavage of protein VI resulting in the C-terminal excision, and second, binding of the protein VI C-terminal fragment to AVP allows its full activation (Russell, 2009; San Martín, 2012). Whether AVP also fulfils a role in virus entry has yet to be shown.

2.3 Genome organization

The adenoviral genome is flanked by inverted terminal repeats of about 100 nucleotides length that contain two identical origins of replication covering about 1-50 base pair. Next to the origin of replication at the left end of the genome, there is the packaging sequence (Ψ), which will guide DNA encapsidation through protein IVa2 (see above). The viral DNA is organized in different transcription units that are sequentially activated: the immediate-early gene E1A; the early genes E1B, E2, E3 and E4; delayed early genes coding for proteins pIX and IVa2, and late genes L1-L5 (Curiel, 2016) (**Figure 2**).

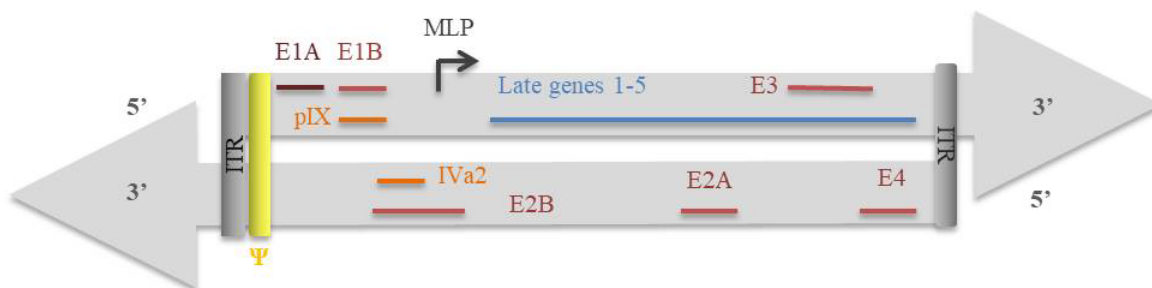


Figure 2. Schematic representation of the adenoviral genome organization. Arrows represent both strands of the AdV dsDNA. Sense of the strands is indicated with 5' or 3' numbers at each extremity. Lines represent major coding regions from the different transcription units. Dark red: immediate early transcription unit. Red: early transcription units. Orange: intermediate transcription units. Blue: late transcription unit. Grey box: ITR. Dark arrow: MLP. MLP: major late promoter; ITR: inverted terminal repeat; Ψ : packaging sequence. Scheme modified from (Ferreira et al. , 2005)

3. ADENOVIRAL INFECTION CYCLE

Like other DNA viruses, AdV need to reach the nucleus in order to replicate and form new infectious particles. The infectious cycle starts with the binding of the virion to the cell surface and subsequent entry into the cytosol. These early steps facilitate a stepwise partial disassembly and transport of the capsid along the microtubules (MT), which will end at the nuclear pore complex (NPC). At this point, the capsid is further disassembled allowing the import of the viral genome inside the nucleus. Once the viral genome has access to the nuclear machinery, it is transcribed and replicated. Finally, viral proteins are produced and thus, new capsids are assembled inside the nucleus and processed in order to egress and infect another cell (**Figure 3**).

3.1 Binding

The adenoviral infection cycle starts with attachment of the virus particle to a specific receptor standing on the cell surface. Initial binding of the viral particle to the cell receptor is mediated by the viral protein fiber. The length and flexibility of this protein, as well as the specificity of its distal domain, determine the receptor preference (Cupelli and Stehle, 2011). Experiments performed in non-permissive hamster cells revealed a specific attachment of HAdV from species A, C, D, E, and F, exclusively at the cell surface of cells overexpressing human Coxsackie and Adenovirus Receptor (CAR) (Bergelson et al., 1997; Roelvink et al., 1998). CAR belongs to a subfamily of immunoglobulin-like surface molecules, implicated in epithelial cell-to-cell tight junctions (Coyne and Bergelson, 2005). HAdV from species B instead recognize either desmoglein 2 (DSG-2) or CD46, a member of the complement regulatory protein family. On the other hand, attachment of the HAdV-D37 fiber to the cell surface is mediated by GD1a glucans via two sialic acid associated residues (Cupelli and Stehle, 2011) (described in **Table 1**). Recently, the scavenger receptor protein MARCO has been shown to increase susceptibilities of certain macrophage subtypes to adenovirus infection (Maler et al., 2017).

HAdV need a second binding to surface α v integrins to be internalized in the cell. This binding is mediated by five flexible loops on the adenoviral penton base containing an arginine, glycine, aspartic acid (RGD) specific sequence (Wickham et al., 1993). Association of the viral penton to integrins facilitate the release of the fiber, presumably due to opposing forces triggered by the fiber/CAR-binding induced motions, versus immobile penton/integrins complexes (Burckhardt et al., 2011). Structural studies have elucidated more

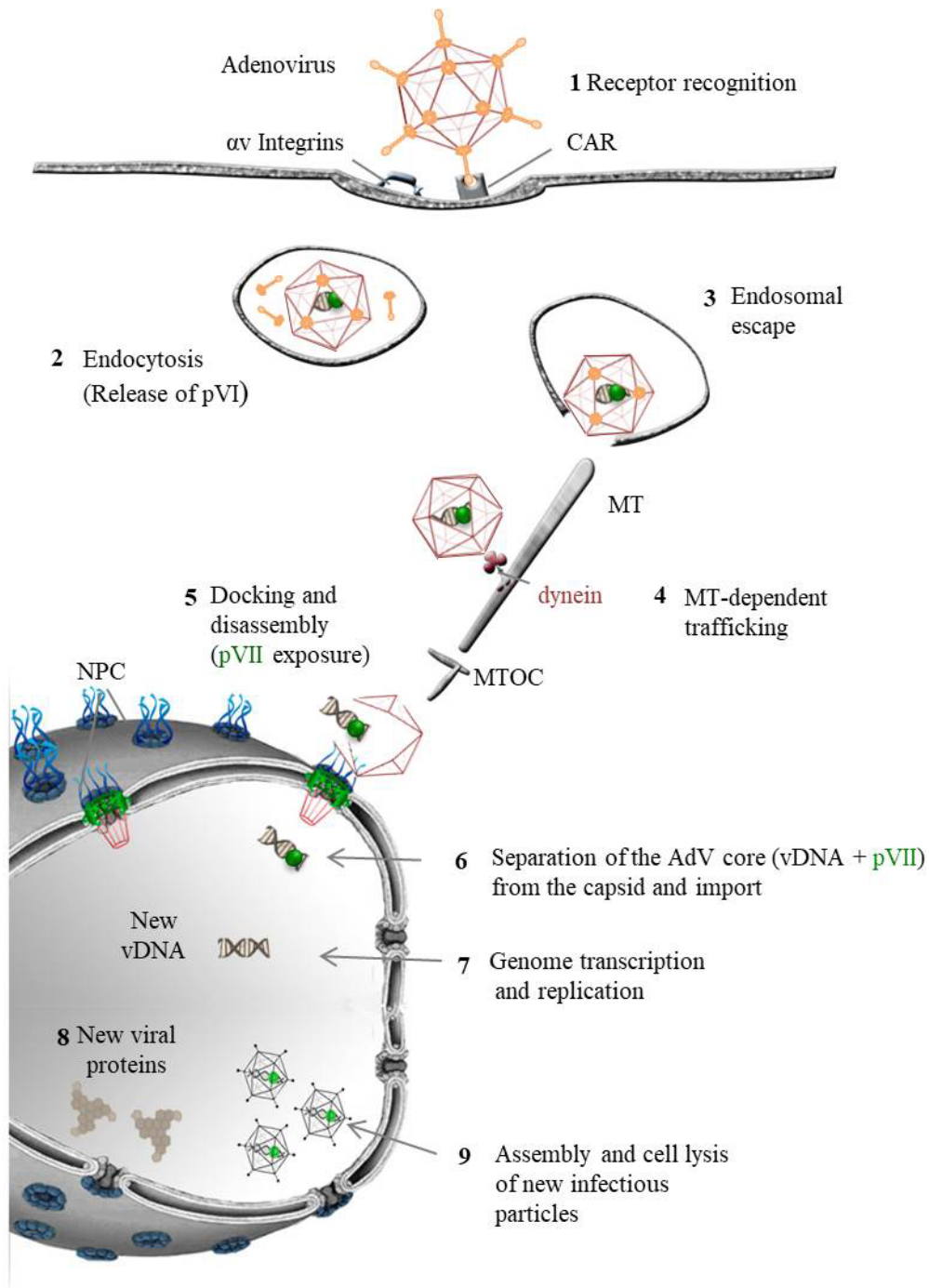


Figure 3. Adenovirus infection cycle. Different steps are shown (1) AdV binding to CAR and αv integrins receptors present at the cell surface. (2) Receptor-mediated clathrin-dependent endocytosis of AdV particles causes release of the fiber and penton base from the capsid. (3) Release of capsid protein VI allows endosomal escape of the capsid. (4) Cytoplasmic transport towards the MTOC via microtubule and dynein association. (5) Docking of the capsid at the cytoplasmic filaments of the NPC triggers disassembly of the capsid. (6) The viral DNA is released and actively imported through the NPC. (7) Viral genome transcription and replication takes place in the nucleus. (8) Viral proteins are synthesized in the cytoplasm and imported into the nucleus. (9) Assembly and egress of new infectious particles.

details about the nature of integrins and penton base association. CryoEM structure analysis indicated that a maximum of four integrins were able to bind the penton base, but due to the close proximity of the RGD domains in the penton monomers, the binding of four integrins simultaneously would only be possible if a conformational untwist takes place (Lindert et al., 2009). Thus, it was suggested that integrins binding to the penton base would induce conformational changes in the capsid vertex that may initiate further uncoating of the capsid. This correlates with atomic force microscopy (ATM) studies in which a selective loss of the vertex region of the virus was observed (Snijder et al., 2013; Ortega-Esteban et al., 2013).

3.2 Entry

CAR-dependent binding to the cell surface facilitates the uptake of the adenoviral particle by clathrin-dependent endocytosis (Wang et al., 1998). This was revealed by using a thermosensitive mutant of dynamin, a crucial protein for excision of the clathrin endosomal vesicle, which allows endocytosis to occur only at a permissive temperature and thus, acts as a dominant negative inhibitor of the adenoviral internalization at 37 °C.

The virion then needs to escape from the endosome in order to avoid autophagic sequestration and further lysosomal degradation. The release of the protein VI from the capsid is critical at this point, since the protein VI is responsible for both, the rupture of the endosomal membrane through its N-terminal amphipathic helix (Wiethoff et al., 2005; Maier et al., 2010) and the escape of the capsid from the endosome through its PPXY motif (Wodrich et al., 2010; Montespan et al., 2017). The exposure to low pH environment has been related to destabilization of the viral capsid (Wiethoff et al., 2005), however there is still some controversy over whether endocytic acidification is indeed necessary for viral entry (Suomalainen et al., 2013).

3.3 Trafficking

After endosomal escape, viral particles engage with the MT network in order to reach the nucleus. The cellular motor protein dynein is responsible for transporting the capsid towards the minus end of MT (Suomalainen et al., 1999; Leopold et al., 2000). It was shown that dynein directly interacts with the viral hexon via the intermediate chains (IC1 and IC2) and light intermediate chain 1 (LIC1); mechanism that differs from that of physiological cargo (Bremner et al., 2009). However, PKA dependent phosphorylation of LIC1 seems to have a predominant role. In agreement with this idea, a LIC1 phosphorylation mutant failed to restore viral capsid trafficking in LIC1 depleted cells (Scherer et al., 2014). Hence, PKA

dependent phosphorylation would tilt the balance towards minus-end-directed motility against positive-end directions (Suomalainen et al., 2001). Studies have also associated low pH treatment with a reversible conformational change of the hexon that would favour dynein recruitment (Scherer and Vallee, 2014).

Although implication of MT in facilitated cytosolic trafficking of AdV has been largely described, MT-independent motility has also been reported, however the mechanism is not known (Glotzer et al., 2001; Yea et al., 2007).

3.4 Genome delivery

Cellular motor proteins mediate transport of adenoviral particles towards the nucleus. They reach the microtubule organizing center (MTOC) in about 1 hour post infection (Suomalainen et al., 1999; Leopold et al., 2000). At this point, viral particles need to engage with nuclear factors to approach the nuclear membrane, as deduced from experiments performed in enucleated epithelial cells, showing an accumulation of incoming virions at the MTOC when the nucleus is removed (Bailey et al., 2003). The cell possesses a sophisticated system for regulating the transport of macro-molecules between the nucleus and the cytoplasm. AdV have the ability to hijack this mechanism to support genome delivery. A detailed description of the different cellular partners involved in nucleo-cytoplasmic transport and the current state-of-the art knowledge about the strategy used by AdV (and other viruses) to deliver viral genomes into the nucleus is provided in sections below (**Sections 4 and 5**).

3.5 Genome transcription and replication

Once the viral genome access the nuclear compartment, the protein E1A activates transcription of the viral genome. Early gene transcription leads to the synthesis of viral proteins involved in both: controlling cellular responses and responses of the immune system (E1B, E3 and E4 regions) or promoting transcription and replication of the viral genome (E2 and E4 region). It has been reported that viral core protein VII enhance early transcription by recruiting the cellular chromatin factor TAF-1/SET (Template activating factor-1), which in turn regulates viral chromatin structure to ensure transcription (Haruki et al., 2006, Komatsu et al., 2011). Later on, protein VII is released from the chromatin (Chen et al., 2007), giving rise to DNA replication activation. DNA synthesis requires priming of the E2 encoded TP precursor by addition of a dCMP residue. Then, the DNA-binding protein (DBP) induces the separation of both DNA strands assisted by cellular factors NFI and Oct-1. This process facilitates initiation of DNA synthesis by the adenoviral DNA pol (Hoeben and Uil, 2013).

The activation of late gene transcription is mediated by the major late promoter (MLP). It requires full activation triggered by DNA replication and newly synthesized protein IVa2. MLP activation then, triggers production of all late genes through alternative splicing of MLP derived transcripts. Adenoviral late proteins are synthesized to either form the structure of the virion, assist in assembly and genome packaging or have regulatory functions (Curiel, 2016).

3.6 Late phases

The assembly of nascent virions occurs in the nucleus, once the viral DNA is synthesized (Weber et al., 1985) and newly produced capsid and core proteins are imported into the nucleus (Wodrich et al., 2003). Recent studies have shown that capsid assembly and genome packaging occur at the periphery of viral replication centers (Condezo and San Martín, 2017). However, it is still not well understood how both processes are coordinated. Proteins IVa2 and L1 52/55K recognize the packaging sequences (Ψ) and help to encapsidate the viral DNA (Perez-Romero et al., 2005). L1 52/55 K are thought to link the association between the viral DNA and the capsid proteins during the assembly process (Ma and Hearing, 2011), and will later be released from the viral particle by proteolytic cleavage during maturation (Pérez-Berná et al., 2014).

Capsid maturation is crucial for correct disassembly during early steps of infection. A thermosensitive mutant known as *tsI*, grown at non-permissive temperature (38.5 °C), is unable to include the viral protease during capsid assembly and thus, further cleavage of precursor proteins is lacking (Rancourt et al., 1995). As a consequence, the *tsI* has a much more compacted capsid and condensed core, which prevent capsid disassembly and the release of the membrane lytic factor protein VI during entry into the cell (Pérez-Berná et al., 2009) leading to lysosomal degradation (Martinez et al., 2015). Main progress in the understanding of the capsid maturation process has been provided by comparing WT and mutant *tsI* capsid structures (reviewed in Mangel and San Martín, 2014).

Once virions are properly assembled and processed, an increased production of the E3 coded adenovirus death protein (ADP) finally leads to the lysis of the infected cell, allowing the egress of newly formed infectious particles (Tollefson et al., 1996).

4. BASIC MECHANISMS OF NUCLEOCYTOPLASMIC TRANSPORT

In comparison to prokaryotes, gene expression in eukaryotes possesses an additional level of control due to spatial segregation of DNA transcription in the nucleus and protein synthesis in the cytoplasm. Both compartments are separated by the nuclear envelope, thus nucleocytoplasmic transport of macro-molecules requires its own machinery and precise regulation. Both compartments are connected through small pores embedded in the nuclear membrane, which are called nuclear pore complexes (NPC). These are macromolecular complexes constituted of individual proteins known as nucleoporins (Nups), which form a symmetric octameric pore around a central channel of 41 nm of diameter (Bui et al., 2013) consistent with the reported size limit of cargo (39 nm; Panté and Kann, 2002). Molecules smaller than \approx 5.3 nm of diameter (Mohr et al., 2009) (corresponding to about 40–60 kDa; Ma et al., 2012) can freely diffuse across the NPC. Instead, larger molecules cannot diffuse through the pore channel and thus, are translocated by a facilitated active transport (Cingolani et al., 1999). For this, they rely on special carrier proteins collectively called karyopherins.

In general, karyopherins are specialized in transporting molecules unidirectional (in or out) with some exceptions mediating bidirectional transport. Consequently, the nomenclature import of molecules into the nucleus is mediated by importins, and transport towards the cytoplasm involves exportins. They are classified in two families: the karyopherin- α family, consisting of 3 subfamilies of importin- α (Pumroy and Cingolani, 2015); and the karyopherin- β family, comprising most of the transport receptors known to date, which are divided into 15 different subfamilies of importins and exportins, in humans (Chook and Süel, 2011) (listed in **Table 2**). For some karyopherins, the crystal structure was solved (e.g importin- β (Cingolani et al., 1999) or transportin-1 (Lee et al., 2006), and reviewed in (Christie et al., 2016)). This revealed common fold of a highly flexible super-helical structure formed by 19-20 HEAT-repeats, which consist in two antiparallel α -helices (A and B) connected by a short loop. These HEAT repeats are arranged as N- and C-terminal arches. The karyopherin- β family possess a conserved N-terminal arch that binds the small GTPase Ran, in its GTP-bound state (reviewed in Cook et al., 2007; Chook and Süel, 2011).

Karyopherin binding to RanGTP determines the interaction between transport receptors and their cargo: importins bind RanGTP and their cargo in an exclusive manner (either cargo or RanGTP), presenting higher affinity for RanGTP; in contrast, exportins need RanGTP to form the cargo complex for export. To drive nucleocytoplasmic transport, cells have established a system to maintain a gradient of RanGTP across the nuclear envelope that ensures directionality of the transport.

Table 2. Human karyopherin- β family¹

Subfamily	Karyopherin- β	Known cargos	Recognized sequence
IMB1	Importin- β	Ad2 pV, pVII; HPV16 E6, L2; H2A,H2B; HIV1 IN	Classical-NLS via Imp α or IBB
IMB2	Transportin-1 (TNPO-1)	Ad2 pV, pVII; hnRNPs; H2B,H2A,H3; HSP70,90; CPSF6	PY-NLS
IMB3	Importin-5	HPV16 L2, HPV18 L2; HIV-1 Rev; H2A,H2B,H3,H4	ND
IMB4	Importin-4	Proteins	ND
IMB5	Importin-9	H2B,H2A,H3,H4; HIV-1 REV; HSP27	ND
IPO8	Importin-7, Importin-8	Ad2 pVII; H1,2B,4; HIV-1 IN Ago2; Smad 1,4	ND
KA120	Importin-11	UbcM2, UbcH6, UBE2E2; Gag (RSV)	ND
TNPO3	Transportin-SR, Importin-13	CPSF6; HPV E2; HIV1 IN Ubc9	RS domains
XPO1	CRM1 (Exportin-1)	(Thakar et al., 2013; Kırılı et al., 2015)	Classical-NES
XPO2	CAS	Importin- α	Importin- α
XPO4	Exportin-4	Proteins	ND
XPO5	Exportin-5	RNA and proteins	Conformational; entire pre-miRNA
XPO6	Exportin-6	Proteins	ND
XPO7	Exportin-7	Proteins	ND
XPOT	Exportin-t (Xpo-t)	t-RNAs	Conformational; entire tR

¹Simplified from (Xu et al., 2010; Chook and Süel, 2011; Twyffels et al., 2014). CPSF6: Cleavage and polyadenylation specificity factor subunit 6; H: Histone; HIV: Human Immunodeficiency virus; hnRNP: Heterogeneous ribonucleoprotein; HPV: Human Papilloma Virus; HSP: Heat-shock protein; IBB: Importin- β binding domain; IN: Integrase; ND: non-determined; RS: Serine residues; RSV: Respiratory Syncytial Virus.

4.1 The RanGTP gradient

The protein Ran belongs to the Ras superfamily of small GTPases. It is present in the cell in two states: either bound to GTP, or bound to GDP (as a result of GTP hydrolysis). Karyopherins are only able to bind the GTP-bound form of Ran, which is asymmetrically distributed in the cell (**Figure 4**).

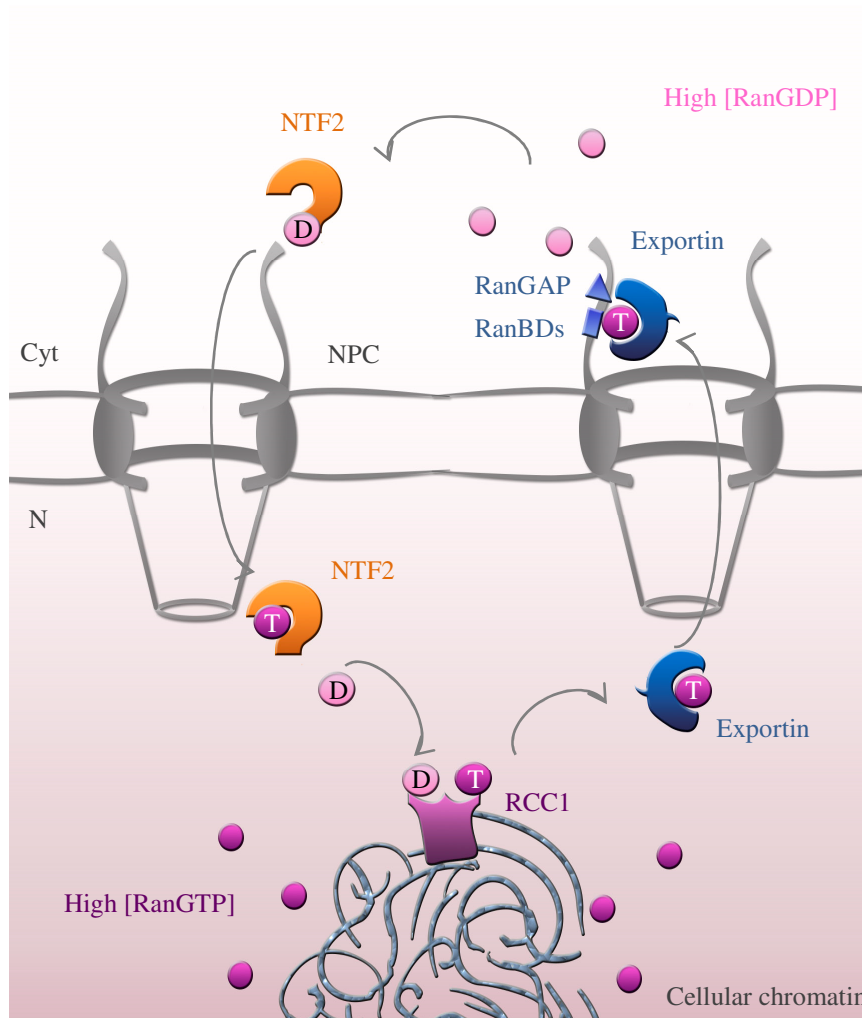


Figure 4. The RanGTP gradient. The RanGTP gradient determines the directionality of nucleocytoplasmic transport. The high concentration of RanGTP (GTP-bound form of Ran) in the nucleus is maintained by chromatin bound RCC1 (Regulator of chromosome condensation 1), which mediates loading of GTP to Ran to generate RanGTP. The high concentration of RanGDP (GDP-bound form of Ran) in the cytosol is maintained by RanGAP (Ran GTPase-activating protein), which is found either soluble in the cytosol or associated with Nup358 at the cytoplasmic filaments of the nuclear pore complex. With the help of the RanBDs (Ran binding domain) of Nup358 or the soluble RanBP1 (Ran binding protein), RanGAP activates the hydrolysis of GTP mediated by Ran. The resulting RanGDP molecule is imported into the nucleus by the specific importin NTF2 (Nuclear transport factor 2). T: RanGTP; D: RanGDP; NPC: nuclear pore complex; Cyt: cytoplasm; N: nucleus

The RanGTP concentration in the nucleus is high, which favours the formation of the export complex consisting of an exportin, a RanGTP molecule, the cargo and other cofactors. The RanGTP concentration in the cytoplasm in contrast is very low, which facilitates recognition and binding of cargo by importins. In order to maintain the gradient of RanGTP between the nucleus and the cytoplasm, two different factors are localized in both compartments. On the cytoplasmic side, the Ran GTPase-activating protein (RanGAP) facilitates the hydrolysis of GTP by Ran, resulting in low RanGTP concentrations. Additional cytosolic factors contribute to GTP hydrolysis, like the Ran-binding proteins (RanBP) (Bischoff and Görlich, 1997; Kehlenbach et al., 1999). The resulting RanGDP molecule is recycled back to the nucleus by using a specific importin called NTF2 (Nuclear Transport Factor 2) (Ribbeck et al., 1998; Smith et al., 1998). Inside the nucleus, a specific RanGEF protein, RCC1 (Regulator of Chromosome Condensation 1), mediates the release of GDP and reloading of Ran with GTP (Bischoff and Ponstingl, 1995). This protein is found associated to the chromatin via histones H2A and H2B (Nemergut et al., 2001). In addition, the presence of RanGTP regulates karyopherin interactions with Nups. In the case of importins, binding to RanGTP induces a conformational change that alters the structure of the Nup-binding site (Bayliss et al., 2000), leading to the release of the transport receptor from the Nup. In the case of exportins is the opposite, binding of RanGTP increase the affinity of karyopherins for Nups (Port et al., 2015; Ritterhoff et al., 2016)

4.2 Nuclear import

In general, transport receptors determine which molecules are transported through the pore by recognizing a specific range of cargoes, although some cargoes can be imported by more than one carrier (as is the case for cellular histones (Mosammaparast et al., 2001) or the adenoviral core protein VII (Wodrich et al., 2006)). Nuclear import starts with the recognition of a specific sequence in the cargo known as nuclear localization signal (NLS) (**Figure 5**). NLSs consist of one or more short sequences of basic amino-acids exposed on the protein surface that interact with importins in absence of RanGTP. Thus, the import complex between cargo and import receptors forms in the cytoplasm and is followed by interactions with the NPC by binding to Nups, which results in import of the complex across the NPC. As mentioned above, inside the nucleus, import receptors preferentially bind to RanGTP, leading to the release of the cargo. Finally, they are recycled back to the cytoplasm for the next round of import.

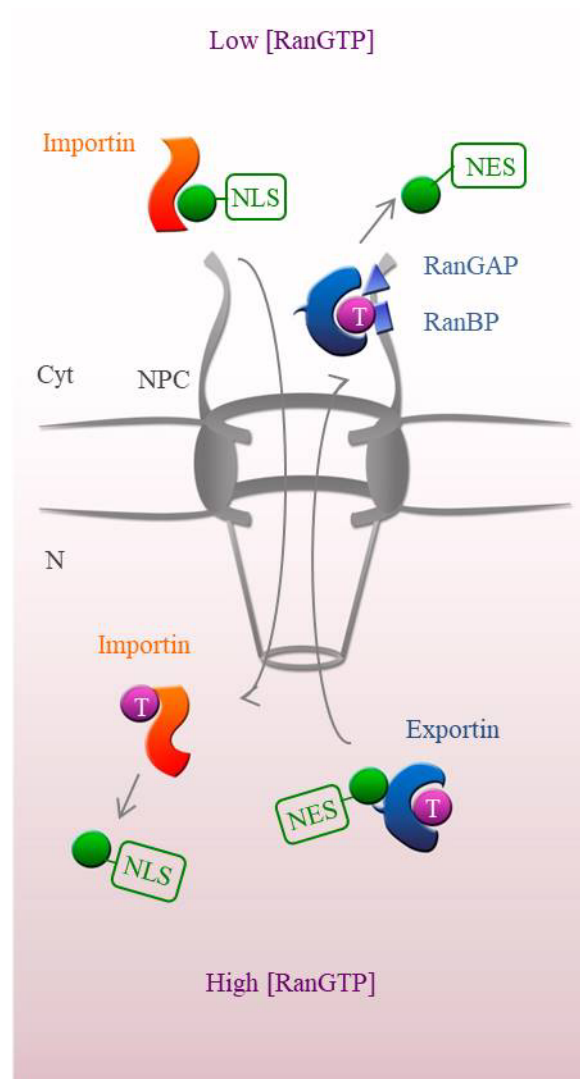


Figure 5. Bidirectional active transport across the NPC. Importins recognize NLS-containing cargoes in the cytosol. Low concentrations of RanGTP in the cytoplasm favor the formation of the import complex, which then translocate across the pore. At the nuclear side of the pore, high concentrations of RanGTP allow RanGTP binding to the import receptor, leading to the release of the cargo inside the nucleus. Exportins behave in the exact opposite way. Export receptors recognize a NES-bearing cargo in the nucleus. High concentrations of RanGTP in this compartment facilitate the formation of the export complex, which then translocate through the pore. At the cytosolic side of the NPC, RanGAP and RanBP facilitate the hydrolysis of GTP by Ran, leading to the disassembly of the complex and release of the cargo into the cytoplasm. NLS: nuclear localization signal; NES: nuclear export signal; T: RanGTP; D: RanGDP; NPC: nuclear pore complex; Cyt: cytoplasm; N: nucleus.

4.2.1 Importin- α/β complex pathway

Importin- β is probably the best studied member of the karyopherin- β family. The prevalent import pathway of a classical-NLS-containing cargo by importin- β involves cargo recognition via an adapter protein. Classical-NLS (cNLS) were first described in the SV40 T-antigen and consist of a consensus monopartite sequence of 4-5 basic residues: K(K/R)X(K/R) (where X is any residue). Detection of the cNLS in the cytoplasm is mediated by the adaptor protein importin- α , which in turn, interacts with importin- β through its importin- β -binding domain (IBB). Once the import complex reaches the nucleus, binding of RanGTP to importin- β displaces the IBB domain of importin- α , which then, competes with the cNLS of the cargo thereby facilitating the release of the cargo inside the nucleus. Finally, importin- β bound to RanGTP is recycled back into the cytosol while importin- α recycling requires a specific exportin (CAS in vertebrates) to come back to the cytoplasm (reviewed in Lange et al., 2007). A bipartite NLS sequence (e.g. in nucleoplasmin (Dingwall et al., 1988)), which contains an extra basic cluster located 10-12 residues downstream of the first cluster is imported in a similar manner. High concentration of importin- β at the NPC periphery (Chi et al., 1995) has been proposed to compete with binding of certain NLS-containing cargo with MT thereby facilitating a switch from MT-dependent trafficking to facilitated import to the nucleus (Roth et al., 2011) (explained in section 5.3).

4.2.2 Transportin-1 pathway

The classical importin- α/β mediated transport, where cargo is recognized through an adapter protein, is more the exception than the rule. All other investigated karyopherins bind and translocate their cargoes directly. Another major import receptor is transportin-1, which binds to proline and tyrosine rich NLS (PY-NLS). PY-NLS are about 30-40 aa sequences that share low similarity between transportin-specific cargoes, making it difficult to predict and establish a consensus sequence. PY-NLS are best known for having structural disorder and overall basic charge. The proposed C-terminal consensus sequence of the PY-NLS is R/K/H-X(2-5)-P-Y (where X is any residue) (Lee et al., 2006). One of the best characterized NLS recognized by transportin-1 is the M9 sequence of the mRNA-binding protein hnRNP A1 (Pollard et al., 1996). Many of the transportin-1 cargoes are mRNA binding proteins and transcription factors (Chook and Süel, 2011), although under non-physiological conditions transportin-1 has been described to mediate import of exogenous DNA through the NPC in *Xenopus* reconstituted nuclei (Lachish-Zalait et al., 2009). Similar to other import receptors, high concentrations of RanGTP in the nucleus favours binding of RanGTP to the N-terminal arch

of transportin-1, leading to the release of cargo. In the case of transportin-1, it contains a large loop that connects the two helices within the HEAT repeat 8. Upon RanGTP binding, a conformational change is proposed to push the acidic H8 loop towards the cargo-binding site in the C-terminal arch of transportin-1, causing cargo release in the nucleus (Chook et al., 2002).

4.3 Nuclear export

Nuclear export of cargoes is initiated in the nucleoplasm with the recognition of a short amino acid sequence present in the protein cargo named nuclear export signal (NES) (**Figure 5**). NESs are peptides of usually 8–15 residues long generally presenting hydrophobic patterns. The exportin binds the cargo together with a RanGTP molecule and some other cofactors (see below) that assist in the formation of the export complex. The export complex interacts with Nups and crosses the NPC to translocate the cargo to the cytoplasmic side. As detailed above, at the cytoplasmic side of the pore, the RanBPs promote the dissociation of RanGTP from the exportin and facilitate the activation of Ran-mediated GTP hydrolysis by RanGAP, leading to cargo release.

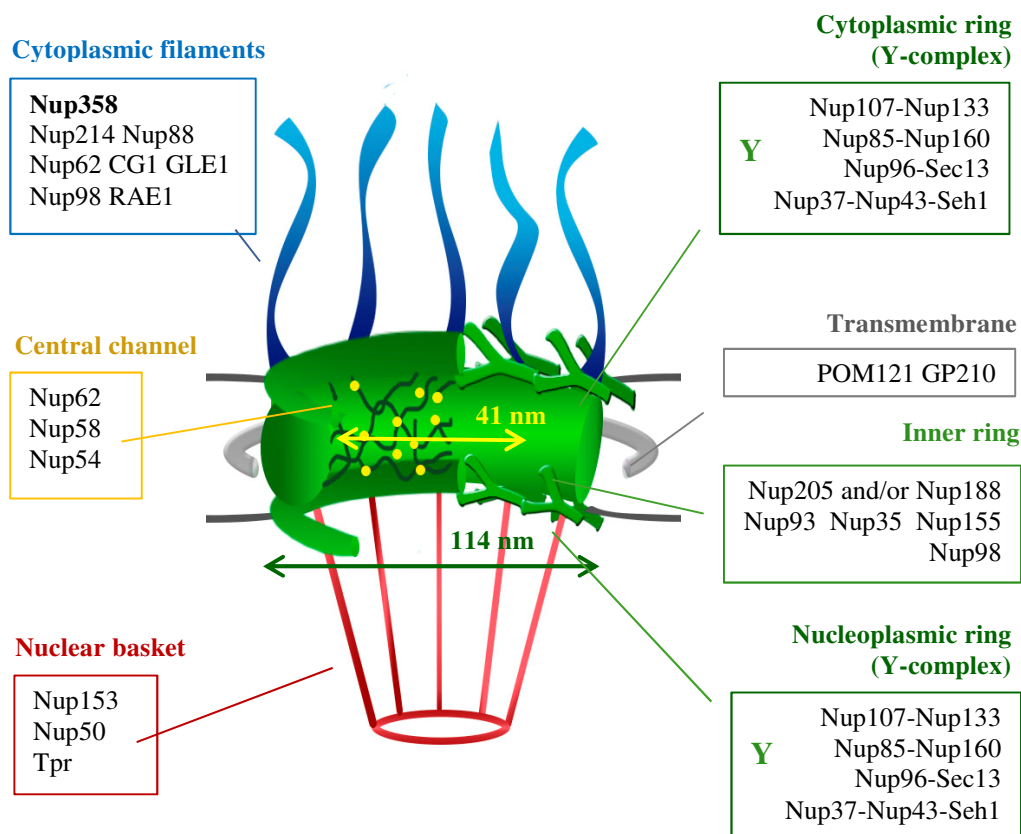
4.3.1 CRM1-dependent export

The exportin CRM1 (Chromosome Region of Maintenance-1) was first discovered in yeast, where its mutation causes abnormal chromosome morphology (Adachi and Yanagida, 1989). Since then, CRM1 function in nuclear export and additional roles in mitosis have been extensively studied. CRM1 recognizes hydrophobic NESs (Fornerod et al., 1997a; Fukuda et al., 1997; Kehlenbach et al., 1998) through a specific binding pocket on the outer surface (Monecke et al., 2013). Prototypical classic NESs recognized by CRM1 are the present in the HIV-1 protein Rev (LPPLERLTL; hydrophobic residues underlined) as well as the inhibitor of cAPK (PKI) NES (LALKLAGLDI) (Fischer et al., 1995; Wen et al., 1995). RanGTP then, binds CRM1 increasing CRM1-cargo affinity (Monecke et al., 2014). RanGTP binds to the N-terminal domain CRM1 which was designed as CRIME (CRM1, Importin-β, Etcetera) due to the high level of similarity to the N-terminus of importin-β (Fornerod et al., 1997b). To form fully functional export complexes, additional adaptor proteins are required (Petosa et al., 2004). One of these cofactors is RanBP3, which increases the affinity of a NES-bearing cargo for CRM1 by simply binding to the exportin, or by promoting high RanGTP concentration in the vicinity of CRM1 (Hutten and Kehlenbach, 2007). In exceptional cases, natural cargoes of CRM1 bind with highly increased affinity independently of RanGTP, as is the case for the

adaptor receptors snurportin-1 or NMD3, whose NES differ from that of the canonical Rev-HIV1 NES (Kutay and Güttinger, 2005). Binding to Nups also assists the translocation of the export complex through the pore. At the cytoplasmic side, Nup214 serves as a terminal docking site for the export complexes allowing access to soluble RanBP1 and Nup358 Ran-binding domains, that facilitate release of the cargo in cooperation with soluble or Nup358-associated RanGAP (Hutten and Kehlenbach, 2007). In steady-state CRM1 is mainly localized inside the nucleus and at the NPC via Nup358 binding (Hutten and Kehlenbach, 2006; Hamada et al., 2011). However a fraction is localizing at the MTOC (Liu et al., 2009). It has been proposed that CRM1 might be targeted to the MTOC by binding with centrosomal RanGTP (Keryer et al., 2003; Liu et al., 2009).

5. THE NUCLEAR PORE COMPLEX

Nuclear pore complexes are large macromolecular protein assemblies of 120 MDa in humans (as a reference, ribosomes have a molecular mass of ~ 3.5 MDa). NPCs are embedded in the nuclear envelope traversing outer and inner nuclear membrane thereby forming a central channel that connects nuclear and cytoplasmic compartments (**Figure 6**).



The overall structure of the NPC presents an eight-fold rotational symmetry and is organized in three stacked rings: a cytoplasmic ring, a central ring embedded in the nuclear membrane and a nuclear ring. From the cytoplasmic ring emanate 8 flexible filaments. At the nuclear side of the NPC, a basket-like structure is anchored to the nuclear ring (recently reviewed in Beck and Hurt, 2017). About 30 different types of Nups compose the NPC. Most of them are distributed in stable subcomplexes, however some Nups are highly mobile. Some Nups seem to have an exclusive scaffold function, like the Nup107/160 complex, also known as Y-complex, constituted of 10 Nup members. Other Nups encode sequences enriched in phenylalanine and glycine residues, so called FG-repeats, which are necessary for the interaction with karyopherins. Beyond its well-known function mediating nucleo-cytoplasmic transport, components of the NPC play also a role in regulating gene expression, DNA replication, as well as mediating different steps during mitosis (Ibarra and Hetzer, 2015).

5.1 FG-Nups involved in transport

As mentioned, FG-repeats of certain Nups bind to karyopherins through low-affinity interactions, allowing transient passage across the pore. The intrinsically disordered structure of FG-repeat-bearing Nups has hindered the understanding of their organization in the central channel. Several models have been conceived from *in vitro* studies (reviewed in Wälde and Kehlenbach, 2010). One of them is known as the *selective phase model* (Frey and Görlich, 2007). This model proposes that hydrophobic clusters of FG-repeats encoded by some Nups would interact within the NPC forming a network with gel-like properties. Consequently, the NPC would allow diffusion of small molecules but restrict translocation of larger ones. Transport receptors would be able to interact with the FG-repeat clusters thereby overcoming the selective permeability barrier. In the *virtual gate* and *the polymer brush model* (Rout et al., 2003) the FG-FG interactions would not be the determinants of the NPC permeability barrier. The model views the NPC as a small volume gate, crowded by FG-Nups, which restricts the movement of incoming molecules through the NPC.

Figure 6. Structure and components of the nuclear pore complex. Schematic representation of the structure and nucleoporin components of the NPC. Names and localization of individual nucleoporins are indicated in colored boxes (Beck and Hurt, 2017; Weberuss and Antonin, 2016). The cytoplasmic, inner and nuclear rings are represented in green. The basic structural element of the external rings is a dimer of two slightly shifted, tandem Y complexes. Nup358 stabilizes the interface between Y-complexes of the cytoplasmic ring (von Appen et al., 2015). The nuclear basket (red) is anchored to the nuclear ring. Attached to the inner ring are the FG-repeat containing Nups (yellow dots), which form a meshwork within the central channel. Transmembrane Nups are represented in a grey ring. Horizontal arrows indicate dimensions of the external diameter of the NPC and the central channel (Bui et al. 2013).

Transport receptors able to interact with FG motifs would need less energy to entry into the narrow pore, and, if the binding is not too strong, transport complexes can dissociate and exit the pore volume. The *polymer brush model* adds that FG-Nups tend to form brush-like structures that are in constant movement and repel large molecules unless they interact with the filaments. The *forest model* (Yamada et al., 2010) is a mixture of previously described models. It estimates two categories of FG-domain conformations: globular collapsed-coil domains, forming the so-called “shrubs”; and groups of extended-coil domains forming the “trees”. The central channel formed by the trees would allow transport of large molecules according to principles described for the selective phase model. Instead, lateral FG-Nups could facilitate transport of cargo-free transport receptors or carrying small cargoes based on the principles of an entropic gate. Finally, the *reduction of dimensionality model* (Peters, 2009), postulates that FG-repeat binding sites of Nups for transport receptors are essentially saturated, forming a narrow central channel through which small molecules can diffuse. Large molecules instead have to bind transport receptors at the entry of the NPC. This binding would allow progressive translocation along the central channel by continuous interactions with the FG repeats. Recently, Lim and coworkers have directly analyzed the native nuclear pores of *Xenopus laevis* oocyte cells using high-speed atomic force microscopy. Their observations favour the *virtual gate/polymer brush model*, in which FG-Nups would be in constant movement, creating an entropic barrier for unspecific cargoes (Sakiyama et al., 2016).

The majority of FG-Nups are therefore localized in the central channel of the NPC. However, some are asymmetrically distributed at the periphery of the NPC, such as Nup153 located at the nuclear basket, or Nup214 and Nup358 that are major components of the cytoplasmic filaments (**Figure 6**). These Nups serve as docking site for incoming transport complexes or are implicated in the terminal step of transport.

5.1.1 Nup214

Nup214 is located on the cytoplasmic side of the NPC where it forms a complex with Nup88 and Nup62 (Brohawn et al., 2009). An important role of Nup214 in nucleo-cytoplasmic transport is to facilitate CRM1-dependent export of certain cargoes (Bernad et al., 2006; Hutten and Kehlenbach, 2006). Nup214 binds and stabilizes the export complex formed by CRM1, a NES-containing cargo and RanGTP, protecting it from premature hydrolysis of GTP (Hutten and Kehlenbach, 2006; Port et al., 2015). Recently, the tetrameric complex formed by interacting regions of Nup214, RanQ69L (a GTP hydrolysis-deficient Ran mutant), NES-

cargo Snurportin-1 and CRM1, was studied by X-ray crystallography and site-directed mutagenesis. The results revealed that several individual FG-repeat motifs of Nup214 drive the interaction with several FG-binding pockets in CRM1 (Port et al., 2015). It is conceivable that as a last step of export, highly flexible FG-repeat C-terminal binding region of Nup214 to CRM1 facilitates access of the export complex to RanBP1 or the RanBD domains of Nup358 which, together with RanGAP, cooperate to disassemble the export complex at the cytoplasmic side of the NPC (**Figure 7**; Hutten and Kehlenbach, 2007).

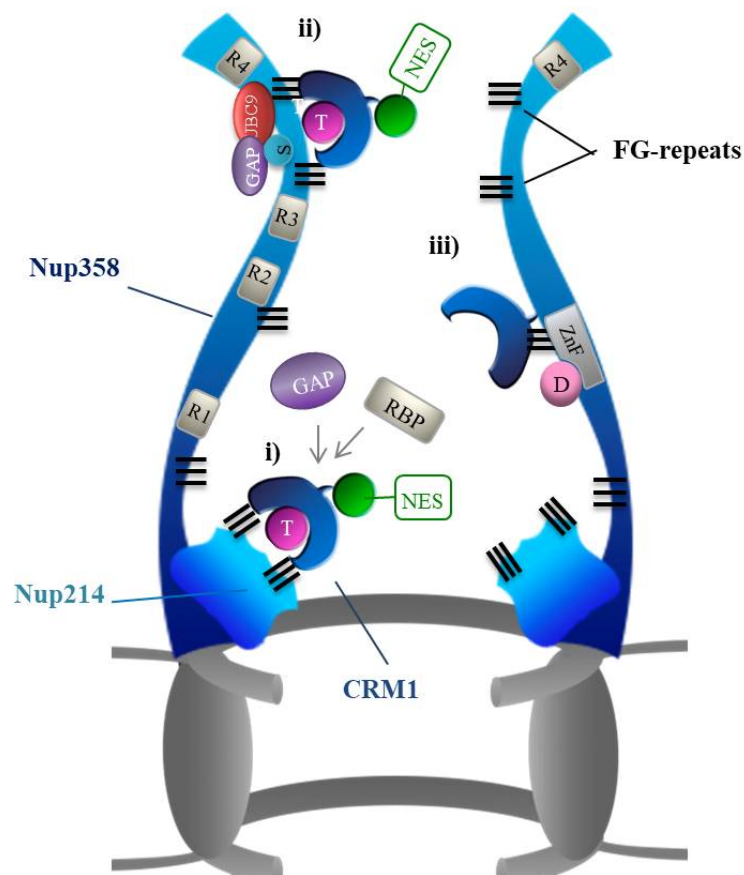


Figure 7. Role of cytoplasmic Nup214 and Nup358 in CRM1-mediated nuclear protein export.

i) Export complexes consisting of CRM1, a RanGTP molecule and a NES-bearing cargo formed inside the nucleus translocate across the pore and dock at Nup214 in the cytoplasmic side of the NPC. Nup214 binds to CRM1 via its FG-repeats (black lines) and stabilizes the complex, preventing premature disassembly. Cytosolic soluble RanGAP and RanBP1 facilitate hydrolysis of GTP by Ran, which leads to the disassembly of the complex and release of NES-cargo in the cytoplasm. ii) Alternatively, Nup358 provides a C-terminal binding site for CRM1-containing export complexes via two FG-repeat clusters. Nup358-associated SUMO* RanGAP and the RanBDs of Nup358 facilitate the hydrolysis of GTP by Ran leading to the release of the cargo in the cytoplasm. iii) After export complex disassembly, the resulting free CRM1 protein can stay associated to the C-terminus of Nup358 or bind to the central zinc finger domains of Nup358. The resulting RanGDP molecule can also associate to Nup358 via the zinc finger domain of Nup358. NES: nuclear export signal; T: RanGTP; D: RanGDP; NPC: nuclear pore complex; ZnF: Zinc fingers Cyt: cytoplasm; N: nucleus. Modified from (Hutten and Kehlenbach, 2007).

5.1.2 Nup358

Nup358 (also known as Ran binding protein 2, RanBP2) is a large (358 kDa) filamentous protein of about 36 nm length (Delphin et al., 1997), which correlates with the dimensions of the cytoplasmic filaments (Beck et al., 2004). The first semi-quantitative analysis of individual Nup stoichiometry estimated 8 copies of Nup358 per NPC, in vertebrates (Cronshaw et al., 2002); however, combination of proteomics and super-resolution microscopy allowed recent determination of human Nup stoichiometry, defining 32 copies of Nup358 per NPC (Ori et al., 2013). In spite of being the major component of cytoplasmic filaments in vertebrates, there is not a Nup358 homologue in yeast (Knockenbauer and Schwartz, 2016). Indeed, Nup358 has been reported to play a scaffold function stabilizing the structure of the cytosolic ring of human NPCs (von Appen et al., 2015) and, interestingly, most of the protein interfaces that contribute to this stabilization appear to be specific for higher eukaryotes. Importantly, depletion of Nup358 does not lead to reduced levels of the other major cytosolic Nup, Nup214, and *vice versa* (contrary to Nup88, which binds to Nup214) (Walther et al., 2002; Hutten and Kehlenbach, 2006; Bui et al., 2013). It is not clear however why Nup358 implies an advantage in higher eukaryotes. It might be required to improve efficiency of nucleo-cytoplasmic transport, which could be specially limiting in cells with large cytoplasm (e.g. neurons). Additionally, Nup358 has specific functions in both interphase and mitosis that might not be required in yeast.

5.1.2.1 Nup358 domains

Nup358 consist of a multi-domain architecture and thus, interacts with many different proteins implicated in various processes such as nucleo-cytoplasmic transport, microtubule regulation or chromosomal segregation during mitosis (**Figure 8**). Nup358 possesses an N-terminal leucine-rich region harbouring the (unmapped) NPC-anchoring domain (Joseph and Dasso, 2008; Hamada et al., 2011). Characteristic of Nup358 are also its four different Ran-binding domains (RanBD1-4) homologous and functionally equivalents to that of RanBP1 (Kehlenbach et al., 1999; Vetter et al., 1999; Yaseen and Blobel, 1999). In addition, the protein encodes several FG-repeat patches, distributed all along the protein (Wu et al., 1995; Yokoyama et al., 1995). The central region contains 8 zinc finger (ZnF) motifs in human Nup358, with a variable number depending on the species (Singh et al., 1999).

The C-terminal region of Nup358 has a natively unfolded region with E3 ligase activity (Pichler et al., 2002). This region is characterized by two internal repeats (IR1 and IR2) separated by a short linker sequence (M). Additionally, there is a SUMO-interaction motif

(SIM) directly N-terminal of IR1. The region M-IR2 is also able to bind SUMO1 *in vitro* (Tatham et al., 2005). Both IR1 and IR2 are able to bind Ubc9 and catalyze SUMOylation, although IR1 has a much more efficient E3 ligase activity compared to IR2 *in vitro* (Tatham et al., 2005). However, *in vivo*, SIM1 and IR1 domains of Nup358 are occupied by RanGAP*SUMO1 and Ubc9, respectively. The binding of RanGAP*SUMO1 and Ubc9 to Nup358 allows catalytic activation of the IR2 domain, constituting the relevant E3 ligase activity *in vivo* (Werner et al., 2012). In this context, Ubc9 has an exclusive structural function. It facilitates recruitment of RanGAP*SUMO1 to the SIM motif and thus, activates by an unclear mechanism the E3 ligase activity of the IR2 region of Nup358 (Zhu et al., 2006; Werner et al., 2012). Finally, at the C-terminal extremity of Nup358 there is a cyclophilin-like domain (Wu et al., 1995; Yokoyama et al., 1995).

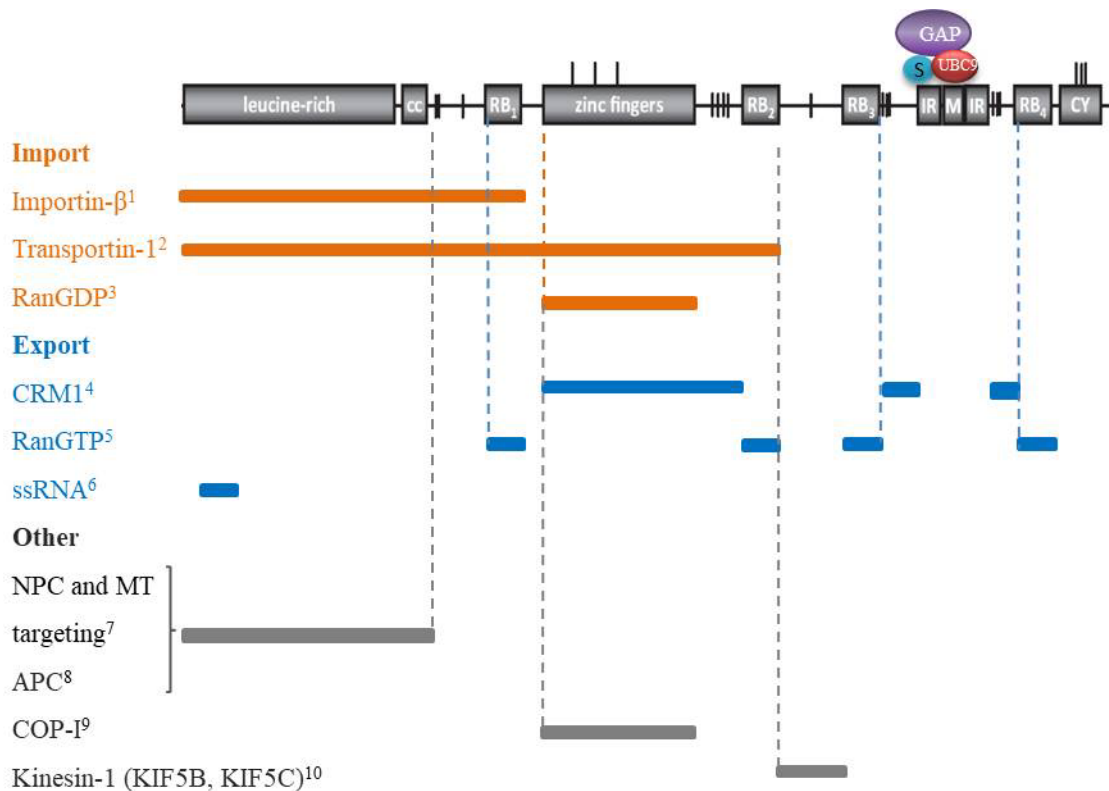


Figure 8. Structure and interacting partners of Nup358. Nup358 is the major component of the cytoplasmic filaments of the NPC and stably form a complex with SUMO**RanGAP* and the SUMO E2 conjugating enzyme Ubc9. The structure of Nup358 is represented at the top of the scheme. Different domains are indicated in grey boxes. FG-repeats are represented with vertical dashes. Cc: coiled-coil; RB1-4: RanBD; IR: internal repeat region; M: middle region; CY: cyclophilin-like domain. The N-terminal of IR1 is a functional SUMO interacting domain (SIM). Interacting proteins or molecules are indicated to the left of the scheme. Regions of Nup358 involved in import are colored in orange, regions involved in export are colored in blue and regions involved in non-transport functions are colored in grey. ^{1,7}Hamada et al., 2011; ²Wälde et al., 2012; ^{3,5}Yaseen and Blobel, 1999; ⁴Singh et al., 1999; ⁴Ritterhoff et al., 2016a; ⁵Kehlenbach et al., 1999; ⁵Vetter et al., 1999; ⁶Kassube et al., 2012; ⁷Joseph and Dasso, 2008; ⁸Murawala et al., 2009; ⁹Prunuske et al., 2006; ¹⁰Cai et al., 2001.

5.1.2.2 Interactions involved in import

Nup358, like Nup214, is an essential protein for mouse development as shown with knock-out mice (Aslanukov et al., 2006; van Deursen et al., 1996). It was demonstrated that the N-terminal region of Nup358 is needed for tethering importin- β to Nup358 in a RanGTP-dependent manner, permitting NLS-mediated cargo complex formation and cell viability (**Figure 8**, Hamada et al., 2011). Indeed, depletion of Nup358 in HeLa cells causes a decrease of importin- α/β - and transportin-mediated import rates (Hutten et al., 2008, 2009). Efficient import of certain cargoes was restored by an excess of transport receptors, suggesting that Nup358 facilitates transport by maintaining high concentration of available transport receptors in close proximity to the NPC. It contains indeed several FG-repeats that could retain available transport receptors to avoid its diffusion to the cytoplasm, and thus facilitating rapid assembly of new transport complexes. Transport receptors have also differential preferences for Nup358 regions. In the case of importin- α/β -facilitated import, the N-terminal third of Nup358 was sufficient. In contrast, transportin-dependent cargoes require a larger N-terminal fragment (Wälde et al., 2012). In the case of importin-7-mediated transport of human telomerase, a N-terminal part of Nup358 containing the zinc finger region of Nup358 is required (Frohnert et al., 2014). Furthermore, Nup358 is able to promote import of cargoes directly (Wälde et al., 2012). However, import of certain cargoes has been shown to occur independently of Nup358 in *Xenopus* oocytes (Walther et al., 2002) or in HeLa cells (i.e. import of the glucocorticoid receptor (Salina et al., 2003) and the transcription factor NFAT (Hutten and Kehlenbach, 2006)), meaning that the function of Nup358 in facilitating transport is cargo- and transport receptor-dependent.

5.1.2.3 Interactions involved in export

In addition to its import function, Nup358 might also participate in nuclear export. As described above, it forms a stable complex with SUMOylated RanGAP. This form of RanGAP is as active as unmodified RanGAP (Swaminathan et al., 2004) and thus, potentiates GTP-hydrolysis by Ran allowing export complex disassembly. Similar to Nup214, Nup358 provides two binding sites for the exportin CRM1 (**Figure 7 and 8**). The first consist of two FG-repeat patches flanking the C-terminal E3 ligase region, thus, the binding site localizes closely to Nup358-associated SUMOylated RanGAP. Moreover, a RanBD site is situated adjacent to each of both FG-repeat patches. Hence, all elements necessary for disassembly of CRM1-dependent export complexes are confined at the C-terminal region of Nup358, constituting an efficient disassembly “machine” for export complexes (Ritterhoff et al., 2016).

However, depletion of Nup358 in HeLa or MCF-7 only caused a mild reduction in CRM1-dependent export (Bernad et al., 2004; Hutten and Kehlenbach, 2006), contrary to the strong impact on CRM1-dependent export caused by Nup214 depletion (Hutten and Kehlenbach, 2006). Whether the function of Nup358 in CRM1-dependent export is redundant or not remains to be elucidated. Nup358-facilitated export might be of particular interest in large cells, in which transport receptors may become rate-limiting due to cytoplasmic diffusion. Interestingly, Nup358 remains active as a SUMO E3 ligase when associated with CRM1 (Ritterhoff et al., 2016). Recently, it has been shown that Ran can be SUMOylated in its GDP-bound form by the Nup358 E3 ligase complex (Sakin et al., 2015). It is possible that Nup358 links CRM1-dependent export with SUMOylation of some cargoes on their way to the cytoplasm, which may be required for their cytoplasmic function.

The second binding site for CRM1 is localized at the central region, which includes the ZnF domain and several FG-repeats. The ZnF motifs were shown to be major determinants for CRM1 binding, although the contribution of FG-repeats was not excluded. CRM1 binding to the ZnF was insensitive to treatment with the non-hydrolysable analogue GTP γ S or the CRM1 inhibitor LMB (see below), instead both inhibitors prevented Ran to bind to the CRM1-ZnF complex (Singh et al., 1999), which is consistent with the observation that exclusively the GDP-bound form of Ran is able to bind to the ZnF domain (Yaseen and Blobel, 1999). Localization of CRM1 at the NPC is dependent on Nup358 (Engelsma et al., 2004; Hamada et al., 2011). It has been proposed that anchoring of CRM1 at Nup358 occurs in a step after cargo release, before its recycling to the nucleus, and that this anchoring is not an essential step in CRM1-mediated export (Hutten and Kehlenbach, 2006).

Nup358 has also been linked to mRNA export. Nup358 was shown to promote NXF1-p15-dependent mRNA export in *Drosophila* S2 cells by providing a major binding site for NXF1-p15 at the cytoplasmic filaments and thus, preventing its cytoplasmic diffusion (Forler et al., 2004). Export of poly-adenylated gene transcripts was shown to be impaired in Nup358 conditional knockout mouse embryonic fibroblasts (MEF); however NXF1-p15 was not mislocalized in these cells, suggesting that Nup358 supported mRNA export by a different mechanism (Hamada et al., 2011). Furthermore, a NPC-anchored N-terminal fragment of Nup358 containing a FG-repeat cluster was the minimal fragment able to restore mRNA export in absence of endogenous Nup358 in MEF, suggesting a role for this specific FG-repeat cluster in promoting mRNA export in mouse cells. Finally, the N-terminal extremity harbours 3 tetratricopeptide repeats (TPRs), which were found to bind single stranded RNA *in vitro* (Kassube et al., 2012).

5.1.2.4 Non-transport functions of Nup358

Nup358 possesses a N-terminal leucine-rich region with overlapping sequences responsible for targeting the protein to the NPC and binding to interphase microtubules (Joseph and Dasso, 2008; Hamada et al., 2011). Additionally, this region interacts with APC (adenomatous polyposis coli) which has implications in polarized cell migration (Murawala et al., 2009). The ZnF domain also serves as a platform for coatmer complex COP-I, which is an important factor in nuclear envelope breakdown (Prunuske et al., 2006). Finally, Nup358 contains a kinesin-binding domain at the C-terminal half, named JX2 (Cai et al., 2001), that together with the flanking RanBDs 2 and 3, mediate kinesin-1 activation and e.g. exert control of mitochondrial motility (Cho et al., 2007, 2009; Patil et al., 2013) (**Figure 8**).

6. REGULATION OF NUCLEOCYTOPLASMIC TRANSPORT

Nucleocytoplasmic transport can be regulated at different levels. These levels include the modulation of transport signals in the cargo, regulation of expression and/or localization of transport receptors, or modifications of the cytoskeleton or the NPC. Modulations of nucleocytoplasmic transport are often caused by developmental or stress stimuli to e.g. altered gene expression; or during cell-cycle progression, but also by viruses in their quest to hijack the transport system to access the nucleus (Terry et al., 2007).

6.1 Modulation of localization signals

Post-transductional modifications in or near transport signals can either mask or increase their recognition by transport receptors. For example, phosphorylation masks the NLS of the nuclear factor of activated T-cells (NFAT), a transcription factor which is only exposed by Calcineurin-dependent dephosphorylation, upon increased cellular Ca^{2+} levels (Belfield et al., 2006). Nuclear localization of 55 kDa phosphoprotein encoded in early region 1B (E1B-55K) of the HAdV-C5 genome is regulated by SUMO modification. It contains both, a NES and a NLS. SUMOylation within the NES disrupts CRM1-dependent export, favouring the NLS mediated import to the nucleus (Kindsmüller et al., 2007). A localization signal can also be formed by structure rearrangements upon ligand binding. This is the case of the fatty acid transporter FABP5. Ligand binding to FABP5 is followed by a conformational change that forms a NLS recognized by importins (Armstrong et al., 2014).

6.2 Regulation of transport factors

Abundance of a specific karyopherin can affect its respective cargo transport rates (Timney et al., 2006). Hence, overexpression of individual transport receptors has been related to dysregulation of transport in different diseases. As an example, high expression of CRM1 has been observed in various cancer cells like multiple myeloma or osteosarcoma cells (Ishizawa et al., 2015). Physical retention of transport receptors in a cellular compartment also influences its activity. In response to stress, an accumulation of importin- α in the nucleus leads to downregulation of importin- α/β -mediated nuclear import (Furuta et al., 2004). In an opposite manner, the ebola virus matrix protein VP35 evades cellular immune response by binding and trapping importin- α in the cytoplasm and thus, prevents nuclear translocation of the transcription factor STAT1 (Reid et al., 2006; Xu et al., 2014).

Small chemical molecules and peptides have been extensively used as inhibitors to study the main nucleo-cytoplasmic transport pathways. The molecule Ivermectin was identified in screening assays as a specific inhibitor of the importin- α/β import pathway (Wagstaff et al., 2012). Another peptide, designed by Cansizoglu and colleagues (Cansizoglu et al., 2007), was conceived to inhibit transportin-1. The peptide combines the N-terminal half of the hnRNP A1 M9 and the PY motif of the C-terminal part of hnRNP M. The resulting M9M peptide is able to bind transportin-1 with very high affinity, preventing the interaction to other cargoes and consequently blocking transportin-dependent import. Finally, the molecule Leptomycin B (LMB) produced by *Streptomyces sp.*, was originally described as a potent antifungal antibiotic (Hamamoto et al., 1983). Years later, CRM1 was identified as the cellular target of LMB (Kudo et al., 1999). The molecule covalently binds to a single cysteine (C528) located in the cargo-binding pocket, sterically preventing interaction of CRM1 with its cargo and interfering with the Ran-binding loop function, thus efficiently inhibiting CRM1-dependent export complex formation (Petosa et al., 2004).

6.3 Cytoskeleton-facilitated nuclear transport

Although acquisition of cytoskeletal motor proteins by viruses is a widely used mechanism to reach the nucleus (reviewed in Dodding and Way, 2011), the use of MT/actine-dependent transport for facilitating nuclear import does not seem to be a predominant feature for cellular proteins (Roth et al., 2007). However, some components of major regulatory signalling pathways need to be transported relatively fast from the cytoplasm to the nucleus upon activation. This is e.g. the case for the tumour-suppressors p53 and retinoblastoma protein (Rb), or the parathyroid hormone-related protein (PTHrP), that use MT-facilitated transport to reach the nucleus. In the case of p53, it interacts with polymerized MT and requires both,

functional MT network as well as dynein, to accumulate in the nucleus after DNA damage. Furthermore, p53 contains a MT-binding domain at the N-terminal region (Giannakakou et al., 2000). The Rb protein also depends on MT integrity and dynamics for efficient nuclear accumulation under normal conditions (Roth et al., 2007). These studies have analyzed the requirement of the MT dynamics for nuclear import; however the connection between the MT network and the import pathway is not addressed. Nevertheless, the study by Roth *et al.* (Roth et al., 2007) suggests that there might be specific MT binding sequences recognized by the importin pathway, since proteins known to bind MT and to be imported to the nucleus, like the telomere repeat-binding factor (TRF1), did not show any MT-dependency for nuclear import. These specific MT association sequences (MTASs) were identified in PTHrP, which uses the MT network to reach the nucleus (Roth et al., 2011). PTHrP contains a MTAS overlapping with an NLS directly recognized by importin- β . High concentrations of importin- β can compete with MT-binding to PTHrP. Since no binding of importin- β to MT was detected, Roth *et al.* suggested that higher concentrations of importin- β at the periphery of the NPC (at the MTOC) would facilitate the switch of PTHrP from MT- to importin- β -dependent transport. This implies that MT-trafficking would accelerate NLS-cargo translocation to the nuclear periphery and consequently, facilitate the formation of importin- β -cargo import complexes at the vicinity of the nucleus. Instead in neurons, formation of import complexes has been reported to occur at axons, thus, at regions considerably far from the nucleus. Importin- α constitutively binds the motor protein dynein in axons. Upon nerve injury, local synthesis of importin- β favours the formation of a NLS-cargo-importin- α/β complex that is transported along MT to facilitate nuclear import (Hanz et al., 2003; Perlson et al., 2005). Cargo recognition by importin- α has been also reported at synaptic sites following activation of synaptic receptors, serving as an adaptor protein between synapsis signalling and synapsis-to-nucleus MT-dependent transport (reviewed in Lever et al., 2015; Panayotis et al., 2015). Hence, MT can facilitate nuclear import in two ways: by directly translocating NLS-bearing cargoes towards the nucleus, where they encounter transport receptors; or by facilitating transport of the import complex from peripheral regions to the nucleus.

6.4 Regulatory mechanisms at the NPC

Cell-type specific differences in Nup composition have been observed in a study performed by Ori *et al.* that compared protein expression of Nups in different cancer-derived cell lines such as K562 (erythroleukemia), RKO (colon), SK-MEL-5 (melanoma) and HeLa (cervix); and non-tumor derived HEK293 cells. Peripheral Nups showed particular heterogeneity on

levels of protein expression among different cell lines. In the case of the cytoplasmic Nup214, it showed an increased stoichiometry in RKO cells compared to HeLa or HEK293 cells, for example. No significant changes were observed in the case of Nup358. Changes on peripheral Nup expression could affect the number of docking sites available for transport factors (Ori et al., 2013). Composition of the NPC can also be regulated by post-transductional modifications. It is known that Nups are released from the NPC by phosphorylation during mitotic progression (Güttinger et al., 2009; Laurell et al., 2011). Changes on NPC composition can affect the permeability barrier of the pore, that is, the mechanism through which NPCs prevent passive diffusion of large molecules to mediate efficient active transport (proposed models described in section 5). The FG-Nup Nup98 has been shown to be essential for maintaining the permeability barrier (Hülsmann et al., 2012), which is consistent with the observation that removal of Nup98 from the NPC is required for further NPC disassembly during mitosis (Laurell et al., 2011). Viruses alter NPC composition to increase NPC permeability with the goal to either, facilitate nuclear import of viral genome (e.g AdV), or accumulate nuclear proteins at the cytosol required for their replication (e.g picornaviruses). In the case of AdV, it has been proposed to induce the mechanical displacement of Nups from the NPC during capsid disassembly (Strunze et al., 2011). Picornaviruses, induce changes in NPC composition by either degradation of Nups or by inducing specific phosphorylation of Nups by host factors (reviewed in Le Sage and Mouland, 2013).

7. ROLE OF THE TRANSPORT MACHINERY IN MITOSIS

During mitosis, nuclear compartmentalization is reversed and thus, the nucleo-cytoplasmic function of Nups and transport receptors is not needed. Instead during mitosis, both Nups and karyopherins play a crucial role in different steps to facilitate cell division.

7.1 Nuclear envelope breakdown (NEBD)

At the onset of mitosis, during G2/M transition, centrosomes need to be localized at opposite sides of the nucleus for ordered chromosome segregation. Correct positioning is assisted by Nups and microtubule motor proteins. Specifically, Nup358 recruits the motor adaptor Bicaudal D through its kinesin-binding domain, which in turn, mediates dynein and kinesin-1-dependent centrosome positioning (Splinter et al., 2010). Nup133 facilitates also centrosome positioning by an independent and non-redundant process during prophase (Bolhy et al., 2011). Entering in prophase, Nup358 and Nup153 participate in NEBD by recruiting the membrane remodeler COPI coatomer complex. The mechanism is not clear, but the COPI

complex is thought to induce the formation of vesicles to disperse the contents of the nuclear envelope that would consequently fuse with the ER (Liu et al., 2003; Prunuske et al., 2006). Disassembly of the NPC also takes place during NEBD. The NPC is dismantled in a step-wise process triggered by phosphorylation of Nups, leading to the release of nucleoporin subcomplexes from the NPC that are dispersed into the mitotic cytosol (Laurell and Kutay, 2011).

7.2 Mitotic spindle formation

In spite of nuclear envelope disruption during mitosis, the high concentration of RanGTP is maintained in proximity to chromatin by the chromatin bound nucleotide exchange factor RCC1 (see above), which positively regulates the assembly of mitotic factors around chromosomes (**Figure 9**; reviewed in Cavazza and Vernos, 2016). Karyopherins (importin- β (reviewed in Harel and Forbes, 2004) and transportin-1 (Bernis et al., 2014)) act as negative regulators during mitosis by sequestering spindle assembly factors (SAF) in regions away from chromatin, where RanGTP concentrations are low. The mitotic spindle then, starts to grow from the centrosomes and from the chromosomal kinetochores. The Nup Y-complex is first recruited at the kinetochores and will function as a platform for γ -tubulin ring complexes (γ -TuRCs), which promote the nucleation of MT. Once the nucleation is initiated, CRM1 is targeted to the Y-complex in a RanGTP-dependent manner and serve as bridge to recruit the Nup358/Ubc9/RanGAP*SUMO1 complex (reviewed in Chatel and Fahrenkrog, 2011 and Forbes et al., 2015). The interaction of CRM1 with Nup358 at the kinetochores is enhanced by phosphorylation of CRM1 at serine 391 (Wu et al., 2013) and can be disrupted by LMB-treatment (Gilistro et al., 2017). SUMO-1 conjugation in turn, is required for RanGAP targeting to kinetochores through Nup358 association (Joseph et al., 2002). The recruitment of this complex towards the kinetochores is important for MT attachment (Arnautov et al., 2005; Joseph et al., 2004). Once at the kinetochores, RanGAP reduces RanGTP concentration by activating the hydrolysis of GTP and balances the growth rate of MT. At kinetochores Nup358 SUMOylates topoisomerase II α allowing its translocation to the centromere where then, it triggers DNA decatenation and facilitates proper separation of sister chromatids during anaphase (Dawlaty et al., 2008). In addition to its kinetochore localization, CRM1 is also found at the centrosome (also in interphase). This localization is dependent on CRM1 binding to centrosomal RanGTP, and is important for NES-dependent pericentrin targeting, which then serves to recruit γ -TuRC for correct nucleation of MT from the centrosomes (Liu et al., 2009).

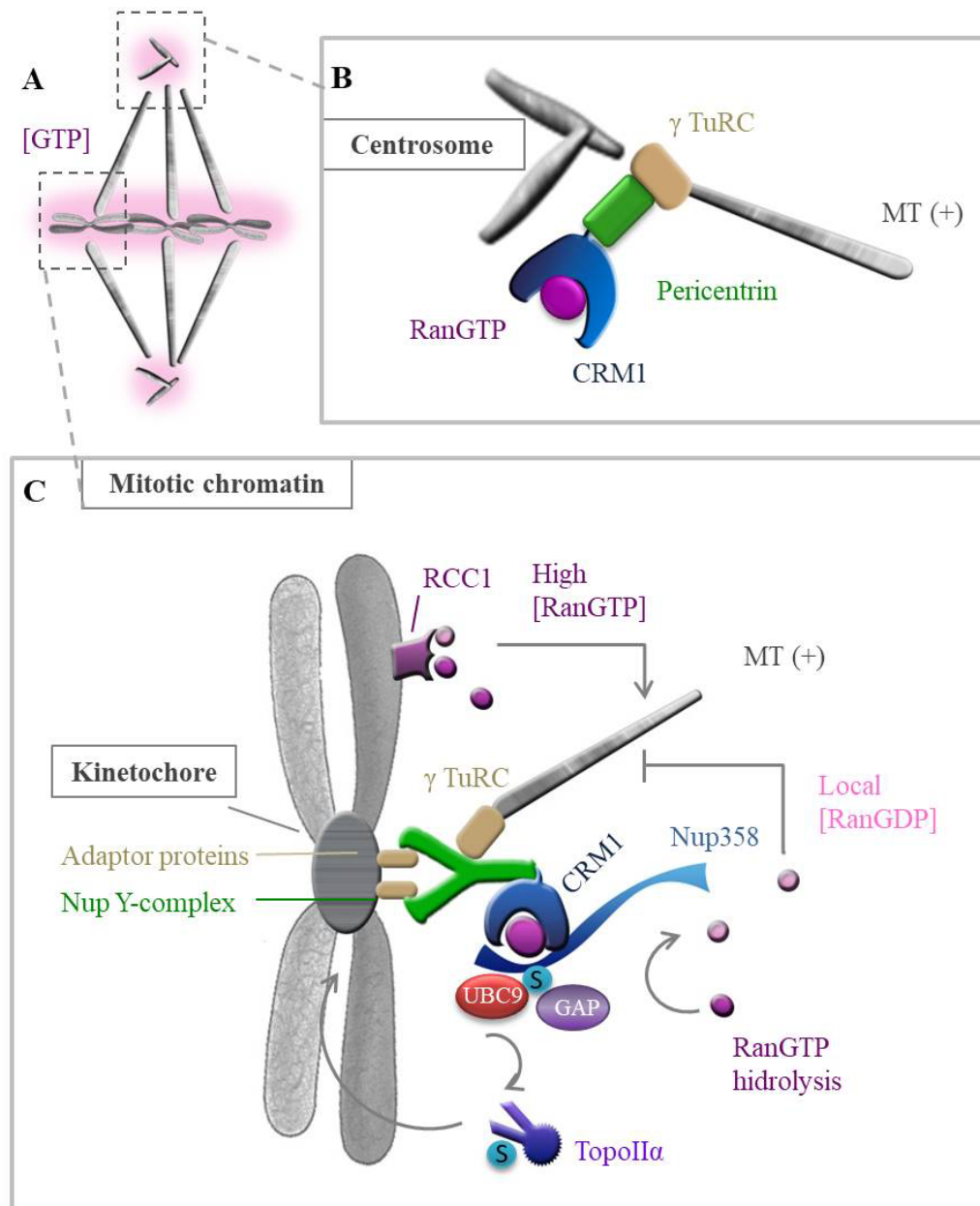


Figure 9. Role of the nucleo-cytoplasmic machinery in mitosis. Schematic representation of the role and localization of Nup358, CRM1 and the RanGTP gradient in mitosis. (A) MT nucleation in mitosis mainly takes place at centrosomal and chromatin regions where concentration of RanGTP is high. (B) CRM1 is targeted to the centrosomes in a RanGTP-dependent manner. Pericentrin is targeted to the centrosomes via NES-binding to CRM1 and mediates recruitment of the γ -TuRC, which in turn, promote MT nucleation at the centrosomes. (C) The Nup Y-complex is targeted to the kinetochores via adaptor proteins. The Y-complex is required for γ -TuRC recruitment thereby allowing MT nucleation at kinetochores. In parallel, chromatin-bound RCC1 maintain high levels of RanGTP at the kinetochores. These conditions favour RanGTP-dependent recruitment of CRM1 to the Nup Y-complex. Nup358 in complex with RanGAP and Ubc9 is also targeted to the kinetochores via CRM1 interaction. The E3 ligase function of Nup358 is important at the kinetochores to e.g. SUMOylate the topoisomerase II. SUMOylated topoII will mediate segregation of two sister chromatids. Nup358-associated SUMO-RanGAP facilitates hydrolysis of RanGTP thereby locally decreasing the concentration of RanGTP, which destabilizes MT nucleation necessary for correct MT-kinetochore attachment. Modified from Chatel and Fahrenkrog, 2011; Forbes et al., 2015.

7.3 NPC post-mitotic assembly

Right after chromatin segregation, the NE and NPCs need to reassemble to reconstitute transport across the pore. Early events of NE assembly are observed at mid-anaphase, and involve the association of certain Nups with the chromatin after dephosphorylation by cellular phosphatases. These early assembled Nups include members of the Y-complex followed by transmembrane Nups. Subsequently, the first FG-repeat containing Nups to assemble are those forming the hydrophobic meshwork within the central NPC and Nup98, constituting NPC assembly intermediates already competent for import (Dultz et al., 2008). Finally during telophase, peripheral Nups such as Nup358 or Nup153 are incorporated in newly formed NPC, but the exact order is not known (reviewed in Weberruss and Antonin, 2016).

8. Nuclear import of viral genome

Because DNA is not a physiological import substrate, viruses which deliver their genomes into the nucleus of non-dividing cells require access to and diverting of existing transport pathways. Several of these viruses use their own structural proteins to interact with the nucleo-cytoplasmic transport machinery (Fay and Panté, 2015).

An example is the enveloped DNA virus herpes simplex virus 1 (HSV). The capsid of HSV is surrounded by a proteinaceous layer known as the tegument. It reaches the nucleus by MT-dependent transport via association with dynein. Docking at the cytoplasmic filaments is RanGTP-sensitive and mediated by importin- β -dependent association to Nup358 (Ojala et al., 2000; Copeland et al., 2009), and probably also involving Nup214 (Copeland et al., 2009; Padeloup et al., 2009). The import of the viral DNA is thought to be independent of transport receptors, and to occur through a unique portal vertex in the capsid that would eject the genome by pressure, a mechanism similar to bacteriophages, although the mechanistic details and spatial organization are unknown (reviewed in Liashkovich et al., 2011).

In the case of the retrovirus human immunodeficiency virus 1 (HIV-1), its RNA genome is retro-transcribed in the cytosol by the viral reverse transcriptase. The resulting DNA molecule reaches the nucleus coated by nucleocapsid proteins forming the so called pre-integration complex (PIC). It is not clear how the capsid structure is disassembled nor how the import of the viral genome takes place. Several cellular factors have been shown to interact with the HIV-1 capsid protein and to be important during genome delivery including the mRNA processing protein CPSF6, the Nups 358 and 153, and transportin-3 (reviewed in Campbell and Hope, 2015). However, a capsid mutant unable to bind the upstream factor CPSF6 was able to evade the import restriction caused by cytoplasmic enrichment of CPSF6, using an

alternative import pathway. These results suggest some level of flexibility that HIV-1 has for engaging with different import pathways (Lee et al., 2010).

Another DNA virus, the hepatitis B virus, requires structural changes in the entering capsid to translocate to the NPC (reviewed in Gallucci and Kann, 2017). Briefly, mature capsids in the cytoplasm extrude the C-terminal part of the core capsid protein through protein kinase C (PKC) phosphorylation (Rabe et al., 2003). This conformational change exposes an otherwise hidden cNLS that is recognized by importin- α/β complex, which translocates the capsid across the NPC. The viral capsid is then retained at nuclear basket of the NPC by direct binding to Nup153 (Schmitz et al., 2010), which mediates capsid disassembly and genome release.

Influenza A virus, in contrast to other RNA viruses, replicates its RNA genome in the nucleus. Its genome is segmented in 8 single-stranded (-)RNAs, which are packaged with the nucleoprotein (NP) and the RNA-dependent RNA polymerase complex (PB2, PB1 and PA subunits) to form a viral ribonucleoprotein (vRNP) (Cros and Palese, 2003). The import of the vRNP is dependent on the classical importin- α/β pathway. Several of the components contain NLSs; however it is unclear which determines import of the vRNP. Major candidates are NP and PB2 (Cros et al., 2005; Gabriel et al., 2008).

9. ADENOVIRAL GENOME DELIVERY

AdV are able to infect non-cycling cells by delivering their genome into the nucleus across the NE through the NPC (Greber et al., 1997). The strategy adopted by AdV to deliver their genomes involves different members of the karyopherin- β family and Nups, some of them also hijacked by other viruses to release their genome into the nucleus. During the process of adenoviral genome delivery, 3 main steps can be differentiated. The first is the docking of the capsids at the NPC. In a next step, the capsid is disassembled, facilitating exposure of the AdV core at the NPC. Finally, AdV genomes are separated from the capsid and imported into the nucleus (**Figure 10**).

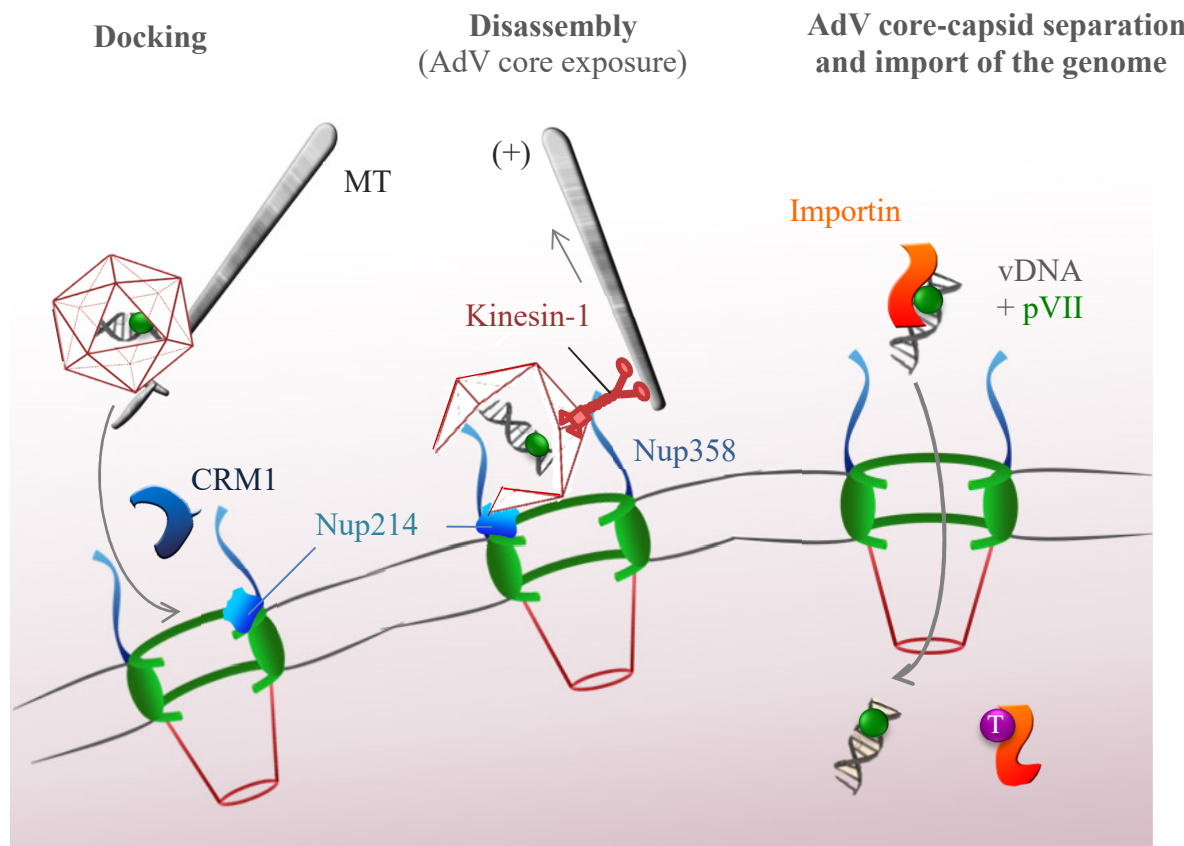


Figure 10. AdV genome delivery. Schematic representation of the different steps during AdV genome delivery. **(A)** Docking of the AdV particle at the NPC. Incoming viral particles traffic along MT towards the nucleus. In the nuclear periphery, a CRM1-dependent mechanism allows docking of the capsid at the NPC via direct binding to cytoplasmic Nup214. **(B)** Disassembly of the capsid. The proposed model for the mechanism mediating AdV capsid disassembly involves direct binding of the motor protein kinesin-1 to the capsid-exposed protein IX. Nup358 activates anterograde motility of kinesin-1 which, according to the model, would create a mechanical tension to the Nup214-anchored capsid leading to its disruption. **(C)** Import of the AdV genome. Capsid disassembly exposes the AdV core, allowing recruitment of import receptors that would finally mediate separation of the core from the capsid and import to the nucleus. In the nucleoplasm, import receptors bind to RanGTP, which leads to the release of the AdV core in the nucleus.

9.1 Docking of the capsid at the NPC

Trafficking of the AdV particle is facilitated by the MT network. Once at the periphery of the nucleus, viral particles dock at the NPC. The mechanism by which these particles translocate from the MT network to the NPC is unknown, but the exportin CRM1 has been shown to be a key factor in this process (Strunze et al., 2005; Smith et al., 2008; Wang et al., 2017). Indeed, LMB treatment prevents AdV docking at the NPC, and depending on the cell type, a dispersed distribution in the cytoplasm or retention of viral particles at the MTOC is observed (Strunze et al., 2005; Wang et al., 2017). As a consequence, capsids can no longer associate with the NPC preventing them from disassembly and thus, blocking genome import and the progression of infection. Recent analysis of AdV capsid motility showed an increased MT-dependent motility of particles at the vicinity of the NE in presence of LMB, suggesting a role

for CRM1 in the unloading of AdV capsids from MT (Wang et al., 2017). At the NPC, the cytosolic Nup214 has been identified as the docking site for HAdV-C2 (Trotman et al., 2001) and HAdV-C5 capsids (Cassany et al., 2015); and this binding is a prerequisite for further capsid disassembly and import of the viral genome. Experiments performed with purified NE suggested that capsid docking does not depend on cytosolic factors nor the RanGTP system (Trotman et al., 2001). The capsid protein hexon directly mediates the specific interaction of the capsid with Nup214 as shown in digitonin-permeabilized cells (Cassany et al., 2015). Depletion of Nup214, but not of the major component of cytosolic filaments, Nup358, resulted in a loss of hexon rim-staining reminiscent of NPC binding.

9.2 Capsid disassembly and genome release

It is believed that AdV use their capsids to protect their genome from cytosolic detection of cellular immune sensors during trafficking to the NE (Rathinam and Fitzgerald, 2011). However, once docked at the NPC, the capsid exceeds the size amenable to nuclear import. Consequently, the viral capsid needs to disassemble in order to expose the viral genome. The disassembled capsid remains associated temporarily with the adenoviral core and then, both are separated leading to the import of the genome into the nucleus; however the mechanism is still not well understood. Nup358 does not appear to be involved in capsid docking. Instead, Strunze *et al.* proposed a model in which Nup358 would play a supportive role in the mechanical disassembly of the capsid for genome release (Strunze et al., 2011). In their model, upon AdV docking at the NPC, the motor protein kinesin-1 serves as a linker between the capsid and Nup358. Kinesin-1 was proposed to bind the capsid protein pIX (located at the capsid surface) through its kinesin light-chain (Klc1), while the JX2 domain of Nup358 binds via the kinesin-1 heavy-chain Kif5C. The binding of Nup358 to Kif5C activates its (+)-end-directed MT-dependent motility (Cho et al., 2009). This active motor force would create a mechanical tension to the Nup214-anchored capsid leading to its disruption. According to the model, the Nup358 activated motor force would also release some Nups from the NPC, explaining the increment in NE permeability observed during infection (Strunze et al., 2011).

9.3 Genome import

Once the capsid undergoes disassembly at the NPC, the adenoviral genome is exposed. Nuclear import of the viral genome remains not well understood. DNA is not a physiological import substrate. Consequently viral genomes, such as the AdV genome, require to be linked into existing import pathways. One possibility is to use genome bound viral or cellular

proteins as transport adapters for the genome, providing the necessary import signals to the transport machinery. The core proteins VII, TP and Mu all remain associated with the viral genome during import (P. K. Chatterjee et al., 1986), and thus, could all potentially contribute to genome import. The viral histone-like protein VII is tightly bound to the viral genome and is the most abundant genome bound protein with about 800 copies per genome. Moreover, it contains several functional NLSs that mediate import of the protein via binding to different transport receptors (Wodrich et al., 2006; Hindley et al., 2007). However, differences in importin recognition between the precursor (preVII) and mature form of the protein VII have been observed. Although preVII is able to bind importins α , β , γ and transportin-1; the mature form binds preferentially classical and/or transportin-1 import receptors, and its import was preferentially mediated by transportin-1 in digitonine-permeabilized cells (Hindley et al., 2007).

9.4 Controversy

In the literature there is a clear consensus for the role of Nup214 as the docking site for AdV capsids (Cassany et al., 2015; Trotman et al., 2001). However, the different studies identified mutually exclusive regions of Nup214 as the interaction site with the capsid. Trotman and colleagues observed that the FG-repeat containing C-terminal fragment of Nup214 was the substrate of a modified Ad2, designed to transfer a biotin moiety onto crosslinked proteins (Trotman et al., 2001). In contrast, Cassany *et al.* showed a direct binding of the purified hexon with a recombinant soluble N-terminal fragment of Nup214, which also contains two FG-repeats (Cassany et al., 2015). There is a less clear picture for the capsid disassembly process taking place at the NPC. The current model for AdV capsid disassembly at the NPC involves the nucleoporin Nup358 at the NPC (Strunze et al., 2011). However, Cassany *et al.* showed that Nup358 is dispensable for AdV infection (Cassany et al., 2015). In the model proposed by Strunze *et al.* there seem to be a strong dependency of the MT network for capsid disruption at the NPC (Strunze et al., 2011). However, it was recently reported that incoming viral particles engage with microtubules until they approach the NE region, where they shift to microtubule-independent motions in a CRM1-sensitive manner (Wang et al., 2017), implying the importance of capsid release from MT to proceed towards a successful docking at the NPC. Other factors have been proposed to be involved in capsid disassembly like the histone-1. However the proposed docking site on the capsid was identified to be a hypervariable loop in hexon. This binding site would be specific for HAdV-C2 but not for other genotypes such as HAdV-B3 (Trotman et al., 2001). Import of the adenoviral genome is mediated by different

transport receptors (Hindley et al., 2007). Although pVII has been thought to be the main adaptor for vDNA import, a recent study showing that pVII positively regulates viral gene transcription concluded that this effect was not due to enhanced import efficiency by pVII (Komatsu et al., 2011). Indeed, transfected AdV cores or reconstituted TP-DNA complexes were imported to the nucleus with similar efficiencies, suggesting that pVII is not an essential factor for facilitated vDNA import. However, transfected complexes could be imported by a different mechanism than released AdV cores from incoming capsids following NPC docking. Indeed, transportin-1 and importin-7 have been shown to mediate import of exogenous DNA through the NPC in reconstituted *Xenopus* nuclei, or in digitonin-permeabilized HeLa cells, respectively (Lachish-Zalait et al., 2009; Dhanoya et al., 2013).

10. AIM OF THE WORK

Recent progress in understanding the mechanism through which AdV deliver their genome into the nucleus has been made in the past years. However, this process is not completely understood. For example, there is not a clear consensus in the literature about the role of Nup358 in AdV genome delivery. Likewise, it is not known how different transport receptors (e.g. exportin CRM1 or import receptors) interact with the viral particle and mediate different steps during AdV genome delivery: docking of the capsid at the NPC, disassembly of the capsid, or genome separation from the capsid and subsequent import to the nucleus. The aim of this work has been to characterize the functional role of Nup358, as well as different nuclear transport receptors during AdV genome delivery. To study the potential transport-related and non-transport related functions of the nuclear transport machinery in AdV genome delivery, we have monitored this process in both, interphase and mitotic cells.

MATERIALS AND METHODS

1. MOLECULAR BIOLOGY METHODS

1.1. Bacterial culture

Plasmids were amplified in *Escherichia coli* DH5 α bacteria strain. This strain is suitable for plasmid amplification since it contains multiple mutations that enable high-efficiency transformations and low homologous recombination activity. Bacteria were grown in liquid LB medium (Luria-Bertani medium: 10 g/L pepton, 5 g/L yeast extract, 5 g/L sodium chloride) or on LB-plates (LB supplemented with 15 g/L agar). Selective antibiotics were added to LB media at 100 $\mu\text{g}/\text{mL}$ in the case of ampicillin, and 50 $\mu\text{g}/\text{mL}$ for kanamycin. Bacteria are grown at 37 $^{\circ}\text{C}$.

1.2. Bacterial transformation

Chemically competent bacteria (~ 100 μL) are first incubated with 1-200 ng of plasmid DNA on ice for 30 min. Cells are subjected to a heat-shock at 42 $^{\circ}\text{C}$ for exactly 45 seconds. Bacteria are then placed on ice for 2 min and then resuspended in pre-warmed (37 $^{\circ}\text{C}$) LB without antibiotics. The bacteria in suspension are incubated for 45 min at 37 $^{\circ}\text{C}$ by shaking at 180 rpm. Transformed bacteria are plated onto LB plates with the appropriate antibiotics and allow growing at 37 $^{\circ}\text{C}$ overnight.

1.3. Polymerase chain reaction (PCR)

Amplification of specific DNA sequences was performed by PCR. Sequences were amplified with the aim of inserting them into plasmids by using the Gateway $^{\circledR}$ Technology (Invitrogen). For this, primers of the PCR were designed to hybridize with the desired sequence (~ 20 nt) and incorporated AttB1 or AttB2 sequences (Bacterial Attachment site). Homologous sequences are present in the pDONR vector thereby allowing insertion of the AttB-flanked PCR by homologous recombination. The list of primers used is summarized in **Table 3**. The reactions were set up as detailed in **Table 4** using Phusion DNA polymerase (Thermo scientific). The thermo-cycler was programmed according to **Table 5**. The annealing time was optimized for each fragment. The resulting PCR products were purified using the kit NucleoSpin Gel and PCR Clean-up (Macherey-Nagel), according to manufacturer's protocol.

Table 3. List of primers¹

AttB site	Hybridizing sequences	Sequence of the primer
AttB1	(for) Nup358 aa 806-814	GGGGACAAGTTTGTACAAAAAAGCAGGCT ccatg GATCAGAATTCTTTACTGAAAATG
AttB1	(for) Nup358 aa 1312-1318	GGGGACAAGTTTGTACAAAAAAGCAGGCT ccatg GTAGCCATGGCGTCAAATC
AttB1	(for) Nup358 aa 1350-1357	GGGGACAAGTTTGTACAAAAAAGCAGGCT ccatg AAGAAAGAAGGGTCTTGGTGGC
AttB1	(for) Nup358 aa 2307-2314	GGGGACCACTTTGTACAAGAAAGCTGGGT ccta GAGTTTCATTAAATTCTGCTGAC
AttB2	(rev) Nup358 aa 2550-2557	GGGGACCACTTTGTACAAGAAAGCTGGGT ccta ATTGTTACTTTTCAAAGGTGC
AttB2	(rev) Nup358 aa 3039-3047	GGGGACCACTTTGTACAAGAAAGCTGGGT ccta GAGTTTCATTAAATTCTGCTGAC
AttB2	(rev) Nup358 aa 2703-2710	GGGGACCACTTTGTACAAGAAAGCTGGGT ccta ACATTCTTTCTCATTATCTGC
AttB2	(rev) C-ter HA-tag of pEF- HA w/ XbaI site	GGGGACCACTTTGTACAAGAAAGCTGGGT ccta CTGGTGGGGTGAATTTCTAG

¹Sequences highlighted in red correspond to the AttB sites. Small letters in the sequences correspond to ATG or stop codons and nucleotides required for a correct reading frame. For: forward; Rev: reversed.

Table 4. Reaction mix for PCR

Reagent	Volume (μL)
5 x HF buffer	10
20 mM dNTP	0.5
2 μM Primer 5'	5
2 μM Primer 3'	5
Template DNA (2-10 ng/μL)	5
Phusion Polymerase	0.5
H ₂ O milliq.	to 50

Table 5. PCR programme¹

Cycle Step	Temperature (°C)	Time (s)
1 Denaturation	98	30
2 Denaturation	98	10
3 Annealing	50-70	15
4 Extension	72	60
5 Extension	72	10 min
6 Cooling	18	∞

¹Steps from 2-4 were repeated 34 times

1.4. Cloning

The Gateway® Technology (Invitrogen) allows inserting a sequence into mammalian or bacterial expression vectors. This technology is based on homologous recombination. First, purified PCR products are cloned into a donor plasmid (pDONR) flanked by recombination sites. This is called the BP reaction. For this, 50-100 ng of purified PCR product, 150 ng of the pDONR plasmid and 1 µL of the BP Clonase II Enzyme mix (Invitrogen) are mixed in a final volume of 5 µL, and incubated for 1 h at RT. Then, 2 µL of the reaction are used to transform DH5α bacteria. Growing colonies should have incorporated the pDONR plasmid with the desired insert, since the pDONR plasmid encodes a toxic gene that result lethal for bacteria. Plasmids are purified after amplification of 2-3 colonies using kanamycin selection media. Purified plasmids are subjected to enzyme restriction digestion and/or sequencing to verify the insert. A second reaction called LR is performed to obtain the expression vector containing the fragment of interest. The principle and the protocol are the same than for the BP reaction. For LR recombination, 1 µL of LR Clonase II Enzyme mix (Invitrogen) is mixed with 50-100 ng pENTRY containing the gene of interest and 150 ng pDEST expression plasmid. Similar than the previous step, 2 µL of the result of the homologous recombination reaction is used to transform DH5α bacteria. Colonies are grown in ampicillin selection media. Plasmids are purified using the kit Nucleo Spin Plasmid (Macherey Nagel) and digested with restriction enzymes and/or sequenced to verify the insert.

1.5. List of plasmids

Table 6. Available plasmids for mammalian cell expression

Vector	Encoding polypeptide	Source	Resistance
pcDNA 3.1	(+)	Invitrogen	Amp
pcDNA3.1(+)	CRM1- C528S D824K K680Q A731Q L679R - HA	R. Kehlenbach ¹	Amp
pcDNA3.1(+)	CRM1- C528S D824K W880A -HA	R. Kehlenbach ¹	Amp
pcDNA3.1(+)	CRM1- C528S P778A V779A -HA	R. Kehlenbach ¹	Amp
pcDNA3.1(+)	CRM1- C528S P967A V968A -HA	R. Kehlenbach ¹	Amp
pcDNA3.1(+)	CRM1- C528S W142A P143A -HA	R. Kehlenbach ¹	Amp
pcDNA3.1(+)	CRM1- C528S W880A F882A -HA	R. Kehlenbach ¹	Amp
pCAG-ME-IP	H2B-tdiRFP	Addgene	Amp
pCS2	myc-MBP-M9M	R. Kehlenbach ¹	Amp

pEGFP-C1	GFP-M9core	R. Kehlenbach ¹	Kan
pEGFP-C1	GFP-cNLS	R. Kehlenbach ¹	Kan
pL30-cGFP	GFP-Nup358 aa 2307-2710	F. Lagadec ^{1,2}	Amp
pL30-cGFP	GFP-Nup358 aa 2307-3047	F. Lagadec ^{1,2}	Amp
pEF-HA	HA-Importin-7 siRNA resistant	R. Kehlenbach ¹	Amp
pEF-HA	HA-Importin-9	R. Kehlenbach ¹	Amp
pEF-HA	HA-Importin- β	R. Kehlenbach ¹	Amp
pEF-HA	HA-Nup358 aa 1-1170	R. Kehlenbach ¹	Amp
pEF-HA	HA-Nup358 aa 1-1306	R. Kehlenbach ¹	Amp
pEF-HA	HA-Nup358 aa 1-1810	R. Kehlenbach ¹	Amp
pEF-HA	HA-Nup358 aa 1-2148	R. Kehlenbach ¹	Amp
pEF-HA	HA-Nup358 aa 1-2448	R. Kehlenbach ¹	Amp
pEF-HA	HA-Nup358 aa 1-3047	R. Kehlenbach ¹	Amp
pEF-HA	HA-Nup358 aa 1312-2557	R. Kehlenbach ¹	Amp
pEF-HA	HA-Nup358 aa 1350-1810	R. Kehlenbach ¹	Amp
pEF-HA	HA-Nup358 aa 1350-2148	R. Kehlenbach ¹	Amp
pEF-HA	HA-Nup358 aa 2011-2445	R. Kehlenbach ¹	Amp
pEF-HA	HA-Nup358 aa 2307-2710	R. Kehlenbach ¹	Amp
pEF-HA	HA-Nup358 aa 2307-3047	R. Kehlenbach ¹	Amp
pEF-HA	HA-Nup358 aa 806-1000	R. Kehlenbach ¹	Amp
pEF-HA	HA-Nup358 aa 806-1133	R. Kehlenbach ¹	Amp
pEF-HA	HA-Nup358 aa 806-1170	R. Kehlenbach ¹	Amp
pEF-HA	HA-Nup358 aa 806-1306	R. Kehlenbach ¹	Amp
pEF-HA	HA-Nup358 FL	R. Kehlenbach ¹	Amp
pmRFP-C1	RFP-Nup214 aa 1975-2090 cNLS	R. Kehlenbach ¹	Kan
pEGFP - H1	Non-targeting RNAi	(Cassany et al., 2015)	Amp
pSUPER	shRNA Nup358 F1R1	(Cassany et al., 2015)	Amp
pEF-HA	HA-Transportin-1	R. Kehlenbach ¹	Amp

¹Univ. Goettingen, Germany. ²Univ. Bordeaux, France

Table 7. Generated plasmids¹

Vector	Encoding polypeptide	Resistance
pDEST15	GST-Nup358 aa 1312-2557	Amp
pDONR221	Nup 358 aa 1312-2557	Kan
pDEST15	GST-Nup358 aa 1350-1810	Amp
pDONR221	Nup 358 aa 1350-1810	Kan
pDEST15	GST-Nup358 aa 1350-2148	Amp
pDONR221	Nup 358 aa 1350-2148	Kan
pDEST15	GST-Nup358 aa 2307-2710	Amp
pDONR221	Nup 358 aa 2307-2710	Kan
pDEST15	GST-Nup358 aa 2307-3047	Amp
pDONR221	Nup 358 aa 2307-3047	Kan
pDEST15	GST-Nup358 aa 806-1000	Amp
pDONR221	Nup 358 aa 806-1000	Kan
pDEST15	GST-Nup358 aa 806-1306	Amp
pDONR221	Nup 358 aa 806-1306	Kan

¹Plasmids included on the list above were generated either for Gateway cloning (pDONR) or for bacterial expression of recombinant proteins (pDEST15).

2. CELL BIOLOGY METHODS

2.1. Cell lines

Table 8. Mammalian cell lines

Cell line	Reference	Description
HEK-293 $\alpha\beta 5$	ATCC CRL-1573	HAdV-C5-transformed, human embryonic kidney cell line stably expressing the AdV E1A and E1B oncoproteins. Provided by G Nemerow, Scrips research institute, La Jolla, USA.
U2OS	ATCC HTB-96	Human osteosarcoma cell line. Provided by M. Piechaczyk, IGMM, Montpellier, France.
U2OS- TAF1-GFP	(Komatsu et al., 2015)	U2OS cells stably expressing the protein TAF-1-GFP. Established by T. Komatsu in our lab.

2.2. Cell maintenance

Cells were maintained in a humidified incubator with 5 % (v/v) CO₂ at 37 °C, in Dulbecco's modified Eagle Medium (DMEM) (GIBCO) supplemented with 10 % foetal bovine serum (FBS; from GIBCO), 100 U/mL of penicillin and 100 µg/mL of streptomycin (GIBCO). In the case of HEK293- $\alpha\beta 5$ and U2OS-TAF-1-GFP cells, media was supplemented with geneticin (G418) in a final concentration of 0.5 mg/mL.

Every 3-4 days, cells were splitted at a 1/10 ratio just before reaching confluence. For this, cells were washed with sterile PBS 1X buffer (PBS pH 7.4, GIBCO), detached from the culture T75 flasks using 0.05% trypsin/EDTA (GIBCO), and diluted with fresh medium.

2.3. Transient transfection of DNA

Cells are seeded on day 1 in order to be ~ 60-80 % confluent the next day. The next day, cells are transfected using Lipofectamine 2000 reagent (Invitrogen). Volumes for reaction are summarized in **Table 9**. For this, a reaction mix is prepared diluting DNA in OPTIMEM reduced serum media without antibiotics (Opti-MEM, GIBCO). In parallel, Lipofectamine 2000 is diluted in equivalent volume of OPTIMEM medium. Next, diluted DNA is added to Lipofectamine 2000 reagent diluted solution (1:1 ratio) and the mixture is incubated for 20 min at room temperature. In the meantime, cells are washed twice with PBS 1X. To increase transfection efficiency of large constructs (e.g. constructs encoding NPC-anchored fragments of Nup358) cells were treated with 5 % DMSO DMEM (~ 300 µL per well of a 12 well-plate) for 2 min and then gently washed twice with PBS 1X. OPTIMEM medium is then added to cells. After 20 min of incubation, the mixture containing DNA-lipid complexes is added to

cells dropwise and cells are placed in the incubator at 37 °C for 3 h. Then, the transfection mixture is removed and replaced with fresh complete DMEM media. Cells are incubated for 1-3 days at 37 °C and either fixed or further treated.

Table 9. Scheme for DNA transfection

Reagent	Volume		
	10 cm dish	6 well-plate	12 well-plate
N° Cells seeded on day 1	2×10^6	$2-3 \times 10^5$	$8 \times 10^4-1.5 \times 10^5$
Lipofectamine 2000	8 μ L	3 μ L	1,5 μ L
DNA (1 μ g/ μ L)	5-12 μ L	2 μ L	0.5-1.5 μ L
Optimem added to DNA	1 mL	200 μ L	100 μ L
Optimem added to Lipofectamine	1 mL	200 μ L	100 μ L
Optimem added on cells	4 mL	800 μ L	400 μ L

2.4. RNA interference-mediated depletion

RNA interference (RNAi) is a specific and efficient method of silencing gene expression on the post-transcriptional level. Methods of RNAi involve small interfering RNA (siRNA) and short hairpin RNA (shRNA). SiRNA directed against the mRNA of Nup358 or the import receptor transportin-1 has been extensively used for study the role of these proteins in nucleocytoplasmic transport in HeLa cells (Hutten and Kehlenbach, 2006; Hutten et al., 2008, 2009; Wälde et al., 2012). The shRNA method has also been used for study the role of the cytoplasmic Nups, Nup214 and Nup358 in AdV genome delivery in HeLa cells (Cassany et al., 2015). In this work, both methods were used to specifically deplete Nup358, and the siRNA method to deplete transportin-1.

2.4.1. siRNA

Validated siRNA oligonucleotides directed against the mRNA of Nup358 or non-specific (used as a control) were obtained from Eurofins Genomics. Specific sequences are indicated in **Table 10**. In the case of transportin-1, oligonucleotides were kindly provided by R. Kehlenbach, University of Goettingen, Germany (Hutten et al., 2009). For efficient depletion of both, Nup358 and transportin-1, experiments were done 72 h after siRNA transfection. U2OS were seeded in a 6 (2×10^5 cells/well) or 12-well plate (10^5 cells/well). The next day, cells were transfected with 100 mM siRNA using Lipofectamine siRNAmix (Invitrogen) following the manufacturer's protocol. Volumes of different reagents used are summarized in

Table 11. On day 3, cells were splitted onto coverslips of 15 mm diameter in a 12-well plate (in order to seed 8×10^4 cells/well). In the case of depletion/restitution experiments of Nup358, a DNA-siRNA co-transfection of the Nup358 constructs with specific or non-targeting siRNA was performed using the protocol for transient transfection on day 4. A pcDNA3.1+ empty vector (Invitrogen) was used as DNA control. Cells were infected or directly fixed on day 5. In the case of WB analysis, cells were collected on day 5.

Table 10. Sequences of oligonucleotides used for RNAi

Targeted protein	Method	Sequence (5' → 3')
Control	SiRNA	AGGUAGUGUAAUCGCCUUG
Control	ShRNA	Ref. in (Cassany et al., 2015)
Nup358	SiRNA	CACAGACAAAGCCGUUGAA
Nup358	shRNA	Ref. in (Cassany et al., 2015)
Transportin-1	siRNA	Ref. in (Hutten et al., 2009)

Table 11. Scheme for siRNA transfection

Reagent	Volume	
	6 well-plate	12 well-plate
Lipofectamine siRNAmix	3 μ L	1.5 μ L
SiRNA (20 μ M)	6 μ L	3 μ L
Optimem added to siRNA	200 μ L	100 μ L
Optimem added to Lipofectamine	200 μ L	100 μ L
Optimem added on cells	800 μ L	400 μ L

2.4.2. shRNA

Gene silencing of Nup358 by shRNA was done as described previously (Cassany et al., 2015). Cells were transfected with the pSUPER vector (Oligoengine) expressing shRNA directed against Nup358. An efficient knock-down of Nup358 was obtained three days post-transfection. A peGFP-H1 vector containing two expression cassettes, one for enhanced GFP (eGFP) and one for non-targeting shRNA, was used as a control. U2OS were seeded in a 12-well plate (10^5 cells/well). The next day, cells were co-transfected with 1 μ g of shRNA coding plasmids and 1 μ g of plasmids expressing different transport receptors by using the protocol for transient transfection. On day 3, cells were splitted onto coverslips of 15 mm diameter (in order to seed 8×10^4 cells/well). Cells were finally infected and fixed on day 5.

2.5. Coating of coverslips with Poly-L-Lysine

Cells were grown on coverslips treated with the positively charged Poly-L-Lysine to improve adherence of mitotic cells. For this, 15 mm diameter coverslips were washed with 2-propanol for 10 min and let dry under the hood. Coverslips were then covered with 0.01 % (v/v) Poly-L-Lysine (Sigma) and incubated for at least 10 min at room temperature. After washing with sterile water, and EtOH, the coverslips are completely dried and used for the experiment.

2.6. Cell-cycle synchronization

U2OS were seeded on coverslips pre-treated with Poly-L-Lysine in a 12-well plate (2×10^5 cells/well). The next day, 4 μ L of colcemid solution (10 μ g/mL; D1925 Sigma) per 1 mL of DMEM were added to cells and incubated during 14-16h. On day 3 about 60-70 % of cells were efficiently synchronized in mitosis.

In the case of experiments in which a transfection of CRM1 or Nup-constructs was performed, 1.5×10^5 U2OS cells/well were seeded onto Poly-L-Lysine coated coverslips in a 12-well plate. On day 2, cells were transfected with 1.5 μ g of DNA following the protocol for transient transfection. On day 3, 4 μ L of colcemid solution per 1 mL of DMEM were added to cells and incubated during 14-16h. On day 4, synchronized cells were infected and fixed for IF staining.

For live-cell-imaging analysis of mitotic cells, U2OS-TAF-1-GFP cells were seeded in a 6-well plate (3×10^5 cells/well). The next day cells were transfected with 2 μ g expression vector for histone H2B-tdiRFP to visualize the chromatin, following the protocol for transient transfection. On day 3 cells were splitted to seed $5-7 \times 10^5$ cells in ibidi μ -slides I (Ibidi). This was performed 3-4 h before colcemid addition to allow cell adhesion to the surface. Four μ L of colcemid solution per 1 mL of DMEM (10 μ g/mL) were added to cells and incubated during 14-16h. On day 4, cells synchronized in mitosis were infected and imaged.

2.7. Leptomycin B (LMB) treatment

Leptomycin B is an anti-fungal antibiotic from *Streptomyces* sp. that inhibits CRM1-dependent nuclear export. LMB binds to a conserved cysteine residue in CRM1, which blocks the binding of CRM1 to proteins containing the nuclear export signal (Kudo et al., 1999).

Cells were treated with 20 nM final concentration of LMB (L2913; Sigma) (0.5 μ L of the stock solution per 1 mL of DMEM medium) for 30 min and then either fixed or infected. Infections were also done in presence of LMB at 20 nM final concentration.

3. VIRAL PRODUCTION

3.1. Viral amplification

AdV vectors used in this study lack the E1A region required for initiation of viral transcription and instead, express the GFP protein. Consequently, these vectors are not able to replicate and need to be produced in HEK293- $\alpha\beta5$ cells, which stably express the AdV E1A and E1B proteins. HEK293- $\alpha\beta5$ cells are grown in a 15-cm-diameter Petri dish until they reach 80-90% confluency. Cells are then infected with about 10^9 physical particles of AdV vectors and incubated at 37 °C. In case of production of the ts1 mutant, infected cells are incubated at the non-permissive temperature 38.5 °C. At this temperature, the *ts1* mutation located in the viral protease results in the production of hyper stable particles due to unprocessed capsid proteins. Cells are collected when they begin to visibly detach from the plate and show round shape, which is typically 48 h after infection. Cells are pelleted by 3500 g centrifugation during 5 min at room temperature and resuspended in 20 mL fresh DMEM medium. Cells are subjected to three cycles of freeze-thaw in order to lyse cells and release viruses into the supernatant. Cellular debris are removed by centrifugation at 3500 rpm during 10 min at room temperature. The supernatant containing liberated AdV is used to infect 80-90 % confluent HEK293- $\alpha\beta5$ cells growing in twenty 15-cm-diameter Petri dishes. In about 48 h, rounded partially detached cells are collected and pelleted by centrifugation at 3500 rpm during 5 min at room temperature. Pelleted cells from twenty 15-cm-diameter Petri dishes are mixed together and resuspended in 40 mL. Resuspended cells are subjected to three cycles of freeze-thaw in order to release viruses into the medium and cellular debris are removed by centrifugation at 3500 rpm during 10 min at room temperature. The resulting supernatant can be stored at - 80 °C for further purification.

3.2. Virus purification

Viruses are purified from the supernatant using a cesium chloride (CsCl for molecular biology, ≥ 98 %; Sigma) density gradient combined with ultracentrifugation. Two successive gradients are used to purify viruses. The first discontinuous gradient is formed by mixing two different CsCl density solutions: 2 mL of 1.4 g/mL and 2 mL of 1.25 g/mL in 50 mM Tris pH 8 and 150 mM NaCl. The second continuous gradient is formed using 10 mL of 1.34 g/mL CsCl density solution. First, 8 mL of supernatant containing AdV in suspension are added to each discontinuous gradient in a polypropylene tube (Beckman) (normally three are done in parallel) and centrifuged for 2 h at 35000 rpm at 18 °C. After centrifugation, viruses are a well-defined whitish band. A thicker band is often found above which corresponds to empty

capsids. Next, viruses concentrated in the lower band are collected by using a 5 ml syringe with 21 G needle. The viruses collected from three independent discontinuous gradients are then transferred to a single new tube with the continuous gradient. Viruses are once again centrifuged during 18 h at 35000 at 18 °C. The lower discrete band corresponding to infectious viruses is collected using a 5 ml syringe with a 21 G needle and transferred to a dialyse cassette (Slide-A-Lyzer Dialysis Cassettes, 10K MWCO; Thermo Scientific) previously equilibrated in PBS 1X. The dialysis is performed immersing the cassette first in 500 mL of PBS 1X in slow agitation during 2 h. The PBS 1X solution is changed and the cassette immersed for another 3 h. The dialysis is complete after overnight immersion of the cassette in 500 mL PBS 1X 10 % glycerol buffer. Purified viruses are finally collected by puncturing the cassette with a 5 ml syringe with 21 G needle, aliquoted and stored at - 80 °C.

3.3. Virus labelling

Purified viruses can be labelled using the “Micro-scale protein labeling kits” from Invitrogen with Alexa488, Alexa594 or Alexa647 (A30006, A30008, A30009). In a reaction tube, 100 µL of purified AdV are mixed with 12 µL of 1M Na-bicarbonate buffer pH 8.3 and 2 µL of the desired dye previously resuspended in 10 µL of DMSO. The reaction is gently mixed and incubated in rotation during about 15 min. The excess of dye is removed from the labelled viruses by filtering the solution through 800 µL of pre-equilibrated desalting Bio-Rad MicroBio-Spin™ 6 columns in PBS 1X 10 % glycerol following manufacturer instructions. The flow through is collected, aliquoted and stored at - 80 °C.

3.4. Virus quantification

Purified viruses were quantified by using two different methods. The first, quantifies number of physical particles based on the estimated copy numbers of viral genomes. For this, purified viruses are diluted at 1/10 or 1/100 (depending on the estimated concentration of the preparation) in lysis buffer (10 mM Tris pH 7.4, 0.1 % SDS and 1 mM EDTA). Diluted viruses are incubated for 10 min at 56 °C to disrupt the capsids and release the viral DNA. The OD is measured at 260 nm. Copy numbers are calculated according to the OD₂₆₀ method (1 OD₂₆₀ = 1.16×10¹² particles/ml (Mittereder et al., 1996)).

The second method quantifies number of infectious particles by plaque assay. For this, the day before infection 10⁶ HEK293-αvβ5 cells are seeded per well in a 6-well plate. The day after plating, cells should be ~ 90 % confluent. The purified sample of viruses is diluted in order to infect with 1, 0.1, 0.01 estimated physical particles per cell and incubated overnight at 37 °C. The next day, the medium containing viruses is removed and substituted by DMEM

(pre-warmed at 37 °C) with 1 % agarose (pre-warmed at 70 °C). Once agarose overlays are solidified, infected cells are incubated at 37 °C. Five to seven days after agarose overlay addition, fluorescent plaques (in the case of GFP vectors) are formed. Each plaque is representative of one infective virus particle. The viral titer of the stock sample is then determined by taking the average number of fluorescent plaques for a dilution and the inverse of the total dilution factor.

4. VIRAL INFECTION

In this work, three different AdV replication-deficient E1-deleted GFP-expressing vectors based on genotype HAdV-C5, were used: Ad5-wt-GFP (Martinez et al., 2015), Ad5-ts1-GFP and Ad5- Δ pIX-GFP (kindly provided by Christopher M. Wiethoff, Stritch School of Medicine, Illinois, USA).

4.1. Time course infection in interphase cells

Cells grown on 15 mm coverslips in a 12 well-plate were seeded in order to have between $1.5\text{-}2 \times 10^5$ cells the day of infection. For this, U2OS were considered to increase in number by 1.5 fold each day, during the first two days after plating. It is important to infect a sub-confluent population of cells to allow homogeneous binding of AdV's to cell surfaces. Depending on the purpose of the experiment, number of physical particles (pp) or infectious particles (pfu/cell = MOI) per cell was considered. For analysis of kinetic of AdV genome delivery, a time course infection was performed considering MOI 30 when using the Ad5-wt-GFP. When comparing different viruses (Ad5-wt-GFP with Ad5- Δ pIX-GFP), 5000 pp/cell was considered for infections. Time course infection for analysis of endosomal escape of AdV particles was performed considering 5000 pp/cell. In all cases, the number of particles internalized per cell is in the range of 50-150.

The day of infection, coverslips are collected and placed on a Parafilm-wrapped culture plate lid. Viruses are diluted in 100 μ L/condition of pre-warmed DMEM (37 °C) and added to cells. A second lid is placed over the coverslips to avoid evaporation of the media. Parafilm allows adhesion of coverslips to the lid and prevents diffusion of the DMEM solution containing viruses. The small volume allows faster binding of AdV to the cell surface. Cells are placed in the incubator for 30 min to allow AdV particle binding and internalization. After 30 min, a fraction of viruses have already entered in the cytosol. Thus, volume on coverslips is removed to avoid successive waves of internalization. This is considered as the time point zero of the

time course. Coverslips are placed again in a 12-well plate filled with 1 mL/well fresh 37 °C pre-warmed DMEM. Then, cells are incubated at 37 °C and fixed at different time points.

4.2. Infection of mitotic cells

The protocol of infection for mitotic cells is similar than interphase cells but with some modifications. Cells grown on Poly-L-Lysine-coated 15 mm-coverslips were seeded in order to have $\sim 3 \times 10^5$ synchronized cells the day of infection. Cells were infected considering 5000 pp/cell of Ad5-GFP vectors. Coverslips are collected and placed on a Parafilm-wrapped culture plate lid, on ice. Viruses are diluted in 100 μ L/condition of cold DMEM (4 °C) and added to cells. The lid is placed on ice at 4 °C during 30 min to allow binding but not internalization of the viral particles. After 30 min, the medium containing viruses is removed and coverslips are placed again in a 12-well plate filled with fresh pre-warmed DMEM (37 °C) to allow internalization. This is considered as the time point zero of the infection. Then, cells are incubated at 37 °C and fixed 1 hpi.

For analysis of AdV genome delivery in synchronized living mitotic cells, medium was replaced by CO₂-independent medium (Life Technologies) supplemented with 10 % FCS and 4 mM Glutamax (Life Technologies). Synchronized mitotic cells growing in an Ibidi slide were infected with viruses diluted in 500 μ L CO₂-independent medium. Infections were done asynchronously at 37 °C using ~ 3000 pp/cell without inoculum removal.

5. IMMUNOFLUORESCENCE (IF) ANALYSIS

5.1. IF staining

U2OS cells grown on 15 mm coverslips were washed with PBS 1X. Cells were fixed using 4 % (v/v) paraformaldehyde in PBS 1X for 15 min and then washed with PBS 1X. If the IF staining was not performed the same day of fixation, cells were stored at 4 °C in PBS 1X.

Immediately prior to start the IF staining, IF-buffer is prepared containing 10 % FCS, and 0.5% Saponin in PBS 1X. The FCS saturates the sample with non-specific proteins to reduce unspecific recognition of antibodies. Saponin gently permeabilizes the cells allowing access of the antibodies to intracellular proteins. Fixed cells were incubated for ~ 15 min at room temperature with 100 μ L/coverslip of IF-buffer. In the meantime, primary antibodies are diluted in 100 μ L/coverslip of IF-buffer and centrifuged at full-speed for 2 min to remove aggregates. The list of antibodies used and their dilutions for IF is summarized in **Table 12**. After 15 min of blocking step, 100 μ L of the antibody solution is added per coverslip and

incubated at 37 °C for 1 h in a humid chamber. After 1 h, coverslips are washed by short rinsing in PBS 1X to remove the antibody solution and then placed in a 12-well plate filled with ~2-3 mL/well of PBS 1X. The plate is gently moved on a shaker for efficient washing for ~15 min. Secondary antibodies coupled with Alexa fluorophores (Alexa fluor, Life Technologies, Invitrogen) were used at a dilution of 1:500. One hundred μ L of the secondary antibody solution is added to the coverslips and incubated at 37 °C for 45 min in a humid chamber. Coverslips are then washed twice with PBS 1X for 10 min each wash. When washing is finished, coverslips are rinsed shortly in PBS 1X, then in distilled water to remove the salt, and finally in pure EtOH. Coverslips are let air dry at room temperature. Finally, coverslips are embedded in fluorescence mounting medium (Dako) containing 1 μ g/mL DAPI (Sigma) (to stain the DNA) on slides and let dry in the dark for at least 30 min before microscopy analysis.

Table 12. List of primary antibodies used for IF and WB analyses.

Antibody	Immunogen	Organism	Source	Dilution
α Actine	Actine Nter.	Rabbit	Sigma A2103	WB: 1:4000
α Ad5 serum	AdV capsid	Rabbit	R. Iggo	IF: 1:1000 WB: 1:5000
α CRM1	Human CRM1	Goat	R. Kehlenbach ^{1,2}	IF: 1:250 WB: 1:1000
α GAPDH	Mouse GAPDH aa 314-333	Mouse	Sigma G9545	WB: 1:1000
α HA clone 3F10	HA-tag, epitope YPYDVPDYA	Rat	Roche	IF: 1:500 WB: 1:2000
α Nup358 aff. pur.	Human HA- Nup358 aa 2553-	Goat	R. Kehlenbach ^{1,2}	IF: 1:1000
α Nup358 aff. pur.	Human HA- Nup358 aa 806-	Guinea pig	(Cassany et al., 2015)	IF: 1:1000
α Nup358 aff. pur.	Human HA- Nup358 aa 3062-	Rabbit	R. Kehlenbach ^{1,2}	IF: 1:1000
α Importin β	Importin β	Rabbit	R. Kehlenbach ^{1,2}	IF: 1:500

α Importin- β	Importin- β	Rabbit	M. Kann ³	WB: 1:4000
α Kinesin light chain clone 1	Bovine brain KLC first 50 aa	Mouse	Sigma MAB1616	WB: 1:1000
α Myc	Myc-tag	Mouse	Molecular probes	IF: 1:400
α Pericentrin	Hu. Pericentrin aa 175-225	Rabbit	Abcam	IF: 1:500
α protein VI clone 9F10 B2 aff. pur.	AdV protein VI	Mouse	Home made	IF: 1:400
α protein VII clone 2–14 aff. pur.	AdV protein VII	Mouse	Home made	IF: 1:100
α RanBP1	RanBP1	Rabbit	L.Gerace ⁴	IF: 1:250
α Transportin clone D45	Human transportin N-ter	Mouse	BD Bioscience	IF: 1:500 WB: 1:1000
α α -Tubulin	Chicken tubulin	Rabbit	Sigma T9026	IF: 1:500 WB: 1:1000

¹ Institut Bergonie, Bordeaux, France ²Univ. Goettingen, Germany ³Univ. Bordeaux, France

⁴ Scripps Research Institute, La Jolla, USA

5.2. Image acquisition

IF preparations were imaged using confocal microscopes SP5 or SP8-CRYO (Leica) equipped with Leica software, from the Bordeaux Imaging Center (BIC) platform. Confocal stacks (~ 10 stacks) were taken every 0.3 μm with a pinhole setting of 1 using threefold oversampling for all channels. Acquisitions were taken setting a resolution of 16 bits and a pixel size of 75 nm.

Record of AdV infections in mitotic living cells was performed using a Leica spinning-disk microscopy system equipped with an environmental chamber heating the whole optical system to 37 °C. Stacks (n=6) were taken every 0.2 μm . Frames were taken every 5 seconds for each color channel using a x100 objective and recorded using MetaMorph software.

5.3. Image quantification

Images were processed using Image J software (National Institutes of Health).

5.3.1. Quantification of fluorescence intensity

Stacks from the channel of interest (fluorescence of Nup358) of confocal images were combined as Z-projection. An image corresponding to the control condition was first analyzed to adjust the settings (see **Figure 11**). Individual cells were selected from maximal projection images by drawing a selection around the cell periphery. Regions of interest (ROI) corresponding to individual cells from one image were added to the ROI manager tool which allows working with multiple selections. Then, a threshold was applied to highlight the area considered as positive signal. Measurement of fluorescence is performed exclusively in the thresholded area. The parameter analyzed is the integrated density which is equivalent to the product of the thresholded area and the mean gray value. The result of the analysis gives the value of the integrated density for each one of the regions of interest (for each cell). A macro was developed to automate quantifications of all images with the same threshold as set for control cells.

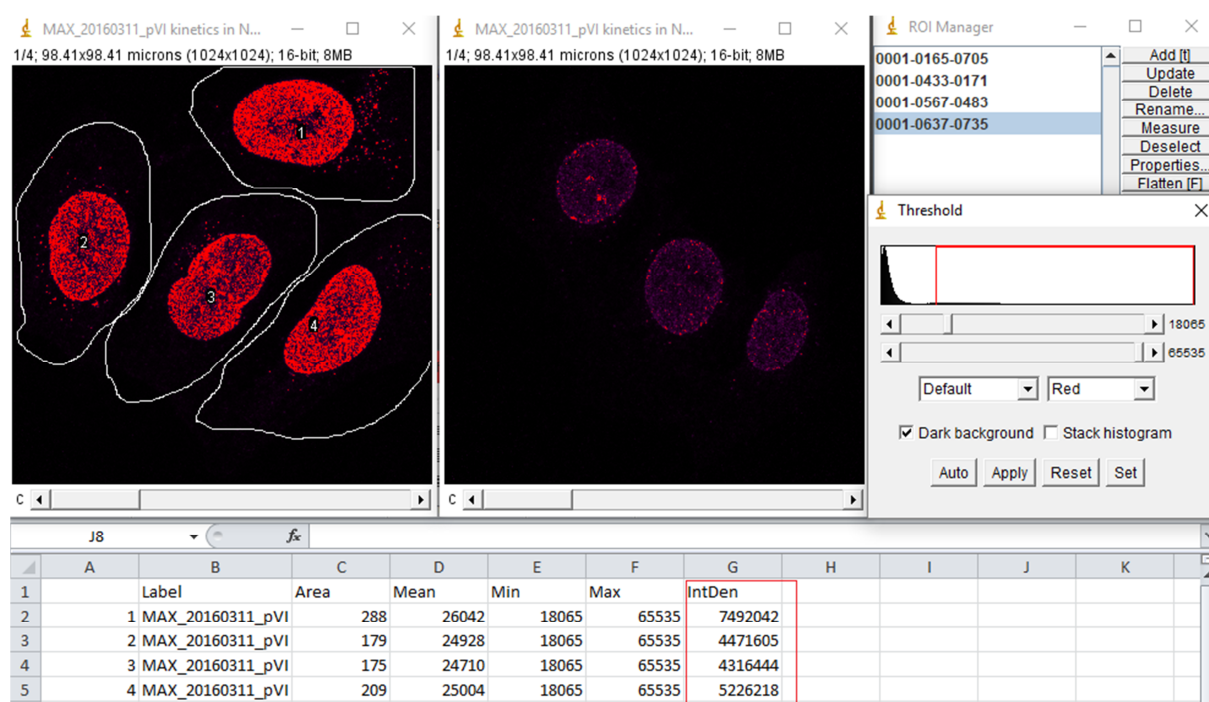


Figure 11. Quantification of fluorescence intensity. Screenshot of the quantification analysis using Image J software. Confocal images correspond to maximal Z-stack projection of the channel for Nup358 fluorescence. Left image correspond to KD control cells and right image to KD Nup358 cells. Cell outlines are shown in white. Selections were included in the ROI manager tool (top right box). Thresholded area is highlighted in red. Same threshold setting was applied for both images using the threshold tool (middle right box). Results for each cell of the KD control image are shown in the panel at the bottom. Parameters shown are: thresholded area, mean gray fluorescence, min. and max. Values applied for the threshold and the integrated density (= Area x Mean).

5.3.2. Quantification of single signal

For every image, channels were separated and stacks were combined as Z-projection. Individual cells were selected from maximal projection images by drawing a selection around the cell periphery (see **Figure 12**). Regions of interest (ROI) corresponding to individual cells were added to the ROI manager tool. This tool allows working with the same selections in different channels of the image. In a given channel of interest (e.g corresponding to fluorescence of pVII), a threshold was applied to highlight the area considered as positive signal. Then, the software is set to quantify the number of objects from the thresholded image that exceed a defined area of pixels. The minimal area of pixels is defined depending on the object of interest: e.g. for pVII quantification the minimal area is set in 10 pixels and for AdV capsids is 5 pixels. The result of the analysis gives the number of objects quantified for each region of interest (for each cell). A semi-automate macro was developed to perform quantifications of all images.

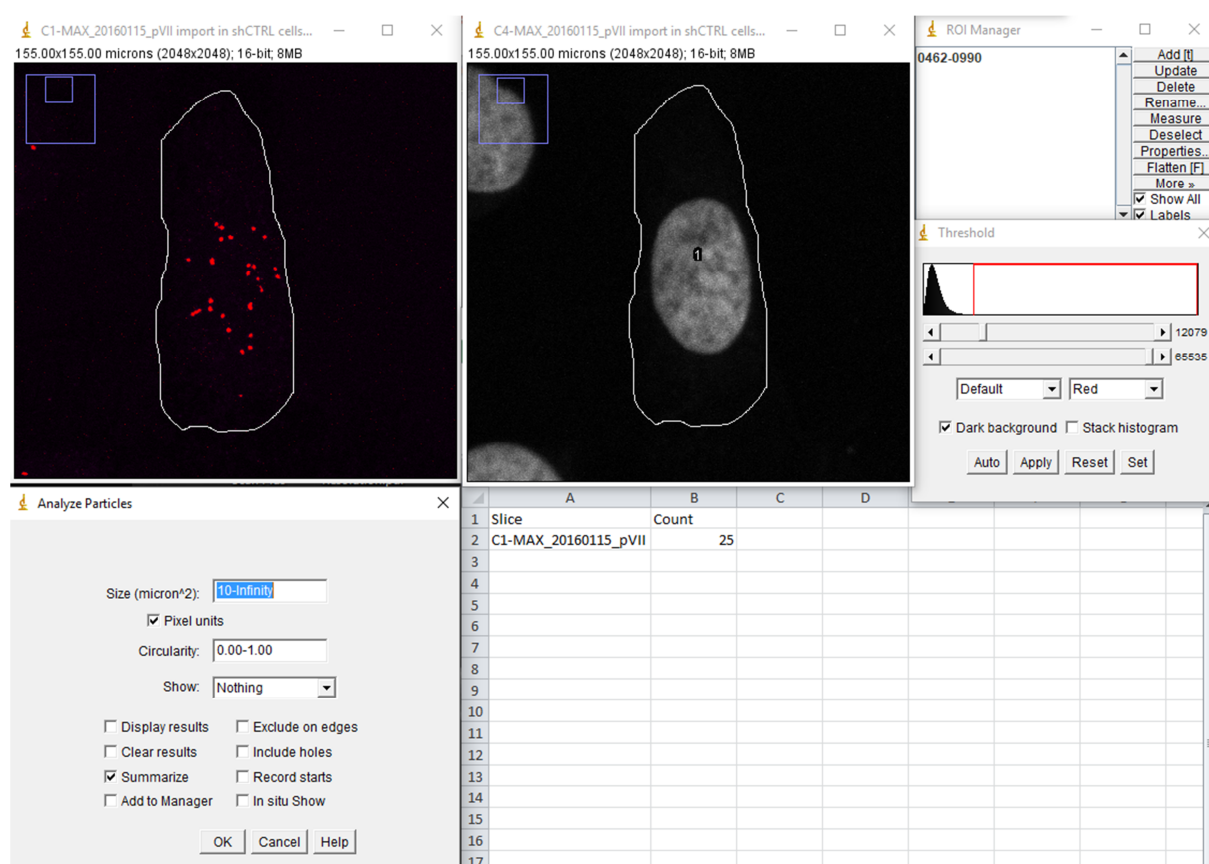


Figure 12. Quantification of single signal. Screenshot of the quantification analysis using Image J software. Confocal images correspond to maximal Z-stack projection of the channel for pVII fluorescence (to the left) and DAPI fluorescence (right). Cell outlines are shown in white. The selection was included in the ROI manager tool (top right box). Thresholded area in the pVII channel is highlighted in red using the threshold tool (middle right box). The analyze particles tool (bottom left box) is set to count thresholded objects exceeding 10 pixels. The result of the quantification of pVII dots in the selected area (ROI) is shown in the panel at the bottom right.

5.3.3. Quantification of co-localization

For quantification of co-localization in interphase cells, channels were separated and stacks were combined as Z-projection. For mitotic cells, quantification of co-localization was performed from a single representative focal plane. Quantification of co-localization between signals from two different channels requires creation of a binary image from each one of the channels of interest (**Figure 13**). For this, a threshold was applied to highlight the area considered as positive signal. Then, the software creates a binary image or “mask” from the highlighted area. Superposition of binary images generates a third binary image which shows the pixels in common. From this image, objects above a defined area of pixels are quantified. A semi-automate macro was developed to perform quantifications of all images.

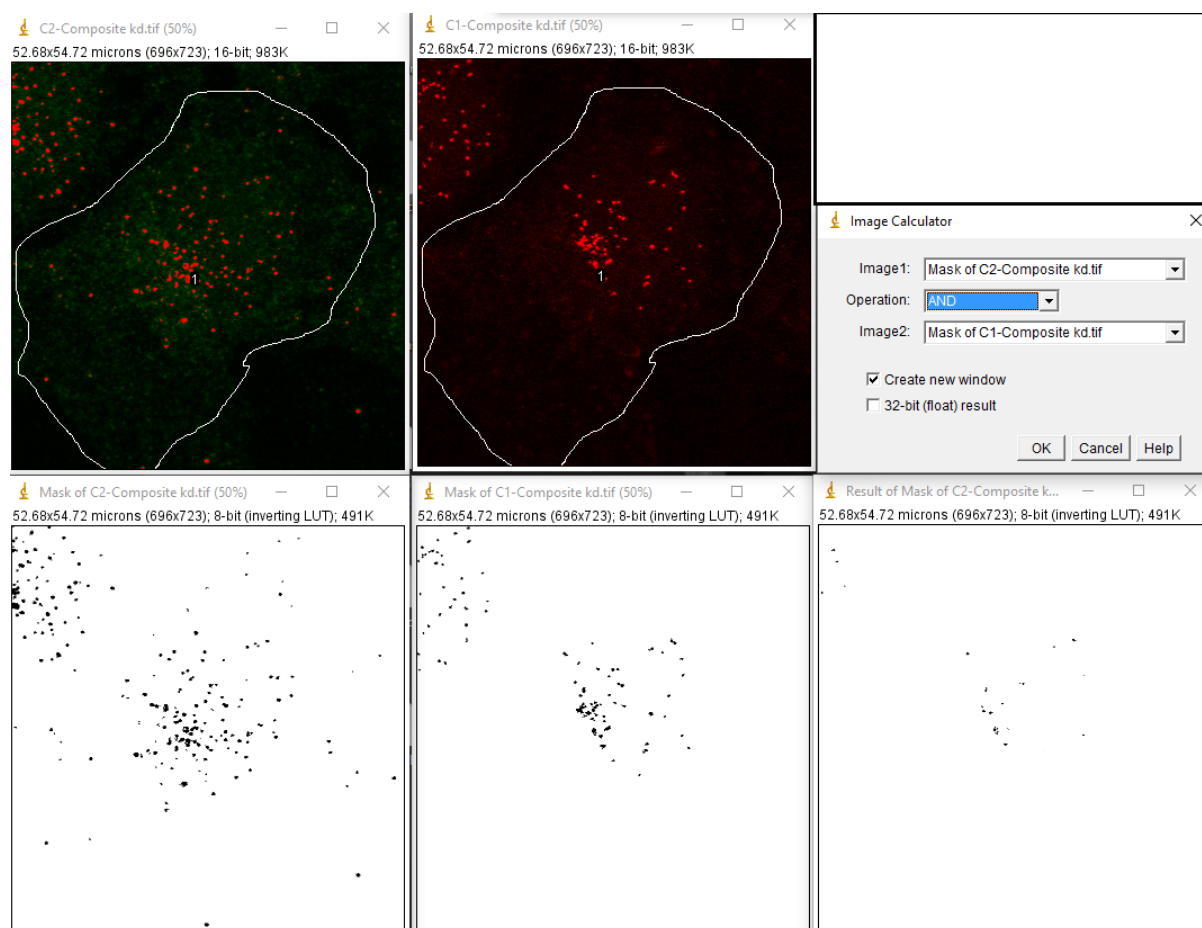


Figure 13. Quantification of co-localization. Screenshot of the quantification analysis using Image J software. Confocal images correspond to maximal Z-stack projection of the channel for AdV capsid fluorescence (to the left) and pVII fluorescence (right). Cell outlines are shown in white. Thresholded area for each channel is highlighted in red. Binary images are created from the highlighted areas, one for each channel (bottom left and middle panels). The image calculator tool (top right) creates a third binary image (bottom right) showing the pixels shared between both binary images. Objects exceeding a defined area of pixels are counted.

5.4. Statistical analysis

Statistical analyses were performed using GraphPad Prism 6 software. Results are presented either in a Tukey box plot, in a scattered plot or in columns, as indicated in the figure legends. In Tukey box plot representation, the box extends from the 25th to 75th percentiles. This range is called the interquartile range (IQR) and represents the distribution of 50 % of the data. The line in the middle of the box is plotted at the median and the dot represents the mean. Different from other box plot representations is the calculation for drawing the “whiskers”. The length of the whiskers does not extend beyond 1.5 times the IQR. The whiskers will be shorter if the extreme values are below that range. If extreme values extend beyond 1.5 times the IQR, they are represented as individual values. In this work, these individual values are not represented but considered for inferential analysis. In scattered plot and column representations, bars indicate the standard deviation (STD). Horizontal lines or the length of the columns represent the mean.

To compare the mean of two populations, statistical analysis was done using unpaired two-tailed student t-test. To compare the mean of more than two conditions, one-way ANOVA (one factor) or two-way ANOVA (two factors) tests were applied, as indicated in the figure legends. Multi-comparison post-hoc corrections were performed to figure out which groups in the sample differ. In the case of one-way ANOVA post-hoc tests, Tukey was used when sample size of groups was equal; otherwise Dunnet’s test was used. In the case of two-way ANOVA test, Sidak’s correction was used for multi-comparison tests (NS: no significant, *:P<0.05; **:P<0.01; ***:P<0.001; ****: P<0.0001).

6. BIOCHEMICAL METHODS

6.1. Cell extracts preparation

Adherent cells are washed with PBS 1X and detached from the plate using 0.6 mM EDTA in PBS 1X and incubating at 37 °C for 15 min. Cells are collected using a scraper in the case of cultivating cells in a 10 cm dish. Then, cells are pelleted by centrifugation at 500 g for 5 min at 4 °C. In the case of the detection of transportin-1 from cell extracts or for the IP-experiment, the pellet is resuspended in IP lysis buffer (Pierce IP Lysis Buffer, ref. 87788 Thermo scientific) supplemented with 1mM PMSF and cocktail protease inhibitors (cOmplete™, Mini, EDTA-free Protease Inhibitor Cocktail, Roche) and incubated for 20 min on ice. Lysates are clarified by centrifugation at 21000 g for 10 min at 4 °C.

In the case of preparation of cell extracts for pull-down experiments, the pellet was resuspended in Transport Buffer 1x (prepared as previously described; Kehlenbach and

Paschal, 2006), supplemented with 1 mM DTT, 1mM PMSF and cocktail protease inhibitors. Cells were lysed on ice by sonication for 1 min alternating 1 sec ON, 1 sec OFF at amplification 20 %. The resulting lysates were clarified by ultracentrifugation at 100000 g for 30 min at 4 °C.

Protein concentration in the cell extracts was quantified by Bio-Rad protein assay which is based on the Bradford dye-binding method (Bradford, 1976). Clarified cell extracts are diluted in Laemmli 4X buffer (8 % SDS, 40 % glycerol, 0.01 % bromophenol blue, 5 % 2-Mercaptoethanol, 200 mM Tris buffer pH 6.8) and boiled at 95 °C for 15 min.

6.2. Co-Immunoprecipitation (co-IP)

Co-IP's were performed using anti-HA Affinity Matrix (Roche) following manufacture's protocol. Briefly, 20 µL of anti-HA coated beads per condition were equilibrated with IP lysis buffer by 3 washing steps and centrifugation at 400 g. From the 350 µL of total cell extract, 5 % was diluted and boiled in Laemmli 4X buffer and considered as "input" fraction. The remaining volume was incubated with the anti-HA beads for 3-4 h at 4 °C while rotating. Afterwards, the beads were washed 3 times with ice-cold IP buffer. The beads were then resuspended in 40 µL Laemmli buffer and boiled at 95 °C.

6.3. Pull-Down

Purified AdV particles in PBS 1X 10 % were diluted (1:2) in 0.1 M sodium citrate buffer adjusted either at pH 5 or pH 7.4 for 1 h at room temperature. After incubation, half of the sample was boiled in Laemmli buffer and referred as "input". The other half was used for the binding reaction with cell extracts. Cell extracts were adjusted at 350 µL or 600 µL when detecting endogenous or exogenous CRM1, respectively. A fraction of the sample was boiled in Laemmli buffer and referred as "input". Cell extracts were then pre-incubated in presence or absence of LMB for 30 min at room temperature. AdV particles were added to cell extracts and incubated at room temperature for 1 h. Pull-down of viral particles was done by centrifugation at 21000 g, 4 °C for 1 h. Supernatant was removed and the non-visible pellet was resuspended in Laemmli buffer and boiled at 95 °C.

6.4. SDS-PAGE electrophoresis

Separation of proteins was performed by SDS polyacrylamide gel electrophoresis (SDS-PAGE). Denaturing and reducing polyacrylamide gels allow separation of proteins according to their molecular weight. In this work, separation of proteins was performed using a

discontinuous or continuous buffer system. The first includes two layers of gel, namely stacking and resolving gel. The stacking gel allows loading and concentration of samples, and consists of 4 % acrylamide/bis-acrylamide solution (Biorad), 125 mM Tris pH 6.8 and 0.1 % SDS. The resolving gel was used at 11 % acrylamide/bis-acrylamide, 375 mM Tris pH 8.8 and 0.1 % SDS. The continuous buffer system allows separation of much greater range of proteins of different molecular weights; therefore it was used for separation of different HA-Nup358 fragments. Gradient gels were performed using a gradient-maker. The gel consists of the resolving buffer at two different acrylamide/bis-acrylamide concentrations: 15 % at the bottom and 4 % at the top.

Gel running is performed at constant voltage of 90 V in TGS 1X buffer (Tris-Glycine-SDS: 25 mM Tris pH 8.3, 192 mM glycine, 1 % SDS). In addition to the samples, a protein ladder was loaded to the gel to estimate the molecular weight of the resolved proteins (PageRuler Plus Prestained Protein Ladder; Thermo Scientific).

6.5. Western blot (WB)

Separated proteins were transferred from the gel onto a nitrocellulose membrane. For this, the gel and the nitrocellulose membrane are placed between buffer-soaked filter papers as a “sandwich”. The assembled “sandwich” was introduced in a transfer tank (Trans-Blot Cell apparatus; Biorad) and filled with transfer buffer (192 mM glycine, 25 mM Tris pH 8.5, 0.01 % SDS, 15 % methanol). The transfer of proteins from the gel to the membrane was performed at constant 600 mA, for 1 h 30', at room temperature. To check uniform blotting, the proteins were stained with Ponceau S solution afterwards. Excess of dye was washed away with water. To detect transferred proteins, the nitrocellulose membrane was first incubated with the blocking solution for 30 min (TBS buffer 1X (Tris-Buffer-Saline: 137 mM NaCl, 2.7 mM KCl, 25 mM Tris pH 7.4 and 0.05 % tween20) + 10% powder milk (Régilait) to avoid unspecific recognition by the antibodies. Then, the membrane was incubated in the blocking solution with diluted primary antibodies, overnight at 4 °C. Antibodies and dilutions used are summarized in **Table 12**. Next day, membranes were washed 3 times in TBS 1X 0.05 % tween buffer and incubated with peroxidase coupled secondary antibodies (Jackson Immuno Research) diluted 1:10000 in blocking solution for 1 h at room temperature. Membranes were washed 2 times in TBS 1X 0.05 % tween and once in TBS 1X. Then, bound antibody was detected by chemiluminescence using the ECL Femto kit (Millipore) and a chemiluminescence imaging system (LAS 4000). Exposure times were chosen according to the strength of the signal.

RESULTS

1. THE ROLE OF NUP358 IN ADV GENOME DELIVERY

Nup358 is the major component of the cytoplasmic filaments of the NPC and is known to support karyopherin-mediated import of cellular (Hamada et al., 2011; Hutten et al., 2008; Wälde et al., 2012; Frohnert et al., 2014) and viral cargoes (Hutten et al., 2009). Nup214 is closely located at the cytoplasmic side of the pore and it was previously identified by our lab and others as the docking site for incoming adenoviral particles (Trotman et al., 2001; Cassany et al., 2015). Our initial analysis suggested that depletion of Nup358 did not impair capsid docking at the NPC, and only marginally affected viral genome import (Cassany et al., 2015). In contrast, a study by Strunze *et al.* observed a 4-fold reduction of AdV infection upon Nup358 depletion and linked this effect to a default in AdV capsid disassembly at the NPC (Strunze et al., 2011). Differences between both studies may be due to different read-out approaches. To better understand the mechanisms of adenoviral genome import, we decided to investigate the role of Nup358 during this process in greater detail.

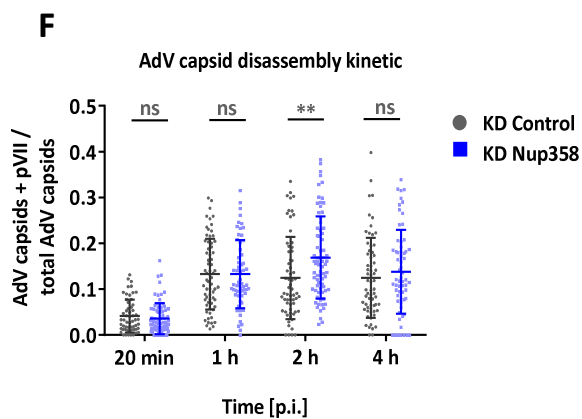
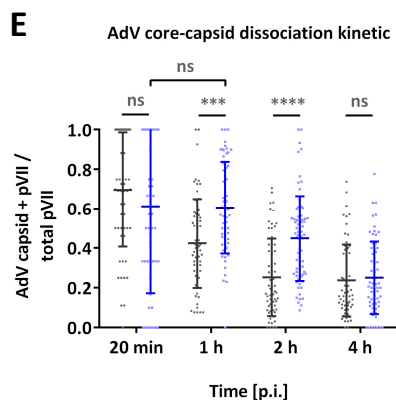
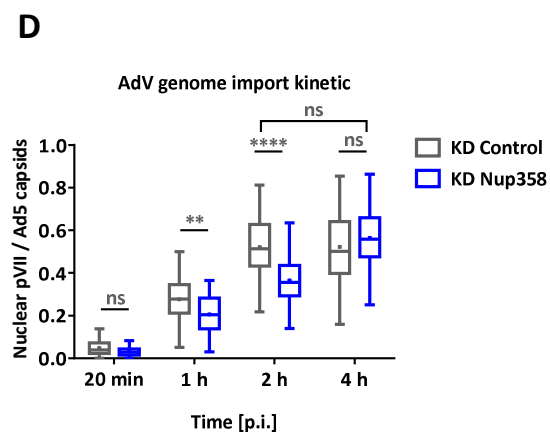
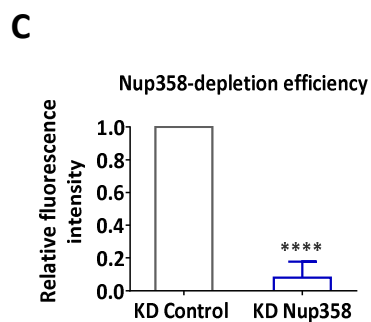
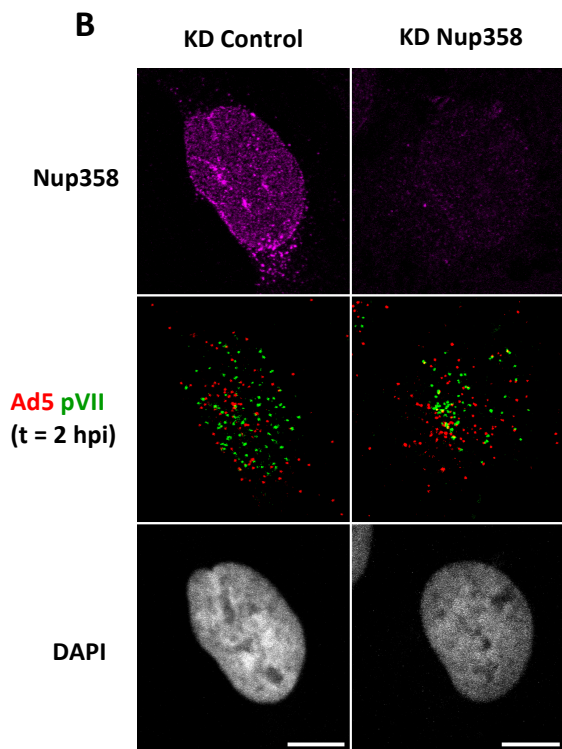
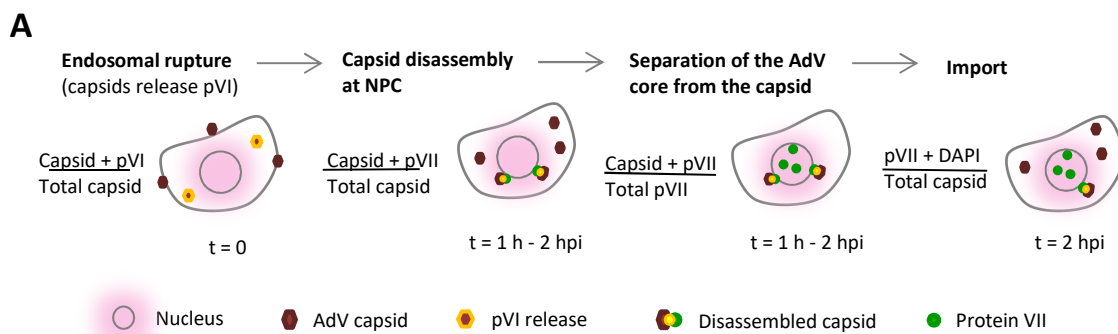
1.1. Nup358 depletion leads to inefficient AdV genome import

Different stages of AdV infection can be studied using quantitative and time-resolved immunofluorescence analysis. Early steps of infection include the entry of the viral particle into the cytoplasm, microtubule-dependent trafficking, and genome delivery into the nucleus. These events can be monitored by using specific antibodies recognizing AdV proteins (**Figure 14a**). For example, during AdV entry, the membrane lytic factor protein VI is released, which leads to the escape of the virion from the endosome (Wiethoff et al., 2005; Wodrich et al., 2010). Escaped particles are again negative for protein VI which is presumed to remain with the endosomal membrane. Hence, detection of AdV protein VI and capsids allows visualization and quantification of this specific step. The relative amount of capsids positive for protein VI in one cell will then represent the relative endosomal escape occurring at a specific time point. As depicted in **Figure 14a**, the analysis of a population of cells at different time points allows us to estimate the kinetic of endosomal escape from a given cell population by estimating the number of pVI positive capsids over time. Similarly, it is possible to monitor AdV genome delivery. It is known that protein VII associates with vDNA during early phases of infection, including import (Chatterjee et al., 1986; Komatsu et al., 2011). Furthermore, a study calculated that pVII-vDNA co-localization linearly correlated with the viral dose in the range of 20-200 physical particles per cell (Wang et al., 2013). However, during the cytosolic transport, the protein VII epitope remains hidden inside the

capsid together with the genome. Therefore, detection of both protein VII and AdV capsids is a useful tool to monitor AdV genome delivery. During AdV genome delivery, viral particles reach the NPC and capsids are further disassembled. As a consequence, AdV cores including the viral genome and the histone-like protein VII are exposed at the cytoplasmic side of the NPC. At this precise moment, capsids are disassembled but still not disintegrated, allowing visualization of both, AdV capsids and pVII together. The proportion of disassembled capsids is thus represented by the relative amount of capsids positive for pVII. Exposed AdV cores then dissociate from the capsid and are finally imported into the nucleus. As depicted in **Figure 14a**, the kinetic of AdV core-capsid dissociation can be calculated as the relative amount of pVII still associating (co-localizing) with AdV capsids. The efficiency of genome import can be estimated by calculating the number of nuclear pVII dots (pVII dots in DAPI area) relative to the amount of cytosolic capsids.

1.1.1. Nup358 depletion delays AdV genome import

To address the question whether Nup358 plays a specific role in AdV genome import we performed depletion analysis using siRNA against Nup358 or non-specific siRNA as control. We first established conditions for efficient depletion under which U2OS cells are still viable, since excessive depletion is lethal (**Figure 14b and c**). Hence, 72h post-siRNA transfection cells were transduced with an Ad5-wt-GFP vector, and number of nuclear pVII dots and viral capsids were quantified at 20 min, 1 h, 2 h and 4 h post-infection (hpi). The results showed a progressive increase of imported AdV genome over time in control cells, reaching a *plateau* at 2 hpi (**Figure 14b and d**). In Nup358-depleted cells no reduction of the overall genome import could be observed at 4 hpi. However, we observed a delay, suggesting that genome delivery was less efficient but not restricted as previously observed upon depletion of Nup214 (Cassany et al., 2015).



1.1.2. Nup358 depletion affects AdV genome release but not capsid disassembly

A delay in nuclear accumulation of AdV genomes can be the consequence of defective upstream events during viral entry. The immediate steps preceding import of the viral genome are the disassembly of the capsid and the separation of the core from the disassembled capsid. Both steps are tightly linked (both parameters share the same numerator) and a default in capsid disassembly would delay dissociation of pVII-containing viral cores from the capsid and conversely, if AdV cores are not efficiently separated from the capsid, this would be reflected in an increment of the relative number of capsids positive for pVII. Therefore, it is essential to compare kinetics of both events to understand which specific step during AdV genome delivery is affected in absence of Nup358.

To see whether Nup358 depletion specifically affects capsid disassembly and/or separation of AdV cores from capsids and import, we further calculated the kinetic of AdV core-capsid dissociation and capsid disassembly from our kinetic assay. The kinetic of AdV core-capsid dissociation (**Figure 14e**) in control and Nup358-depleted cells showed that at 20 min pi, most of detectable pVII was still associated with the viral capsid (values close to 1), while some had already been separated from the capsid (values close to 0) and have been imported into the nucleus.

Figure 14: Nup358 depletion delays AdV genome import. U2OS cells grown on coverslips were transfected with siRNA control or targeting Nup358. Three days after transfection cells were infected with Ad5-wt-GFP vector at 37 °C followed by inoculum removal after 30 min ($t = 0$). Cells were then fixed at 20 min, 1 h, 2 h or 4 hpi and stained using specific antibodies to detect endogenous Nup358 (magenta), the viral capsid (red), and the core protein VII (green). DAPI staining was used to visualize the chromatin. **(A)** Schematic representation of the detection and quantification of viral particles during different steps of entry and AdV genome delivery. Viral particles and the corresponding degrees of capsid disassembly viral components are specified in the legend. Approximate time points for each entry step are indicated below the illustrations. **(B)** Representative confocal images of AdV pVII-containing core delivery in KD control and KD Nup358 cells at 2 hpi. Maximal projection images are shown. Antibodies used are indicated to the left of each row. Scale bars 10 μ m. **(C)** Quantification of the mean fluorescence intensity of endogenous Nup358 (blue bar) relative to control cells (grey bar). Bars represent the SD of the mean of 3 independent experiments; $n=60$ cells for each condition, for each experiment; $p<0,0001$ two-tailed T-test. **(D)** Quantification of the kinetic of genome import efficiency in control (grey) or Nup358-depleted cells (blue), calculated as the number of nuclear pVII dots (pVII dots in DAPI area) relative to the total amount of capsids per cell. Normalized numbers are represented as box plots. Data obtained from individual cells, from two independent experiments ($n \geq 30$ cells per condition, for each experiment) were represented in a Tukey box plot **(E)** Quantification of the kinetic of dissociation of AdV cores from capsids in control (grey) or Nup358-depleted cells (blue), calculated as the number of co-localization events pVII + AdV capsids, relative to the total amount of pVII dots per cell. **(F)** Quantification of the kinetic of AdV capsid disassembly in control (grey) or Nup358-depleted cells (blue), calculated as the number of co-localization events AdV capsids + pVII, relative to the total amount of AdV capsids per cell. Data obtained from individual cells, from two independent experiments ($n \geq 30$ cells per condition, for each experiment) were represented in a scatter plot (E;F). Bars in the scatter plot represent the mean and SD. Results in (D-F) were analyzed using a two-way ANOVA test and Sidak's multiple comparisons post hoc test. ****: $p < 0,0001$; ***: $p \leq 0,001$; **: $p \leq 0,01$; ns $\geq 0,05$

In control cells, the ratio of pVII positive for AdV capsids decreased over time with most pVII separating from the capsid as early as 2 hpi. In contrast, in Nup358-depleted cells, the separation of viral cores from the capsid did not occur as fast as in control cells since at 1 h and 2 hpi, the proportion of detectable pVII still associated with AdV capsids was significantly higher in Nup358-depleted cells compared to control cells. In addition, statistically equivalent ratios of pVII separation were observed at 20 min and 1 hpi in absence of Nup358. Finally at 4 hpi, most of pVII were not associated with viral capsids in both conditions, which correlate with equivalent absolute rates of genome import at this time point (**Figure 14d**). These results suggest that depletion of Nup358 leads to inefficient separation of viral genomes from the capsid, and consequently, there is a delay in adenoviral genome import; however this result can be also the consequence of a defective capsid disassembly.

The ratio of disassembled capsids (marked by being pVII positive) vs total viral particles in control cells increased from 20 min to 1 hpi, coinciding with their arrival at the NPC environment, and later, from 1 h to 4 hpi this ratio stabilizes (**Figure 14f**). Strikingly, in Nup358-depleted cells, the relative amount of disassembled capsids at 20 min and 1 hpi was statistically non-significant compared to control cells, meaning that capsids in Nup358-depleted cells disassembled as efficiently and with similar kinetics as in control cells at early time points. However, at 2 hpi, the ratio of disassembled capsids in Nup358-depleted cells was significantly higher, while at 4 hpi the rate of capsid disassembly is no longer statistically different in control vs Nup358-depleted cells, coinciding with the moment at which AdV genome import is compensated in cells lacking Nup358. The differences observed at 2 hpi probably reflect an accumulation of AdV cores still associating with the capsid due to an inefficient import of the AdV genome.

Taken together, these results show that depletion of Nup358 delays AdV genome delivery by affecting specifically the import step, rather than disassembly of AdV capsids at the NPC, since capsids were similarly disassembled at early time points (20 min and 1 hpi) in control and Nup358-depleted cells, but accumulated at 2 hpi before absolute import rates caught up with control cells at 4 hpi.

1.1.3. Nup358 depletion does not affect virion entry into the cytoplasm

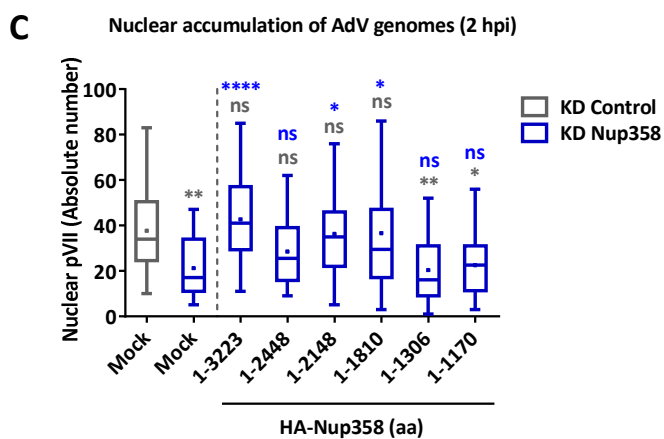
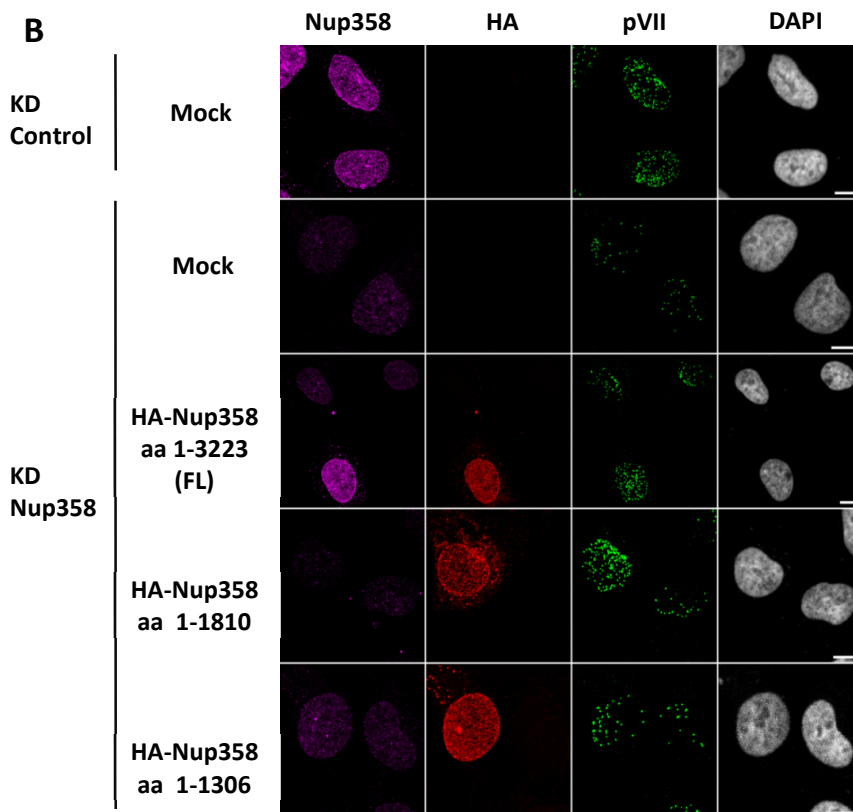
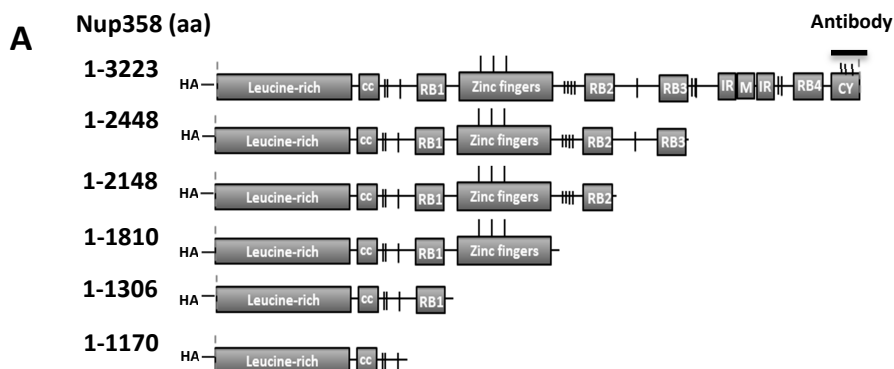
To confirm that depletion of Nup358 does influence only genome import and did not affect upstream trafficking events, we next monitored the kinetic of protein VI exposure, which reflects the escape of AdV particles from the endosome. We performed a similar experiment depleting cells with specific siRNA against Nup358 or using non-targeting siRNA as a control. Cells were transduced with 5000 pp/cell (about 100 internalized pp) of Ad5-wt-GFP following the time course for visualizing pVI exposure previously described by our lab (Montespan et al., 2017). We observed that in control and Nup358-depleted cells, capsids positive for pVI peak about 30 min post virus addition (**Figure 15a and b**). In both depleted and control conditions, this was followed by a decrease of pVI-associated capsids over time, reflecting the progressive entry of viral particles to the cytosol and showing that early AdV entry steps are not affected by Nup358 depletion.

Taken together, these results suggest that Nup358 is not essential for AdV genome import but point to a role of Nup358 in accelerating AdV core-capsid dissociation and import of the viral genome to the nucleus, which would be in agreement with a role in facilitating viral genome import by promoting import complex formation.

1.2. The N-terminal half of Nup358 is sufficient for promoting efficient AdV genome import

To confirm a role for Nup358 in AdV genome import and to exclude off-target effects in the siRNA experiment, as well as to identify the region of Nup358 facilitating adenoviral genome import, we used a combined depletion/reconstitution approach. This approach was previously developed for studying the involvement of Nup358 in nucleo-cytoplasmic transport of cellular cargoes (Wälde et al., 2012). In this study, Wälde and colleagues generated several siRNA resistant constructs, encoding different fragments of Nup358 all harbouring the N-terminal NPC-anchoring domain, to reconstitute nucleo-cytoplasmic transport (**Figure 16a**). We took advantage of this system and performed systematic depletion/reconstitution of Nup358 and followed the import kinetic of the AdV genome upon infection. In order to confirm the efficient siRNA-depletion of endogenous Nup358 and discriminate endogenous from reconstituted Nup358, we used antibodies against the C-terminal cyclophilin-like domain of Nup358 which detects endogenous Nup358 but is absent in the truncated fragments. In contrast, all constructs included an N-terminal HA-epitope, allowing specific analysis of Nup358-reconstituted cells. To ensure high depletion rates for Nup358, we depleted endogenous Nup358 using double siRNA transfections. Since the antibody specific for the C-terminal domain of Nup358 recognized both, the endogenous and the full-length reconstituted Nup358 (thus masking the efficiency of the depletion), we analyzed only cells surrounded by cells that clearly lacked Nup358, suggesting an efficiently transfected area of cells (**Figure 16b, third row**). To analyze if we could fully or partially restore the genome import efficiency in absence of endogenous Nup358, cells were transfected with the full-length or truncation mutants constructs of Nup358. The following day, cells were transduced with the Ad5-wt-GFP vector and analyzed the 2 hpi time point which gave the statistically highest differences in AdV genome import efficiency between control and Nup358-depleted cells (**Figure 16d**). The absolute number of pVII dots in the nucleus of control-depleted *vs* Nup358-depleted cells was significantly increased, confirming that nuclear accumulation of viral genomes is less efficient at 2 hpi in absence of Nup358 (**Figure 16c**). Strikingly, full-length reconstituted Nup358-expressing cells accumulated nuclear pVII-containing AdV cores as efficiently as control cells. In contrast, fragments containing exclusively the first 1306 amino-acids (aa) of Nup358 or shorter fragments did not restore the efficiency of AdV genome import. To restore AdV genome import into the nucleus to wild type levels a minimal fragment containing the first N-terminal 1810 aa was required.

These results confirm that Nup358 facilitates AdV genome import and identifies the N-terminal half of Nup358 as the minimal region necessary for promoting an efficient import of the AdV genome into the nucleus.



1.3. Transport receptors compensate for the lack of Nup358

The AdV core contains ~ 800 copies of the protein VII tightly associated with the vDNA. pVII encode several functional NLSs (Wodrich et al., 2006) and is able to interact with different transport receptors (Wodrich et al., 2006; Hindley et al., 2007). These studies revealed a possible scenario where recruitment of available import receptors to genome-bound protein VII would drive the import of the AdV genome. In agreement with this model, Nup358 was shown to facilitate import of certain cellular cargoes by maintaining a local pool of available transport receptors (avoiding diffusion of free import receptors and/or facilitating its recycling to the cytosol) (Hutten et al., 2008, 2009). Hence, in absence of Nup358, transport receptors could become rate-limiting also for viral genomes and consequently, import of AdV genome would be delayed. To test this hypothesis, we decided to overexpress HA-tagged transport receptors in Nup358-depleted cells.

In this assay, we included transport receptors whose import is known to be facilitated by Nup358 (importin- β , transportin-1 and importin-7) (Hutten et al., 2008, 2009; Wälde et al., 2012; Frohnert et al., 2014). Furthermore they have been described to promote unphysiological DNA import (transportin-1 (Lachish-Zalait et al., 2009) and importin-7 (Dhanoya et al., 2013)) and to bind either both forms of pVII (transportin-1 and importin-7), or exclusively the non-mature form (importin- β) (Wodrich et al., 2006; Hindley et al., 2007). Moreover, we included importin-9 since among its cargo are several cellular histones (described in the introduction, Table 2) and the HIV-1 protein Rev (Hutten et al., 2009).

Figure 16: The N-terminal half of Nup358 is sufficient for promoting efficient AdV genome import. Control or Nup358 siRNA-depleted cells were transfected with an empty plasmid or with NPC-anchored truncation mutants of Nup358. The day after, cells were infected with Ad5-wt-GFP vector at 37 °C followed by inoculum removal after 30 min ($t = 0$). Cells were fixed at 2 hpi and stained using specific antibodies to detect endogenous Nup358 (magenta), the HA-tag of Nup358 constructs (red), and the core protein VII (green). DAPI staining was used to visualize the chromatin. **(A)** Schematic representation of the siRNA resistant HA-tagged constructs of Nup358 used in this assay, indicating the corresponding amino-acids (aa) present in each fragment. Domains of Nup358 are represented in grey boxes and vertical sticks represent the FG-repeats. The rabbit antibody used in this assay recognizes an epitope in the cyclophilin-like domain (CY) of Nup358, which is missing in the truncation mutants. **(B)** Representative confocal images of pVII accumulation in the nucleus of control and KD Nup358 cells, either mock treated or expressing the full-length (FL) or truncation mutants of Nup358 as indicated to the left of each row. Note that the Nup358 antibody recognizes the FL construct but not the truncation mutants. Maximal projection images are shown. Scale bar 10 μ m. **(C)** Quantification of the nuclear accumulation of AdV genomes in control (grey) or Nup358-depleted cells (blue), calculated as the number of pVII dots co-localizing with the DAPI staining per cell. Data obtained from individual cell values ($n > 30$ per condition) are represented in a Tukey box plot. Results were analyzed using a one-way ANOVA test and Tukey's multiple comparisons post hoc test. ****: $p < 0,0001$; **: $p < 0,01$; *: $p < 0,05$; ns $\geq 0,05$. Grey asterisks represent significance with respect to KD control and blue asterisks with respect to mock KD Nup358 cells.

Cells were thus co-transfected with HA-tagged constructs of different importins (Hutten et al., 2008, 2009), together with shRNA-encoding plasmids targeting Nup358 that were previously used in our lab to study Nup358 involvement in AdV genome delivery (Cassany et al., 2015). Nup358-depleted or control cells overexpressing transport receptors were transduced with Ad5-wt-GFP and analysed at 2 hpi. We could observe again a statistically significant decrease of nuclear pVII dots in Nup358-depleted cells compared to control cells at 2 hpi (**Figure 17a and b**). Interestingly, this was completely restored in cells lacking Nup358 but overexpressing transportin-1. To a lesser extent, excess of importin-9 also restored the defect induced by Nup358-depletion. Overexpression of importin- β and importin-7 in contrast did not compensate for the lack of Nup358. Importantly, overexpression of transportin-1, importin- β or importin-9 in cells conserving endogenous Nup358 did not increase AdV genome import rates, suggesting that Nup358 regulates genome import through access to specific transport receptors (**Figure 17b and c**). In presence of endogenous Nup358 overexpression of importin-7 could not be determined due to high rates of cell death. Together, these results show that transport receptors can be rate-limiting for AdV genome import in absence of Nup358 and suggest a role for Nup358 in maintaining high concentration of available importins at the NPC to facilitate the formation of AdV core import complexes, preferentially with transportin-1.

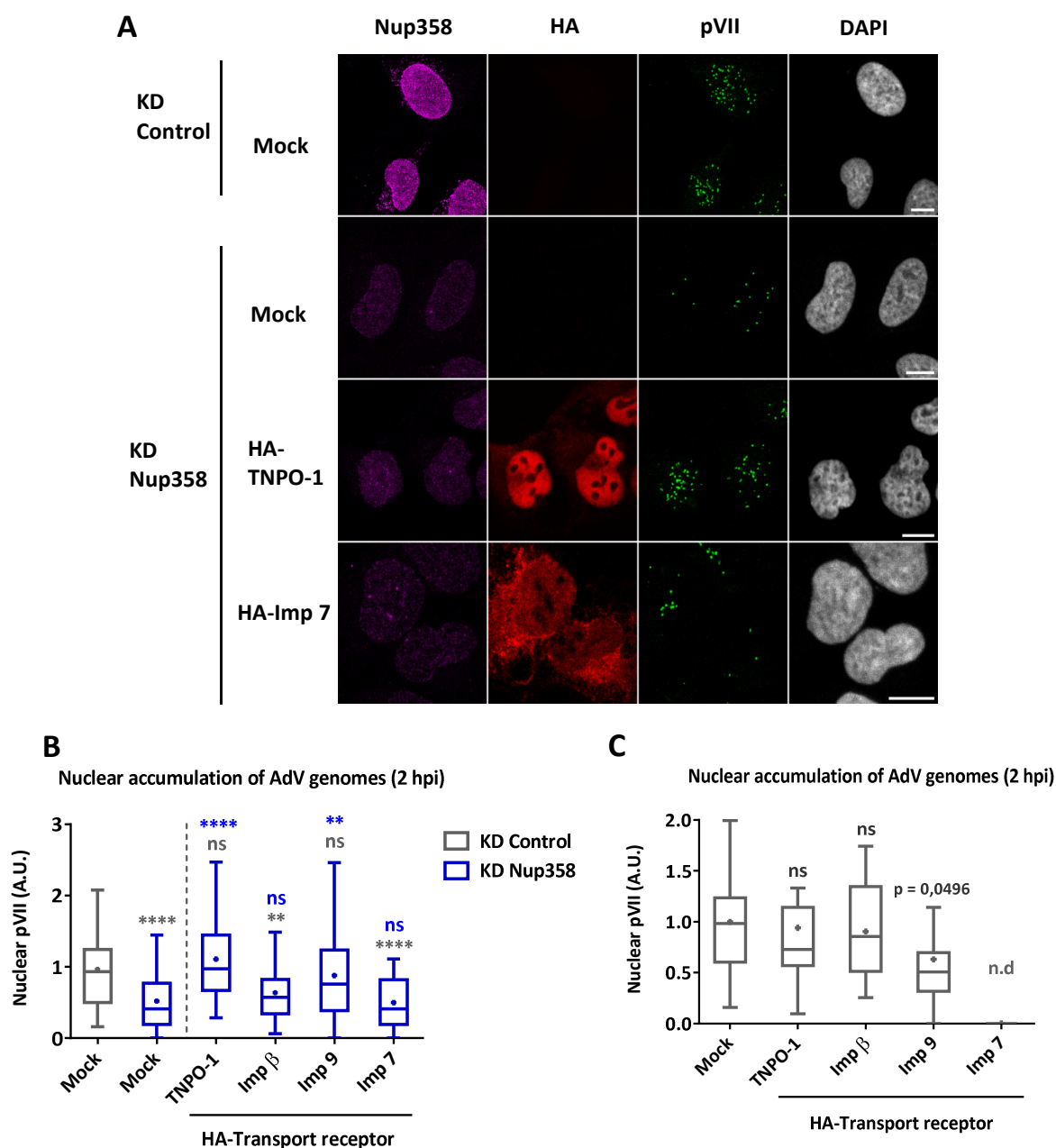


Figure 17: Transport receptors compensate the lack of Nup358. Cells were co-transfected with shRNA expression plasmids against Nup358 or non-specific (control) and an empty vector (mock) or HA-tagged constructs coding for HA-transportin-1 (TNPO-1), HA-importin- β , HA-importin-9 or HA-importin-7. Three days later cells were infected with Ad5-wt-GFP and fixed at 2 hpi after inoculum removal. Cells were stained using specific antibodies to detect endogenous Nup358 (magenta), the HA-tag of transport receptor constructs (red), and the core protein VII (green). DAPI staining was used to visualize the chromatin. **(A)** Representative confocal images of pVII accumulation in the nucleus of control and KD Nup358 cells, either mock treated or expressing different HA-tagged import receptors as indicated to the left of each row. Maximal projection images are shown. Scale bar 10 μ m. **(B-C)** Quantification of the nuclear accumulation of AdV genomes in control (grey) or Nup358-depleted cells (blue), calculated as the number of pVII dots co-localizing with the DAPI staining per cell. Individual cell values were normalized relative to the control of each experiment and represented as arbitrary units (A.U.). Values of two independent (B) or one (C) experiment with at least 25 cells per condition, for each experiment, are represented in a Tukey box plot. Importin-7 condition in control cells could not be determined due to low cell viability (nd). Results were analyzed using a one-way ANOVA test and Tukey's multiple comparisons post hoc test. ****: $p < 0,0001$; **: $p < 0,01$; ns $\geq 0,05$. Grey asterisks represent significance with respect to KD control and blue asterisks with respect to mock KD Nup358 cells.

1.3.1. AdV genome import is not exclusively mediated by transportin-1

We then asked whether transportin-1 would be the main transport receptor mediating import of AdV cores *in vivo*. To answer this question we used two different approaches: specific RNAi depletion or inhibition of transportin-1. In the depletion approach, efficient knock-down of transportin-1 was reached 72 h post siRNA transfection (**Figure 18a and b**). Cells were then transduced with Ad5-wt-GFP and analysed 2 hpi. Only a slight reduction in AdV genome import was observed in transportin-1-depleted cells compared to control cells (**Figure 18b and c**).

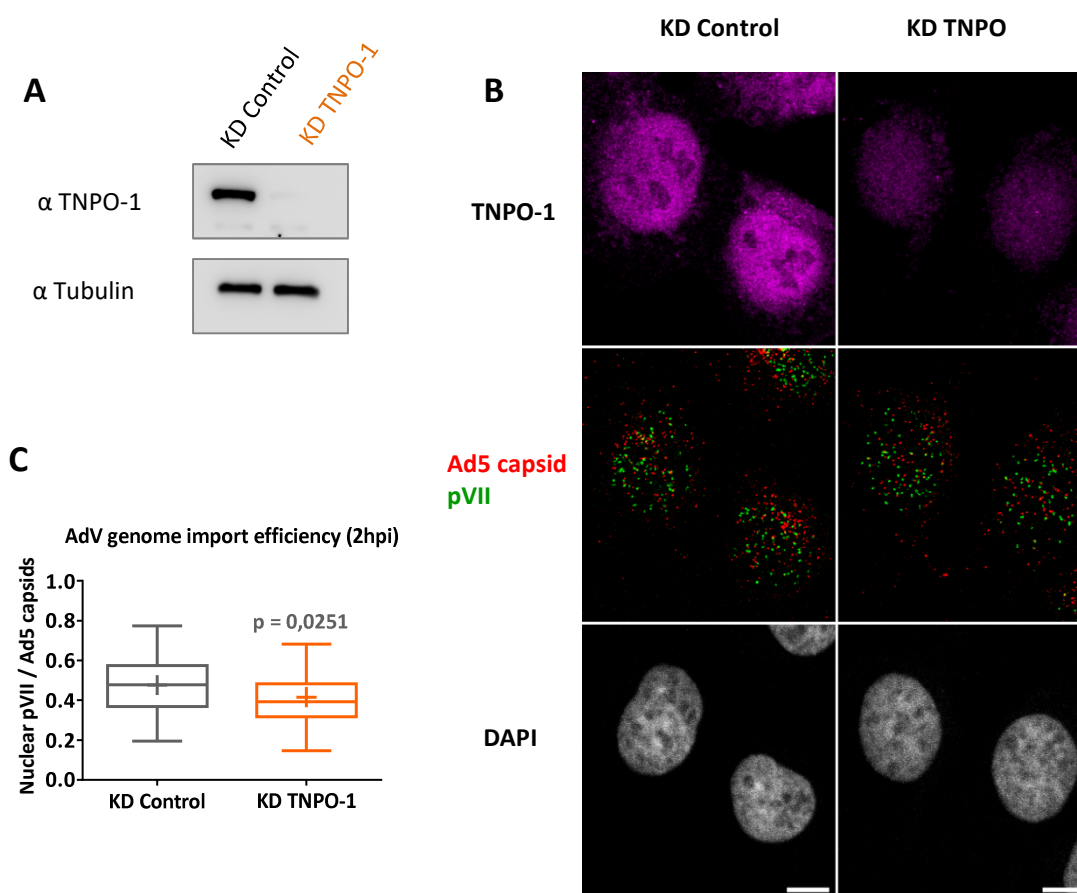


Figure 18: Depletion of transportin-1 does not impact AdV genome import. (A) WB analysis of the efficiency of transportin-1 (TNPO-1) KD. Cells were transfected with non-specific siRNA or siRNA's against TNPO-1. Cells were collected 72 h later and total cell lysates were analyzed by WB using antibodies against TNPO-1 and tubulin as indicated. (B) Representative confocal images of the AdV core delivery in control and KD TNPO-1 cells fixed 2 hpi. Cells were stained using specific antibodies to detect endogenous TNPO-1 (magenta), the AdV capsid (red), and the core protein VII (green). DAPI staining was used to visualize the chromatin. Scale bar 10 μ m. (C) Quantification of AdV genome import efficiency in control (grey) or TNPO-1-depleted cells (orange), calculated as the number of nuclear pVII dots relative to the total amount of AdV capsids per cell. Data obtained from individual cell values ($n > 30$ per condition), from two independent experiments are represented in a Tukey box plot. Results were analyzed using a two-tailed T-test.

To confirm this observation, an inhibition assay was performed. Cells were transfected with a construct coding for a myc-tagged M9M peptide, a well-known high affinity cargo inhibitor of transportin-1 (Cansizoglu et al., 2007). To control specific inhibition of the transportin-1 pathway, cells were co-transfected with either a plasmid coding for GFP-tagged M9-NLS of the protein hnRNP A1 which is specifically recognized by transportin-1, or with a GFP-tagged cNLS recognized by the importin- α/β complex. In parallel, cells were transfected with the myc-tagged M9M peptide inhibitor and transduced with Ad5-wt-GFP. Expression of myc-M9M caused partial re-localization of the GFP-tagged M9-NLS peptide from the nucleus to the cytoplasm, probing the specific inhibition of transportin-1-dependent import (**Figure 19a**). However, excess of myc-M9M did not cause any reduction in AdV genome import compared to mock-treated cells at 2 hpi (**Figure 19b and c**). These results show that specific depletion or partial inhibition of transportin-1 does not impair import of the AdV genome into the nucleus, suggesting that other import receptors may compensate the lack of transportin-1 to promote import of the AdV genome into the nucleus or that the remaining pool is sufficient to drive genome import (e.g. facilitated by Nup358).

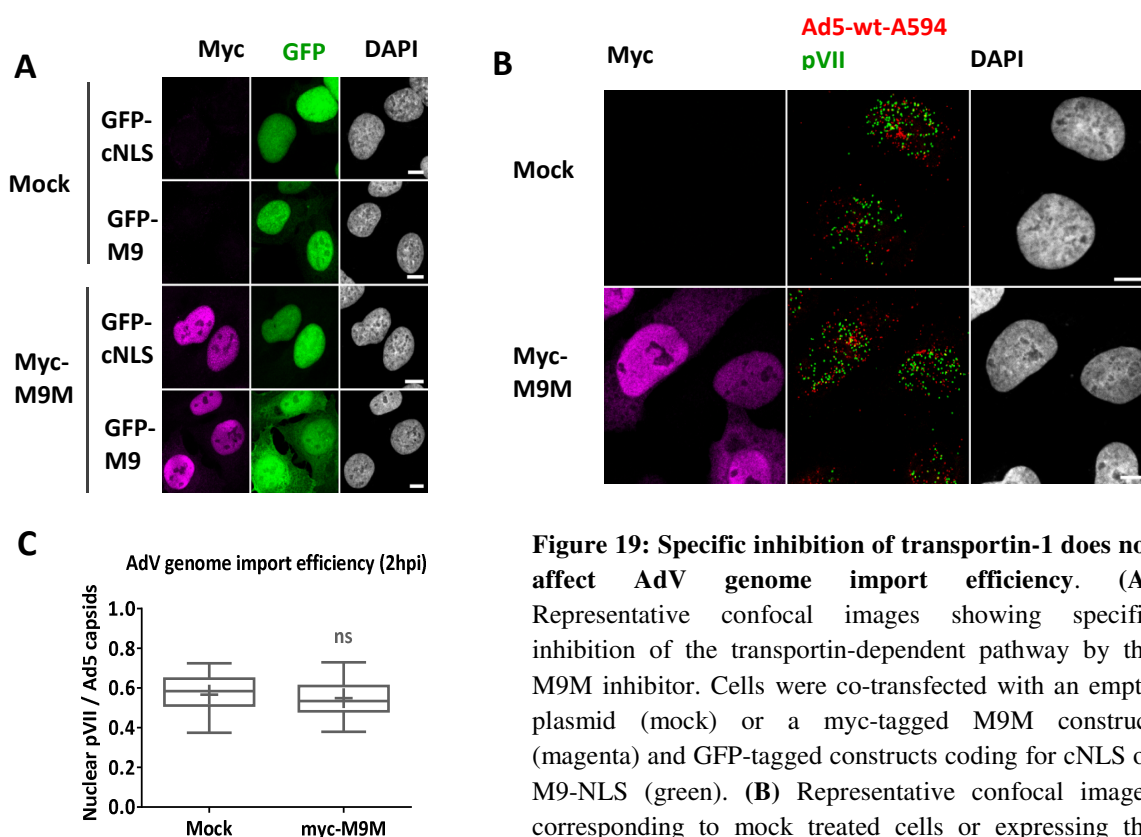


Figure 19: Specific inhibition of transportin-1 does not affect AdV genome import efficiency. (A) Representative confocal images showing specific inhibition of the transportin-dependent pathway by the M9M inhibitor. Cells were co-transfected with an empty plasmid (mock) or a myc-tagged M9M construct (magenta) and GFP-tagged constructs coding for cNLS or M9-NLS (green). (B) Representative confocal images corresponding to mock treated cells or expressing the myc-M9M construct infected with Ad5-wt-GFP-A594

(red) and fixed 2 hpi. Cells were stained using specific antibodies to detect the myc-tag (magenta) and the core protein VII (green). DAPI staining was used to visualize the chromatin. Scale bar 10 μ m. (C) Quantification of AdV genome import efficiency in mock or myc-M9M expressing cells, calculated as the number of nuclear pVII dots relative to the total amount of AdV capsids per cell. Data obtained from individual cell values ($n > 30$ per condition) are represented in a Tukey box plot. Results were analyzed using a two-tailed T-test. $Ns \geq 0,05$

1.4. The N-terminal FG-cluster of Nup358 recruits transport receptors

We have observed that excess of transport receptors can compensate for the absence of Nup358, which suggest a role for Nup358 in facilitating AdV genome import by maintaining high concentration of available transport receptors near the NPC. Likewise, we have observed that the N-terminal half of Nup358 was able to restore efficient import of AdV genomes in cells depleted for Nup358. Thus, we wanted to know if this fragment contains functional domains suitable to explain receptor enrichment at the NPC. As shown in **Figure 20**, this N-terminal fragment contains one RanBD that could be involved in recycling of importins back to the cytoplasm. In addition, the fragment encodes several FG-repeats that potentially bind free transport receptors directly. Finally, the fragment encodes a group of zinc fingers that were suggested to be the docking site for the exportin CRM1 on its way back to the nucleus (Singh et al., 1999). We thus investigated the recruitment of different transport receptors by soluble or NPC-anchored fragments of Nup358.

1.4.1. The FG-repeat patch- and RanBD1-containing fragment of Nup358 recruits endogenous transportin-1

To study the contribution of the different domains in the recruitment of transport receptors, we first used HA-tagged constructs containing fragments of Nup358 lacking the NPC-anchoring region, and stained for endogenous transportin-1. Cells were transfected with either a plasmid containing the aa 806-1306 of Nup358, comprising a coiled-coil domain, a cluster of FG-repeats and the first RanBD; a fragment comprising the contiguous region of aa 1350-2148 harbouring several zinc fingers, another cluster of FG-repeats and the second RanBD of Nup358; or the aa 2307-2710 C-terminal region (**Figure 20a**). The staining of endogenous transportin-1 was predominantly nuclear in mock treated cells (**Figure 20b**). In contrast, in cells overexpressing the N-terminal fragment of aa 806-1306, the endogenous transportin-1 was re-distributed to the cytoplasm and co-localized with the NPC-non-anchored fragment of Nup358. Strikingly, this was not the case in cells overexpressing fragments of aa 1350-2148 or aa 2307-2710 since endogenous transportin-1 still localized inside the nucleus regardless of the subcellular localization of the exogenous fragment of Nup358. These results suggest that the most N-terminal fragment comprising the first patch of FG-repeats and RanBD1 is more efficient in recruiting endogenous transportin-1 than other FG-repeats or RanBDs in adjacent regions of Nup358, which is in agreement with our observation that the N-terminal NPC-anchoring fragment of Nup358 can rescue AdV genome import.

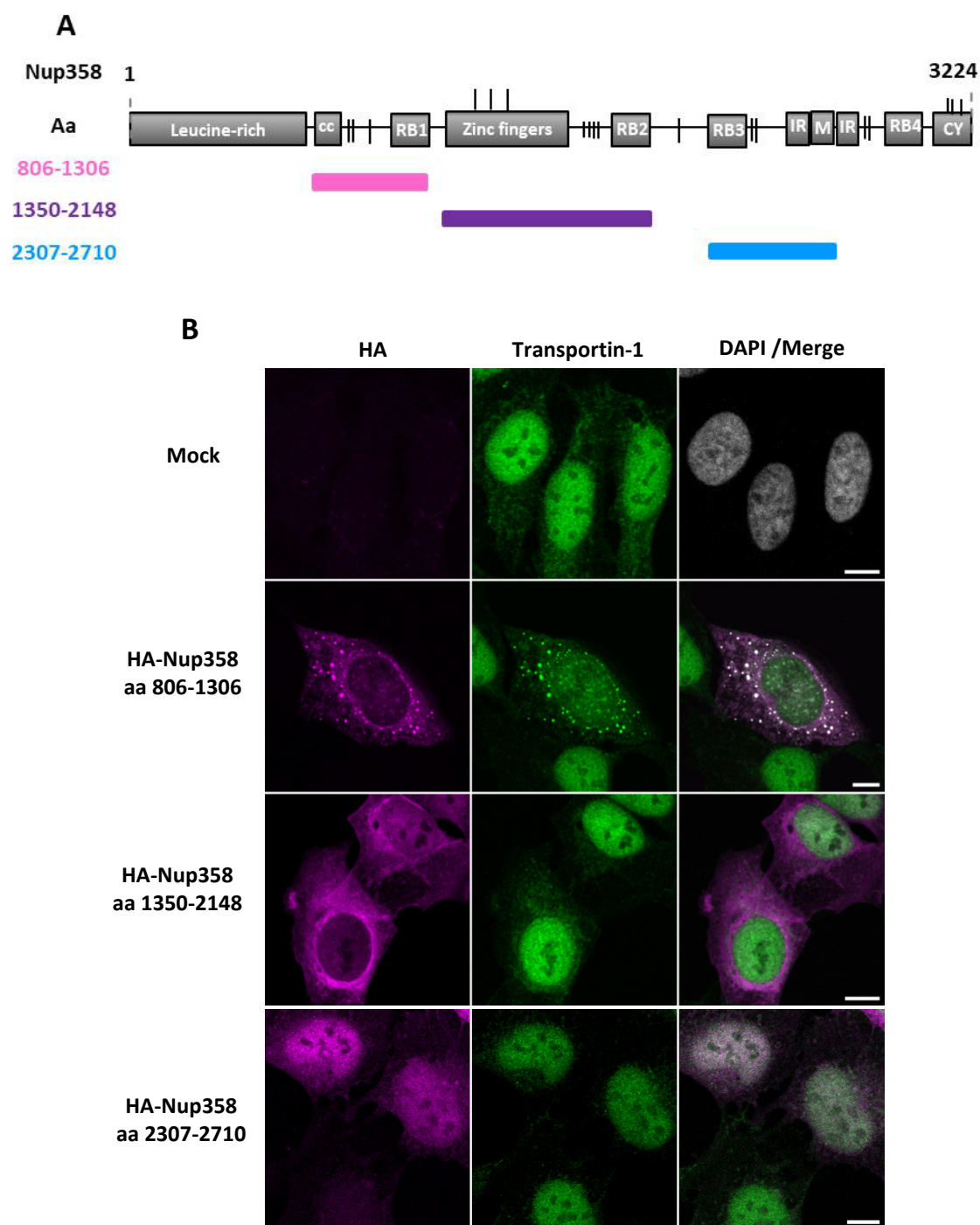


Figure 20: The N-terminal soluble fragment of Nup358 (aa 806-1306) mislocalizes transportin-1. (A) Schematic representation of the structure of Nup358. Soluble HA-tagged fragments of Nup358 used in this assay with the corresponding amino acid residues (aa) are represented in different colours. (B) Representative confocal images of endogenous TNPO-1 distribution in cells transfected with an empty plasmid (mock) or expressing the indicated HA-tagged soluble fragments of Nup358. Transfected cells were stained using specific antibodies against HA-tag (magenta) and the endogenous TNPO-1 (green). Co-localization of HA-Nup358 fragments with endogenous TNPO-1 is depicted in the right column as overlay (white signal). Maximal projection images are shown. Scale bars 10 μ m.

1.4.2. The N-terminal FG-repeat cluster of Nup358 recruits endogenous transportin-1 and importin- β

We then asked whether this recruitment was specific for transportin-1 or shared as docking site with other transport receptors. We also wondered which of the specific domain in the fragment (the coiled-coil domain, the FG-repeats or the first RanBD) was driving the recruitment. We repeated the experiment but this time focusing our analysis on the aa 806-1306 region. Cells were transfected with either the aa 806-1306 HA-tagged construct or plasmids containing shorter regions: a fragment aa 806-1170, devoid of the RanBD, a fragment comprising aa 806-1133 lacking some FG-repeats and a fragment harbouring exclusively the coiled-coil domain (**Figure 21a**). Cells were then stained using either specific antibodies against endogenous transportin-1 or importin- β . Endogenous transportin-1 localization was mainly nuclear and endogenous importin- β localized mainly at the nuclear rim in mock treated cells (**Figure 21b**). Expression of the largest fragment of aa 806-1306 caused a re-localization of both transportin-1 and importin- β towards cytoplasmic regions co-localizing with the HA-tagged fragment. The RanBD was not responsible for this redistribution since the aa 806-1170 fragment lacking this domain was still able to re-localize both endogenous importins. Removal of some FG-repeats caused only a partial redistribution of importin- β but still co-localized clearly with transportin-1. Finally, the fragment containing exclusively the coiled-coiled domain of Nup358 did not relocate any of the transport receptors tested. These results suggest that the most N-terminal cluster of FG-repeats is able to recruit at least the most common importins: importin- β and transportin-1.

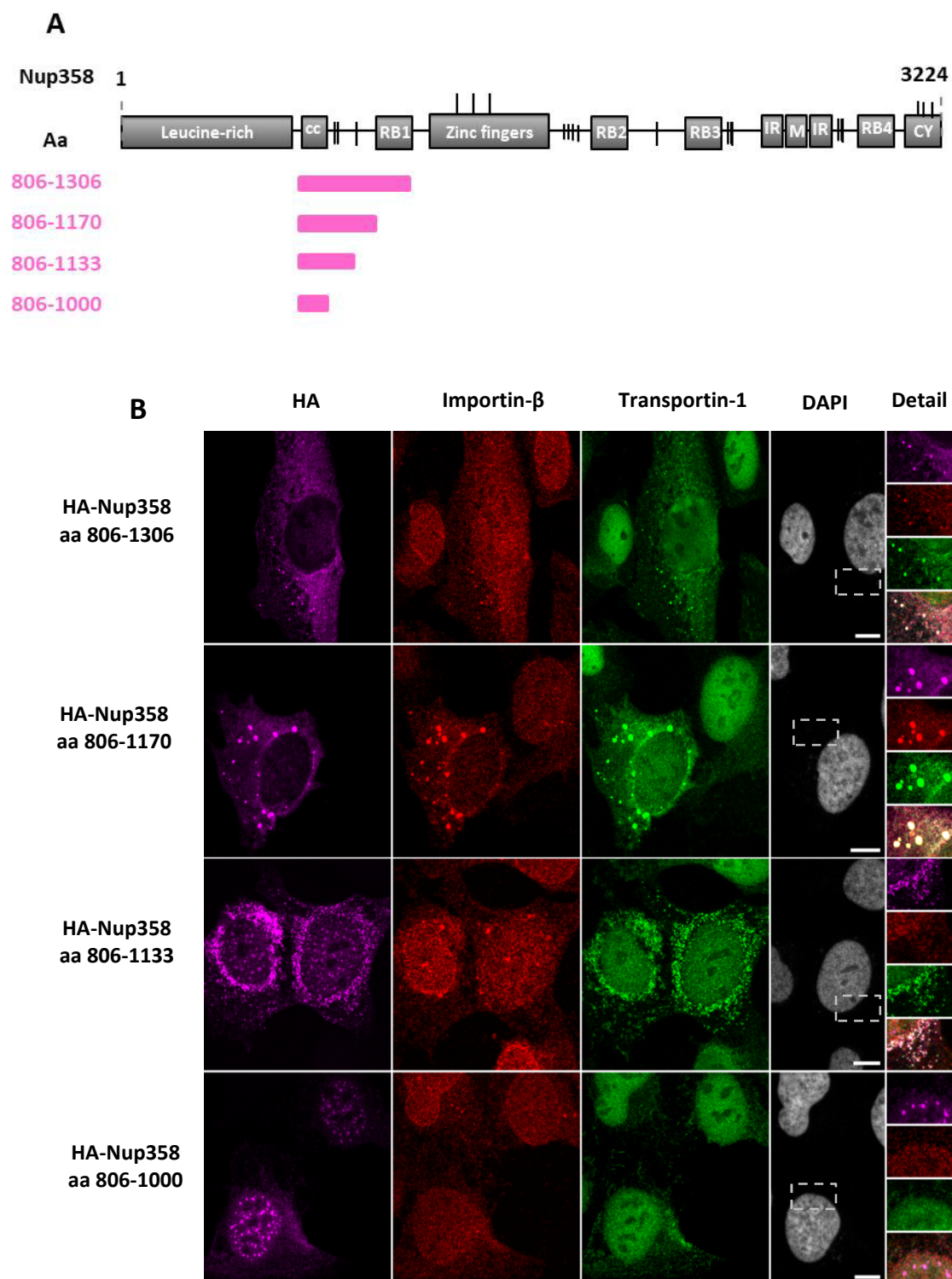


Figure 21: The N-terminal FG-repeats of Nup358 mislocalizes both transportin-1 and importin- β . (A) Schematic representation of the structure of Nup358. Soluble HA-tagged fragments of Nup358 used in this assay with the corresponding amino acid residues (aa) are represented in pink. (B) Representative confocal images of endogenous transportin-1 (TNPO-1) and importin- β distribution in cells transfected with the indicated HA-tagged soluble fragments of Nup358. Transfected cells were stained using specific antibodies against HA-tag (magenta), the endogenous importin- β (red) and the endogenous TNPO-1 (green). DAPI staining was used to visualize the chromatin. A detail of the co-localization of HA-Nup358 fragments with endogenous transport receptors is shown in the right column. Maximal projection images are shown. Scale bars 10 μ m.

To confirm that transport receptors were binding to the N-terminal region of Nup358, we perform a co-immunoprecipitation (Co-IP) assay. This time, cells were transfected with plasmids coding for different parts of Nup358: the N-terminal fragments aa 806-1306 and aa 806-1000 (containing exclusively the coiled-coil domain); a central fragment comprising the zinc finger region, FG-repeats and the second and third RanBDs (aa 1312-2557); and a C-terminal fragment (aa 2307-3047) (**Figure 22a**). Total lysates of cells expressing different fragments of Nup358 were incubated with beads coated with anti-HA antibodies. The input and the resulting anti-HA bound fraction were blotted using antibodies against either importin- β or transportin-1 (**Figure 22b**). To control the IP efficiency of the HA-tagged fragments, an anti-HA antibody was used, and in parallel, the GAPDH was detected as a loading control. Results showed a specific binding of importin- β to the N-terminal fragment aa 806-1306 confirming the observed redistribution results. In addition, importin- β also bound to the central fragment comprising the second FG-repeat cluster (aa 1312-2557), although with reduced affinity. The fragment including exclusively the coiled-coil domain did not bind importin- β . Likewise we did not observe binding for the most C-terminal fragment even though it harbours two FG-repeat clusters and RanBD 3 and 4. Unfortunately, we could not obtain conclusive results regarding binding of transportin-1 to Nup358 since a similar band corresponding to transportin-1 was observed in all the conditions included the non-transfected control. These results show that under our IP conditions, importin- β was able to specifically bind the N-terminal FG-repeat and RanBD1 containing fragment of aa 806-1306, and to a lower extent the adjacent central fragment of aa 1312-2557, which also harbours a FG-repeat cluster and RanBD2 and 3, but not the C-terminal fragment containing equivalent domains, suggesting a higher specificity of the N-terminal half of Nup358 in recruiting endogenous importin- β . In contrast, we were unable to confirm specific transportin-1 binding under these conditions.

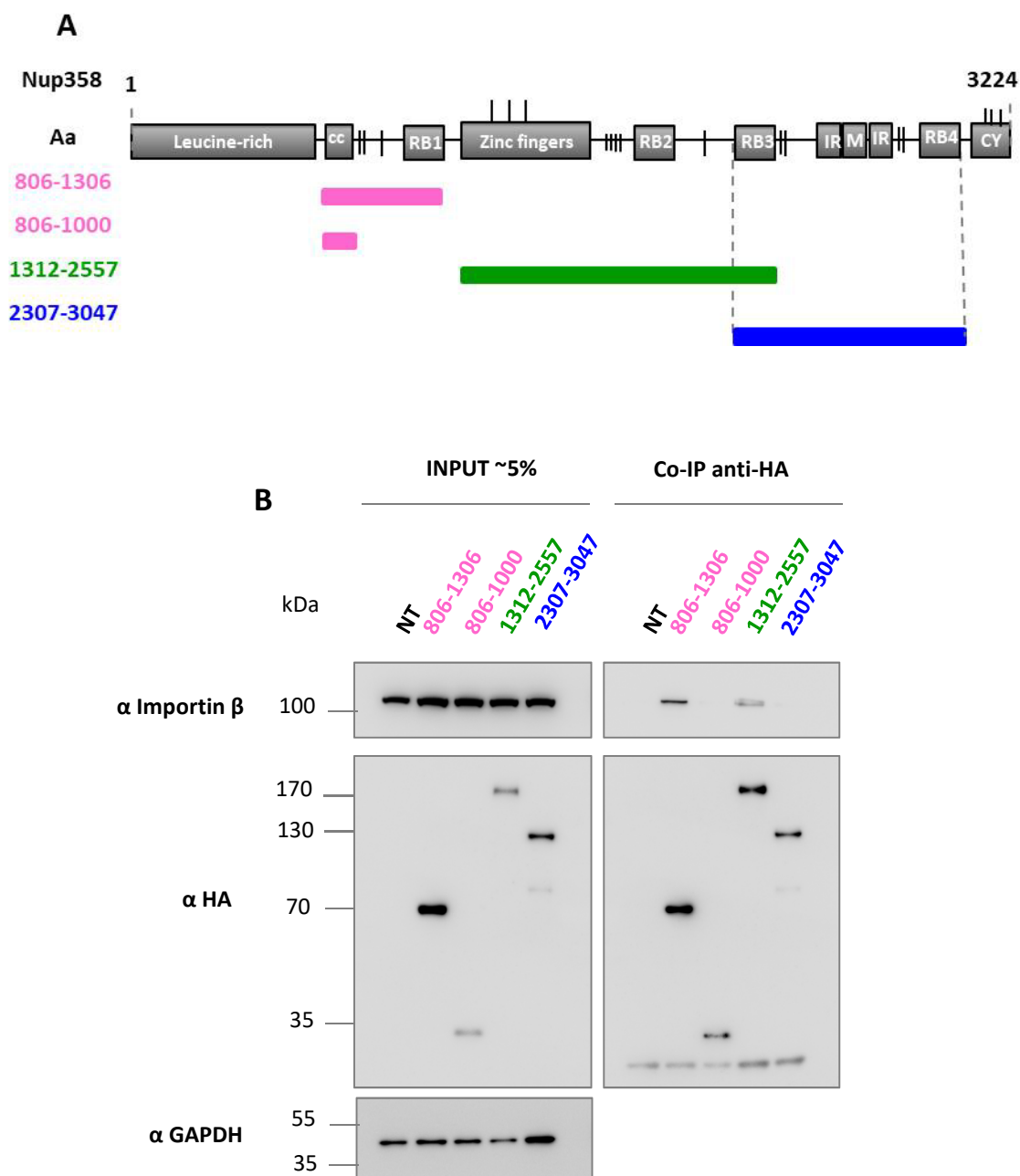


Figure 22: The N-terminal soluble fragment of Nup358 (aa 806-1306) binds endogenous importin- β . (A) Schematic representation of the structure of Nup358. Soluble HA-tagged fragments of Nup358 used in this assay with corresponding amino acid residues (aa) are represented in different colours. (B) WB of lysates of HEK293- α V β 5 non-transfected (NT) or transfected with HA-tagged soluble fragments of Nup358 (left panel) and Co-IP of HA-Nup358 fragments and interacting importin- β . Cells were transfected with the indicated constructs and proteins were precipitated from total lysates using anti-HA coated beads. Input and bound fractions were separated by SDS-PAGE and proteins were detected using specific antibodies against HA-tag, importin- β and the GAPDH as loading control.

1.4.3. The N-terminal half of Nup358 is not sufficient to tether CRM1 to the NPC.

We next wanted to understand the possible contribution of the zinc finger domain included in the NPC-anchored N-terminal fragment of Nup358 necessary to restore an efficient import of the AdV genome into the nucleus (**Figure 23b**). This region has been shown to bind the exportin CRM1 (Singh et al., 1999). Previous work showed that depletion of Nup358 leads to mislocalization of CRM1 from the nuclear rim (Bernad et al., 2004), however this mislocalization seems to be dispensable for CRM1 export function (Hutten and Kehlenbach, 2006). Moreover, CRM1 was shown to be critical for translocation of AdV particles towards the NPC, through an unknown mechanism (Strunze et al., 2005). We thus asked whether the N-terminal zinc finger containing fragment of Nup358 contributes to the import AdV genomes by facilitating accumulation of CRM1 at the NPC. To test this, cells were depleted for Nup358 by siRNA and transfected with either the HA-tagged N-terminal fragment necessary for restoring AdV genome import efficiency (aa 1-1810); the immediately shorter, without the zinc finger region (aa 1-1306); or the immediately longer, comprising the second FG-repeat cluster and the RanBD2 (aa 1-2148) (**Figure 23a**). Cells were then stained for the HA-tag, to confirm fragment transfection and localization; for the endogenous Nup358, to confirm the knock-down efficiency; and CRM1, using specific antibodies. Fluorescence of both endogenous Nup358 and CRM1 was reduced in cells treated with specific siRNAs against Nup358 (**Figure 23b**). None of the N-terminal Nup358 constructs tested was able to efficiently accumulate endogenous CRM1 at the NE, consistent with previous observations (Hamada et al., 2011). The fragment containing the zinc finger domain and accessory FG-repeats and RanBD2, showed clear co-localization with CRM1 in dot like structures in cytosolic regions, contrary to other fragments tested. However, levels of endogenous CRM1 at the NE were still reduced compared to control cells.

Taken together, these results show that the N-terminal half of Nup358 harbours a FG-repeat region able to recruit importin- β and transportin-1. CRM1 instead could not be recruited by the N-terminal half of Nup358. Additional downstream FG-repeats were required to tether CRM1 to the N-terminal fragment of Nup358 but still accumulation of CRM1 at the NE was not as efficient as in control cells conserving the endogenous Nup358, suggesting that the docking site for CRM1 is located within the C-terminal part of Nup358, in agreement with previous observations (Hamada et al., 2011). Thus, the NPC-anchored fragment comprising aa 1-1810 could favour import complex formation with incoming AdV cores in two ways: by providing binding sites for importins, and/or by enhancing recycling of transport receptors. It

is however unlikely that Nup358 facilitates AdV genome import by supporting accumulation of CRM1 at the NPC.

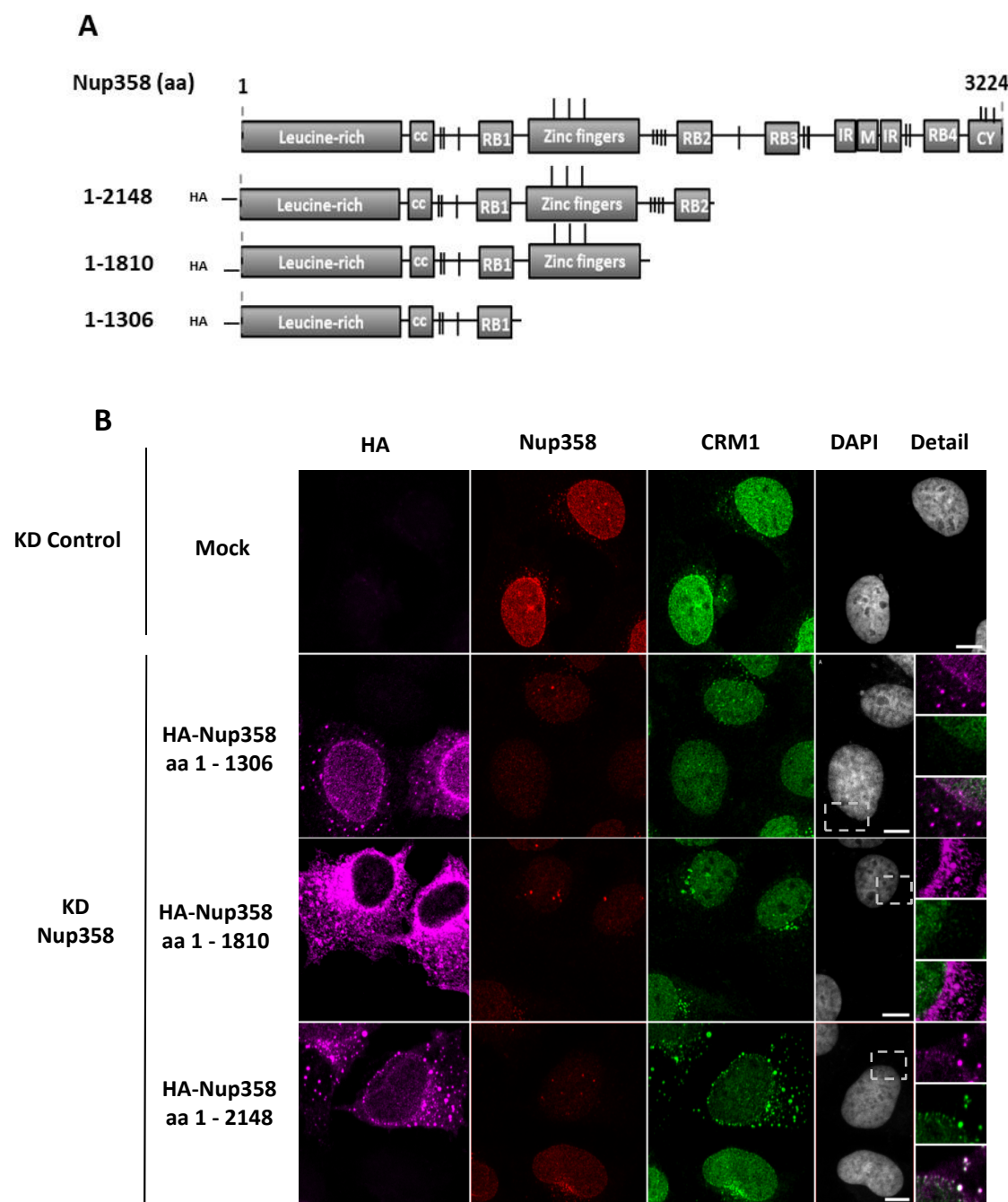


Figure 23: The N-terminal half of Nup358 is not sufficient to target CRM1 to the NPC. (A) Schematic representation of the structure of Nup358. NPC-anchoring HA-tagged fragments of Nup358 used in this assay with the corresponding amino acid residues (aa) are indicated to the left of the scheme. (B) Representative confocal images of endogenous CRM1 distribution in control or Nup358-depleted cells transfected with an empty plasmid (mock) or with the indicated HA-tagged soluble fragments of Nup358. Cells were stained using specific antibodies against HA-tag (magenta), the endogenous Nup358 (red) and the endogenous CRM1 (green). DAPI staining was used to visualize the chromatin. A detail of the co-localization of HA-Nup358 fragments with endogenous CRM1 is shown in the right column depicted as overlay (white signal). Maximal projection images are shown. Scale bars 10 μ m.

2. THE ROLE OF CRM1 IN ADV GENOME DELIVERY

A major role for CRM1 in translocation of AdV capsids from the MTOC to the NPC was shown by treating infected cells with Leptomycin B (LMB) (Strunze et al., 2005). Under LMB condition AdV capsids accumulate at the MTOC and no genome import is observed. LMB covalently binds to a cysteine present in the cargo-binding pocket of CRM1 avoiding interaction with NES-containing cargo (Kudo et al., 1999). However, the mechanism by which CRM1 promotes translocation of the capsid from the MTOC to the NPC and whether it is directly involved or indirectly via a CRM1-dependent cargo is still unclear. CRM1 is able to interact with Nups upon nuclear export as a component of the export complex (Nup214 (Port et al., 2015); Nup358 (Ritterhoff et al., 2016)) or after export complex disassembly (Nup358, (Singh et al., 1999; Hutten and Kehlenbach, 2006)). Since Nup214 act as docking site for incoming AdV capsids (Cassany et al., 2015; Trotman et al., 2001), it is possible that CRM1 links the arrival of AdV capsids at the periphery of the nuclear envelope and NPC-anchoring through interactions with Nups. To study the function of CRM1 in AdV genome delivery, we used NPC non-anchored fragments of the main cytoplasmic components of the NPC: Nup358 and Nup214; and analyzed their effect on AdV genome delivery in interphase and mitotic cells, in which nuclear compartmentalization is suspended.

2.1. Soluble fragments of cytoplasmic Nups impair AdV genome delivery in interphase

Cytoplasmic FG-repeat containing Nups, Nup358 and Nup214, have been shown to bind the main export receptor CRM1. Nup358 has been shown to be principally involved in import but not in export (Hutten et al., 2008, 2009; Hamada et al., 2011; Wälde et al., 2012). For Nup214 it is the opposite (Bernad et al., 2006; Hutten and Kehlenbach, 2006), although it is able to bind a subset of import receptors (Moroianu et al., 1995; Yaseen and Blobel, 1997). A recent study showed the crystal structure of the export complex, including CRM1 bound to a FG-repeat-containing C-terminal fragment of Nup214 (Port et al., 2015). No crystal structure has yet been reported for the Nup358-CRM1 complex. Nevertheless, biochemical studies have identified two binding sites for CRM1 on Nup358: the first at the zinc finger central region (Singh et al., 1999), and the second at the FG-repeat-containing C-terminal region of Nup358 (Ritterhoff et al., 2016). Binding of CRM1 export complexes to the C-terminal region of both cytoplasmic Nups involves several FG-repeats. This binding is functionally different: while binding to Nup214 stabilizes the export complex, the Nup358 binding disassembles the

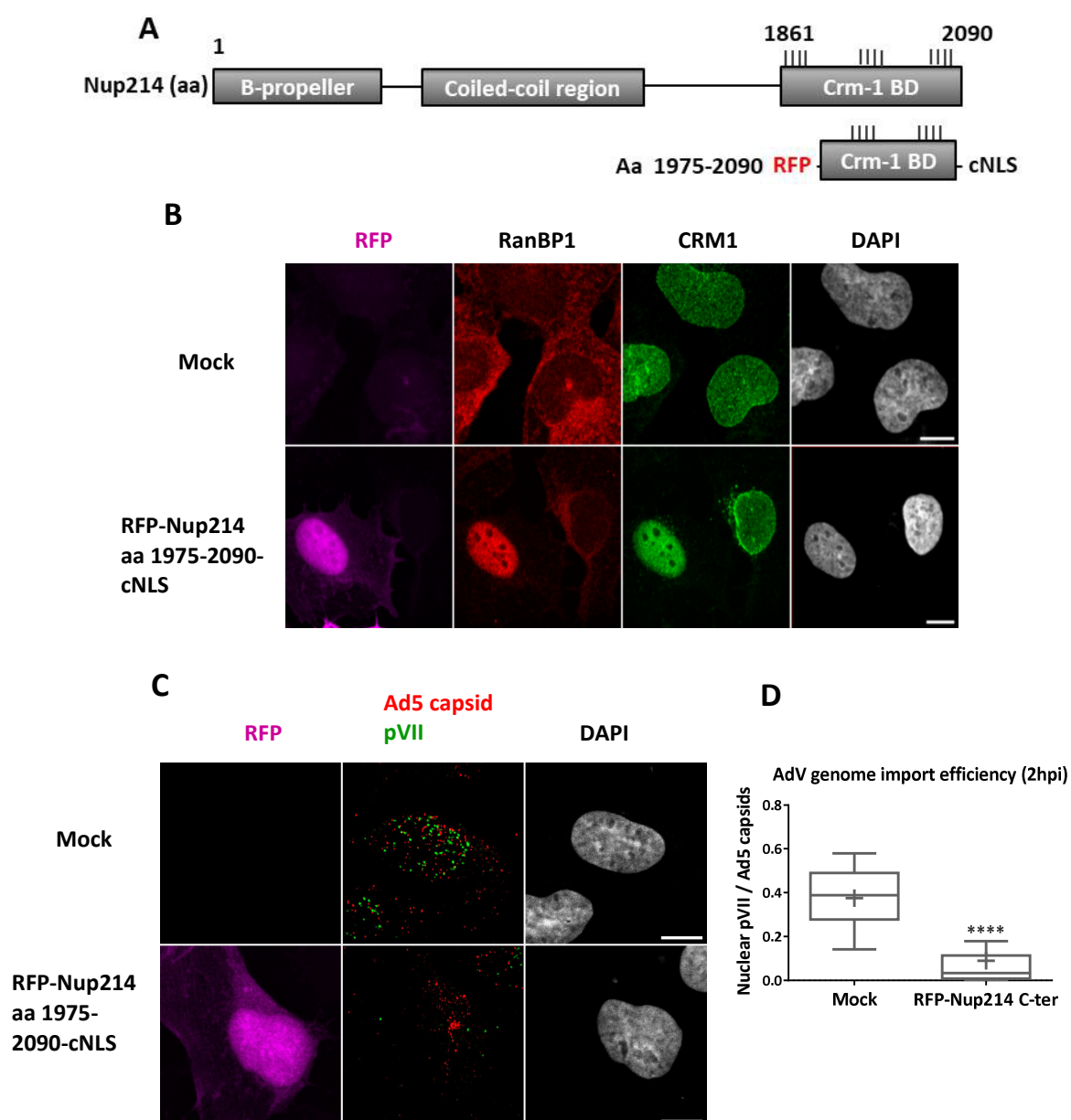
export complex. Stabilization of CRM1 export complexes by Nup214 is an essential step for export of some cargos like NFAT or HIV-1 Rev, presumably to avoid premature disassembly of the complex before reaching the cytosolic compartment (Hutten and Kehlenbach, 2006). Disassembly of export complexes by Nup358 could be a redundant alternative in general nuclear export since soluble RanGAP and RanBP1 are also able to facilitate the export complex dissociation (Hutten et al., 2008). Finally, binding of CRM1 to alternative central sites of Nup358 occurs in a RanGTP- and LMB-independent manner (Singh et al., 1999) so it has been proposed to bind empty CRM1 before being recycled back to the nucleus (Bernad et al., 2004; Engelsma et al., 2004). Because it was reported that AdV requires functional CRM1 to dock at the NPC (Strunze et al., 2005; Wang et al., 2017) we decided to investigate the implication of CRM1 interaction with cytosolic Nups on AdV genome delivery focusing on Nup358.

2.1.1. The C-terminal CRM1-binding fragment of Nup214 disrupts nuclear targeting of AdV capsids

To study the role of CRM1 in AdV genome delivery and investigate whether Nup binding to CRM1 was important during this process, we first used a fragment of Nup214 which is known to act as dominant negative for CRM1-dependent export by entrapping CRM1 inside the nucleus. Nup214 harbours a FG-repeat enriched region at its C-terminal extremity (**Figure 24a**). Within this region, there are 3 FG-repeat clusters included between the aa 1916 to 2033, that mediate binding with several FG-binding pockets of CRM1 (Port et al., 2015). Characterization of the Nup214-CRM1 interaction revealed that a shorter fragment comprising the last two FG-repeat patches (aa 1968-2033) was still able to bind CRM1 and was more appropriate to study the binding defects of CRM1 mutants (Port et al., 2015). Expression of this shorter fragment in cells was shown to specifically impair CRM1-mediated nuclear export (Roloff et al., 2013). Hence, we decided to use the shorter C-terminal fragment of Nup214 including the second and third FG-patches, comprising aa 1975-2090 (**Figure 24a**), to see whether it could also compete with AdV genome delivery. First, we wanted to confirm whether overexpression of this C-terminal fragment impaired export of the NES-containing cargo RanBP1. The C-terminal fragment of Nup214 used in this experiment contained a RFP-tag at the N-terminus and a cNLS at the C-terminal extremity. Cells expressing this fragment or mock treated were stained using specific antibodies against endogenous RanBP1 and CRM1. Results showed again a cytosolic localization of RanBP1 in control cells, contrary to cells expressing the nuclear RFP-Nup214 C-terminal fragment,

which redistributed RanBP1 to the nucleus confirming its specific inhibitory function (**Figure 24b**). Upon expression of the C-terminal Nup214 fragment, endogenous CRM1 lost the rim-staining present in control cells and got trapped inside the nucleus. We next analyzed the efficiency of AdV genome delivery in cells expressing the Nup214 fragment. For this purpose, we followed our infection protocol and stained cells for AdV capsids and pVII. As expected, a clear accumulation of capsids was observed at 2 hpi, coinciding with the presumed location of the MTOC, which resulted in strong impairment of AdV genome import **Figure 24c and d**.

These results confirmed that the C-terminal fragment of Nup214 trap endogenous CRM1 inside the nucleus thereby blocking CRM1-dependent export. Specific impairment of CRM1 thus, blocks AdV genome docking at the NPC with the consequence of impairing AdV genome import into the nucleus.



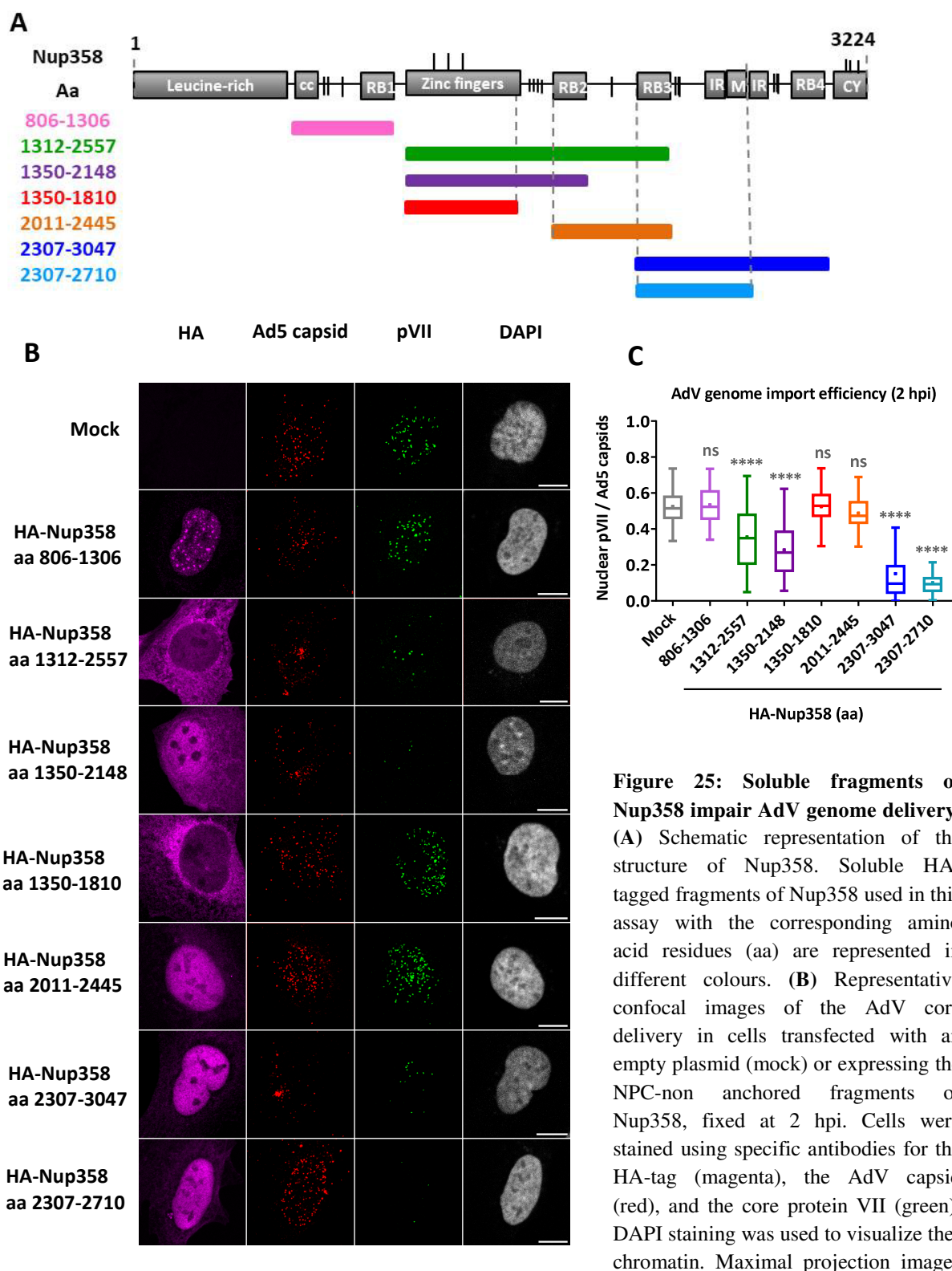
2.1.2. Soluble fragments of Nup358 impair AdV genome delivery

Because Nup358 also provides binding sites for CRM1 (Singh et al., 1999; Ritterhoff et al., 2016), we tested whether different soluble fragments of Nup358 (NPC-non-anchored fragments) could also compete with AdV translocation to the NPC. With this aim, cells were transfected with different HA-tagged soluble fragments (**Figure 25a**) and infected with Ad5-wt-GFP vectors. Cells were stained using specific antibodies against viral pVII, Ad5 capsids and HA, and efficiency of viral genome import was then calculated for 2 hpi. Results showed that overexpression of the construct containing the non-binding region of Nup358 to CRM1 of aa 806-1306 (able to recruit import receptors) allowed delivery of AdV genomes as efficiently as in mock treated cells (**Figure 25b and c**). The central region containing the zinc fingers-CRM1 binding site (aa 1312-2557) instead caused a statistically significant decrease in AdV genomes accumulating in the nucleus. Furthermore, an accumulation of viral capsids could be observed at one discrete location near the NE, presumably the MTOC. These effects were not due to an excess of the kinesin-1 binding domain of Nup358 (JX2) nor the third RanBD, since the shorter soluble fragment of aa 1350-2148 devoid of these domains also caused an accumulation of viral capsids at the specific location near the NE, preventing efficient AdV genome delivery. In contrast, the soluble fragment of Nup358 consisting exclusively of the zinc finger domain (aa 1350-1810) did not affect neither AdV genome delivery nor capsid distribution. This was also the case for the fragment of aa 2011-2445 containing the JX2 domain flanked by the second and third RanBDs. These results suggested that at least the zinc finger domain and the adjacent central FG-repeat patch and RanBD2 were necessary to compete with AdV genome delivery by sequestration of the capsids at the presumed MTOC location.

Figure 24: The C-terminal CRM1-binding fragment of Nup214 competes with AdV genome delivery. (A) Schematic representation of the structure of Nup214. Soluble RFP-tagged fragment of Nup214 used in this assay with corresponding amino acid residues (aa) indicated to the left of the scheme. (B) Representative confocal images of endogenous CRM1 and RanBP-1 distribution. Cells were transfected with an empty plasmid (mock) or with the indicated soluble RFP-tagged C-terminal fragment of Nup214 (magenta). Cells were stained using specific antibodies against RanBP1 (red) and CRM1 (green). (C) Representative confocal images of the AdV core delivery in mock-treated or cells expressing the C-terminal fragment of Nup214 fixed at 2 hpi. Cells were stained using specific antibodies to detect the AdV capsid (red), and the core protein VII (green). (D) Quantification of AdV genome import efficiency in mock or cells expressing the C-terminal fragment of Nup214, calculated as the number of nuclear pVII dots relative to the total amount of AdV capsids per cell. Data obtained from individual cell values (n>25 per condition) were represented in a Tukey box plot. Results were analyzed using a two-tailed T-test. *****: P < 0,0001 (B-C) DAPI staining was used to visualize the chromatin. Maximal projection images are shown. Scale bars 10 μ m.

Interestingly, when we transfected cells with constructs containing the C-terminal part of Nup358 we also impaired AdV genome delivery. The longer fragment flanked by the RanBD 3 and 4 and therefore, comprising the two FG-repeat clusters and the E3 ligase activity (aa 2307-3047), strongly impaired AdV genome delivery compared to control cells. This effect was accompanied by a prominent accumulation of capsids at the presumed MTOC. In contrast the shorter C-terminal fragment of Nup358 (aa 2307-2710), which neither contained the fourth RanBD nor the Nup component of the mature E3-ligase activity complex (Werner et al., 2012) or the second patch of FG-repeats necessary for CRM1 binding (Ritterhoff et al., 2016) also caused a strong impairment of AdV genome delivery compared to control cells. Different from the longer C-terminal fragment, capsid distribution was normal and no MTOC accumulation could be observed, suggesting that this fragment impaired AdV genome import through different mechanisms.

These results showed that regions containing the described binding sites for CRM1 in Nup358 and Nup214 competed for efficient AdV genome import and accumulate viral capsids at a discrete location near the NE. In the case of central region of Nup358, the minimal fragment responsible of this impairment included not only the zinc finger domain but also an extended FG-repeats-containing region. In addition, we observed a strong impairment of AdV genome delivery in presence of an excess of the C-terminal CRM1 non-binding region of Nup358 comprising aa 2307-2710. This fragment did not compete with AdV translocation but presumably with a downstream step involved in AdV genome delivery.



are shown. Scale bars 10 μ m. (C) Quantification of AdV genome import efficiency in control or cells expressing the soluble fragments of Nup358, calculated as the number of nuclear pVII dots relative to the total amount of AdV capsids per cell. Data obtained from individual cell values, from three different experiments ($n > 30$ per condition) are represented in a Tukey box plot. Results were analyzed using a one-way ANOVA test and Tukey's multiple comparisons post hoc test. ****: $p < 0,0001$; ns $> 0,05$.

2.1.3. CRM1-binding fragments of Nup358 induce accumulation of AdV capsids at the MTOC

Previous studies showed that inhibition of CRM1 by LMB treatment leads to an accumulation of AdV capsids at the MTOC, blocking their translocation to the NPC with subsequent inhibition of the infection (Strunze et al., 2005). We thus wanted to confirm whether the accumulation of AdV capsids in presence of CRM1-binding fragments of Nup358 was indeed located at the MTOC. Cells expressing soluble fragments of Nup358 for which we have observed an inhibition of AdV genome delivery (the central aa 1350-2148, and both C-terminal fragments of aa 2307-3047 and 2307-2710; **Figure 26a**) were infected with Ad5-wt GFP vector during 2 h. Cells were stained for endogenous pericentrin, which is a protein located at the MTOC. Infected cells treated with LMB were used as a positive control for AdV capsid accumulation at the MTOC. Results showed that in non-treated control cells, capsids had already reached the nucleus and distributed around the nuclear membrane (**Figure 26b**). In contrast, cells treated with LMB showed a clear co-localization of AdV capsids at the MTOC. Similarly, cells overexpressing CRM1-binding sites of Nup358 (aa 1350-2148 and aa 2307-3047) induced an accumulation of AdV capsids co-localizing with pericentrin staining. Opposing effect was observed in cells expressing an excess of the short C-terminal fragment of aa 2307-2710, which strongly impaired AdV genome delivery in the previous experiment (**Figure 25c**), but did not cause an abnormal distribution of capsids and no co-localization with pericentrin was observed (**Figure 26b**).

These results confirm that CRM1 binding fragments of Nup358 compete with proper AdV genome delivery by inducing an accumulation of AdV capsids at the MTOC. In contrast, the shorter C-terminal CRM1 non-binding fragment of Nup358 did not block AdV particles at the MTOC, confirming that this fragment is not a dominant negative for AdV capsid targeting to the NPC, but for a downstream event during AdV genome delivery.

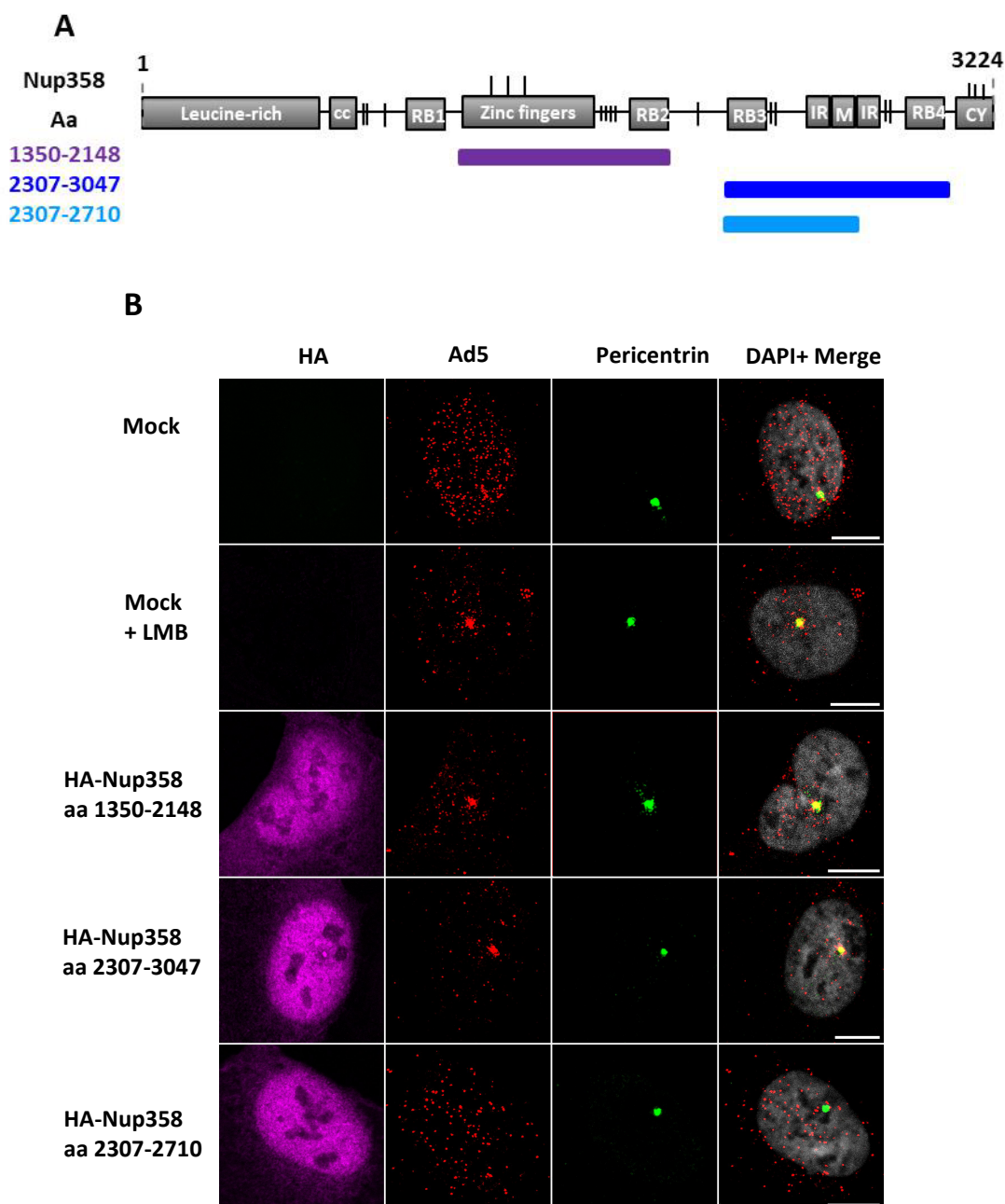


Figure 26: Soluble CRM1-binding fragments of Nup358 induce accumulation of AdV capsids at the MTOC. (A) Schematic representation of the structure of Nup358. Soluble HA-tagged fragments of Nup358 used in this assay with the corresponding amino acid residues (aa) are represented in different colors. (B) Representative confocal images of AdV particle distribution with respect of the MTOC in cells transfected with an empty plasmid (mock) or expressing the indicated HA-tagged soluble fragments of Nup358. LMB treatment was used as a positive control inducing the accumulation of AdV capsids at the MTOC. Transfected cells were stained using specific antibodies for HA-tag (magenta), AdV capsid (red) and the endogenous pericentrin to visualize the MTOC (green). DAPI staining was used to visualize the chromatin. Co-localization of the viral particles with the MTOC is shown in the right column (yellow). Maximal projection images are shown. Scale bars 10 μ m.

2.1.4. CRM1-binding fragments of Nup358 disrupt CRM1 export function necessary for nuclear targeting of AdV.

CRM1 is the major exportin in human cells. We therefore asked whether soluble CRM1-binding fragments of Nup358 could impair the export function of CRM1, which in turn could be required for AdV genome delivery. To monitor functional protein export in cells, we used the well-known CRM1 NES-cargo RanBP1 as a reporter protein which is found in the cytosol in steady-state (Richards et al., 1996). We included in the analysis several soluble fragments of Nup358 (**Figure 27a**): the central CRM1-binding fragment of aa 1170-2148 that also caused an accumulation of AdV capsids at the MTOC; the zinc finger domain (aa 1350-1810) which did not; and the two C-terminal soluble fragments (aa 2307-3047 and 2307-2710). Cells were either transfected with HA-Nup358 fragments or mock treated and stained for endogenous RanBP1 and CRM1. Control cells showed a clear cytosolic and diffused distribution of RanBP1, reflecting normal protein export (**Figure 27b**). In contrast, export of RanBP1 was disrupted upon specific inhibition of CRM1 by LMB treatment, resulting in a predominant nuclear staining for the CRM1 cargo RanBP1. In both, treated and non-treated cells with LMB, endogenous CRM1 was distributed forming the characteristic rim-staining at the nuclear membrane. Interestingly, in presence of either the central or the C-terminal CRM1-binding fragments of Nup358, endogenous RanBP1 distribution switched to a predominantly nuclear localization, and similarly, endogenous CRM1 disappeared from the cytoplasmic side of the nuclear envelope becoming trapped inside the nucleus. On the contrary, the soluble fragment containing exclusively the zinc finger region was not able to trap CRM1 inside the nucleus and protein export occurred normally regarding RanBP1 distribution. Similar results were observed in cells expressing the C-terminal fragment of Nup358 not able to bind CRM1.

Taken together, these results show that soluble CRM1-binding fragments of Nup358, similar to Nup214, prevent endogenous CRM1 localization at the cytoplasmic side of the NE and act as dominant negatives for CRM1 export function, which in turn, is necessary for correct targeting of AdV capsids to the nucleus. Thus, nuclear retention of CRM1 inside the nucleus is not an effect specific for a single Nup and it is induced by CRM1-binding fragments regardless of the functional context of the CRM1-Nup binding. In addition, we observed that the zinc finger region by itself is not sufficient to neither retain CRM1 inside the nucleus nor block CRM1 export function, and thus, it does not alter AdV genome delivery. Finally, the C-terminal part of Nup358 harbours the region of aa 2307-2710 that even though its overexpression does not affect CRM1-dependent protein export, it strongly impairs AdV

genome delivery at a downstream step of nuclear targeting of the AdV capsids, presumably in a CRM1-independent manner.

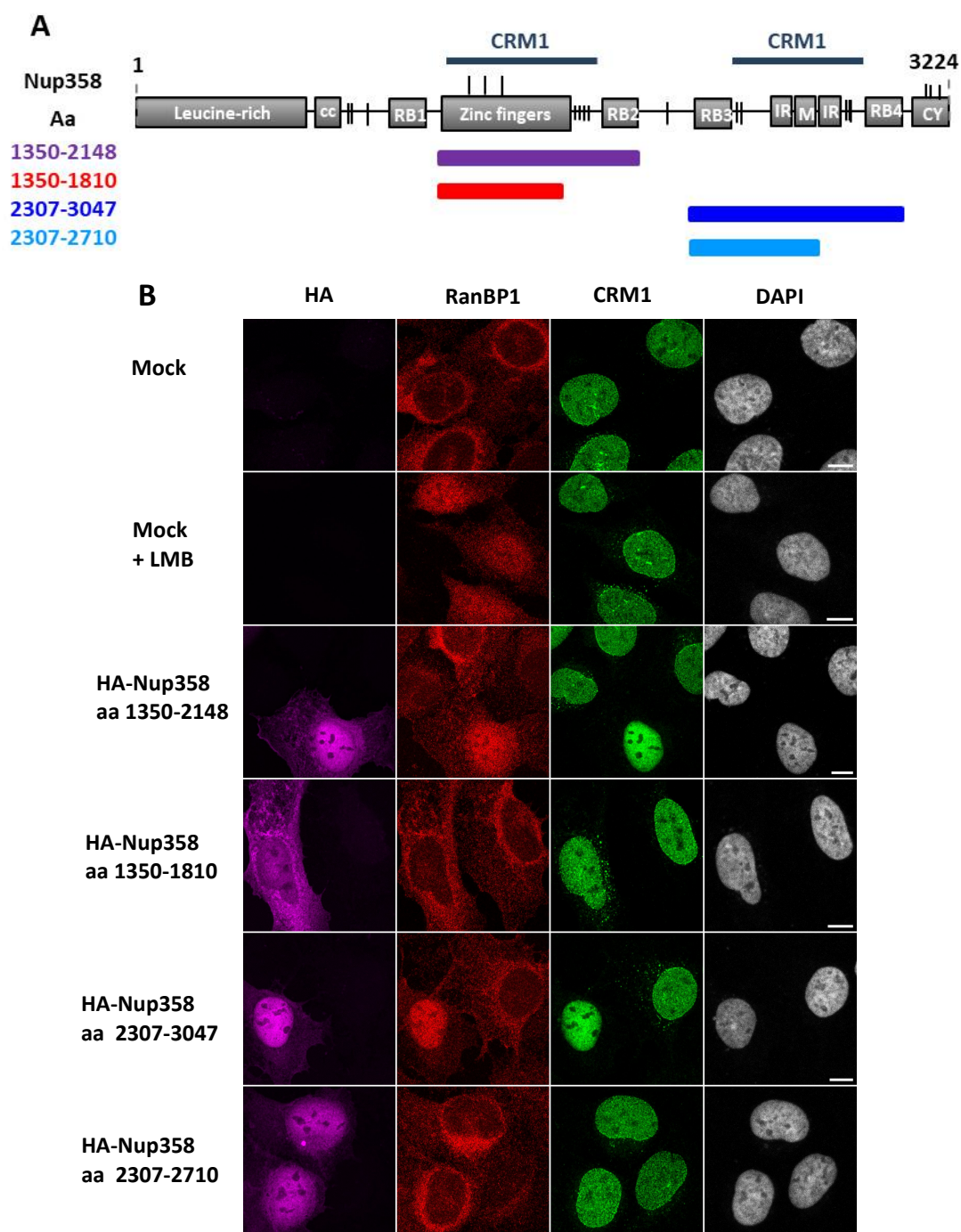


Figure 27: CRM1-binding fragments of Nup358 disrupt CRM1 export function. Cells expressing CRM1-binding fragments of Nup358 trap CRM1 inside the nucleus, blocking CRM1-dependent export of RanBP1 (A) Schematic representation of the structure of Nup358 with the described binding sites for CRM1 represented with bars above the scheme. Soluble HA-tagged fragments of Nup358 used in this assay with the amino acid residues (aa) comprised are represented in different colors below the scheme. (B) Representative confocal images of endogenous CRM1 and RanBP-1 distribution in cells transfected with an empty plasmid (mock) or with the indicated soluble Nup358 fragments. LMB treatment was used as a positive control for specific inhibition of CRM1-dependent export pathway. Cells were stained using specific antibodies for HA-tag (magenta), endogenous RanBP1 (red) and CRM1 (green). DAPI staining was used to visualize the chromatin. Maximal projection images are shown. Scale bars 10 μ m.

2.1.5. The C-terminal fragment of Nup358 impairs AdV genome delivery in a CRM1-dependent and -independent manner.

We have observed that soluble fragments of Nup358 impair AdV genome delivery at two levels: translocation of AdV capsids to the nucleus and at an undetermined downstream step. We decided to focus on the C-terminal part of Nup358 and ask whether effects caused by the two analyzed fragments were CRM1-dependent or not. If the competition with AdV genome import induced by overexpression of both C-terminal Nup358 fragments is CRM1-dependent in both cases, an excess of CRM1 might be able to bypass the import defects and restore AdV genome delivery. To investigate which effect induced by fragments was dependent on CRM1, cells were co-transfected with GFP-tagged C-terminal fragments of Nup358 (aa 2307-3047 or 2307-2710; **Figure 28a and 29a**), together with an HA-tag construct of CRM1. Cells were transduced with Ad5-wt-GFP and stained using specific antibodies for the HA-tag to visualize exogenous CRM1, and to detect either pVII or AdV capsids. GFP-tagged C-terminal Nup358 constructs showed predominant nuclear localization, similar to previously used HA-tagged fragments (**Figures 28b**). Firstly, we analysed the nuclear accumulation of viral pVII under different conditions (**Figure 28b**). Overexpression of CRM1 or the GFP-tag alone did not cause any impairment of AdV genome delivery. Furthermore, we could confirm that both C-terminal CRM1-binding and non-binding fragments of Nup358 prevent nuclear accumulation of AdV genomes, meaning that the N-terminal GFP-tag did not modify their competition activity. Strikingly, co-transfection of HA-CRM1 with either the larger or the shorter C-terminal fragment of Nup358 did not restore the impairment of nuclear accumulation of AdV genomes.

Similar experiment was performed to analyze AdV capsid distribution. Again, we observed an accumulation of AdV capsids at the MTOC when expressing the larger CRM1-binding fragment of Nup358 (**Figure 29b**). The shorter fragment, on the other hand, did not impair nuclear targeting of AdV capsids, similar to the HA-tagged construct. Interestingly, an excess of HA-CRM1 in cells co-expressing the largest C-terminal fragment of Nup358 reversed MTOC accumulation of AdV capsids. In parallel, AdV capsid distribution in the condition in which the shorter C-terminal fragment was co-transfected with HA-CRM1 stayed unaltered.

These results show that AdV capsid accumulation at the MTOC induced by the larger CRM1-binding C-terminal fragment of Nup358 (aa 2307-3047) is caused by specific impairment of CRM1. Hence, excess of CRM1 could overcome the defect on nuclear translocation of AdV capsids and unmasked a competition effect caused downstream of nuclear AdV capsid targeting by the shorter C-terminal region (aa 2307-2710) which was independent of CRM1.

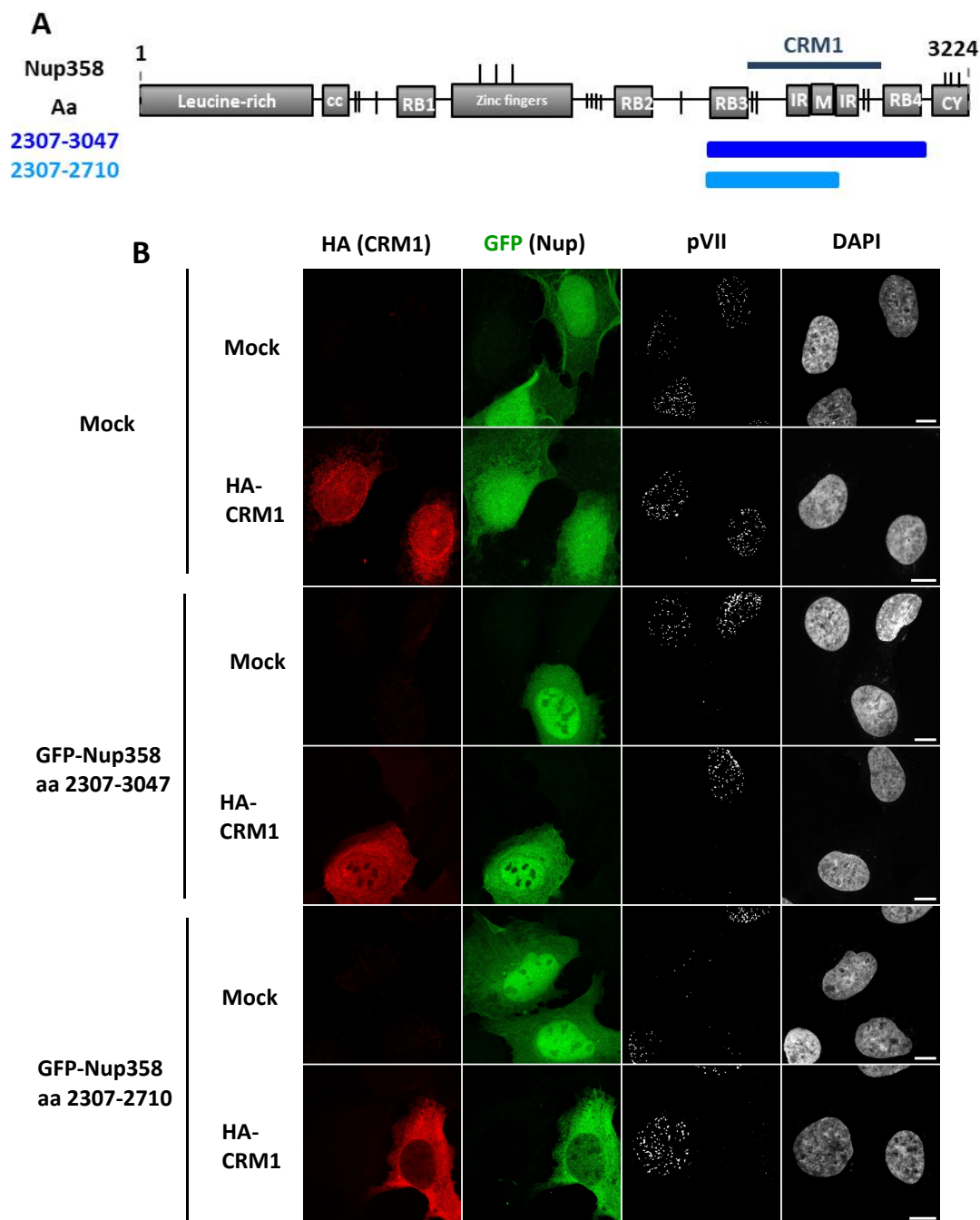


Figure 28: The C-terminal fragments of Nup358 impair nuclear accumulation of AdV cores in a CRM1-dependent and -independent manner. Cells expressing C-terminal fragments of Nup358 prevent pVII detection in the nucleus (A) Schematic representation of the structure of Nup358 with the binding site for CRM1 indicated at the C-terminal region of Nup358. Soluble HA-tagged fragments of Nup358 used in this assay with the corresponding amino acid residues (aa) are represented in different colors below the scheme. (B) Representative confocal images of nuclear accumulation of AdV cores in cells co-transfected with an empty plasmid (mock) or with HA-CRM1 and with an GFP-empty plasmid or with the indicated soluble GFP-tagged Nup358 fragments (green). Cells were stained using specific antibodies for HA-tag to detect exogenous CRM1 (red), and for pVII (grey dots). DAPI staining was used to visualize the chromatin. Maximal projection images are shown. Scale bars 10 μ m.

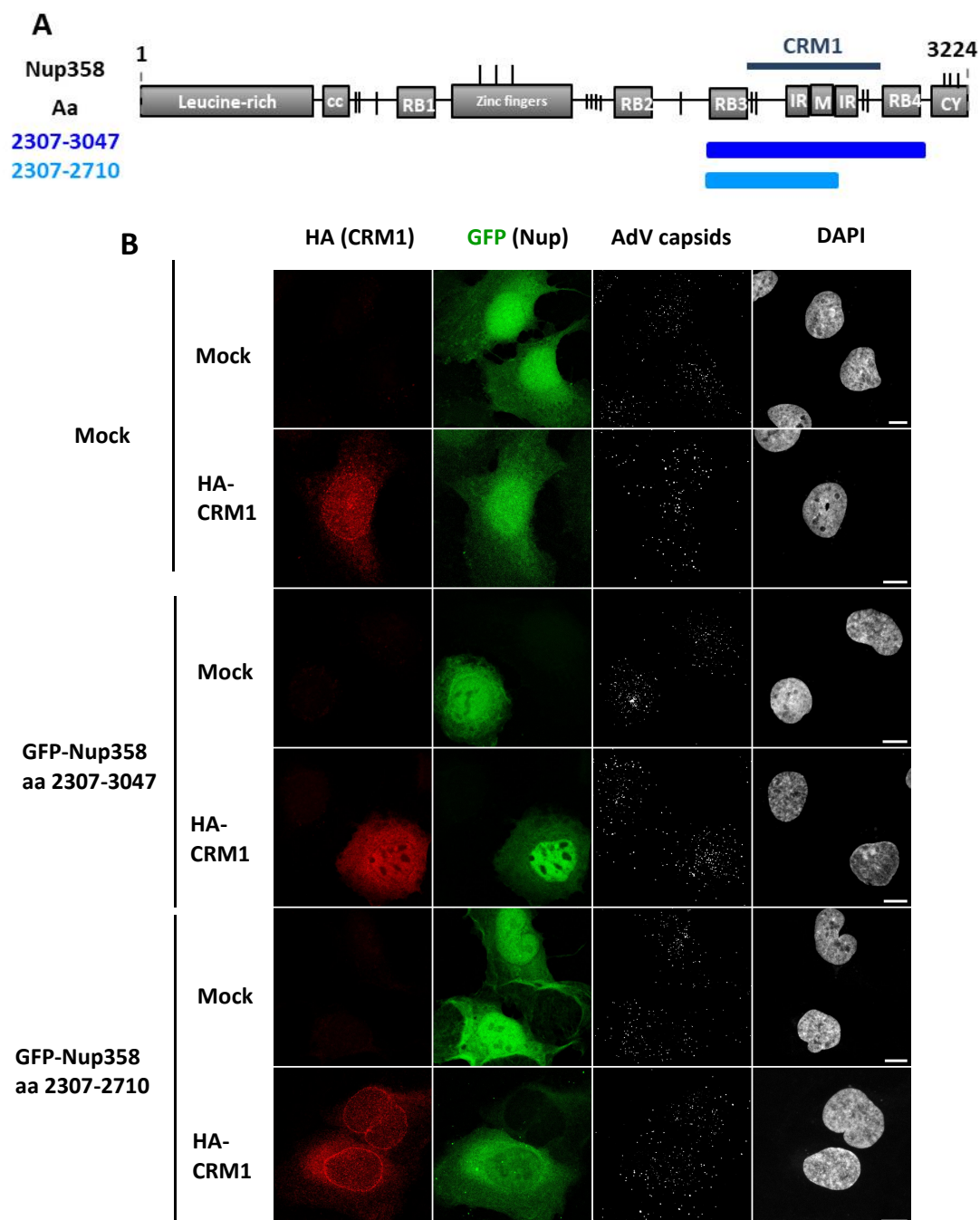


Figure 29: The C-terminal CRM1-binding fragment of Nup358 impairs nuclear targeting of AdV capsids in a CRM1-dependent manner. Overexpression of CRM1 overcomes AdV capsid accumulation at the MTOC induced by the C-terminal CRM1-binding fragment of Nup358 (A) Schematic representation of the structure of Nup358 with the binding site for CRM1 indicated at the C-terminal region of Nup358. Soluble HA-tagged fragments of Nup358 used in this assay with the corresponding amino acid residues (aa) are represented in different colors below the scheme. (B) Representative confocal images of AdV particle distribution in cells co-transfected with an empty plasmid (mock) or with HA-CRM1 and with an GFP-empty plasmid or with the indicated soluble GFP-tagged Nup358 fragments (green). Cells were stained using specific antibodies for HA-tag to detect exogenous CRM1 (red), and for AdV capsids (grey dots). DAPI staining was used to visualize the chromatin. Maximal projection images are shown. Scale bars 10 μ m.

2.2. Infection of mitotic cells as a model system to study AdV genome delivery

Up to now, we have observed that overexpression of CRM1-binding fragments of Nup358 or Nup214 caused a strong impairment of CRM1-dependent translocation of AdV capsids from the MTOC to the NE, similar to the effect observed upon CRM1 inhibition by LMB treatment. Overexpression of CRM1-binding fragments of Nups caused a loss of CRM1 from the NE contrary to LMB treatment, which did not cause any apparent redistribution of CRM1. We then asked whether the role of CRM1 in AdV genome delivery and/or the defect observed in presence of dominant negative Nup-fragments were conditioned by the presence of the NE. In mitotic cells, the NE is not present. However, AdV genome delivery into mitotic cells has not been characterized yet. We thus decided to take advantage of this natural disintegration of the NE taking place during mitosis, to study AdV genome delivery in the absence of NE and assembled NPC. Exploiting mitotic conditions allow us to determine the role of the nuclear transport machinery in addition to their nucleo-cytoplasmic transport function.

2.2.1. Establishment of an infection protocol for mitotic cells

First, we established conditions to ensure that infected cells were actually in mitosis at the moment of infection. For this, an enriched population of mitotic cells was obtained by colcemid-induced synchronization of cells in prometaphase. This drug, also known as demecolcine, together with nocodazole or colchicine, is commonly used to block microtubule polymerization. Contrary to colchicine, nocodazole and colcemid treatments are reversible, and mitotic arrest of at least half of the cell population has been described to be stable for ~ 30 min after nocodazole release and up to ~ 2 h after colcemid release, in HeLa cells (Zieve et al., 1980). We tested both treatments in U2OS cells but finally chose colcemid for our infection assays, since we observed lower toxicity and higher yield of synchronized mitotic cells compared to treatment with similar concentrations of nocodazole. A ~ 80 % semi-confluent asynchronous population of cells was incubated in presence of colcemid for 14 to 16 h (**Figure 30a**). Then, cells were released from colcemid by carefully washing with ice cold DMEM medium. Ad5-wt-GFP were incubated with mitotic cells during 30 min at 4 °C to allow attachment of virions to the cell surface and later transferred to 37 °C pre-heated DMEM medium (t=0) to permit viral particle internalization and microtubule polymerization. Cells were fixed at 1 hpi at the latest to avoid cell cycle progression and analysed by IF. At 5 min post infection, about 60-70 % of cells were still in mitotic stage (**Figure 30b**). Moreover, most viral particles were mainly localized in the peripheral areas of the cytoplasm. At 1 hpi,

about 50 % of cells were still arrested in mitosis and AdV capsids were observed closer to the mitotic chromatin, suggesting that they were probably able to access the cytoplasm.

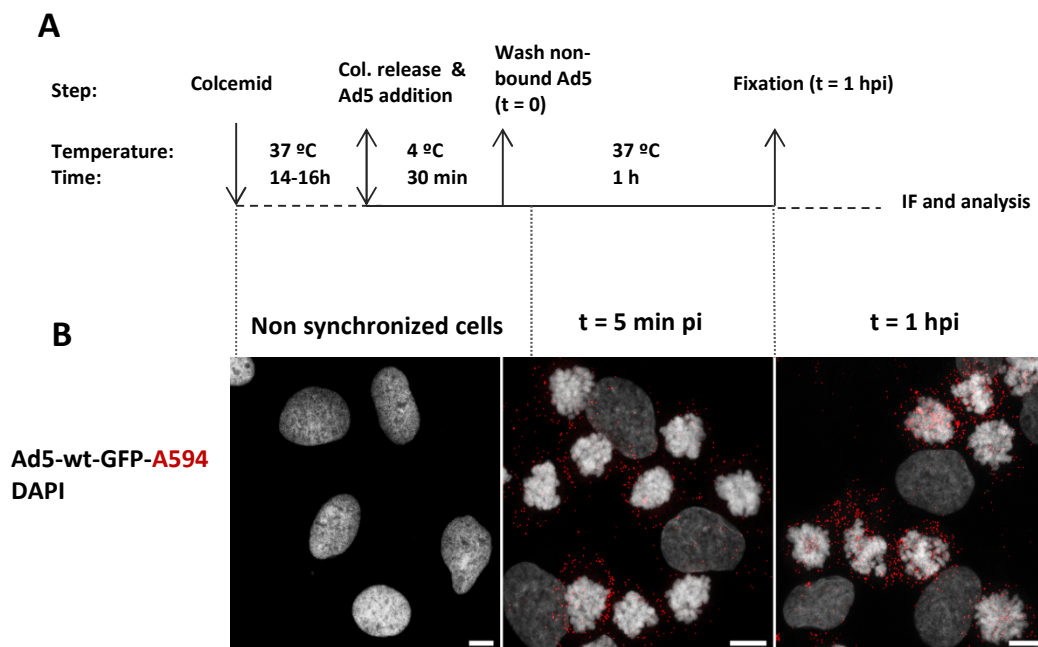


Figure 30: Infection protocol for mitotic cells to study AdV genome delivery. (A) Schematic representation of the experimental setup for cell cycle synchronization and infection of mitotic cells. Cells grown on coverslips are synchronized in mitosis by treatment with the MT-depolymerizing agent colcemid. Synchronized cells are infected with A594 labelled viruses at 4 °C, followed by inoculum removal. Cells are next incubated at 37 °C to allow virus internalization (t=0) and fixed at 1 hpi. Fixed cells are used for indirect immunofluorescence, further confocal microscopy and quantification analysis. (B) Representative confocal images of cells before colcemid treatment (left panel), infected mitotic cells 5 min pi (middle panel) or 1 hpi (right panel). AdV particles were coupled to the A594 fluorophore (red) and DAPI staining was used to visualize the chromatin. Maximal projection images are shown. Scale bars 10 μ m.

2.2.2. Mitotic spindles are reconstituted upon release from colcemid-treatment

In order to further characterize infected mitotic cells we wanted to visualize the integrity of the mitotic spindle of cells 1 h after release from colcemid treatment and infection with Ad5-wt-GFP. For this purpose, the previously described protocol was followed and cells were later stained by using specific antibodies against pericentrin, to detect the centrosomes, and α -tubuline to detect the microtubules. A bipolar mitotic spindle was observed 1 hpi in cells released from colcemid treatment (**Figure 31**). Instead, cells non-released from colcemid inhibition were not able to form mitotic spindles and the pericentrin was completely mislocalized. In our infection conditions, capsids distributed quite homogeneously all over the cytoplasm with some capsids associating with chromatin. This experiment showed that synchronized mitotic cells released from colcemid treatment were able to reconstitute the mitotic spindle upon 1 h of colcemid treatment release even under infection conditions.

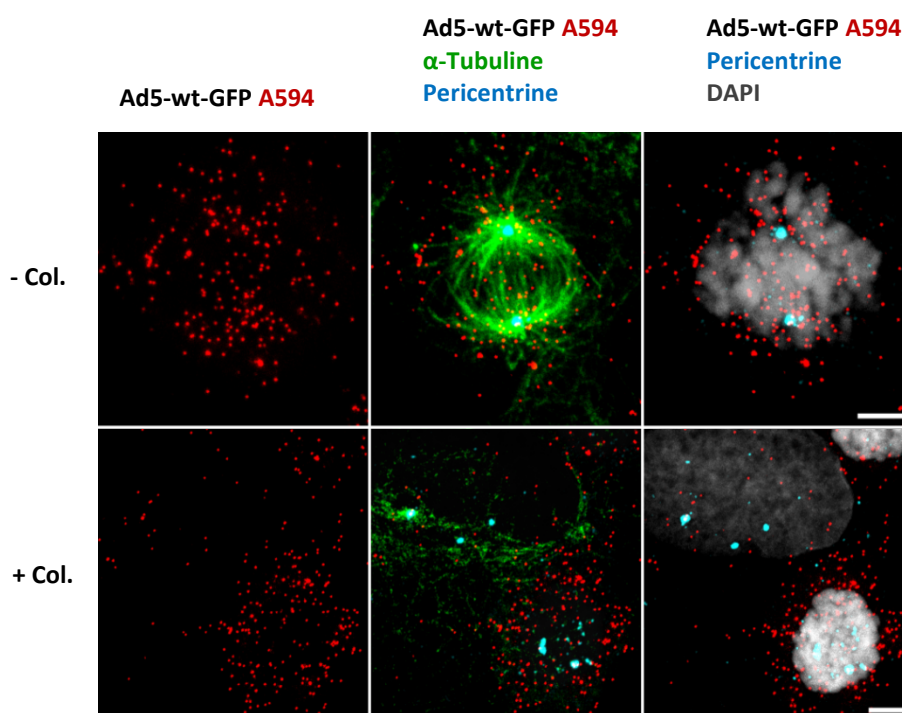


Figure 31: Mitotic spindles are reconstituted in infected cells upon release from colcemid-treatment. Representative confocal images of mitotic infected cells 1 hpi in absence (upper row) or presence (lower row) of colcemid (Col). AdV particles are coupled to the A594 fluorophore (red) and DAPI staining was used to visualize the chromatin. Specific antibodies were used against α -tubuline or pericentrin. Maximal projection images are shown. Scale bars 5 μ m.

2.2.3. AdV are able to deliver their genome in mitotic cells

In order to know whether indeed viral capsids can enter inside the mitotic cell and disassemble their capsid, cells were either infected with the Ad5-wt-GFP or an Ad5-ts1-GFP vector as a negative control. The mutant ts1 capsid lacks the viral protease, meaning that capsid proteins have not been processed, which causes this mutant to have a hyper-stable capsid. As a consequence, the ts1 mutant virus is taken up into cells by receptor-mediated endocytosis but is unable to release the membrane lytic protein VI (Rancourt et al., 1995; Pérez-Berná et al., 2009; Martinez et al., 2015). Consequently ts1 virions stay trapped inside the endosome and are degraded by the lysosomal pathway. Thus, in case capsid disassembly can occur in mitotic cells as it happens in interphase, it should be possible to visualize the viral pVII of the wt Ad5 vector but not that of the ts1 mutant. Synchronized mitotic cells were thus infected with equivalent amounts of physical particles of AdV vectors per cell and later stained for detecting AdV capsids and viral pVII. After 1 hpi, discrete dots corresponding to Ad5-wt pVII were detected mainly localizing at the mitotic chromatin (**Figure 32**). In contrast, mitotic cells infected with the ts1 mutant vector showed hardly any dot corresponding to pVII. In addition, AdV ts1 capsids were localizing predominantly at the cell periphery forming aggregates, suggesting lysosomal degradation.

Taken together, these observations showed that the established protocol allows a successful internalization and disassembly of AdV particles in mitotic cells, meaning that AdV capsids are able to deliver their genome without specific requirement of an assembled NE or NPC structure. Therefore, AdV infection in mitotic cells can be exploited as a simplified system to study the implication of the nuclear-transport machinery and individual Nups in the AdV genome delivery in absence of nucleo-cytoplasmic compartmentalization.

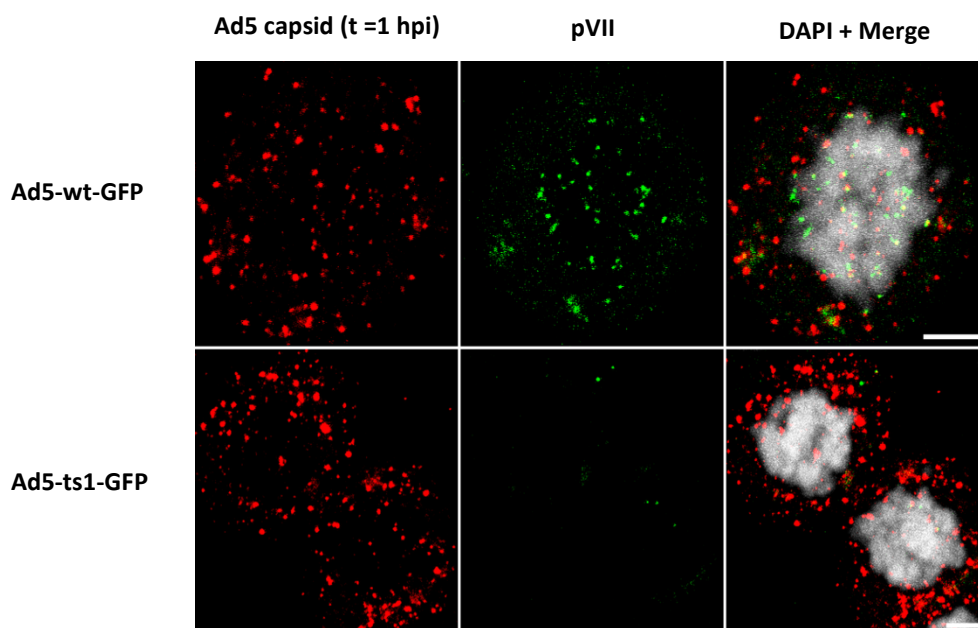


Figure 32: AdV deliver their genome in mitotic cells. Representative confocal images of mitotic infected cells 1 hpi. Cells were infected with the Ad5-wt-GFP vector or the hyper-stable capsid mutant ts1. AdV particles are coupled to the A594 fluorophore (red) and DAPI staining was used to visualize the chromatin. Specific antibodies were used against pVII. Maximal projection images are shown. Scale bars 5 μ m.

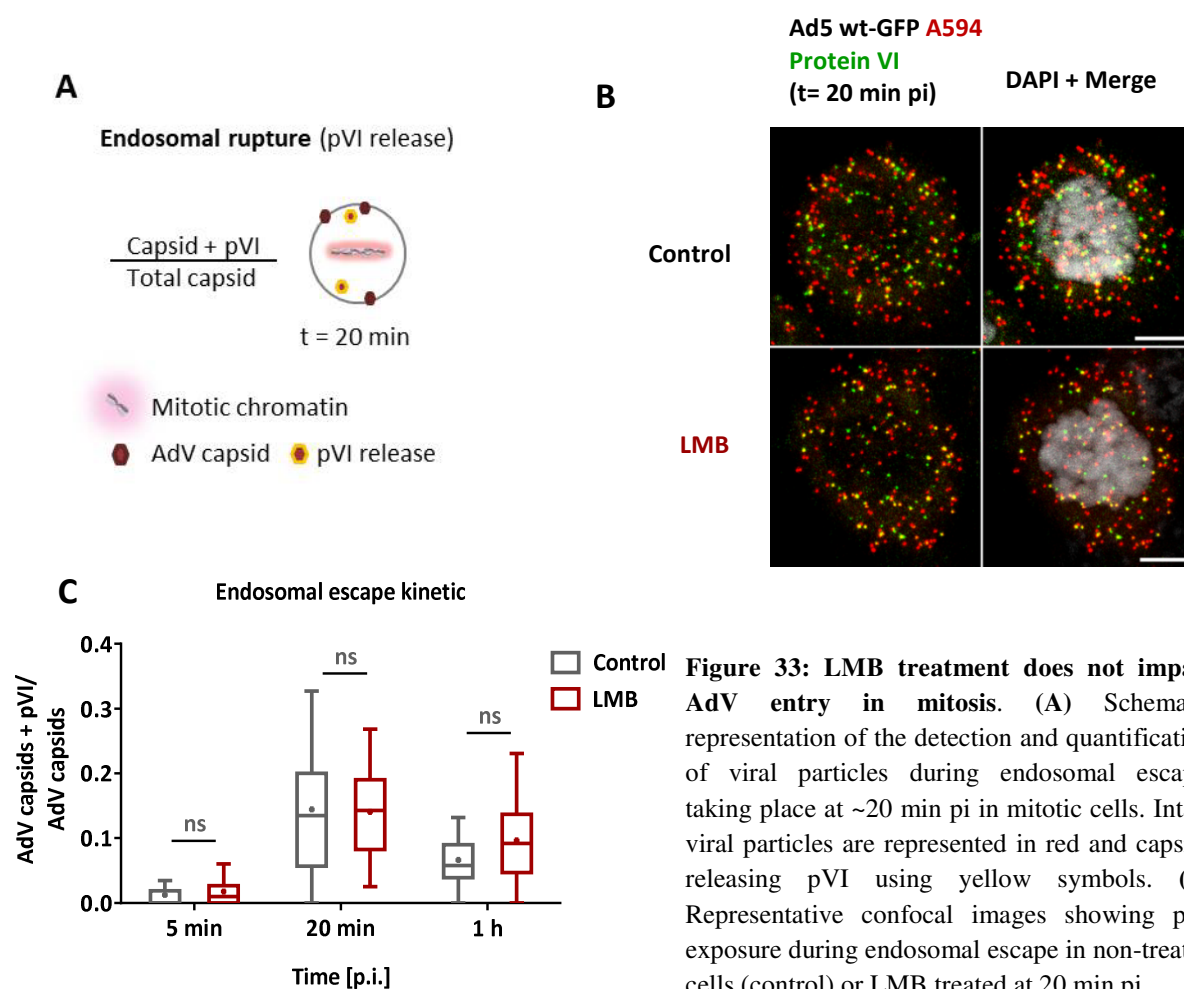
2.3. The role of CRM1 in promoting AdV capsid disassembly

We have confirmed that CRM1 plays a crucial role in translocation of AdV capsids to the NPC in interphase. However in mitosis, nuclear compartmentalization does not exist anymore and thus, AdV capsids do not need to circumvent the NE barrier. We have observed that in mitosis, AdV particles can deliver their genome to the chromatin without specific requirement of a NPC. The fact that viral particles are able to deliver their genome implies a previous entry of capsids to the mitotic cell by endocytosis, with subsequent capsid protein VI release and endosomal escape. Later instead, it is not known whether translocation of viral capsids is required for AdV capsid disassembly. Discrete pVII dots could be observed at the mitotic chromatin 1 hpi, suggesting that AdV cores could be dissociated from the capsid and stably associate with cellular DNA. Hence, we decided to monitor early stages of AdV infection also for mitotic cells and investigate the potential implication of CRM1 during this process.

2.3.1. Functional inactivation of CRM1 does not impair AdV entry in mitosis

In interphase cells, as well as in mitosis, the endosomal escape step is reflected by the kinetic of capsids releasing pVI. In order to assess whether AdV internalization occurs with the same efficiency in control and LMB treated cells, we monitored the endosomal escape of AdV

capsids by analyzing the relative amount of AdV capsids positive for protein VI at different time points, in presence or absence of LMB (**Figure 33a**). For this purpose, a synchronized mitotic cell population was infected with Ad5-wt-GFP in presence or absence of LMB and fixed at 5 min, 20 min or 1 hpi. Viral capsids were pre-stained with Alexa 594, and viral protein VI was detected using specific antibodies. Results showed that at 5 min pi, only few viral capsids had entered into the mitotic cell (**Figure 33b and c**). The maximal rate of capsids exposing pVI was observed at 20 min pi, with statistically similar efficiency in control or LMB treated cells. Finally, at 1 hpi levels of AdV capsids positive for pVI had dropped, meaning that most of the capsids had already entered the cell. These results showed that entry into mitotic cells occurs through endosomal escape and that CRM1 inhibition does not affect AdV capsid internalization in mitotic cells.



AdV particles are A594 labelled (red) and DAPI staining was used to visualize the chromatin. Specific antibodies were used for pVI detection (green). Co-localization of AdV capsids with capsid protein VI appear yellow. Maximal projection images are shown. Scale bars 5 μm . (**C**) Quantification of the kinetic of endosomal escape of AdV particles in control (grey) or LMB treated cells (red) at the indicated time points. Endosomal escape was calculated as the number of AdV capsids positive for pVI (yellow dots), relative to the total amount of capsids per cell. Individual cell values from at least 30 cells per condition are represented in a Tukey box plot. Results were analyzed using a two-way ANOVA test and Sidak's multiple comparisons post hoc test. ns \geq 0,05.

2.3.2. Inhibition of CRM1 prevents the disassembly of AdV capsids

Specific inhibition of CRM1 does not affect entry of AdV particles into the mitotic cell. We then asked whether downstream steps during early phases of infection would be dependent on CRM1 and thus, could be altered in presence of LMB in mitosis. After AdV entry, it is not known whether AdV capsid translocation or anchoring to the chromatin is a prerequisite for genome uncoating during mitosis. We therefore decided to first focus our analyses on calculating the efficiency of AdV capsid disassembly (**Figure 34a**). In interphase cells, genome import occurs rapidly after capsid disassembly at the NPC, thus, the number of pVII dots relative to the amount of AdV capsids reflects the efficiency of viral import. In contrast, in absence of the NE during mitosis, the import step does not take place. Therefore, the number of pVII dots relative to the total amount of AdV capsids will not reflect efficiency of import but that of capsid disassembly. We thus used this parameter to evaluate CRM1 implication in AdV capsid disassembly. For this, we monitored capsid disassembly in absence or presence of LMB. In addition, we used an LMB-resistant HA-tagged mutant of CRM1 that possesses a serine instead of a cysteine residue in position 528 (CRM1 C528S). This position is where the LMB covalently binds to CRM1. Thereby, this point mutation confers CRM1 resistance to LMB allowing export of NES-containing cargo even in presence of LMB. Cells were either transfected with an empty plasmid (mock treated) or transfected with the HA-tagged CRM1 C528S mutant. The next day, cells were synchronized by overnight treatment with colcemid and pre-treated or not with LMB before infecting them with Ad5-wt-GFP. After 1 hpi, cells were fixed and stained with specific antibodies recognizing the viral pVII or the HA-tag. The Ad5 capsids were detected via direct coupling to Alexa 594 fluorophore. Quantification analyses were performed to calculate the pVII to AdV capsid ratio. Results showed that in control cells, the efficiency of capsid disassembly was approximately one third (**Figure 34b and c**). In striking contrast, AdV capsids were hardly disassembled in cells treated with LMB, since only very low amount of pVII dots were detected in spite of the relatively high number of internalized AdV particles. Interestingly, cells expressing an excess of the HA-tagged CRM1 C528S mutant not only restored AdV capsid disassembly but increased almost by two fold the rate of disassembly. These results show that the efficiency of AdV capsid disassembly is directly proportional to the amount of functional CRM1 present in the cell: the efficiency of AdV capsid disassembly is strongly reduced in absence of functional CRM1 and enhanced in presence of an excess of CRM1, suggesting a crucial role of CRM1 in capsid disassembly.

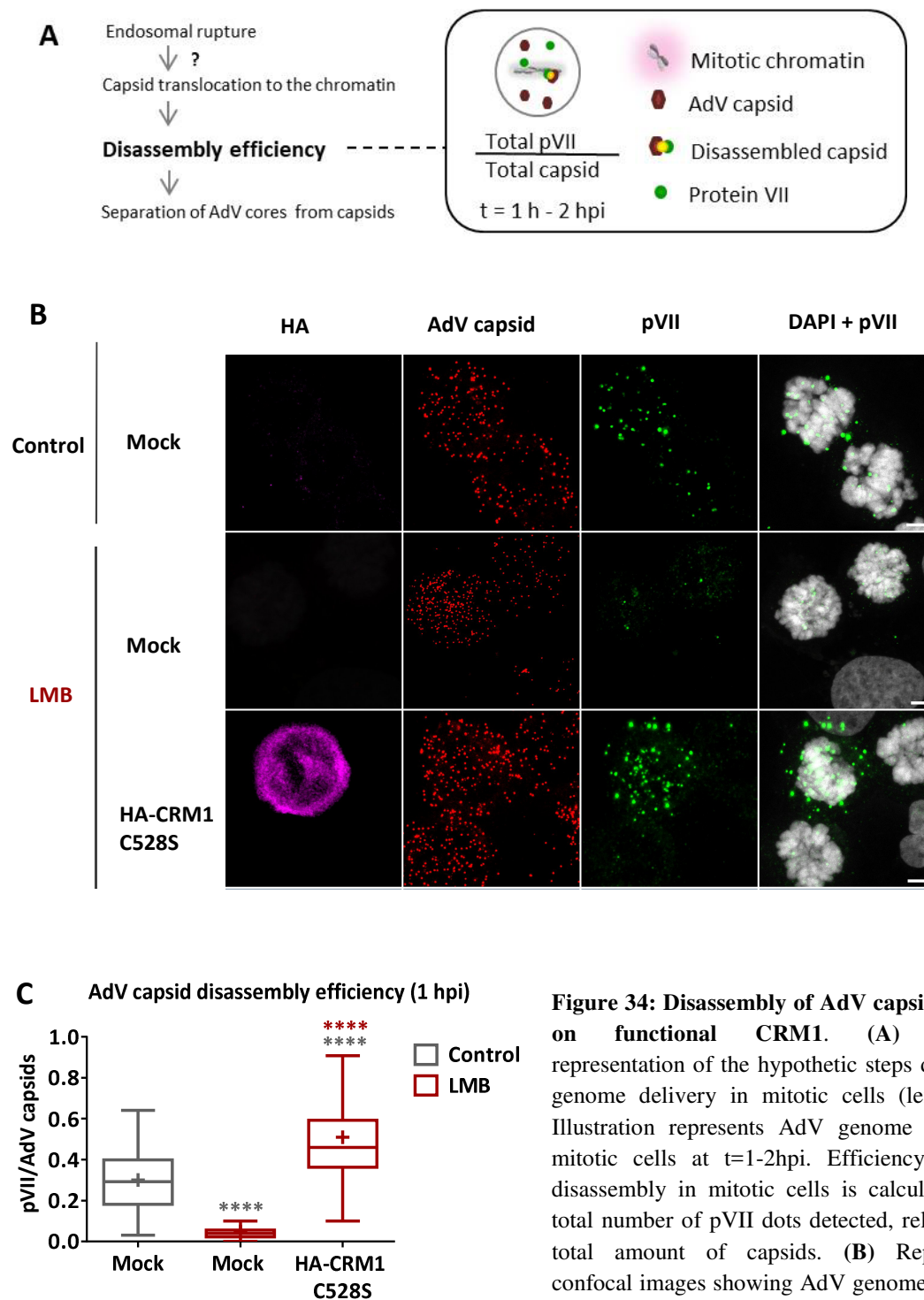


Figure 34: Disassembly of AdV capsids depends on functional CRM1. (A) Schematic representation of the hypothetical steps during AdV genome delivery in mitotic cells (left column). Illustration represents AdV genome delivery in mitotic cells at t=1-2hpi. Efficiency of capsid disassembly in mitotic cells is calculated as the total number of pVII dots detected, relative to the total amount of capsids. (B) Representative confocal images showing AdV genome delivery in mitotic cells. Cells were transfected with an empty

plasmid (mock) or with an HA-CRM1 C528S construct, and treated or not (control) with LMB before and during infection. AdV particles are A594 labelled (red) and DAPI staining was used to visualize the chromatin. Specific antibodies were used for pVII detection (green). Maximal projection images are shown. Scale bars 5 μ m (C) Quantification of the efficiency of AdV capsid disassembly in the indicated conditions. AdV capsid disassembly was calculated as described in (A). Data obtained from individual cell values (n>15 per condition, for each experiment), from three independent experiments, are represented in a Tukey box plot. Results were analyzed using a one-way ANOVA test and Tukey's multiple comparisons post hoc test. ****: p < 0,0001. Grey asterisks represent significance with respect to control and red asterisks with respect to mock LMB treated cells.

2.3.3. Exposure of AdV core accelerates AdV capsid targeting to the chromatin

CRM1 is necessary for nuclear targeting of AdV capsids in interphase and this translocation allows disassembly and import at the NPC. In mitotic cells, CRM1 is still required for efficient disassembly of AdV capsids. However, it is not clear whether AdV capsid disassembly requires targeting of AdV particles to the chromatin. Thus, CRM1 could be involved in translocation of AdV particles from the cell periphery to the chromatin thereby facilitating AdV capsid disassembly by a CRM1-independent mechanism. Alternatively, chromatin targeting is not a pre-requisite for AdV capsid disassembly and CRM1 is directly involved in AdV capsid disassembly. We decided then to characterize the localization of AdV capsids in respect to the chromatin in presence or absence of functional CRM1. For this, we quantified the proportion of AdV capsids (both disassembled or not) that were localizing at the chromatin (co-localizing with the DAPI staining) in control or LMB-treated cells, expressing or not the CRM1 LMB-resistant mutant, at 1 hpi (**Figure 35a**).

For this type of co-localization analyses in mitotic cells, we exclusively quantified the middle focal plane obtained from confocal images of figure 34. The middle plane was considered as representative of the whole cell, since statistically equivalent absolute numbers of capsids were quantified per condition on average (**Figure 35b**).

Results showed that in control cells, nearly 50 % of capsids localized at the chromatin (**Figure 35c**). LMB treatment caused a statistically significant reduction of AdV capsids at the chromatin, although the effect was not as strong as the block on AdV capsid disassembly. However, expression of the CRM1 C528S mutant did not significantly reverse distancing of AdV capsids from the chromatin. These results show that enhanced AdV capsid disassembly induced by the CRM1 C528S mutant is not a consequence of an accelerated translocation towards the chromatin.

AdV capsids were more distanced from the chromatin in LMB treated cells even in the presence of the CRM1 C528S mutant resistant to LMB, suggesting that translocation to the chromatin is not a prerequisite *per se* to allow capsid disassembly. One possibility is that AdV capsids are targeted to the chromatin after disassembly (= after AdV core exposure). This would explain why in LMB treated cells, in which AdV capsid disassembly is strongly impaired, AdV capsids are more distanced from the chromatin. In presence of CRM1 C528S, a more efficient disassembly of AdV capsids could also lead to a more efficient AdV core-capsid dissociation thereby reducing the amount of capsids targeted to the chromatin.

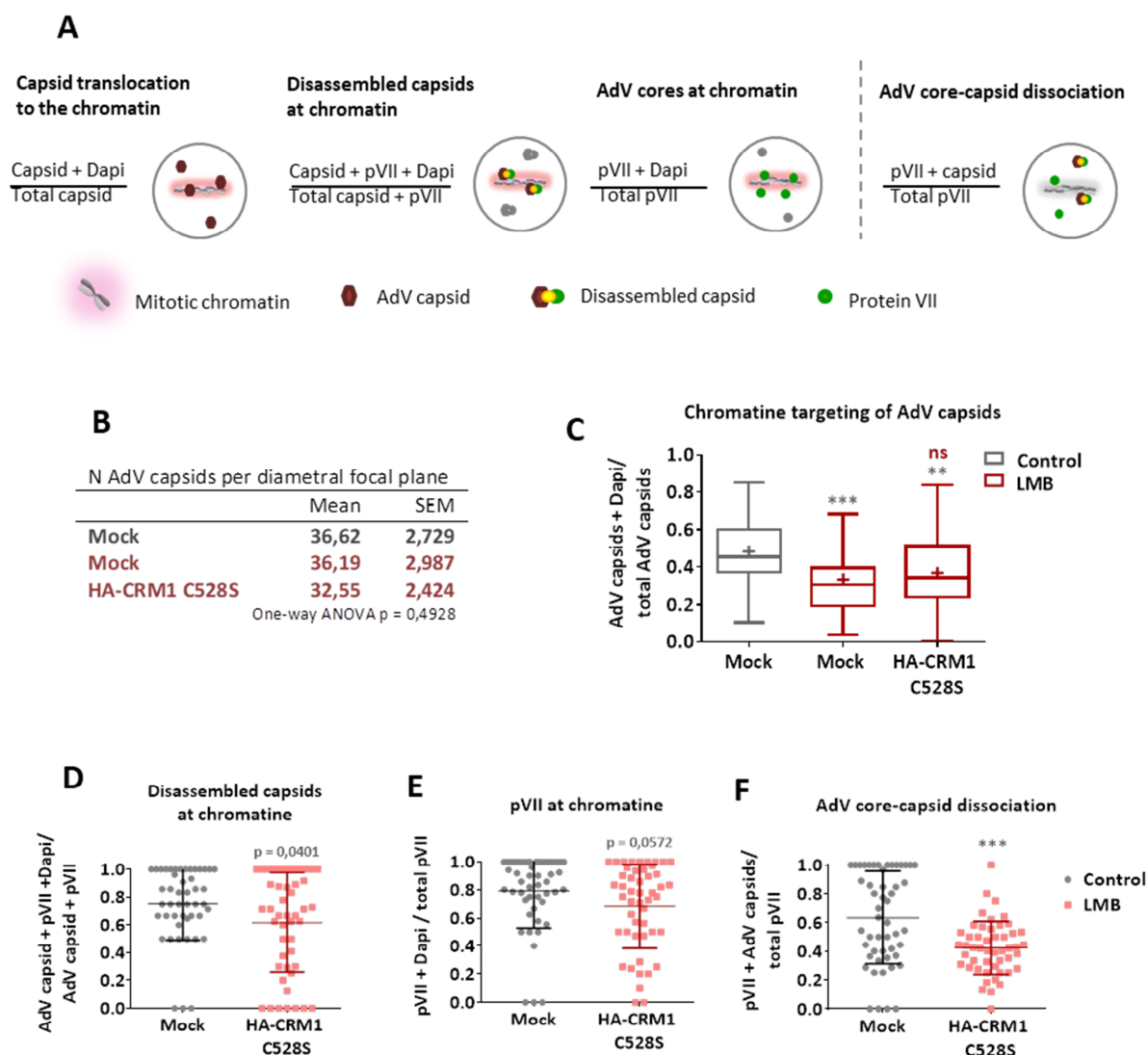


Figure 35: Exposure of AdV core accelerates AdV capsid targeting to the chromatin. (A) Schematic representation of the quantifications used to characterize the AdV particle localization with respect to the cellular chromatin (to the left of the dashed line) and the quantification to estimate the proportion of AdV cores separated from capsids (to the right of the dashed line). Illustration represents distribution of different components of the AdV particles using colored symbols given in the legend. (B) Table including absolute numbers of quantified AdV capsids in one focal plane from confocal images of figure 34. The mean, SEM and statistical analysis is indicated. (C) Quantification of the localization of AdV capsids at the chromatin relative to total AdV capsids detected. Data from individual cell values, from same experiments than figure 34, are represented in a Tukey box plot. Results were analyzed using a one-way ANOVA test and Tukey's multiple comparisons post hoc test. ***: $p < 0,001$; **: $p < 0,01$. Grey asterisks represent significance with respect to control and in red with respect to mock LMB treated cells. (D) Quantification of the localization of disassembled capsids at the chromatin relative to total disassembled capsids detected. (E) Quantification of the localization of AdV cores at the chromatin relative to total disassembled capsids detected (F) Quantification of the proportion of AdV cores still associated with capsids relative to the total amount of pVII detected. (D-F) Data obtained from individual cell values, from same experiments than figure 34 are represented in a scatter blot. Bars in the scatter plot represent the mean and SD. Results were analyzed using a two-tailed T-test. ***: $p = 0,0001$

We then analyzed the localization of disassembled capsids in respect of the chromatin, in control or CRM1-C528S expressing cells. For this, we identified disassembled capsids as AdV capsids positive for pVII and quantified the proportion of them that were docking at the chromatin (co-localizing with the DAPI staining) (**Figure 35a**). Results showed that disassembled capsids were mainly localized at the chromatin in control cells, with an average of about 75 % of disassembled capsids co-localizing with the DAPI staining. Disassembled AdV capsids in CRM1 C528S expressing cells showed similar localization relative to the chromatin with a slight tendency to distribute at non-chromatin regions (**Figure 35d**). Likewise, we analyzed the localization of AdV cores in respect of the chromatin. Distribution of AdV cores was monitored again via pVII detection. The pattern of pVII dots localization was similar to that of disassembled capsids, with most of pVII localizing at chromatin in control and CRM1 C528S expressing cells (about 80% on average) (**Figure 35e**).

These results show that disassembled capsids as well as AdV cores are similarly targeted to the chromatin in both control or LMB treated cells expressing CRM1 C528S. Thus, docking of AdV cores or disassembled capsids to the chromatin is not influenced by the amount of functional CRM1 present in the cell, contrary to the efficiency of AdV capsid disassembly. Results suggest that the viral core (still associated or not to the capsid) is specifically targeted to the chromatin, independently of CRM1. Taken together, results suggest that CRM1 is directly required for the disassembly of the viral capsid and does not influence the efficiency of AdV capsid disassembly by facilitating an upstream event.

2.3.4. Separation of AdV cores from disassembled capsids is accelerated by overexpression of CRM1

Both disassembled capsids and total pVII dots showed similar localization pattern towards chromatin in control as well as in CRM1 C528S expressing cells. These results could reflect in both cases a low AdV core separation rate from capsids (i.e more than 50 % of AdV cores associating with capsids, as observed in interphase cells up to 1 hpi), meaning that disassembled capsids and AdV cores would translocate together to the chromatin prior to core release. In the opposite case, AdV core separation from capsids would be high (i.e less than 50 % of AdV cores associating with capsids, as observed in interphase cells from 2 hpi), meaning that AdV cores can be targeted to the cellular chromatin independently of the AdV capsid. To address this question, we analyzed the proportion of still associated AdV cores with capsids, in control or CRM1 C528S expressing infected cells (**Figure 35a**). Results showed that in control cells, about 60 % of detected pVII dots remained associated to the

AdV capsid (**Figure 35f**), which resembles results observed for interphase cells at 1 hpi (**Figure 14e**). Instead, in cells expressing an excess of functional CRM1, we observed an increase in AdV cores that had separated from the capsid (**Figure 35f**).

These results show that the enhanced efficiency of AdV capsid disassembly caused by an excess of CRM1 C528S also leads to an accelerated separation of the viral cores from the capsid compared to control cells. We have observed that independently of the level of expression of functional CRM1, disassembled capsids exposing the AdV core are efficiently targeted to the chromatin similar than dissociated AdV cores. However, capsids that do not expose de viral core (at least not enough to be detected using specific antibodies against pVII), prevalent in LMB treated cells, do not efficiently reach the chromatin region. This suggests that is the AdV core which determines the localization of the viral particle with respect to the cellular chromatin and not the capsid. Thus, chromatin targeting of the AdV particle would be the consequence of AdV core exposure upon capsid disassembly and not the cause of disassembly. Taken together, these results show that CRM1 is still crucial during AdV genome delivery in mitotic cells being specifically involved in AdV capsid disassembly.

2.3.5. Disassembled capsids are targeted to the mitotic chromatin

In interphase cells, disassembly of AdV capsids occurs at the NPC and thus, disassembly events are rarely observed in cytosolic regions or at the cell periphery. In contrast, in mitotic cells, we have observed that at least 25 % of disassembled capsids can be found in regions away from the chromatin, which is far from being an isolated event. We thus asked whether these non-chromatin disassembled capsids were dead-end products or instead they could still be targeted towards the mitotic chromatin. To answer this question, analyses of AdV genome delivery were done using live cell imaging in mitotic cells. For this, we used the U2OS-TAF-1-GFP cell line, which has been established in our lab and constitutes a useful tool to directly visualize AdV core exposure *in vivo* (Komatsu et al., 2015). In non-infected cells, the protein TAF-1 diffusely distributes inside the nucleus and is recruited to incoming viral genomes by targeting genome associated pVII as soon as the latter is exposed in the nucleus thereby forming discrete dots corresponding to individual AdV cores. In mitosis, the TAF-1 protein diffuses all over the cell, meaning that in principle, exposure of AdV cores in mitosis should be also detected by specific recruitment of TAF-1-GFP to the viral pVII. To monitor AdV genome delivery in mitotic cells then, U2OS-TAF-1-GFP cells were firstly transfected with a construct coding for the histone 2B tagged with the iRFP protein, to visualize the chromatin. The day after, cells were splitted and synchronized in mitosis overnight using a specific

support for live cell imaging. The mitotic population of cells was infected asynchronously at 37 °C with Ad5 vectors coupled to the A594 fluorophore in presence of colcemid treatment to allow monitoring of AdV genome delivery for prolonged time post infection. Movies of 10 min duration using triple-colour detection with high temporal resolution were obtained using a Spinning disk microscope in non-infected cells, or cells infected with either the ts1 mutant or the wt vectors. In non-infected cells or cells infected with the ts1, some discrete TAF-1-GFP dots were observed localizing at the chromatin. However, these dots were rarely at non chromatin regions, did not co-localize with viral particles and seemed to be larger than the characteristic AdV-induced TAF-1-GFP dots, thus unlikely to be related to viral genome release. In the case of mitotic cells infected with Ad5 wt, cytosolic or chromatin-associated dots of TAF-1 GFP positive for AdV capsids were readily visualized from ~ 1 hpi. In the **Figure 36**, an assembly of 18 frames corresponding to 90 seconds of a 10 min video is shown for the time point ~ 2 hpi. The frames depict an event showing the docking of a disassembled capsid (in red) with exposed core (marked by TAF-1-GFP in green) to the cellular chromatin. This specific core exposing AdV capsid moved in the surroundings of the chromatin during several minutes and finally docked at the chromatin. Once docked at the chromatin, the capsid and associated core remained immobile at the docking site, suggesting strong chromatin interaction. Presumably, a similar event had occurred next to the described disassembled capsid before starting the movie, since another disassembled capsid stayed immobile associated to the chromatin during the whole time of the record. These results suggest that disassembly of capsids in non-chromatin regions is not a defective event in mitotic cells but instead, disassembled capsids can be targeted to chromatin.

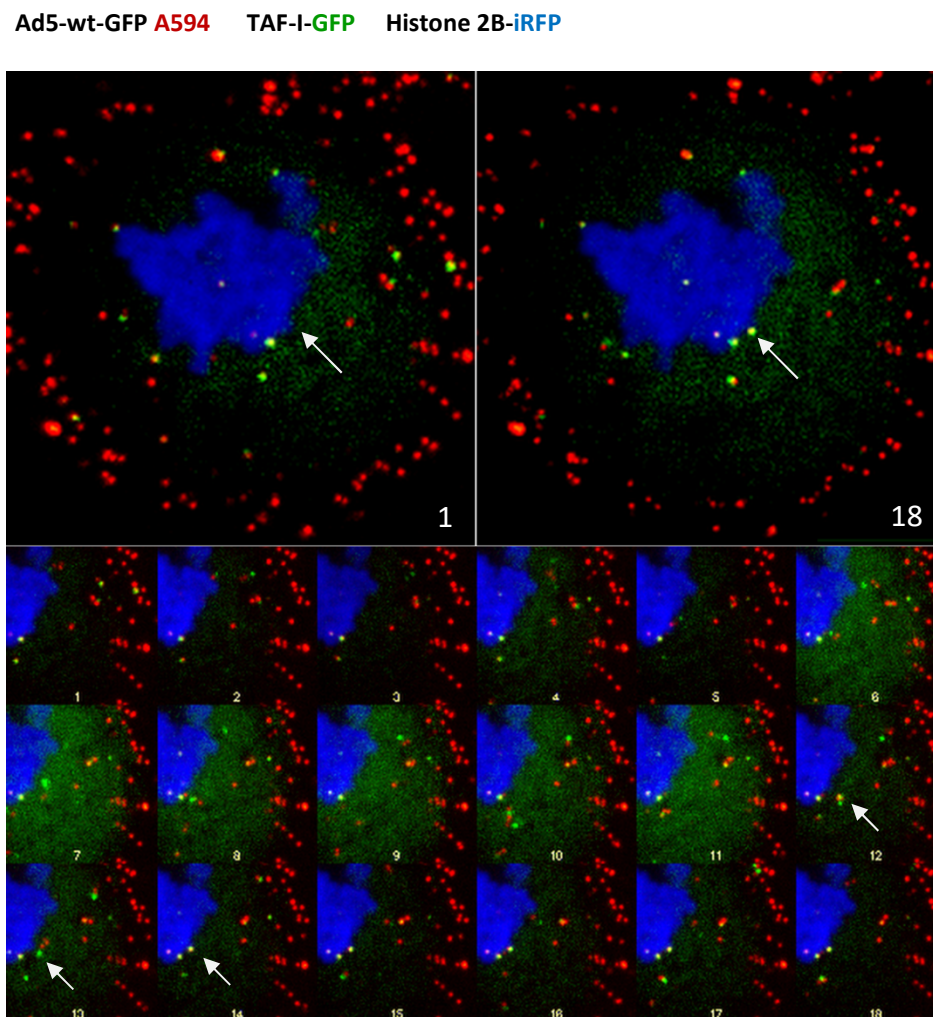


Figure 36: Disassembled capsids are targeted to the chromatin in mitotic cells. (A) Three-colour Live-cell imaging showing docking of a disassembled capsid (in red) with exposed core (green) at cellular chromatin (blue). Stably expressing U2OS-TAF-1-GFP cells were transfected with H2B tagged with the iRFP protein to visualize the chromatin. Synchronized cells in mitosis were infected with Alexa594 coupled Ad5-wt-GFP vector and imaged using spinning-disk confocal microscopy. The top two images show individual frames separated by ~ 90 seconds. The arrow on the left top panel points to the condensed chromatin. On the right top panel the arrow points at a disassembled capsid (yellow) moving in the vicinity and finally docking at the chromatin. The bottom panel shows a higher magnification and frame resolution of the same event.

2.3.6. Soluble fragments of Nups affect AdV genome delivery differently in mitosis

The previous results revealed a novel role of CRM1 in promoting AdV capsid disassembly. This role became evident in mitotic cells, in which the chromatin is not protected by the nuclear membrane and NPC-targeting is not a requirement for capsid disassembly anymore. On the other hand, soluble CRM1-binding fragments of Nup358 or Nup214 trapped CRM1 inside the nucleus and impaired both, CRM1 dependent AdV genome delivery and protein export. Overexpression of CRM1 led to saturation of the CRM1 binding fragment of Nup358 (aa 2307-3047) and restored CRM1-dependent nuclear targeting of AdV capsids. However, a shorter region encoded by the C-terminal part of Nup358 (aa 2307-2710) specifically competed with a step in AdV genome delivery downstream of CRM1-dependent nuclear targeting of AdV capsids. To know whether this competition effect could be bypassed in absence of NE, we analysed the effect of different soluble Nup fragments in mitotic cells.

To test this, cells were first transfected with either the C-terminal fragments of Nup358 (aa 2307-3047 or aa 2307-2710) or the C-terminal CRM1-binding fragment of Nup214 (aa 1975-2090). Two days later, synchronized mitotic cells were infected with Ad5-wt-GFP coupled with A488 during 1 h, in presence or absence of LMB. Specific antibodies were used to detect the viral pVII or the HA-tag of Nup358 fragments, and the Nup214 fragment was detected via its RFP-tag. The AdV capsid disassembly efficiency was then represented as the total number of pVII to AdV capsid ratio. In control cells, the disassembly efficiency was about 25 % and strongly impaired in presence of LMB (**Figure 37a and b**), as observed before. Surprisingly, cells without LMB treatment but expressing the C-terminal CRM1 binding fragment of Nup358 (aa 2307-3047), did not prevent AdV capsid disassembly unlike what we observed in interphase cells, instead this fragment almost doubled the efficiency of disassembly. This effect was completely abrogated in presence of LMB. The shorter C-terminal fragment of Nup358 also augmented AdV capsid disassembly contrary to what was observed in interphase cells, but again LMB treatment impaired AdV capsid disassembly in presence of this fragment. Unlike the two Nup358 fragments, cells expressing the C-terminal CRM1-binding fragment of Nup214 did not significantly alter AdV capsid disassembly efficiency compared to control cells, but were also sensitive to LMB treatment, which abrogated capsid disassembly.

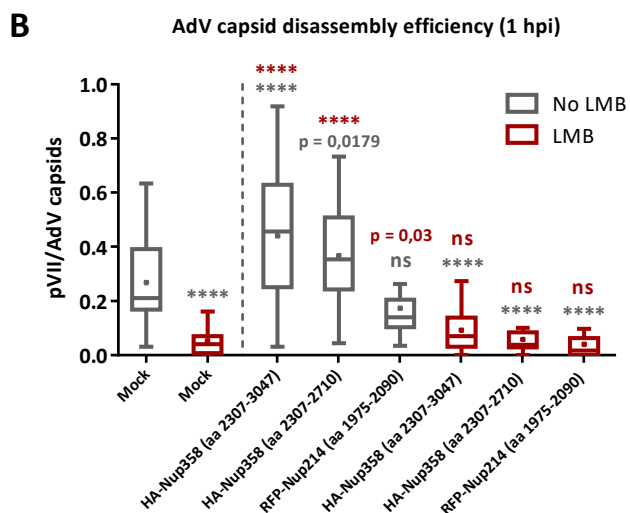
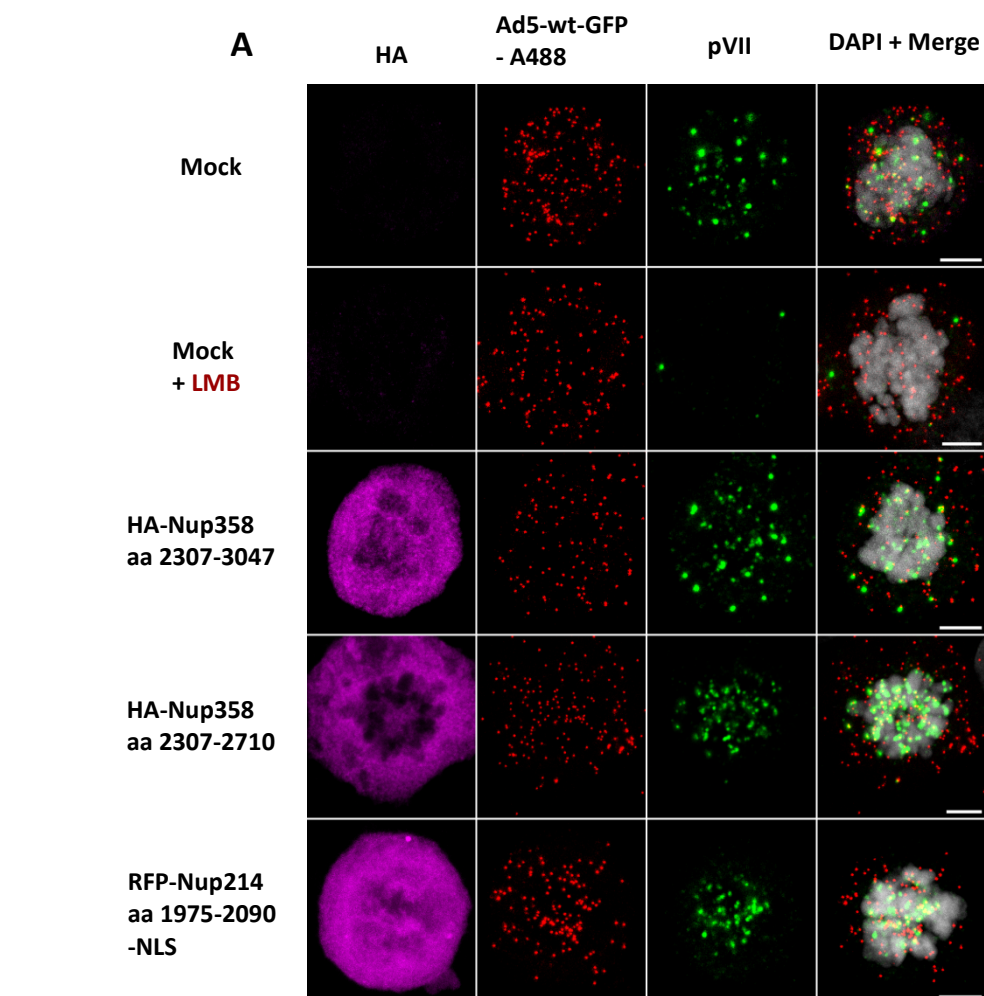


Figure 37: NPC-non-anchored fragments of Nups affect AdV genome delivery differently in mitosis (A) Representative confocal images showing AdV genome delivery in mitotic cells. Cells were transfected with either an empty plasmid (mock), with the C-terminal HA-Nup358 fragments or with the RFP-tagged C-terminal fragment of Nup214, in absence or presence of LMB. Cells were synchronized in mitosis and infected with Alexa 488 labelled viruses (here shown in red) for 1 h. Cells were next fixed and stained using specific antibodies for the HA-tag (magenta) and the core protein VII (green). DAPI staining was used to visualize the chromatin. Maximal projection

images are shown. Scale bars 5 μ m. **(B)** Quantification of the efficiency of AdV capsid disassembly in the indicated conditions. AdV capsid disassembly was calculated as the total amount of detected pVII relative to the number of AdV capsids. Data obtained from individual cell values, from two independent experiments (except in RFP-Nup214 conditions and HA-Nup358 aa 2307-2710 with LMB that results are from one experiment; $n > 15$ per condition, for each experiment), are represented in a Tukey box plot. Results were analyzed using a one-way ANOVA test and Dunnett's multiple comparisons post hoc test. ****: $p < 0,0001$; ns $> 0,05$. Grey asterisks represent significance with respect to control and red asterisks with respect to mock LMB treated cells.

To see whether overexpression of the C-terminal fragments of Nup358 influenced localization of viral capsids and AdV cores in respect of the chromatin, we further analyzed relative localization of total capsids, disassembled capsids and AdV cores, in respect of their chromatin association. We observed again that capsids were less targeted to chromatin under LMB treatment in mock treated cells (**Figure 38 b**). A similar tendency was conserved even in presence of the aa 2307-3047 Nup358 fragment which enhanced genome uncoating. In presence of the shorter C-terminal fragment of Nup358 no difference in capsid localization was observed with or without LMB treatment. Analysis of the localization of the disassembled capsids and AdV cores in presence of the different fragments was predominantly at the chromatin (**Figure 38c and d**).

We also analyzed the proportion of AdV cores still associated with capsids, in the presence of the C-terminal Nup358 fragments (aa 2307-3047 and aa 2307-2710) with or without LMB treatment (**Figure 38a**). Interestingly, the proportion of AdV cores still associated with capsids in cells expressing the CRM1-binding fragment of Nup358 (aa 2307-3047) was significantly reduced compare to mock treated cells, which is in agreement with an enhanced disassembly of the capsid compared to control cells. In contrast, the shorter C-terminal fragment (aa 2307-2710) did not increased the proportion of AdV cores separated from the capsids (**Figure 38e**), consistent with the observation that this fragment only induced a mild increase in the efficiency of AdV capsid disassembly.

Taken together, these results show that the inhibitory effect caused by overexpression of soluble CRM1 binding fragments of Nups or by the not CRM1-binding fragment of Nup358 in interphase could be overcome in the absence of the NE. Moreover, results show that the C-terminal region of Nup358 has a positive effect on AdV capsid disassembly and thus, accelerates AdV core release from the capsid. This enhancement of genome uncoating was less evident in cells expressing the shorter (not CRM1 binding) fragment of Nup358, and accordingly, separation of AdV cores from capsids was not increased. Finally, excess of the CRM1-binding fragment of Nup214 did not caused any evident effect. These results suggest that the C-terminal fragment of Nup358, which functions as a disassembly machine for export complexes, might promote CRM1-dependent function(s), which favour AdV genome uncoating. In contrast, overexpression of the C-terminal of Nup214, which increase stabilization of CRM1-RanGTP-NES-cargo complexes, might not provide any benefit for the disassembly of AdV capsids.

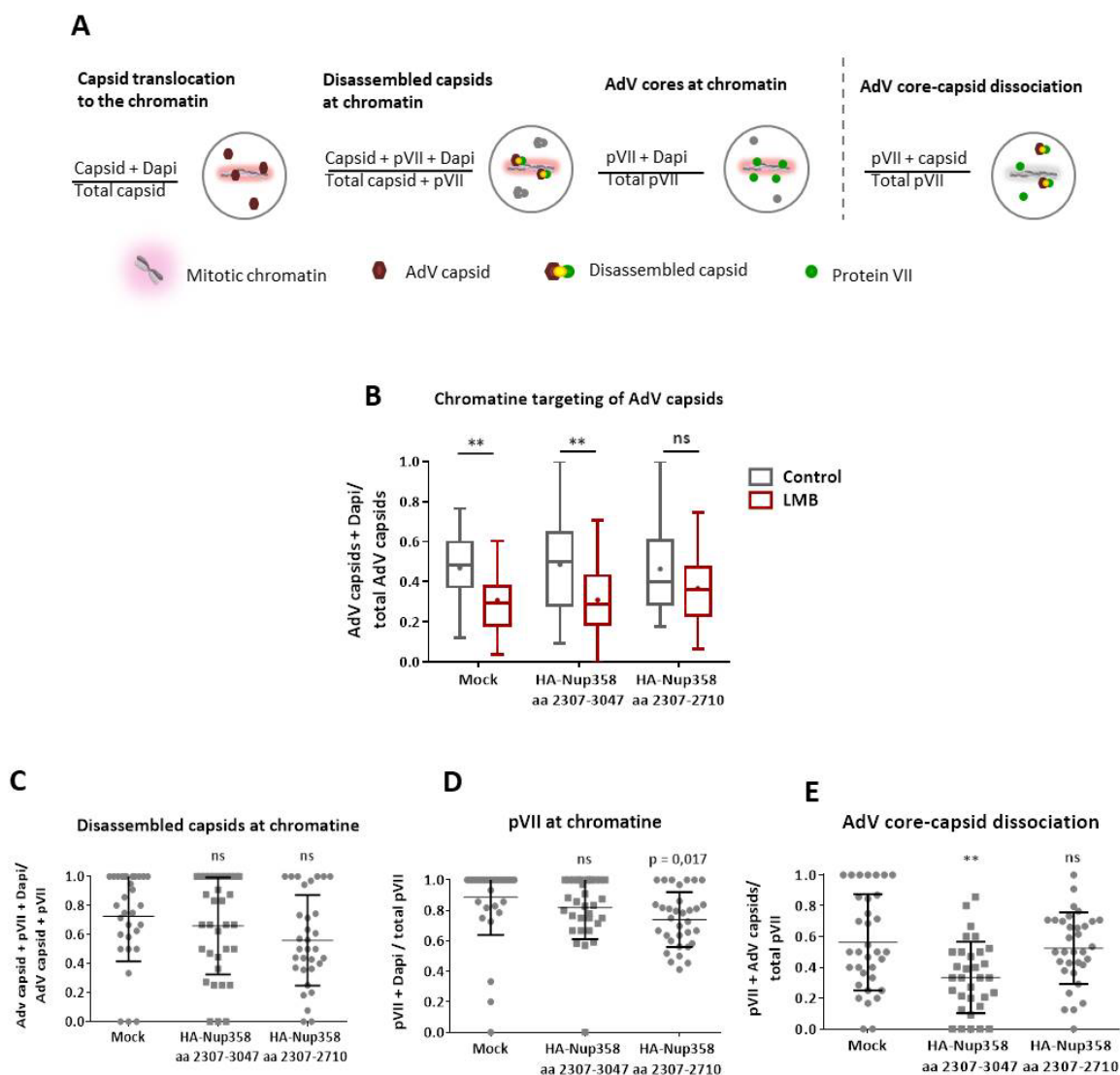


Figure 38: The C-terminal CRM1 binding fragment of Nup358 increases separation of AdV cores from disassembled capsids. (A) Schematic representation of the quantifications used to characterize of the AdV particle localization with respect to the chromatin (to the left of the dashed line) and the quantification used to estimate the proportion of AdV cores separated from capsids (to the right of the dashed line). Illustrations represent distribution of different components of the AdV particles in colored symbols as indicated in the legend. (B) Quantification of the localization of AdV capsids at the chromatin relative to total AdV capsids detected. Quantification performed from a single focal plane of confocal images from figure 37. Data obtained from individual cells (same cells than figure 37) are represented in a Tukey box plot. Results were analyzed using a two-way ANOVA test and Sidak's multiple comparisons post hoc test. **: $p < 0,01$; ns $> 0,05$. (C) Quantification of the localization of disassembled capsids at the chromatin relative to total disassembled capsids detected. (D) Quantification of the localization of AdV cores at the chromatin relative to total disassembled capsids detected. (E) Quantification of the proportion of AdV cores still associated with capsids relative to the total amount of pVII detected. (C-E) Data obtained from individual cell values, from same cells than figure 37 are represented in a scatter blot. Bars in the scatter plot represent the mean and SD. Results were analyzed using a one-way ANOVA test and Tukey's multiple comparisons post hoc test. **: $p < 0,01$; ns $> 0,05$

2.4. Specific point mutations at the N-terminus of CRM1 impair AdV genome delivery

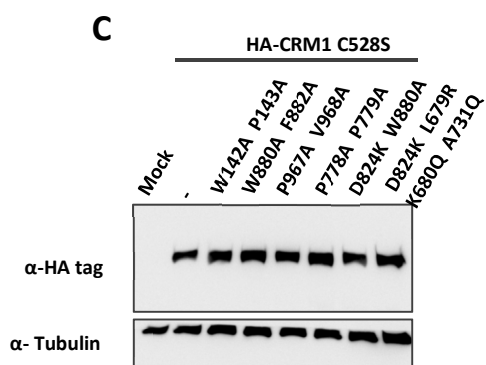
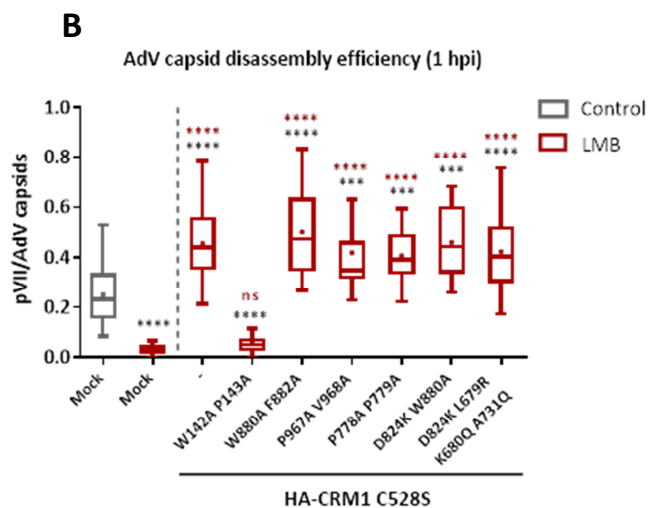
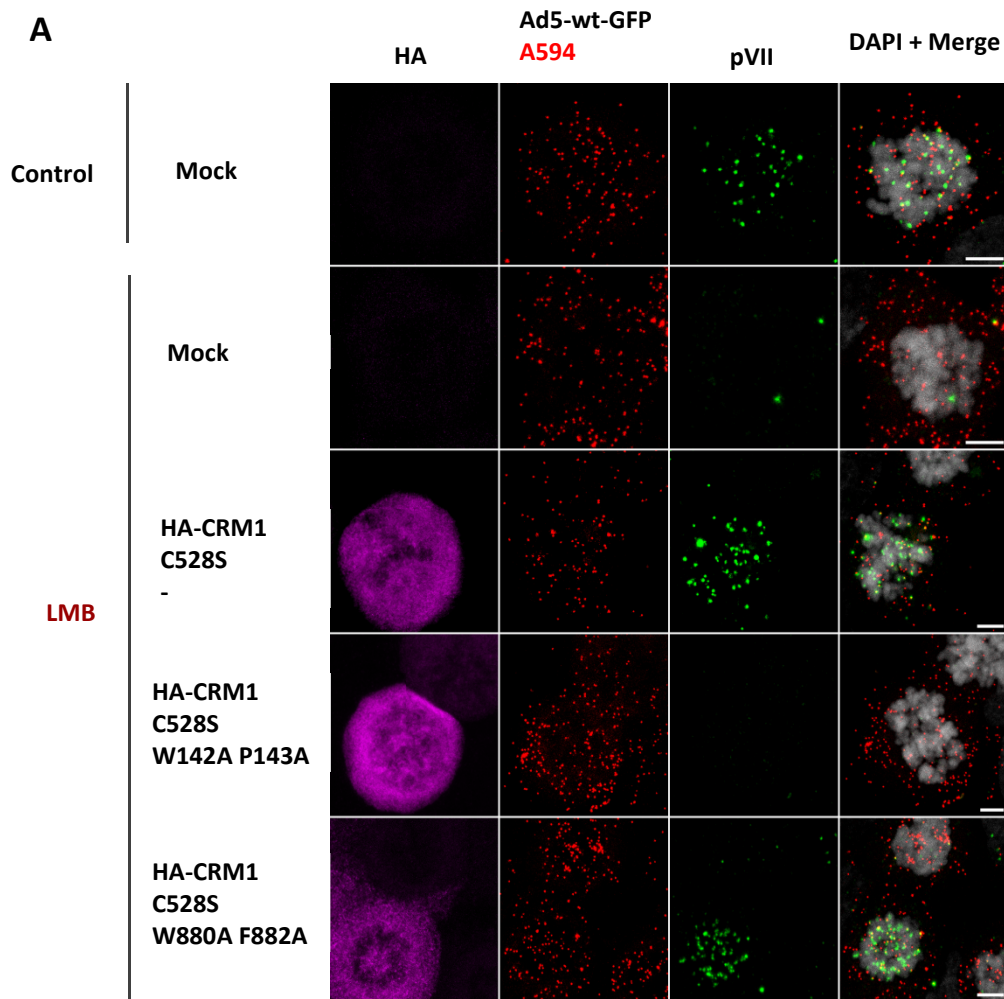
Upon nuclear envelope breakdown (NEBD), the C-terminal fragments of cytosolic Nups lose their ability to compete with AdV genome delivery. Under mitotic conditions, CRM1-binding fragments of Nups cannot cause nuclear retention of CRM1 and the viral particle has unrestricted access to the transport receptor. However, the shorter C-terminal fragment of Nup358 which does not bind CRM1 also lost the ability to compete with AdV genome delivery. This intriguing result raised the question whether overexpression of soluble fragments of Nup358 or Nup214 might still interfere with a proper binding of CRM1 to endogenous Nup358 on its way back to the nucleus, which is not problematic for protein export (Hutten and Kehlenbach, 2006) but may could hinder proper AdV capsid anchoring and disassembly at the NPC. This step might be crucial in interphase but not in mitosis, during which Nup sub-complexes are available by diffusion in the cytoplasm. To test whether proper binding of CRM1 to cytosolic Nups is important for AdV genome delivery, we investigated the ability of different Nup-binding defective CRM1 mutants (Port et al., 2015; Ritterhoff et al., 2016) to restore the impairment of AdV genome delivery caused by LMB treatment, in both: mitotic and interphase conditions.

2.4.1. Mutations in CRM1 prevent AdV genome delivery in mitotic cells

All CRM1 mutants included in this analysis possess the point mutation in position 528 (C528S) that confers resistance to LMB. Importantly, they have specific point mutations inside or close to one or two out of many conserved FG-binding pockets present in CRM1, which were identified by analysing the crystallography structure between Nup214 and CRM1 (Port et al., 2015). In particular, the mutation in position 880 (W880A) has been shown to reduce the affinity of CRM1 for CRM1-binding fragments of Nup214 without affecting its ability to bind RanGTP or NES-cargo; and another study revealed that this residue is also important for CRM1 binding to the C-terminal fragment of Nup358 (Ritterhoff et al., 2016). We thus tested whether these CRM1 mutants were able to restore AdV genome delivery under LMB treatment conditions, in mitotic cells. For this, cells were transfected with the different HA-tagged CRM1 mutants or mock treated, and synchronized in mitosis. Mitotic cells were infected with A594 labelled Ad5-wt-GFP after colcemid release and fixed 1 hpi. Specific antibodies were used to detect viral pVII and the HA-tag of the CRM1 constructs. AdV capsid disassembly efficiency was then calculated as the pVII to AdV capsid ratio. Results confirmed a strong inhibition of AdV capsid disassembly in LMB treated cells

compare to non-treated cells (**Figure 39a and b**). This effect was reversed in presence of the HA-CRM1 C528S construct, which is resistant to LMB and completely functional. Again, we observed that an excess of CRM1 C528S, in addition to restoring the effect of LMB, doubled the efficiency of AdV capsid disassembly compared to control cells. In striking contrast, the CRM1 mutant C528S where residues W142 and P143 were substituted by alanine, did not rescued AdV capsid disassembly at all, even though these residues were not especially close to a FG-binding pocket. CRM1 mutants containing mutations W880A or D824K, which are located inside two different conserved FG-binding pockets, were capable of restoring AdV capsid disassembly without any observable defect when compared to non-treated cells. Similar results were obtained for CRM1 constructs containing point mutations close to some FG-binding pockets. Moreover, all mutants except the W142A P143A nearly doubled the efficiency of the AdV capsid disassembly compared to control cells. Differences between the CRM1 mutants tested and the CRM1 mutated in W142 and P143 were not related to differences in expression, as judged by results obtained in WB (**Figure 39c**).

These results show that residues W142 and P143 of the N-terminal region of CRM1 are necessary for CRM1-dependent AdV capsid disassembly. This specific CRM1 mutant has not been characterized for its ability to bind to Nups or RanGTP/NES cargo, however both point mutations are localized in the conserved RanGTP-binding region (CRIME domain), suggesting that this mutant could have an impaired ability to bind RanGTP, which might be important for AdV capsid disassembly. Unexpectedly, mutations in aa W880 or D824, known to reduce the binding affinity of CRM1 to fragments of nucleoporins Nup214 and Nup358, were able to restore AdV capsid disassembly in the presence of LMB, suggesting that reduced ability of CRM1 to bind cytosolic Nups is not limiting for promoting efficient AdV capsid disassembly.

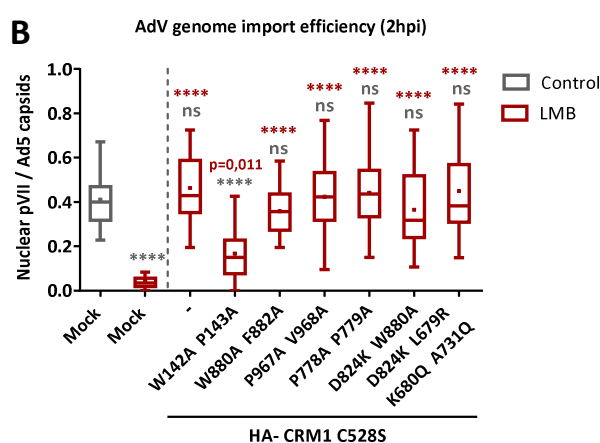
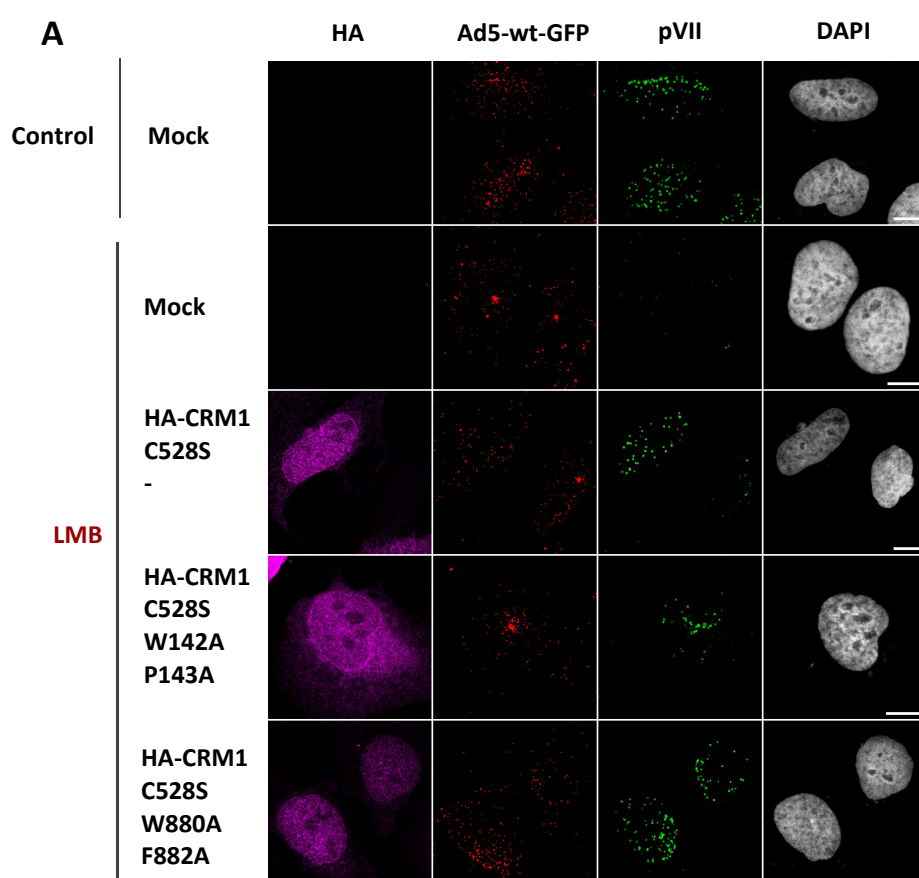


2.4.2. Mutations in CRM1 affect AdV genome delivery in interphase cells

We have identified two residues localized in the N-terminal region of CRM1 that are essential for AdV capsid disassembly in mitosis. We then asked whether this was also the case in interphase cells. To test this, cells were transfected with the same set of HA-tag CRM1 mutant constructs. The day after, cells were pre-incubated with LMB and then infected with Ad5-wt-GFP in presence or absence of LMB, depending on the condition. Cells were fixed 2 hpi and stained for viral pVII, AdV capsid and HA tagged CRM1 constructs, using specific antibodies. The efficiency of AdV genome import was calculated as the number of nuclear pVII to AdV capsid ratio. In control cells, we observed an efficiency of AdV genome import of 40 %, on average (**Figure 40a and b**). This was strongly reduced in cells treated with LMB, in which capsids accumulated at the MTOC. In contrast, cells expressing the HA-CRM1 C528S construct could restore viral import to levels comparable to those of control cells. Of note, in interphase cells contrary to mitotic cells, the LMB resistant CRM1 does not increase the efficiency of AdV genome import compared to control cells. On the other hand, the LMB resistant CRM1 mutant harbouring two point mutations in the N-terminal region (W142A and P143A) only partially restored AdV genome import in cells treated with LMB to the levels of control cells. However, unlike in mitotic cells, a partial rescue of genome import was observed in interphase cells. Moreover, AdV capsids still partially accumulate at the MTOC, suggesting that both events are linked. All other mutants restored the efficiency of AdV genome import to the same extent as control cells.

Figure 39: Point mutations in residues W142A and P143A of CRM1 impair AdV genome delivery in mitosis. (A) Representative confocal images showing AdV genome delivery in mitotic cells. Cells were transfected with either an empty plasmid (mock) or with HA-CRM1 C528S constructs encoding specific point mutations (indicated to the left of each row) or not (-). Transfected cells were synchronized in mitosis and infected with Alexa 594 labelled viruses in absence or presence of LMB. Cells were next fixed and stained using specific antibodies for the HA-tag (magenta) and the core protein VII (green). DAPI staining was used to visualize the chromatin. Maximal projection images are shown. Scale bars 5 μ m. (B) Quantification of the efficiency of AdV capsid disassembly in the indicated conditions. AdV capsid disassembly was calculated as the total amount of detected pVII relative to the number of AdV capsids. Data obtained from individual cell values, from two independent experiments (except in HA-CRM1 C528S P967A V968A and P788A P799A conditions that results come from one experiment; $n > 15$ per condition, for each experiment), are represented in a Tukey box plot. Results were analyzed using a one-way ANOVA test and Dunnett's multiple comparisons post hoc test. ****: $p < 0,0001$; ns $> 0,05$. Grey asterisks represent significance with respect to control and red asterisks with respect to mock LMB treated cells. (C) WB showing HA-CRM1 C528S mutants expression in U2OS cells. Total lysates of transfected cells with an empty plasmid or with different HA-CRM1 C528S constructs were separated by SDS-PAGE and proteins were detected using specific antibodies against HA-tag and α -tubulin, as loading control.

These results show that point mutations W142A and P143A in the N-terminal region of CRM1 still affect AdV genome delivery in interphase cells although less dramatically than in mitosis. Interestingly, it is known that CRM1 is targeted to the MTOC via its N-terminal CRIME domain and suggested to be targeted by binding to centrosomal RanGTP (Keryer et al., 2003; Liu et al., 2009). Thus, it is possible that CRM1 in the context of a CRM1-RanGTP complex rather than alone is necessary to unload the capsids from the MTOC area at least in interphase. In contrast, mutations in the conserved FG-binding pockets of CRM1 did not cause any effect on AdV genome delivery neither in interphase nor in mitotic cells, suggesting that reduced ability of CRM1 to bind cytosolic Nups is not limiting for promoting efficient AdV genome delivery.



2.4.3. The CRM1 mutant W142A P143A conserves the protein export function

We have observed that in cells expressing the LMB-resistant W142A P143A CRM1 mutant, AdV genome delivery could not be fully restored in presence of LMB, contrary to cells expressing the CRM1 construct exclusively harbouring the C528S mutation. This phenotype was more evident in mitotic than in interphase cells. However, in interphase cells, some accumulation of capsids near the NE could be observed. We then asked whether the two point mutations in the N-terminal region of CRM1 impaired its export function. To test this, cells were transfected with the set of HA-CRM1 C528S constructs. The day after, cells were incubated for 20 min with LMB and fixed to visualize endogenous RanBP1 localization and the HA-tagged constructs, using specific antibodies. In control cells, a clear cytosolic localization of RanBP1 was observed (**Figure 41**). As expected following LMB treatment, endogenous RanBP1 was trapped inside the nucleus. Upon expression of the CRM1 LMB resistant mutant, RanBP1 efficiently re-localized to the cytoplasm of LMB treated cells. The CRM1 construct containing point mutations in positions W142 and P143 was able to restore RanBP1 export to the cytoplasm. However, we cannot exclude that these point mutations at the N-terminal part of CRM1 do not reduce its ability to efficiently restore protein export compared to the “wt” CRM1 construct. Arguing with this idea, some cells showing low expression of the “wt” construct restored protein export with high efficiency contrary to cells showing low expression of the W142A P143A CRM1 mutant.

These results show that the W142A P143A CRM1 mutant, deficient for restoring AdV genome delivery, is able to restore protein export in LMB treated cells, although we cannot exclude that it does so with slightly reduced efficiency compared to the “wt” CRM1 LMB resistant construct.

Figure 40: Point mutations in residues W142A and P143A of CRM1 impair AdV genome delivery in interphase. (A) Representative confocal images showing AdV genome delivery in interphase cells. Cells were transfected with either an empty plasmid (mock) or with HA-CRM1 C528S constructs encoding specific point mutations (indicated to the left of each row) or not (-). Transfected cells were infected in absence (control) or presence of LMB. Cells were next fixed and stained using specific antibodies for the HA-tag (magenta), the AdV capsid (red) the core protein VII (green). DAPI staining was used to visualize the chromatin. Maximal projection images are shown. Scale bars 10 μ m. **B)** Quantification of the efficiency of AdV capsid disassembly in the indicated conditions. AdV capsid disassembly was calculated as the number of nuclear pVII relative to the number of AdV capsids. Data obtained from individual cell values ($n > 30$ per condition) are represented in a Tukey box plot. Results were analyzed using a one-way ANOVA test and Tukey's multiple comparisons post hoc test. ****: $p < 0,0001$; ns $> 0,05$. Grey asterisks represent significance with respect to control and red asterisks with respect to mock LMB treated cells.

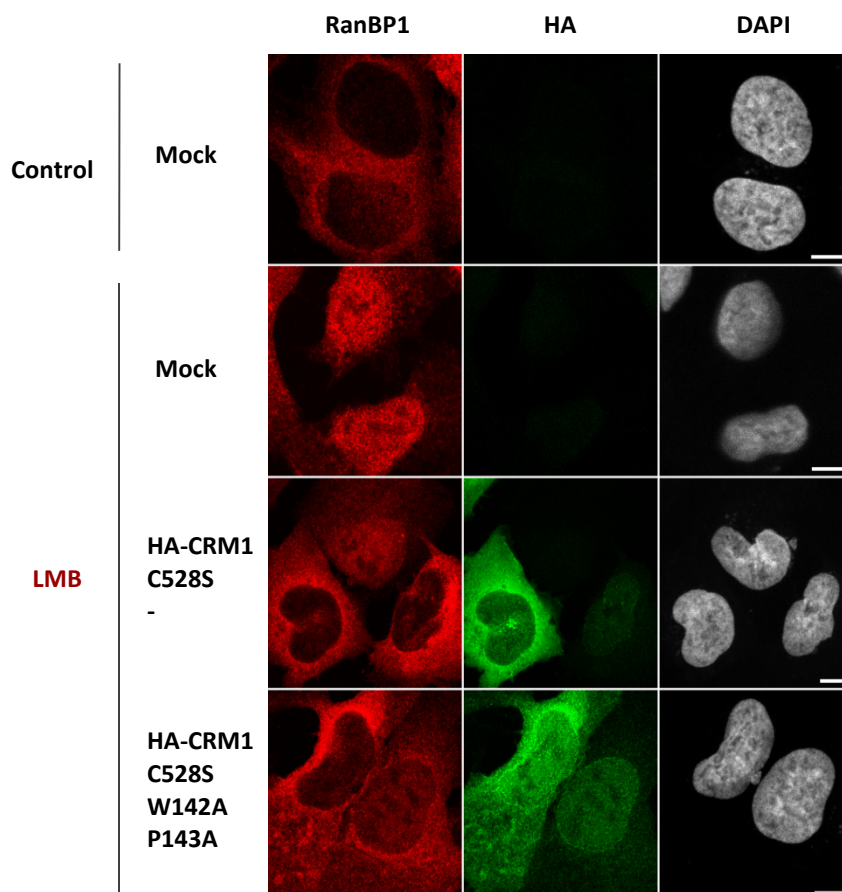


Figure 41: CRM1 mutant W142A P143A conserves the ability to export RanBP1. Representative confocal images showing CRM1-dependent export of endogenous RanBP1. Cells were transfected with either an empty plasmid (mock) or with HA-CRM1 C528S constructs encoding specific point mutations (indicated to the left of each row) or not (-). Transfected cells treated or not (control) with LMB. Cells were stained using specific antibodies for RanBP1 (red) and the HA-tag (green). DAPI staining was used to visualize the chromatin. Maximal projection images are shown. Scale bars 10 μ m.

2.4.4. The CRM1 W142A P143A mutant is able to bind Nup214 and Nup358

Residues W142 and P143 of CRM1 are not positioned at the FG-binding pockets where Nup214 was shown to bind CRM1 (Port et al., 2015). However, these point mutations could still affect Nup214 or Nup358 interaction with CRM1. To test whether this was the case, we tested the ability of this CRM1 mutant to bind either the RFP-Nup214 fragment of aa 1975-2090, which contains the second and third FG-containing regions (**Figure 42a**); or the GFP tagged C-terminal fragment of Nup358 comprising the two FG-repeat patches necessary to bind CRM1 (aa 2307-3047) (**Figure 42b**). In the case of the RFP-Nup214 construct, it is accompanied of a cNLS signal which ensures its nuclear localization. We previously observed that binding of the Nup214 C-terminal fragment to endogenous CRM1 forces its nuclear retention and the export of the reporter NES-cargo RanBP1 is abolished. In this assay, both CRM1 C528S mutants: “wt” and W142A P143A, localized at the NE showing a rim-staining as it is observed for the endogenous CRM1. When CRM1 was co-transfected with the RFP-Nup214 fragment, all were retained inside the nucleus and the export of RanBP1 was completely disrupted (**Figure 42a**).

The GFP-Nup358 fragment localizes to the nucleus at steady-state (**Figure 42b**). When an excess of exogenous CRM1 C528S was expressed, the fragment favoured a cytoplasmic localization and RanBP1 export was restored, suggesting that CRM1 overexpression compensated for the induced CRM1 retention at the nucleus and restored CRM1-dependent export of RanBP1. In the case of the CRM1 C528S W142A P143A mutant, a similar phenotype was observed in most cells. However few cells expressing the soluble fragment of Nup358 still conserved the ability to retain both, endogenous and HA-CRM1 C528S W142A P143A inside the nucleus, with the consequent block in CRM1-dependent RanBP1 export.

These results show that soluble C-terminal fragments of cytosolic Nups bind to CRM1 LMB resistant constructs regardless of the point mutations W142A P143A in the N-terminal region of CRM1.

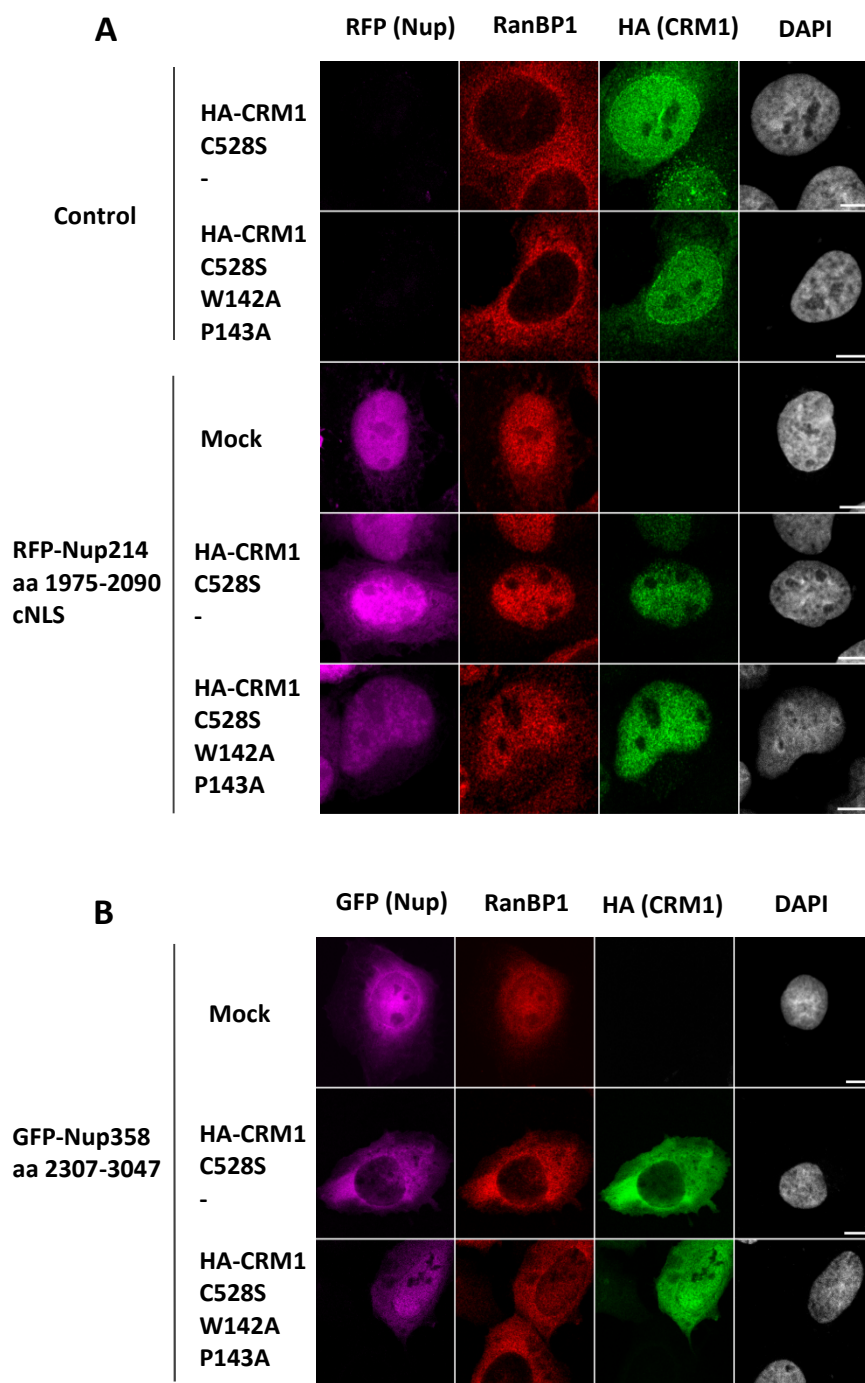


Figure 42: CRM1 mutant W142A P143A is able to bind soluble fragments of Nup214 and Nup358. Representative confocal images showing distribution of exogenous CRM1 and endogenous RanBP1 in presence of C-terminal CRM1-binding domains of cytosolic Nups. (A) Cells were co-transfected with either an empty plasmid (control) or with a C-terminal CRM1 binding fragment of Nup214 (RFP tagged, shown in magenta) and with an empty plasmid (mock) or a HA-tagged construct of CRM1 C528S with specific point mutations or not (-). Cells were fixed and stained using specific antibodies against endogenous RanBP1 (red) and HA-tag (green) to visualize exogenous CRM1. (B) Cells were co-transfected with a C-terminal CRM1 binding fragment of Nup358 (GFP tagged, here shown in magenta) and with an empty plasmid (mock) or an HA-tagged construct of CRM1 C528S with specific point mutations or not (-). Cells were fixed and stained using specific antibodies against endogenous RanBP1 (red) and HA-tag (green) to visualize exogenous CRM1. DAPI staining was used to visualize the chromatin. Scale bars 10 μ m.

2.5. Viral components involved in CRM1-dependent AdV genome delivery

Previous results point to a direct role of CRM1 in promoting nuclear targeting and capsid disassembly of AdV capsids at the NPC. However, the mechanism used by the virus to hijack CRM1 for delivering its genome is not understood. In the literature, the proposed mechanism through which capsids are disassembled at the NPC does not include CRM1 but involves the AdV capsid protein IX (Strunze et al., 2011, see the introduction for details). We therefore investigated in more detail the hypothetical interaction between the AdV capsids and CRM1, and whether the defect in capsid disassembly proposed by Strunze *et al.* for the Δ pIX AdV mutant capsids would be dependent on CRM1.

2.5.1. CRM1 does not interact with purified Ad5 particles

At first, we wanted to investigate whether CRM1 is recruited to the AdV capsid. For this we performed pull-down assays with purified AdV capsids incubated with cellular extracts of U2OS cells. We tested in parallel to pull-down endogenous CRM1 or exogenous HA-CRM1 C528S by using the capsid as bait. To investigate whether LMB treatment could disrupt the hypothetical interaction between the viral capsid and CRM1, we included a condition in which capsids were incubated with non-transfected cell extracts in presence of LMB. Purified Ad5 capsids were pre-treated at pH 7 or pH 5, with the aim to mimic the conditions that viral particles encounter inside early endosomes. An aliquot corresponding to 5×10^9 physical particles of pre-treated viruses at pH 7 or pH 5 was kept as input to control the pull-down efficiency. An aliquot of cell extracts was taken as input control as well. Then, 5×10^9 physical AdV particles were incubated with either non-transfected or containing exogenous HA-CRM1 C528S cell extracts for 1 h at room temperature. Samples were centrifuged under conditions allowing efficient pull-down of stably assembled capsids, and the input and resulting pull-down fractions were analyzed by western-blot. The light chain of kinesin-1 (KLC) has been described to bind the capsid protein IX (Strunze et al., 2011). Therefore, this protein was used as a positive control to confirm that capsids were stable enough to form complexes with cellular factors. A band corresponding to KLC was observed specifically in conditions in which capsids were included in the reaction, confirming co-sedimentation of KLC and capsids (**Figure 43**). In contrast, under our pulldown conditions, no signal for either endogenous or exogenous HA-CRM1 was detected, despite high input levels of the proteins and high recovery rates of capsids. These results show that under these conditions, CRM1 does not bind AdV capsids.

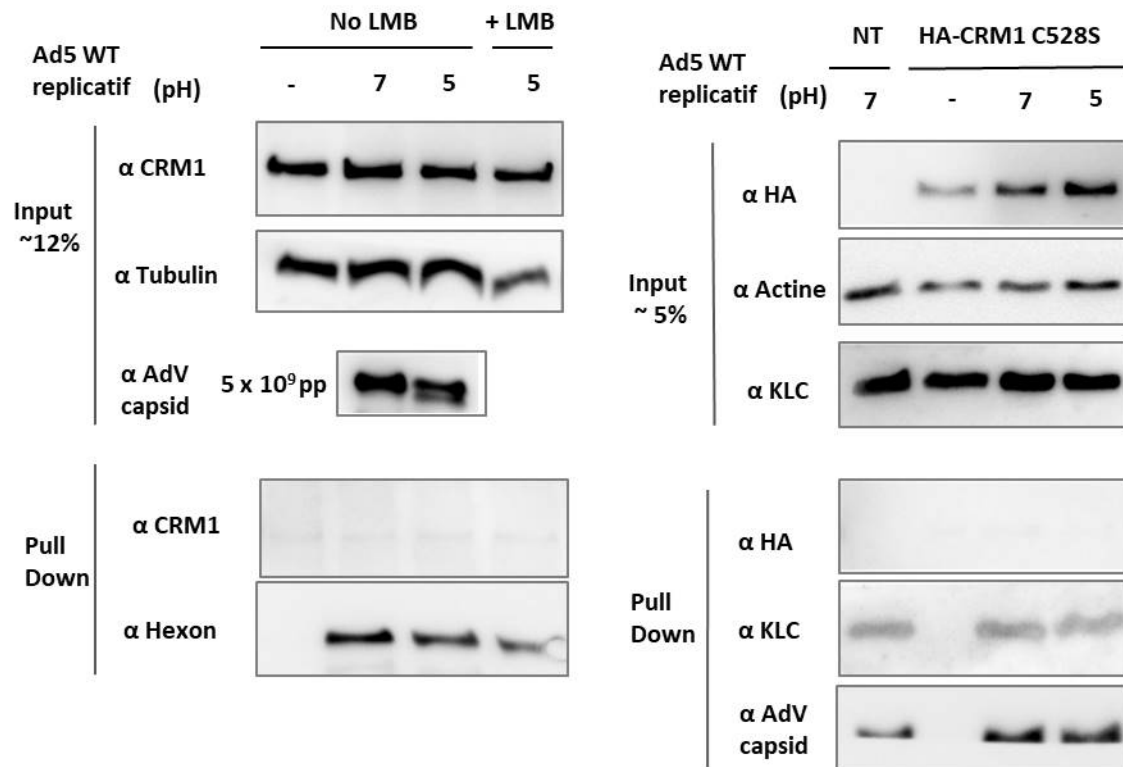


Figure 43: CRM1 does not interact with purified Ad5 particles. Pull down of purified AdV particles incubated with U2OS cell extracts expressing endogenous CRM1 (left panel) or an excess of HA-CRM1 C528S (right panel). Cells were non-transfected (left panel and NT in right panel) or transfected with a HA-CRM1 C528S construct as indicated on the top. Purified viruses were pre-treated at the indicated pH for 1 h. Equivalent amounts of purified viruses were kept as input control or incubated with total cell extracts for ~ 45 min in presence or absence of LMB as indicated. Input and pull-down fractions were separated by SDS-PAGE and proteins were detected by WB using specific antibodies for CRM1 and HA-tag, to detect endogenous or exogenous CRM1, respectively; α -tubuline and actine as loading controls; AdV capsid to detect the hexon protein and evaluate the pull-down efficiency; and the kinesin-light chain (KLC) as a positive control for the binding to the AdV capsid.

2.5.2. The Δ pIX AdV mutant shows premature disassembly of the capsid

The Δ pIX AdV mutant is less infectious than the WT virus (Sargent et al., 2004; Strunze et al., 2011). This mutant lacking the protein IX has been shown to be unable to recruit kinesin-1 to the capsid (Strunze et al., 2011). Given that kinesin-1 is thought to be required for AdV capsid disassembly and that it binds to viral pIX, this interaction has been proposed to support the uncoating of incoming AdV particles (Strunze et al., 2011). Thus, infectivity defects of the Δ pIX AdV mutant have been explained to result from disassembly defects because of this lack of interaction with kinesin-1.

In a first approach, we wanted to characterize the distribution of Δ pIX AdV capsids over time and the kinetic of genome delivery of this mutant compared to the wt AdV. For this, cells were infected with similar amounts of physical particles of either the Δ pIX mutant or wt AdV. Cells at 20 min, 1 h, 2 h or 4 hpi were stained for detecting the viral pVII or the capsids using specific antibodies. In the case of the wt AdV nuclear genome delivery kinetic, capsids were detected during the whole time course and genome import resembled previous kinetics (**Figure 44a**). In contrast Δ pIX AdV capsids were hard to detect after 1 hpi. Furthermore, in the case of the Δ pIX AdV, pVII dots were readily detected in the cytoplasm as early as 20 min pi, often localizing at the cell periphery. Cytoplasmic pVII appeared smaller than the nuclear pVII dots and disappeared over time, while nuclear pVII dots increased in number over time similar to the wt AdV. The simplest explanation for our observation was that Δ pIX AdV capsids have reduced stability, a notion that was described previously (Colby and Shenk, 1981; Furcinitti et al., 1989). For this reason, the parameter analysed in this experiment is not the pVII to AdV capsid ratio but the relation between the numbers of nuclear pVII to the total amount of pVII dots detected (**Figure 44b and c**). The % of nuclear pVII in the time course of the wt AdV was close to the 100 %, with a slight increase in the ratio of cytosolic pVII at 1 hpi, coincident with the arrival of capsids at the nucleus. Not surprisingly the Δ pIX AdV capsids showed a strong tendency to expose AdV cores in the cytoplasm (**Figure 44a**). However at the end of the time course (4 hpi), the ratio of nuclear pVII was closer to the levels of the wt AdV. These results show that the mutant AdV lacking the capsid protein pIX disassembles in the cytosol thereby exposing its viral core; however a large fraction of capsids is still able to deliver its genome into the nucleus.

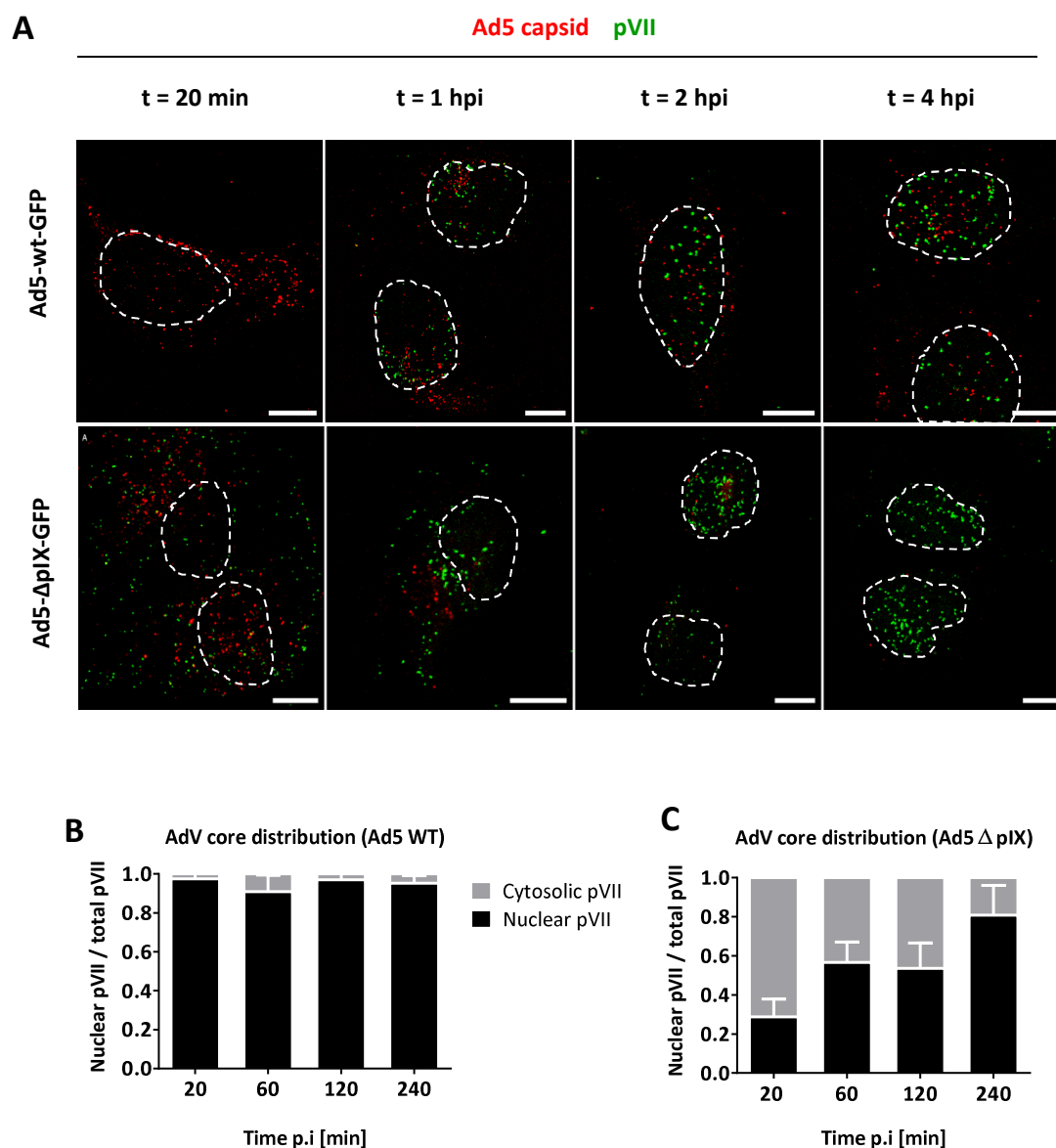


Figure 44: The Δ pIX AdV mutant shows premature disassembly of the capsid. AdV lacking the capsid-surface -exposed structural protein IX abnormally deliver their genomes in the cytosol (A) Representative confocal images of the kinetic of genome delivery of wt Ad5-GFP (upper row) or Δ pIX Ad5 mutant viruses (lower row). Cells were infected with equivalent number of physical particles of wt or Δ pIX Ad5 vectors and fixed at the indicated time points. Fixed cells were stained using specific antibodies for AdV capsid (red) and the core protein VII (green). DAPI staining was used to visualize the chromatin, here dashed lines represent the edges of DAPI staining. Maximal projection images are shown. Scale bars 10 μ m. (B-C) Quantification of the mean of nuclear (black bar) and cytosolic (grey bar) pVII dots represented as the proportion of the total number of pVII dots detected, which was normalized to 1. Data obtained from individual cell values ($n > 10$ per condition) are represented in stacked bars for the wt Ad5 (B) or the Δ pIX Ad5 mutant (C). Bars represent the SD.

2.5.3. CRM1-dependent nuclear targeting of AdV capsids does not depend on viral pIX

The Δ pIX AdV mutant showed a different phenotype regarding the delivery of its genome compared to the wt virus. Cytosolic pVII dots were detected at early time post infection. In contrast, at later time points, nuclear accumulation of pVII dots was observed. The cytosolic AdV cores could be either the result of premature disassembly of the capsids or instead, stem from an accelerated transport to the NPC that would cause capsid disassembly at the NPC, followed by a defect in genome import and cytosolic accumulation of genomes from those capsids. We considered this possibility and hypothesized that Δ pIX AdV mutant capsids should not dock at the NPC upon specific inhibition of CRM1 by LMB treatment and thus, they should not disassemble and not release genomes in the cytosol. In contrast, if genomes were released prior to NPC docking, this would reveal if cytosolic genomes can still be imported into the nucleus. To answer these questions, cells were infected with the Δ pIX AdV mutant in presence or in absence of LMB for 20 min, 1 h and 2 h. Cells were then stained for viral pVII and capsids, using specific antibodies. In absence of LMB, we could confirm previous results in which cytosolic pVII was already detected at 20 min pi (**Figure 45a**) while at 1 and 2 hpi accumulation of nuclear pVII was observed. In presence of LMB, pVII dots were still observed in the cytoplasmic region at 20 min pi similar to non-treated control cells. However, at 1 and 2 hpi some cytosolic pVII could still be detected but no nuclear pVII was observed. Furthermore, Δ pIX capsids accumulated at the MTOC at 1 hpi as do wt AdV capsids upon inhibition of CRM1. At 2 hpi this accumulation was less evident, concomitant with a general loss of capsid signal at this time point. These results show unequivocally that some capsids are disintegrated rather than disassembled even in the presence of LMB, and prematurely expose the AdV core in the cytoplasm. These genomes are rapidly degraded and do not contribute to the nuclear pool of imported viral genomes. However, there seem to be another population of capsids that are stable enough to reach the perinuclear region. These capsids are affected by LMB treatment, suggesting that they use the same CRM1 dependent disassembly mechanism as do wt capsids even though they lack the pIX capsid protein. To further confirm that AdV capsid protein IX is not involved in CRM1-dependent AdV genome delivery, cells were transfected with HA-CRM1 C528S or mock treated and infected with the Δ pIX AdV mutant in presence or absence of LMB. Nuclear accumulation of pVII was then analysed at 2 hpi. Similar than the wt AdV, LMB completely prevented nuclear accumulation of Δ pIX AdV genomes compared to non-treated cells (**Figure 45b and c**).

Conversely, overexpression of the HA-CRM1 construct, resistant to LMB, restored Δ pIX AdV genome import.

Taken together, these results show that capsids devoid of the capsid protein IX are less stable. Consequently, they disintegrate on their way to the nucleus and prematurely expose their viral core. These cytoplasmic released AdV cores are not able to reach the nuclear compartment, suggesting that they are probably degraded. On the other hand, a subpopulation of Δ pIX AdV particles succeeds in reaching the nuclear periphery and depends on CRM1 to deliver the viral genome, similar to WT AdV particles. These data also suggest that protein IX is dispensable for AdV genome delivery unlike previously reported (Strunze et al., 2011).

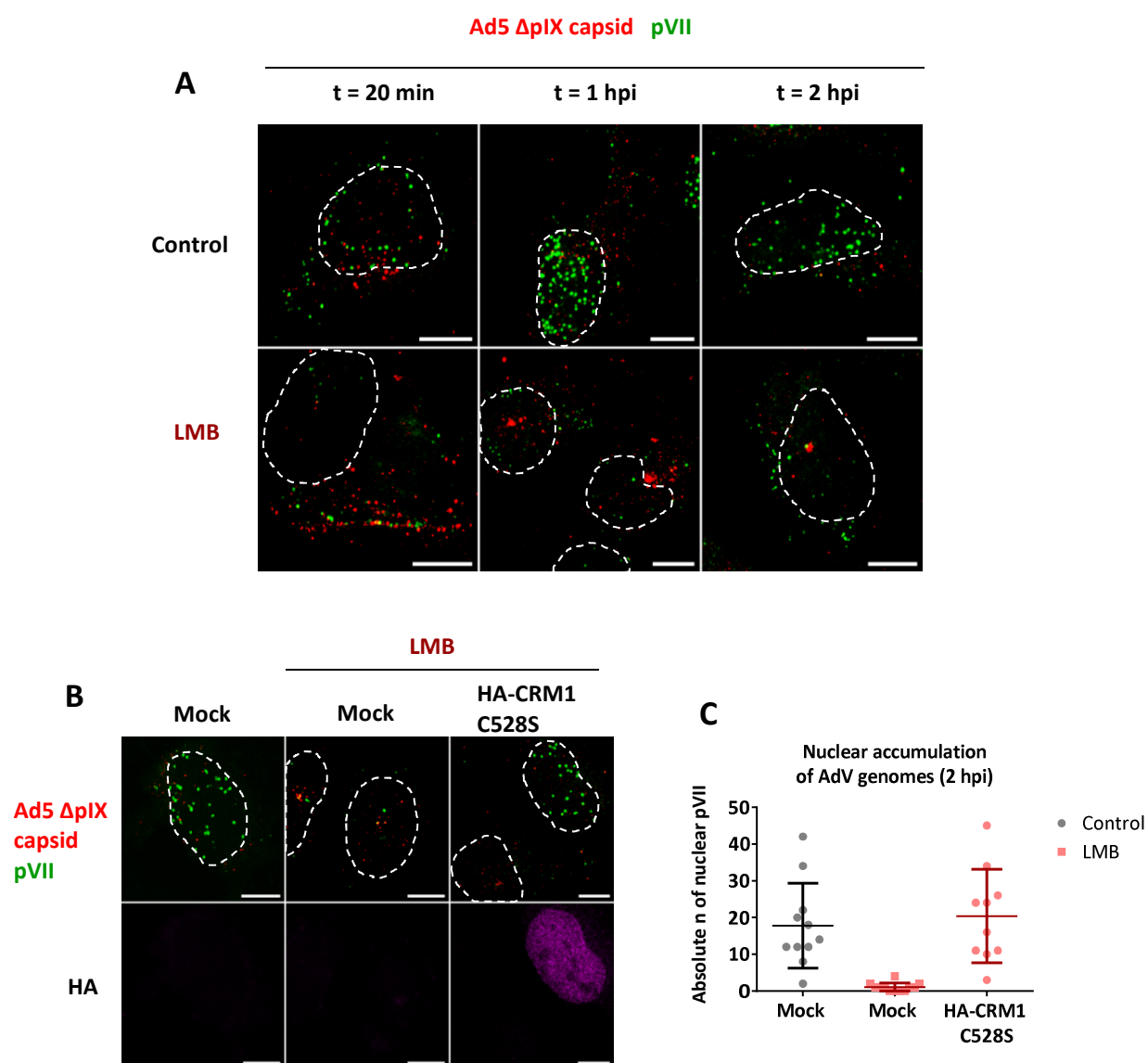


Figure 45: Δ pIX AdV genome delivery requires CRM1. LMB treatment impairs nuclear delivery of Δ pIX AdV genomes (A) Representative confocal images of the kinetic of genome delivery of Δ pIX Ad5 mutant viruses in absence (control) or presence of LMB. Cells were infected with Δ pIX Ad5 vectors and fixed at the indicated time points in presence or absence or LMB. Fixed cells were stained using specific antibodies for AdV capsid (red) and the core protein VII (green). DAPI staining was used to visualize the chromatin. Dashed lines represent the edges of DAPI staining. Maximal projection images are shown. Scale bars 10 μ m. (B) Representative confocal images of the nuclear accumulation of of Δ pIX AdV cores in absence (control) or presence of LMB. Cells were transfected with either an empty plasmid (mock) or with a HA-CRM1 C528S mutant and infected with Δ pIX Ad5 vectors for 2 h. Fixed cells were stained using specific antibodies for AdV capsid (red), the core protein VII (green) and HA to detect exogenous CRM1. DAPI staining was used to visualize the chromatin. Dashed lines represent the edges of DAPI staining. Maximal projection images are shown. Scale bars 10 μ m. (C) Quantification of the absolute number of nuclear pVII (pVII co-localizing with DAPI) in the indicated conditions. Data obtained from individual cell values ($n > 10$ per condition) are represented in a scatter blot. Bars in the scatter plot represent the mean and SD.

DISCUSSION

AdV need to reach the nucleus of infected cells in order to replicate. Because import of DNA to the nucleus is not a physiological process, AdV have evolved strategies to access and divert the existing cellular transport machinery. In this work, we addressed the involvement of the major component of the cytoplasmic filaments of the NPC, Nup358, as well as the contribution of CRM1 and several import receptors in different steps of AdV genome delivery.

1. THE ROLE OF NUP358 IN ADENOVIRUS GENOME IMPORT

Previous studies have identified the cytoplasmic Nups Nup214 and Nup358 in key steps of AdV genome delivery (Trotman et al., 2001; Strunze et al., 2011; Cassany et al., 2015). While in the literature there is a consensus about the role of Nup214 as AdV capsid docking at the NPC, conflicting results were obtained regarding the role Nup358 in AdV genome delivery (Strunze et al., 2011; Cassany et al., 2015). Transport receptors have also been linked to AdV genome delivery. Docking of the viral capsid to the NPC requires functional CRM1 (Strunze et al., 2005) and import of the viral genome has been suggested to be mediated by several import receptors (Trotman et al., 2001; Wodrich et al., 2006; Hindley et al., 2007). Among them, transportin-1 was highlighted as key transport receptor mediating nuclear import of AdV cores in digitonin-permeabilized cells (Hindley et al., 2007). We thus addressed the role of Nup358 and transport receptors in AdV genome delivery in more detail.

1.1. Depletion of Nup358 delays AdV genome import

Previous work by Strunze *et al.* showed strong inhibition of AdV infection as well as impaired disassembly of AdV capsids by using RNAi-mediated depletion of Nup358. Additionally, the authors observed disassembled capsids co-localizing with Nups, including Nup358 at the cell periphery 3 hpi, which was paralleled with an increase in nuclear permeability. The study further showed that kinesin-1 can bind the capsid exposed protein IX. Because it was known that the kinesin-binding domain of Nup358 (JX2) can bind and activate the anterograde motor protein kinesin-1 (Cai et al., 2001; Cho et al., 2009), whose depletion also reduced the number of disassembled capsids, the authors proposed a model in which kinesin-1 anterograde movement via Nup358 activation results in protein IX-mediated capsid disassembly at the NPC. The model further suggests that kinesin-1-driven forces trigger the release of Nups, (e.g. Nup358), from the NPC towards the cell periphery thereby increasing

permeability of the NPC and thus, facilitating progression of viral infection (Strunze et al., 2011).

These results are in conflict with the study of Cassany *et al.* which shows that genome import is impaired in Nup214 depleted HeLa cells, while Nup358 is dispensable (Cassany et al., 2015). Depletion of Nup214 but not Nup358 impaired docking of purified hexon to the NPC in digitonin-permeabilized cells. Thus, authors confirmed previous studies (Trotman et al., 2001) showing that Nup214 is the docking site for incoming AdV capsids, and additionally concluded that Nup358 is not required during AdV genome delivery.

In the present study, we have observed that depletion of Nup358 delays accumulation of AdV genomes in the nucleus, suggesting that Nup358 is not essential but facilitates AdV genome delivery. We further analyzed kinetics of AdV core separation from capsids and capsid disassembly, and observed an accumulation of non-separated AdV cores in absence of Nup358 but an efficient exposure of AdV cores at the nuclear periphery, suggesting intact disassembly.

The differences between the 3 studies might be related to the read-outs employed in each case. Strunze *et al.* analyzed transduction of an Ad5-GFP vector to evaluate AdV infection, and observed a 4-fold reduction of GFP-positive cells in Nup358 depleted cells. This approach however does not allow discerning whether AdV genome delivery has been impaired or if the block occurs at a later step. As it was mentioned in the introduction (section 5), Nup358 depletion strongly impairs mRNA export in *Drosophila* or mouse cells (Forler et al., 2004; Hamada et al., 2011) and also in HeLa cells, although to a lower extent compared to insect cells (Hutten and Kehlenbach, 2006). Thus, export of GFP-mRNA from the Ad5-GFP vector might have been altered after Nup358 depletion. The study of Strunze *et al.* further showed that depletion of Nup358 decreased by 1.5-fold the disassembly of AdV capsids at 3 hpi instead of 4-fold as observed in Ad5-GFP vector expression, suggesting that additional steps during Ad5-GFP transduction should be impaired in Nup358-depleted cells. Detection of disassembled viral capsids was performed by using a polyclonal anti-hexon antibody (R70). This antibody preferentially recognizes epitopes in AdV hexon that are substantially more exposed after disassembly of capsids at the NPC (Greber et al., 1993; Trotman et al., 2001; Puntener et al., 2011). Quantification of disassembled AdV was calculated as the mean fluorescence intensity of R70 staining. However, quantification of total fluorescence intensity does not reflect a specific degree of disassembly of the capsids; they could still be associated to viral cores or disintegrated. Therefore, information about the state of detected capsids is missing and the observed reduction in exposure of otherwise hidden

hexon epitopes, could have been the result of defective release of AdV cores that would delay complete disruption of viral capsids.

In the analysis by Cassany *et al*, AdV genome import was monitored by detection of the vDNA using fluorescence in situ hybridization (FISH). This technique suffers from the harsh specimen preparation. Thus, coated genomes at the NPC might be accidentally detected even prior to capsid disassembly and genome import. Cassany *et al* also indirectly detected vDNA by using specific antibodies against the core protein VII. This approach has been shown to be simple and reliable for monitoring AdV genome delivery in fixed cells because the protein VII epitope is hidden when genomes are still protected by the capsid. A study from Greber and co-workers showed that the vast majority of nuclear AdV genomes labelled with “clickable” nucleoside analogues such as EdC are protein VII-positive (Wang *et al.*, 2013). Indeed, reduction of genome import at 3 hpi upon Nup214 depletion was much more evident when analysing total fluorescence of nuclear pVII (~ 80 % reduction) than total nuclear genome staining (~ 50 % reduction). In parallel, detection of total nuclear genome staining in Nup358 depleted cells was not altered compared to the control, but detection of total nuclear pVII showed about 40 % reduction, although still non statistically significant. The latter results show that the readout might not be sensitive enough, as it does not allow to monitor kinetic differences in genome import.

These results encourage us to analyze the kinetic of AdV genome delivery in Nup358 depleted cells by using specific antibodies recognizing protein VII and viral capsids. In this analysis, instead of quantifying total fluorescence of pVII and AdV capsids, individual dots were quantified by using semi-automated software. This method allowed us to precisely quantify individual AdV cores and thus, evaluate the proportion of disassembled capsids and released genomes. Thus, we observed a delayed AdV genome delivery in Nup358 depleted cells compared to control cells, which correlated with an accumulation of exposed but non separated viral cores during the first 2 hpi. These results show that incoming capsids were able to efficiently expose their associated cores at the NPC but a defective separation of AdV cores from the capsids and import reduced efficiency of AdV genome delivery.

We have observed that Nup358 depletion affects kinetics of AdV genome delivery but does not affect the overall import. Thus, several aspects might be critical to observe an effect on AdV genome delivery after depletion of Nup358. First, it is the time point after infection at which the analysis is performed. In this respect, we observed the maximal difference at 2 hpi but at later time points the differences between control- or Nup358-depleted cells were non-

significant. In the study by Strunze *et al.* the analysis of Ad5-GFP vector expression was done at 6 hpi. Taking into account our results, the differences observed in efficiency of Ad5-GFP transduction between control and Nup358 depleted cells are probably not exclusively related to a default in import. Strunze *et al.* also analyzed capsid disassembly at 3 hpi. The analysis of AdV genome import in the study of Cassany *et al.* was similarly performed 3 hpi. In our analyses the time point zero was considered 30 min after addition of the AdV particles to cells at 37 °C, when most of viral particles have entered into the cytosol. Instead previous studies performed a pre-binding of capsids at 4 °C and considered the time point zero when switching the incubation temperature to 37 °C. Thus, previous analyses performed at 3 hpi are slightly later but somewhat comparable to our time point 2 hpi. Indeed, 1.5-fold reduction in AdV capsid disassembly (Strunze et al., 2011) and 40% reduction in nuclear accumulation of pVII (Cassany et al., 2015) in Nup358-depleted compared to control cells do not necessarily contradict our results at 2 hpi.

Finally, another aspect that might be important is the viral load used for infection. Strunze *et al.* used relatively high viral loads (in the range of 8000 physical particles per cell) and observed an impaired permeability barrier at 3 hpi. Cassany *et al.* used 10000 pp/cell for FISH analyses and 1000 pp/cell for pVII detection, and observed a clearer effect of Nups depletion in the case of pVII analyses. In this study, cells were infected at MOI 30 which is in the range of 3000-5000 pp/cell. It is possible that the progression of infection disrupts the permeability barrier, making incoming AdV particles less dependent on the nucleocytoplasmic transport machinery overtime, and this effect might be directly proportional to the MOI used. However, this hypothesis should be confirmed experimentally.

1.2. The N-terminal half of Nup358 is required for efficient genome import

Previous work by Hutten *et al.* demonstrated that depletion of Nup358 leads to reduced efficiency of importin- α/β - and transportin-dependent import in HeLa cells (Hutten et al., 2008, 2009). Inactivation of Nup358 in conditional knockout MEFs was also shown to cause defects on transportin- and importin- α/β import pathways as well as cell death (Hamada et al., 2011). Both cell viability and import defects were restored in MEFs lacking endogenous Nup358 but stably expressing a N-terminal construct of Nup358 containing the first FG-repeat cluster and a RanBD (aa 1-1306). Using a set of different NPC-anchored truncated mutants of Nup358, Hamada *et al.* observed that the N-terminal FG-repeat cluster was sufficient for efficient mRNA export and transportin-dependent import, but one additional RanBD was needed to restore importin α/β -mediated import. In another study, importin- α/β -

mediated import was similarly dependent on the aa 1-1306 fragment of Nup358 in Nup358-depleted HeLa cells, however transportin-dependent import required additional sequences further downstream, including a RanBD and the zinc finger region (Wälde et al., 2012). A similar approach revealed that a N-terminal fragment of Nup358 containing the zinc finger region was also important to restore importin-7-mediated import of the protein component of the human telomerase (hTERT) into the nucleus of HeLa cells lacking endogenous Nup358 (Frohnert et al., 2014). These studies (Hamada et al., 2011; Wälde et al., 2012; Frohnert et al., 2014) revealed that the role of Nup358 in facilitating nuclear import was predominantly exerted by the N-terminal region of Nup358 and suggested that the RanGAP-interacting region and the SUMO-E3 ligase activity of Nup358 were dispensable.

We thus mapped the minimal region of Nup358 required for an efficient AdV genome delivery. For this, we used a similar approach in U2OS cells and performed depletion/reconstitution experiments using either full-length or truncation mutants of Nup358 harbouring the NPC-anchoring region. This assay allowed us to test whether the observed delay of AdV genome delivery could be restored with full-length exogenous Nup358, and whether some specific domains of Nup358 are dispensable for facilitating delivery of AdV genomes. We observed that defects on nuclear accumulation of viral genomes were restored in cells lacking endogenous Nup358 by expressing the full-length Nup358 construct, but also with a relatively short fragment containing only the N-terminal half of Nup358. This fragment comprises a FG-repeat cluster, one RanBD and the zinc finger domain, suggesting that absence of the C-terminal half of Nup358 does not limit either AdV capsid disassembly or import of the viral genome into the nucleus.

This is *a priori* in conflict with results from the study by Strunze *et al.* showing that overexpression of the kinesin-1 binding domain of Nup358, JX2, which is downstream of the zinc finger region, reduces Ad2 transduction by 1.5-fold (Strunze et al., 2011). Again, the competition effect caused by an excess of JX2 in transduction of the Ad2 vector can be the result of either an impaired AdV genome delivery or a defective export of, in this case, mRNA of the RFP gene. Kinesin-1 family motors (KIF5) are known to directly bind and transport messenger ribonucleoprotein (mRNP) complexes in neurons (Kanai et al., 2004). The kinesin-1 family member identified to be involved in AdV genome delivery is specifically KIF5C (Strunze et al., 2011) and it is preferentially expressed in brain tissue (Kanai et al., 2000; Cai et al., 2001). It may be possible that Nup358 cooperate with KIF5C in neuronal cells to mediate traffic of exported mRNA to cytosolic sites of translation and, consequently, indirectly facilitate efficient translation of exported mRNA. Although function

of KIF5C in epithelial cells is not well known (Astania and Jacob, 2010) it could potentially interact with Nup358 in epithelial cells and cooperatively facilitate mRNA trafficking and translation.

Kinesin-1 has been recently described to link export of the oncogenic transcription factor c-Myc from the nucleus with cytosolic proteasomal-dependent degradation, avoiding formation of c-Myc aggregates in the cytoplasm (Lee, 2014). It is also possible that incoming partially disassembled AdV capsids are recognized at the level of the NPC as protein aggregates and binding to kinesin-1 promotes its traffic back to the cytoplasm to facilitate degradation of viral particles. This process could indirectly favour disassembly of AdV capsids at the NPC. However our results do not suggest a specific requirement of Nup358 to promote activation of kinesin-1 at the NPC, since the region comprising the RanBD2-JX2-RanBD3 necessary for an efficient activation of kinesin-1 (Cai et al., 2001; Cho et al., 2009; Patil et al., 2013) is dispensable for AdV genome delivery. Instead, results suggested a possible function of the N-terminal half of Nup358 in facilitating import of the AdV cores into the nucleus.

1.3. Transport receptors are rate-limiting for AdV genome delivery

In cells lacking Nup358, an excess of transport receptors could restore the defects observed in nuclear import of the generic reporter protein NES-GFP₂-cNLS or HIV-1 Rev, dependent on the importin- α/β or transportin-1 pathways, respectively (Hutten et al., 2008, 2009). However import of specific proteins identified as cargoes of importin α/β (DBC-1, deleted in breast cancer-1) or transportin-1 (DMAP-1, DNA methyltransferase 1 associated protein 1) could not be restored in cells lacking Nup358 by using an excess of transport receptors. These proteins were shown to interact with Nup358 in a receptor-independent manner, suggesting that Nup358 can stimulate efficient import of certain cargoes by at least two ways: by increasing the active concentration of transport receptors at the NPC and by providing receptor-independent binding sites to selective cargoes (Wälde et al., 2012). Importin-7 and Nup358 were shown to cooperate in import of hTERT, however overexpression of importin-7 in Nup358 could not restore the import defect observed in absence of Nup358, suggesting a tight cooperation between importin-7 and Nup358 (Frohnert et al., 2014).

Transport receptors were also shown to be limiting for AdV genome delivery. Antibody microinjection against importin- β or importin-7 reduced the number of accessible capsids (recognized by the anti-hexon antibody R70) at 120 min post infection. These importins were suggested to facilitate Histone 1-mediated disassembly by facilitating translocation of H1-hexon complexes into the nucleus to help in capsid disassembly (Trotman et al., 2001). The

proposed mechanism is unlikely since i) the mapped binding site for Histone 1 (H1) on hexon is in the non-conserved hypervariable loop (and thus only present in select AdV genotypes) and ii) efficient import of hexon has been shown to be mediated by NLS-containing premature protein VI (Wodrich et al., 2003) while purified hexon could not be imported into the nucleus of digitonin-permeabilized cells after addition of energy and cytosol (Cassany et al., 2015), suggesting that import of hexon occurs during viral assembly but is less likely to be of importance during AdV genome delivery. However, it could still be possible that a partially exposed viral genome is recognized by cellular histones in the vicinity of the nucleus, acting as adaptors for importin-facilitated release and import of viral genome. A more likely scenario is that the core associated protein VII, which encodes several functional NLS, acts as adaptor for importin-facilitated transport of the viral genome. Transportin-1 was shown to be limiting for AdV genome import in *in vitro* assays (Hindley et al., 2007). Importin- β , -7 and transportin-1 have been shown to bind and import pre-pVII in digitonin-permeabilized cells (Wodrich et al., 2006). In addition, transportin-1 and importin-7 are also able to bind the mature form of protein VII (Hindley et al., 2007). In these studies however, importin-9 was not included, but it constitutes a good candidate, since it can mediate import of cellular histones (Mühlhäusser et al., 2001). Furthermore, both importin-9 and transportin-1 can mediate HIV-1 Rev import to the nucleus (Hutten et al., 2009).

We thus analyzed whether the reduced efficiency of AdV genome import observed in cells depleted for Nup358 could be compensated by expressing an excess of transport receptors. We observed that both mainly transportin-1 and to a lesser extent importin-9 were able to restore an efficient accumulation of AdV cores in the nucleus of Nup358-depleted cells; instead it was not the case for importin- β or importin-7. These results showed that transport receptors can become limiting for AdV genome import in absence of Nup358, and suggested a specific role for transportin-1 and/or importin-9 in mediating this process. We thus, analyzed import of viral genomes in absence of a functional transportin-1. However, AdV genome import in these conditions was not affected, suggesting that a lack of transportin-1 can be compensated by other transport receptors similarly able to mediate an efficient import of the vDNA. One possibility is that importin-9 is as functional as transportin-1 in mediating import of AdV genome, which would explain why absence of transportin-1 does not cause major impact on vDNA import. Both transportin-1 and importin-9 were shown to be functional in mediating import of HIV-1 Rev (Hutten et al., 2009). However in the case of HIV-1 Rev, depletion or specific inhibition of transportin-1 strongly blocked import, suggesting that endogenous levels of importin-9 were not sufficient to compensate absence of

transportin-1. Only cells expressing an excess of importin-9 (but not importin- β) could restore the block of HIV-1 Rev import induced by specific inhibition of the transportin-1 pathway. The case of AdV genome import seems to be different from that of the HIV-1 protein Rev, since absence or specific inhibition of transportin-1 does not compromise efficiency of AdV genome import. It could be possible that transportin-1 binds to a specific site of Nup358 shared with other import receptors. In this case, depletion of transportin-1 might liberate the site and gives room to different import receptors capable to efficiently mediate import of AdV genome. In this case, depletion of transportin-1 would not be effective in genome import, and would explain our results showing that in presence of functional transportin-1, AdV cores are preferentially imported by transportin-1.

An alternative transport receptor mediating AdV genome import could still be importin-7. It was shown to be limiting in AdV infection (Trotman et al., 2001) and to bind protein VII (Wodrich et al., 2006). Moreover importin-7 cooperates with Nup358 for import of certain substrates (Frohnert et al., 2014). It could be possible that the AdV genome is a substrate for importin-7 and that this transport receptor requires cooperation with Nup358 to mediate import. That would explain why excess of importin-7 does not restore AdV genome import in absence of Nup358. Furthermore cooperative importin-7-mediated transport of hTERT with Nup358 specifically required a NPC-anchored N-terminal fragment of the Nup containing the zinc finger domain, similar to AdV infection. It would be interesting to test whether importin-7-depletion affects AdV genome import as it does for hTERT (Frohnert et al., 2014).

We also analyzed the effect of expressing an excess of importin- β in Nup358-depleted cells on the efficiency of AdV genome import. Similar to importin-7, importin- β was not able to restore efficient import of the vDNA. We cannot exclude however a cooperative role of importin-7 and β , since it is known that they can function as heterodimer to promote import of H1 (Jäkel et al., 1999). Similarly, we cannot exclude the contribution of other import receptors non-tested in this study.

Hence, it seems likely that Nup358 participate in AdV genome delivery by maintaining an available pool of importins close to the NPC via recruitment of free transport receptors (through FG-repeat binding) or in complex with RanGTP (through the RanBDs), rather than providing direct binding sites for AdV genome, since an excess of some transport receptors could restore efficient genome import in absence of Nup358. Our results also show that transportin-1 is the most efficient transport receptor mediating import of AdV genomes in absence of Nup358, suggesting that transportin-1 could be the major import receptor of AdV cores *in vivo*.

1.4. The N-terminal half of Nup358 recruits import receptors

Nup358 is well known as binding site for importin- β (Delphin et al., 1997). Importin- β can bind Nup358 by two different mechanisms: either by direct interaction with the FG-repeat motifs of Nup358, or via indirect binding with RanGTP to the RanBDs. Two different regions of recombinant Nup358 containing equivalent number of FG-repeats and RanBDs were shown to bind either purified importin- β alone or in complex with RanGTP, with very similar affinities, localized either at the N-terminal half or at the C-terminal part of Nup358 (Ben-Efraim and Gerace, 2001). However, Ritterhoff *et al.* showed recently that C-terminal FG-repeat patches of Nup358 preferentially interact with CRM1 compared to several other transport receptors, included importin- β and transportin-1 (Ritterhoff et al., 2016). It is possible that the C-terminal region of Nup358 is normally occupied by CRM1 thereby preventing the binding of other transport receptors *in vivo*. Studies in MEF cells confirmed that an N-terminal NPC-anchoring fragment of Nup358 containing the first FG-repeat cluster and RanBD1 was necessary to bind importin- β in complex with RanGTP, however not the importin- β alone (Hamada et al., 2011). Accordingly, only the NPC-anchored fragment of Nup358 containing the RanBD1 restored importin- β targeting to the NE and importin α/β -dependent transport in conditional knockout MEFs for Nup358. Thus, *in vivo*, importin- β -mediated transport shows strong dependency on RanGTP for targeting importin- β to the RanBD1 of Nup358.

Binding of transportin-1 with Nup358 has been less characterized. Transportin-1 was shown to bind Nup358 although with reduced affinity compared to importin- β (Bonifaci et al., 1997). Recombinant transportin-1 was shown to pull-down Nup358 from *Xenopus* oocyte extracts in a RanGTP-insensitive and M9M-sensitive manner (Lau et al., 2009; Bernis et al., 2014). Different N-terminal NPC-anchoring fragments of Nup358 of variable lengths have been shown to promote efficient transportin-1-dependent import (Hamada et al., 2011; Wälde et al., 2012). However the exact region of Nup358 serving as docking site for transportin-1 is not known. Interestingly, importin- β and transportin-1 do not share the same binding sites in Nup153 (Shah and Forbes, 1998), component of the NPC at the nuclear basket, but both have common binding sites at the mobile Nup98 (Bonifaci et al., 1997). Furthermore, an excess of transportin-1 inhibits importin- α/β -dependent import and *vice versa*, in digitonin-permeabilized HeLa cells (Bonifaci et al., 1997), suggesting that both could share similar docking sites at the cytoplasmic filaments of the NPC.

RanGTP-dependent binding of importin-7 to RanBD1- or RanBD2-3-containing regions of Nup358 has also been reported (Frohnert et al., 2014). Instead interaction of importin-9 with Nup358 remains to be investigated.

Our results show that a soluble fragment comprising the N-terminal coiled-coil domain, a FG-repeat cluster and RanBD1 of Nup358, efficiently recruits both: importin- β and transportin-1, as observed in IF assays. In the case of importin- β , we could further confirm this recruitment by a Co-IP assay. Moreover, we observed an additional binding site for importin- β at the central region of Nup358 with apparent lower affinity, but not in the case of the C-terminal fragment, which is consistent with previous observations showing that the C-terminal part of Nup358 specifically binds to CRM1 and not to importin- β (Ritterhoff et al., 2016). However, we could not obtain conclusive results for transportin-1 in Co-IP assays. It is known that importin- β is highly expressed in cancer cells compared to normal cells (van der Watt et al., 2009; Kuusisto and Jans, 2015). It might be possible that both import receptors share the same binding site in Nup358 as they do in Nup98 (Bonifaci et al., 1997). If this would be the case, detection of importin- β -Nup358 binding might be favoured in detriment of transportin-1-Nup358 binding when using total cell extracts of transformed HEK293- α V β 5 cells in Co-IP assays. Alternatively, the binding of transportin-1 to Nup358 might be less dependent on RanGTP than importin- β and could mainly occur through direct binding to the FG-repeats. Binding of transport receptors to the FG-repeats of Nups is known to be of low affinity and to occur transiently; otherwise transport across the pore would become impossible (reviewed in Aramburu and Lemke, 2017). Indeed, we observed a stronger co-localization of transportin-1 compared to importin- β with soluble fragments of Nup358 that did not contain the RanBD1. In addition, transportin-1, contrary to importin- β , localizes at the nucleus rather than at the NE, favouring the hypothesis that it does not stably dock at the cytoplasmic filaments in a RanGTP-dependent manner. It would be interesting to analyze the interaction of transportin-1 with different recombinant fragments of Nup358 as well as to investigate possible competition with importin- β for the same binding site.

The N-terminal half of Nup358 necessary to restore efficient AdV genome import also harbours the zinc finger region. This domain was shown to directly bind the exportin CRM1 (Singh et al., 1999). Depletion of Nup358 reduces CRM1 localization at the NE (Bernad et al., 2004; Hamada et al., 2011). Even though nuclear targeting of AdV capsids was not impaired in Nup358-depleted cells, we considered the possibility that impaired docking of CRM1 at the NE would affect downstream steps during AdV genome delivery. We thus investigated whether the N-terminal half of Nup358 required for promoting an efficient

genome delivery could restore endogenous levels of CRM1 at the NE. Our results show that endogenous CRM1 cannot efficiently accumulate at the NE by expression of C-terminal truncated constructs of Nup358, in cells devoid of endogenous Nup358, which is consistent with previous observations (Hamada et al., 2011). A fragment containing the zinc finger domain, additional FG-repeats and RanBD2 co-localized with endogenous CRM1, but was still not efficient in accumulating CRM1 at the NE. These results support the hypothesis that endogenous CRM1 accumulates at the NE by binding to the C-terminal instead of the central region of Nup358. Moreover, these observations suggest a requirement of the central FG-repeat cluster in addition to the zinc finger domain to interact with endogenous CRM1. It is therefore unlikely that the N-terminal half of Nup358 facilitates AdV genome delivery by recruiting CRM1 at the NPC.

1.5. Conclusion

This study shows that Nup358 promotes efficient delivery of the AdV genome but it is not essentially required. The C-terminal part of Nup358 was dispensable to promote efficient accumulation of viral genomes in the nucleus. Therefore, Nup358 does not play a major role in supporting CRM1-dependent delivery of AdV genome. Instead, we propose that the mechanism through which Nup358 facilitate AdV genome delivery is by maintaining the concentration of available import receptors near the NPC, which become otherwise limiting for efficient AdV genome import during at least the first 2 h of infection. Later in infection, two different scenarios could explain the recovery of genome import rates. Either incoming AdV actively disrupt the permeability barrier of the NPC thereby reducing its dependency on transport receptors to delivery their genome or, the limited concentration of transport receptors are sufficient to promote genome import of remaining AdV particles.

2. THE ROLE OF CRM1 IN ADENOVIRUS GENOME DELIVERY

Nuclear targeting of incoming AdV capsids occurs through an unknown mechanism which is dependent on functional CRM1 (Strunze et al., 2005; Wang et al., 2017). Specific inhibition of CRM1 by LMB treatment was shown to block incoming AdV particles at the MTOC thereby preventing AdV capsid disassembly at the NPC and consequently, inhibiting infection (Strunze et al., 2005). Recently, Wang *et al.* have suggested that functional CRM1 is required for unloading incoming AdV particles from MT at the nuclear periphery (Wang et al., 2017). It is not clear whether this process directly involves CRM1 binding to incoming viral particles or if instead a CRM1-dependent NES-bearing cargo is responsible for this translocation. In the case nuclear targeting of AdV capsids directly depends on CRM1, Strunze *et al.* proposed 3 different scenarios (Strunze et al., 2005). The first considers the interaction of CRM1 alone with incoming viral particles. In this case, the interaction has to be of supraphysiological affinity and to occur independently of RanGTP (Engelsma et al., 2004). The second possibility involves a short-lived CRM1-NES-RanGTP complex that would unload viral particles from MT upon GTP hydrolysis triggered by cytosolic RanGAP. The third possibility takes into account the interaction of CRM1 with cytosolic Nups which could facilitate CRM1-dependent nuclear targeting of incoming AdV particles. We thus used different approaches to address these possibilities in both, interphase and mitotic cells.

2.1. A novel role for CRM1 in promoting AdV capsid disassembly

In interphase cells, nuclear targeting of AdV capsids has been shown to be strongly dependent on functional CRM1 export (Strunze et al., 2005; Wang et al., 2017). Docking of capsids at the NPC was shown to be a pre-requisite for AdV capsid disassembly (Trotman et al., 2001; Cassany et al., 2015). In interphase, capsid docking to the NPC precedes AdV disassembly, thus accumulation of AdV capsids at the MTOC due to specific inhibition of CRM1 does not allow to study the involvement of CRM1 at immediate downstream steps of AdV genome delivery. CRM1-dependent export and assembled NPC are specific for interphase cells. During mitosis, NPC are substantially disassembled and some of its components engage in mitotic functions unrelated to nucleo-cytoplasmic transport. If AdV depend on nucleo-cytoplasmic transport and assembled NPC to deliver AdV genomes only because a nuclear membrane prevents access to the nuclear interior, viral capsids should be able to disassemble and deliver their genomes in mitosis. Infection experiments in mitotic cells demonstrated that capsids were able to deliver their genomes in mitotic conditions, showing that AdV do not require nucleo-cytoplasmic transport *per se* nor assembled NPC to deliver their genomes.

Instead, endocytic uptake and intra-endosomal partial disassembly appeared crucial for further disassembly, similar to the situation in interphase cells. In addition, most of the released viral cores localized at the chromatin, suggesting that they could reach the chromatin in absence of the NE and that they possess a specific chromatin binding domain.

When we investigated whether a functional CRM1 was also required for efficient AdV genome delivery in mitosis, we could show that specific inhibition of CRM1 by LMB treatment of mitotic cells did not affect viral entry to the mitotic cell but strongly impaired AdV capsid disassembly. Overexpression of a CRM1 mutant resistant to LMB could not only restore capsid disassembly and AdV core release but drastically increased the efficiency compared to control cells. These results highlight the unprecedented involvement of CRM1 in promoting AdV capsid disassembly. However, this analysis does not allow us to know whether CRM1 is directly implicated in the capsid disassembly step or if it is implicated in an upstream step also in mitosis.

Since a high proportion of disassembled capsids and viral cores were localizing at the chromatin in control or CRM1 LMB resistant expressing cells, we considered the possibility that CRM1 enhanced AdV capsid disassembly by somehow facilitating translocation of AdV capsids to the chromatin, similar to what we observed in interphase. In a previous study by Strunze *et al.* (Strunze et al., 2005), AdV capsids were shown to strongly accumulate at mitotic centrosomes in presence of LMB. In our conditions, we observed a tendency of the AdV capsids to localize at regions away from the chromatin compared to control cells and indeed, some cells presented an accumulation of capsids at two discrete opposing regions, probably corresponding to both spindle poles. However, while accumulation at the MTOC was evident in co-cultivated cells that had progressed into interphase, mitotic LMB treated cells did not show such a strong accumulation at centrosomes. This effect became more evident in mitotic cells infected with much higher viral loads and observed at later times post infection (not shown). Overexpression of LMB resistant CRM1, which restored and enhanced AdV capsid disassembly, could not completely reverse the proportion of capsids localizing at the chromatin compared to control cells. Thus, it seems that translocation of capsids to the chromatin is not a pre-requisite for AdV capsid disassembly contrary to interphase cells. It is however possible that under normal conditions in mitotic cells, capsid disassembly mainly takes place at the chromatin, since CRM1 is targeted to the mitotic chromatin in a RanGTP-dependent manner. Even though CRM1 is somehow involved in preventing capsid accumulation at mitotic and interphase centrosomes, results in mitotic cells suggest that this function is independent of its role during AdV genome delivery at the disassembly step.

Another observation is that both released and capsid-associated AdV cores co-localized preferentially at the chromatin in a similar manner, either in control or CRM1 overexpressing cells, contrary to the overall capsid population that was less targeted in presence of LMB compared to control cells. This suggests that it is the core and not a capsid component that guides AdV capsids towards the chromatin in mitotic cells. Strongly supporting this idea, we observed capsid-associated AdV cores in living mitotic cells being targeted and stably docking at the chromatin. It is thus likely that a partially exposed genome is bound by cellular factors that facilitate translocation of the capsid to the chromatin. Alternatively, affinity of components of the viral core for chromatin could trigger targeting and docking of the viral particle to the chromatin.

2.2. Effect of soluble C-terminal fragments of Nup214

We analyzed the effect of overexpressing the CRM1 binding C-terminal fragment of Nup214 in AdV genome delivery. This fragment was shown to bind CRM1 and to induce its nuclear retention inside the nucleus (Fornerod et al., 1997). Expression of this FG-repeat containing fragment in cells was shown to also specifically impair CRM1-mediated nuclear export (Roloff et al., 2013). Inducible expression of the C-terminal fragment of Nup214 was also used to study the involvement of CRM1 in export of AdV mRNA transcripts (Schmid et al., 2012). We thus used this fragment to study the competition effect with AdV genome delivery and, as expected, we observed an accumulation of incoming AdV capsids at the MTOC. Similar to previous observations, CRM1 was trapped inside the nucleus of cells expressing the C-terminal fragment of Nup214 and CRM1-dependent protein export was impaired. This result confirmed the requirement of a functional CRM1-dependent export for nuclear targeting of incoming AdV. The observation that AdV genome delivery also takes place in mitotic cells allowed us to study the requirement of CRM1-binding to Nups regardless of the nucleo-cytoplasmic transport function of CRM1. AdV genome delivery was not blocked in mitotic cells expressing the CRM1-binding fragment of Nup214 and occurred with equivalent efficiency compared to control cells. This result suggests that CRM1 binding to endogenous Nup214 is not required *per se* to allow AdV genome delivery. The precise function of Nup214 and its interaction with CRM1 in mitosis remains elusive, although Nup214 has been also shown to localize at the mitotic spindle and to promote correct chromosome segregation and mitotic progression (Hashizume et al., 2010; Bhattacharjya et al., 2015). It is possible that overexpression of the C-terminal fragment alters localization of CRM1 in mitosis, thus probably affecting its mitotic functions at the chromatin. However, it seems unlikely that overexpression of C-terminal Nup214 impairs CRM1 ability to assemble or disassemble

RanGTP-cargo complexes (in presence of soluble RanGAP and RanBP), which might be the function required for AdV genome delivery in mitosis rather than the nucleo-cytoplasmic transport function of CRM1.

2.3. Effect of soluble C-terminal fragments of Nup358

We also included in our analysis soluble fragments comprising the C-terminal region of Nup358 to test whether they behave as dominant inhibitors for AdV genome import. The largest fragment (aa 2307-3047) incorporates the E3 ligase region as well as flanking FG-repeat patches and RanBDs (3 and 4). Stable interaction with CRM1 and with CRM1-containing export complexes has been shown to require both FG-repeat patches (Ritterhoff et al., 2016). In addition, stable interaction of Nup358 with RanGAP and Ubc9 involves the SIM1 and IR1 domains in the E3 ligase region, respectively (Werner et al., 2012). Thus, this fragment is able to bind CRM1, forms a stable complex with RanGAP and Ubc9, and has a functional E3 ligase region. Furthermore, this fragment has been shown to be autonomously functional for the disassembly of CRM1-containing export complexes *in vitro* (Ritterhoff et al., 2016). The second C-terminal fragment (aa 2307-2710) used in analyses also harbours the RanBD3 and adjacent FG-repeats but lacks the IR2 of the E3 ligase region and downstream domains. Consequently, it is not able to bind CRM1 and it does not possess a functional E3 ligase domain, since the SIM1 and IR1 are occupied by endogenous RanGAP and Ubc9.

Both fragments strongly impaired AdV genome delivery in interphase cells, however not in a similar manner. The largest fragment impaired nuclear targeting of AdV capsids by causing an accumulation of incoming viral particles at the MTOC. In addition, it caused retention of endogenous CRM1 inside the nucleus with the consequent block of protein export. We observed that accumulation of AdV capsids at the MTOC was reversed by expressing an excess of CRM1, meaning that the effect caused by the large C-terminal fragment of Nup358 is CRM1-dependent. However, AdV genome delivery was still impaired in these conditions. Similarly, excess of the short C-terminal fragment of Nup358 caused an inhibition of AdV genome delivery that could not be reversed with exogenous CRM1, showing that a step downstream of capsid docking at the NPC was still disrupted independently of CRM1. Accordingly, overexpression of the short C-terminal fragment did not alter endogenous CRM1 localization nor efficient CRM1-dependent protein export but still prevented AdV genome import.

These results suggest on one hand that the C-terminal CRM1-binding fragment of Nup358 impairs CRM1-dependent export and consequently AdV genome delivery by retaining CRM1 inside the nucleus, similar than the C-terminal CRM1-binding fragment of Nup214. On the

other hand, the competition effect caused by the short C-terminal CRM1-non-binding fragment of Nup358 unmasks the involvement of additional factors in AdV genome delivery downstream of the MTOC relief.

2.3.1. Additional Nup358-associated factors may be implicated in AdV genome delivery

Possible candidates to exert this unknown function are RanGAP and Ubc9. It has been shown that overexpression of the E3 ligase region of Nup358 strongly reduce the concentration of RanGAP at the NE (Hutten et al., 2008; Werner et al., 2012). Similar redistribution of RanGAP was observed after depletion of Nup358 (Hutten et al., 2008). Lack of a NPC-associated RanGAP does not impair import of a cNLS-reporter protein in presence of the endogenous Nup358. However, importin- α/β -dependent import is strongly impaired in cells depleted for Nup358, suggesting that NPC-associated RanGAP is not responsible for the effects observed in Nup358-depleted cells (Hutten et al., 2008). AdV genome delivery is strongly inhibited by RanGAP-binding soluble fragments of Nup358. In contrast, depletion of Nup358 cause a delay but not a block of AdV genome import, which can be reversed by expressing an excess of transport receptors, suggesting that the lack of NPC-associated RanGAP is not the major cause of AdV genome delivery disruption in cells expressing any of the C-terminal fragments of Nup358 tested.

Another possible factor whose distribution and function can be altered upon expression of C-terminal fragments of Nup358 is Ubc9. Ubc9 is a E2 SUMO-conjugating enzyme that is present in the cell either in a soluble shuttling form, located predominantly in the nucleoplasm (Geiss-Friedlander and Melchior, 2007), or in a NPC-associated form, where Nup358 is the major binding site (Zhang et al., 2002). Nup358-depletion leads to substantial loss of Ubc9 from the NPC, but soluble nuclear levels of Ubc9 are not altered (Datta et al., 2014). Expression of a GFP-tagged construct of the IR1-M-IR2 Nup358 region in COS-7 cells, caused a specific re-localization of soluble Ubc9 from the nucleus to the cytoplasm (Saitoh et al., 2002). This region does not bind SUMOylated RanGAP due the lack of the SIM1. Thus, excess of the IR1-M-IR2 fragment did not disrupt stable RanGAP-Ubc9 association to endogenous Nup358. Similarly, cytoplasmic distribution of Ubc9 did not affect the general distribution of the transport machinery. However SUMO and certain SUMOylated proteins were mislocalized after IR1-M-IR2 expression thereby altering their functionality. There are two aspects in our study that could cause a different outcome. First, the GFP-IR1-M-IR2 construct used in Saitoh *et al.*, predominantly localized in the cytoplasm, which caused

substantial re-localization of the soluble nucleoplasmic Ubc9 to the cytoplasmic compartment. Instead the fragments used in our study are mainly nuclear, independently of their tag, and may not alter Ubc9 steady-state localization. Second, both soluble fragments of the C-terminus of Nup358 possess SIM1 and IR1 required for binding RanGAP and Ubc9. Hence, excess of any of these fragments would probably cause removal of both RanGAP and Ubc9 from the endogenous Nup358 and/or mislocalization of their soluble forms. This would not allow discrimination between an effect on AdV genome delivery due to Ubc9 dissociation from the NPC or an altered distribution of its soluble form. Still our C-terminal Nup358 fragments may prevent correct shuttling of Ubc9 between the cytoplasm and the nucleus thereby altering the availability of this enzyme in the correct compartment.

Ubc9 has been shown to be involved in different steps of viral infection either dependent or independently of its SUMO-conjugating function (reviewed in Varadaraj et al., 2014). In the case of AdV, Ubc9 was shown to directly interact with the immediate early E1A protein independent of the catalytic competence of Ubc9 (Hateboer et al., 1996). It is possible that Ubc9 contributes towards the SUMOylation of a cellular or viral component required for AdV genome delivery. Alternatively, it might directly facilitate viral genome delivery by remodelling the capsid using its chaperone activity or mediating import by binding to the viral core (reviewed in Varadaraj et al., 2014). It would be interesting to test whether excess of RanGAP or Ubc9 can overcome the block on AdV genome delivery caused by overexpression of the C-terminal fragments of Nup358. Similarly, it would be interesting to test whether a soluble fragment of Nup358 lacking the SIM1 domain necessary to bind SUMOylated RanGAP conserves the ability to compete with AdV genome delivery.

Taken together, competition of soluble C-terminal fragments of Nup358 with AdV genome delivery in interphase confirms the requirement of a functional CRM1 dependent export and revealed the possible involvement of additional Nup358-associated factors independently of CRM1.

2.3.2. C-terminal CRM1-binding region of Nup358 potentiates CRM1-dependent disassembly of AdV capsids

Analysis of the effect caused by overexpression of these fragments in mitotic cells provided additional information. In striking contrast to interphase cells, none of the fragments blocked AdV genome delivery in mitotic cells, meaning that soluble competing fragments of Nup358 block AdV genome delivery by redistribution and compartmentalization of Nup358-associated factors in interphase cells rather than by direct functional inhibition.

The shorter C-terminal CRM1-non-binding fragment of Nup358 (aa 2307-2710) slightly increased the efficiency of AdV capsid disassembly compared to control cells in mitosis. This short fragment does not bind CRM1 but contains the RanGAP and Ubc9 binding domains and thus, is able to re-localize both factors from the endogenous Nup358 at least in interphase cells. This possible re-localization of RanGAP and Ubc9 from endogenous Nup358 in mitotic cells does not seem to be important for AdV genome delivery.

Interestingly, the C-terminal CRM1-binding fragment (aa 2307-3047) of Nup358 did not compete with AdV genome delivery in mitosis unlike what we observed in interphase cells. To the contrary, it enhanced AdV capsid disassembly and core release. This enhancing effect was comparable to that observed in mitotic cells overexpressing CRM1. As mentioned in the introduction, it is known that the gradient of CRM1-RanGTP-cargo complexes around the chromatin exists in both, interphase and mitosis. In mitotic cells the gradient is maintained by the balance between the production of RanGTP by RCC1 at the chromatin and facilitated hydrolysis of GTP by RanGAP. If the assembly and disassembly of CRM1-RanGTP-cargo complexes is what favours AdV capsid uncoating, capsid disassembly would preferably take place where all factors converge (RanGTP, RanGAP and CRM1). Thus, it would be restricted to the vicinity of the NE in interphase cells, and preferentially occur near the chromatin of mitotic cells. The presence of an excess of the C-terminal fragment of Nup358 in mitosis, may become a useful platform for recruiting both CRM1-containing complexes and the disassembly machinery, in regions away from chromatin, which favours AdV capsid disassembly.

Specific inhibition of CRM1 with LMB treatment impaired AdV genome delivery in mitotic cells even in presence of Nup fragments, suggesting that the C-terminal CRM1-binding fragment of Nup358 boosts AdV capsid disassembly by specifically promoting CRM1 function(s).

2.4. Effect of soluble N-terminal and central fragments of Nup358

The N-terminal fragment containing the coiled-coil domain, several FG-repeats and the RanBD1 (aa 806-1306), has not been described to bind CRM1. Instead we have shown that this fragment can re-localize both importin- β and transportin-1, and co-precipitates at least with importin- β ; therefore, we hypothesized that it could compete with efficient AdV genome import. An excess of the aa 806-1306 fragment in interphase cells did not affect the efficiency of AdV import in presence of endogenous Nup358. This N-terminal fragment was previously shown to also not compete with import of cNLS- or M9-containing reporter constructs (neither other soluble fragments) (Wälde *et al.*, 2012). It is possible that the endogenous Nup358 is still able to recruit enough transport receptors at the NPC to promote efficient import, or simply, the levels of soluble fragment does not remove enough transport receptors from the nuclear periphery to compromise import efficiency. As expected, overexpression of the aa 806-1306 N-terminal fragment of Nup358 did not affect CRM1 accumulation at the NE nor CRM1-dependent export.

Several fragments containing the central zinc finger domain of Nup358 were included in the analysis as well. The zinc fingers were previously shown to interact with CRM1 (Singh *et al.*, 1999). In the study by Singh *et al.*, the recombinant fragment used for analysis corresponded to the zinc fingers and immediate downstream FG-repeat region of the bovine Nup358. The study shows that the main difference between human and bovine zinc fingers is that the first contained 8, instead of 5 zinc fingers found in bovine Nup358, but the immediately downstream region is equivalent. Authors support the idea of the zinc fingers as binding site of CRM1. Although the study does not exclude contribution of the FG-repeats, this region is not considered as major determinant for the formation of the ZnF-CRM1 complex. However, in our analysis, a fragment containing exclusively the zinc finger domain (aa 1350-1810) did not alter CRM1 localization at the NE nor did it alter CRM1-dependent export. Similarly, it was not able to compete with AdV genome delivery. Instead, additional FG-repeats and the RanBD2 (aa 1350-2148 or aa 1312-2557) were necessary to retain CRM1 inside the nucleus and disrupt CRM1-dependent protein export, as well as to accumulate AdV capsids at the MTOC, suggesting that additional FG-repeats considerably contribute to the interaction with CRM1. The RanBD2 may not be relevant in this interaction and neither is the adjacent JX2 domain or the RanBD3, because the fragment containing this region (aa 2011-2445) did not alter CRM1 localization and function, nor did it impaired AdV genome delivery.

The inability of the RanBD2-JX2-RanBD3 fragment (aa 2011-2445) in competing with AdV genome delivery seems to contradict previous results by Strunze *et al.* showing that

overexpression of the JX2 fragment of Nup358 reduced Ad2-mRFP transduction (Strunze et al., 2011). Excess of free JX2 has been shown to compete with recombinant JX2 interaction with kinesin-1 (Cai et al., 2001), and overexpression of this fragment in different cell lines caused perinuclear clustering of mitochondria (Cho et al., 2007). Overexpression of the RanBD2-JX2-RanBD3 fragment in cells also caused a defect of mitochondria motility. The proposed mechanism involves a tight interaction of the fragment RanBD2-JX2-RanBD3 with kinesin-1 that prevents cargo binding and boosts free-kinesin-1 anterograde motility (Cho et al., 2009; Patil et al., 2013). Thus, in case the interaction of AdV capsid with kinesin-1 would be required for further capsid disassembly, the soluble RanBD2-JX2-RanBD3 fragment should be an efficient competitor of AdV genome delivery. Taken together with the results presented above showing that the JX2 domain was dispensable for restoring an efficient AdV genome delivery in Nup358 depleted cells, it is unlikely that the crucial step for capsid disassembly at the NPC involves the kinesin-binding domain of Nup358.

2.5. Specific point mutations at the N-terminus of CRM1 impair AdV genome delivery

We have shown that AdV do not need an assembled NPC in order to deliver their genome, but still require CRM1 for capsid disassembly, even in mitosis. This result revealed that the nuclear transport machinery participate in AdV genome delivery regardless of its nucleocytoplasmic transport function. In addition, we have shown that overexpression of the C-terminal soluble fragment of Nup358 enhance CRM1-dependent disassembly of AdV capsids. Therefore, we address the question whether the interaction of CRM1 with cytosolic Nups is needed for triggering capsid disruption. Crystallography analyses by Port *et al.* identified the conserved FG-binding pockets of CRM1 allowing interaction with Nup214 (Port et al., 2015). The authors further characterized the interaction between Nup214 and different mutants of CRM1 harbouring specific point mutations at one or two out of several identified FG-binding pockets. Thus, we included in our experiments some of these mutants of CRM1 that were shown to have an impaired ability to bind Nup214 or Nup358 (Port et al., 2015; Ritterhoff et al., 2016). Importantly, these mutants also harboured the mutation in the residue C528 conferring resistance to the LMB. We tested if they were able to restore AdV genome delivery in interphase or mitotic LMB treated cells. All tested mutants, except one, were able to efficiently restore and further enhance the efficiency of AdV capsid disassembly similar than the CRM1 “wt” in mitotic cells. This suggested that CRM1/Nup214 or Nup358 interaction via specific binding pockets was not a prerequisite for AdV capsid disassembly. The exception was a mutant harbouring two point mutations in residues W142 and P143. We

then investigated whether binding to the C-terminal fragment of cytoplasmic Nups could be compromised because of these mutations and whether normal protein export could be restored by this mutant in interphase cells treated with LMB. Both the ability to bind cytosolic Nups and protein export were preserved in spite of the point mutations in residues W142 and P143, although protein export seem to be slightly less efficient. Thus, we performed similar experiment in interphase cells and again the CRM1 W142A P143A but no other mutant, lost the ability to efficiently restore AdV genome delivery in LMB treated cells. However, the result was slightly different from that of mitotic cells, since we observed a partial rescue of AdV genome delivery in presence of the CRM1 W142A P143A mutant contrary to almost any restoration in mitotic cells. In interphase cells it became also evident that the W142A P143A mutant was not completely able to prevent viral capsid accumulation at the MTOC in LMB treated cells.

These mutations at residues W142 P143 could be specific for promoting a step of viral disassembly and not affect CRM1-dependent function in the cell. However, we still cannot exclude that binding of this mutant to Nups or its ability to bind RanGTP/NES-cargoes is not compromised to some extent resulting in a less efficient rescue phenotype. These point mutations might not have strong effects on the overall nuclear export or on Nups interactions but might affect the efficiency of CRM1 function, becoming critical for certain cargoes or in this case, for promoting efficient AdV capsid disassembly. Quantitative biochemical analyses would be useful to address this issue. In the study by Port *et al.*, binding of different CRM1 mutants to Nup214 or a NES-cargo was characterized by quantifying the ability of the complex to protect RanGTP from RanGAP facilitated hydrolysis. Most of the CRM1 mutants included in the study by Port *et al.* conserved the ability to bind RanGTP/NES-cargo but presented reduced affinity for Nup214. However, two mutants of CRM1 showed clear differences in RanGTP/cargo binding compared to WT CRM1. These mutants included a point mutation in the residue S928 or A156. It would be interesting to test if these CRM1 mutants are also unable to restore efficient AdV genome delivery in presence of LMB, as control for an impaired ability to bind RanGTP/NES-cargo. However, these point mutations are not specifically situated in close proximity to the RanGTP or cargo-binding regions. Likewise residues W142 and P143 are not localized specifically in the FG-repeat binding pockets of CRM1 (Port *et al.*, 2015) but in the RanGTP-binding domain known as CRIME domain (aa 75–154) (Fornerod *et al.*, 1997) (and not so far from the residue A156). In addition, residues W142 and P143 are conserved among human, *S.cerevisiae* and *S.pombe* CRM1 homologues. Therefore, it is possible that RanGTP does not interact with the W142A

P143A mutant as efficiently as with WT CRM1 and thus, CRM1 dependent function and consequently AdV capsid disassembly are not completely restored in cells treated with LMB. If the W142A P143A CRM1 mutant had an impaired ability to bind RanGTP, this would be against the hypothesis that CRM1 facilitates nuclear targeting of capsids through direct binding to a NES-signal in the viral particle with supraphysiological affinity, since in this case the binding with the cargo would occur independently of RanGTP, and mutations at the CRIME domain should not impair binding with the incoming viral capsid.

The W142A P143A CRM1 mutant showed some efficiency to restore AdV genome delivery in interphase LMB treated cells unlike in mitotic cells. If this mutant has a reduced affinity for RanGTP it is possible that interphase conditions are more favourable to assemble CRM1-RanGTP-cargo complexes due to the high concentration of RanGTP inside the nucleus. Instead during mitosis, the absence of a nuclear membrane favours diffusion of CRM1 and RanGTP and thus, may reduce the chances of forming a CRM1-RanGTP-cargo complex to very specific regions (e.g. at kinetochores). Therefore, point mutations impairing the ability of CRM1 to bind RanGTP may be more restraining in mitosis compared to interphase.

In mitotic cells expressing the W142A P143A CRM1 mutant, we also observed that AdV capsids still partially accumulate at the MTOC. Interestingly, a fraction of CRM1 was shown to localize at centrosomes during the whole cell cycle (Liu et al., 2009). A fragment of CRM1 containing the CRIME domain, but not other regions, was similarly targeted to the MTOC, and competed for pericentrin targeting to the MTOC (which shuttles between the nucleus and the MTOC in a CRM1-dependent manner (Keryer et al., 2003)). Since a pool of Ran resides at the centrosome and is present, at least in part, as RanGTP (Keryer et al., 2003) (reviewed in Lavia, 2016) it is possible that centrosomal CRM1 in complex with RanGTP engages with the AdV capsid thereby mediating its translocation towards the NPC.

Interestingly, we have observed that overexpression of WT CRM1 in interphase cells, contrary to mitotic cells, does not increase the efficiency of AdV genome delivery compared to control cells. Following the previous argument, if higher concentrations of CRM1 increased the efficiency of AdV genome delivery in mitotic cells compared to control cells, in interphase, during which assembly of CRM1-RanGTP-cargo complexes may be more efficient, AdV genome delivery should have also been enhanced with an excess of CRM1 even under LMB treatment. However in this case, the limiting factor may not be the formation of the CRM1-RanGTP-cargo complex but the transport through the NPC, which could act as bottleneck for the export of CRM1-containing complexes, and therefore excess of CRM1 does not enhance efficiency of AdV genome delivery with respect to control cells.

2.6. Viral components involved in CRM1-dependent AdV genome delivery

2.6.1. Potential interaction of CRM1 with the AdV capsid

Our analyses were mainly focused on the cellular machinery required for viral genome delivery. However, it is not known which viral components complement the activity of CRM1 leading to delivery of AdV genomes into the nucleus. We considered the possibility that CRM1 directly interacts with the viral capsid. For this, pull-down assays were performed with purified Ad5 particles and total cell extracts of mock treated or cells expressing an excess of CRM1. We could see specific pull-down of the kinesin-1 light chain (KLC) with purified AdV particles as previously reported (Strunze et al., 2011), however not for endogenous nor exogenous CRM1.

In the case a direct binding of free CRM1 with incoming viral particles takes place in the cell, pull-down using total cell extracts may not be optimal, since other cellular factors could share the same binding site to the capsid with CRM1 (e.g motor proteins) and prevent binding of CRM1 to the viral capsid by competition. However, an excess of CRM1 should have overcome this problem. To enhance a potential affinity for CRM1, purified Ad5 vectors were treated either at neutral pH or pH 5 with the aim to mimic the conformational changes of the AdV capsid taking place during entry. If the interaction of CRM1 with the viral particle is through an epitope or a core protein that is only exposed once the capsid has undergone a particular degree of disassembly, this may be challenging to reproduce *in vitro*, since thermal or pH treatment of viral particles induce different degrees of capsid disassembly but probably do not mimic cellular processes (Pérez-Berná et al., 2012).

In the case that CRM1 binds to incoming AdV particles in complex with RanGTP, it would not be possible to observe an interaction under the conditions tested. High RanGTP concentration in the cell is maintained by RCC1. Thus, in total cell extracts the low concentration of RanGTP may not be sufficient to promote CRM1-RanGTP complexes formation and consequently, it would not be possible to see the potential interaction of CRM1-RanGTP with incoming AdV particles. Indeed, our previous results favour an implication of CRM1 in AdV genome delivery in complex with RanGTP. It is possible that a NES-containing component of the incoming AdV particle forms a complex with CRM1 and RanGTP at the MTOC. The formation of the complex could trigger the translocation of the capsid to the NPC were high concentrations of RanGAP would disassembly the complex and destabilize the capsid, leading to complete uncoating of the capsid.

Another possibility is that CRM1 in complex with RanGTP at the MTOC regulates the centrosomal targeting of NES-bearing CRM1 cargo that might either mediate a motor protein

switch at the vicinity of the nucleus or mediate the unloading of incoming viral particles from the MT. A recent study analyzed motility of AdV particles in absence or presence of LMB, and suggested that AdV particles are unloaded from MT at the nuclear periphery by a CRM1-dependent mechanism (Wang et al., 2017). In that case, CRM1 cargo substrates modulating microtubule trafficking might be good candidates (Thakar et al., 2013). One example is the tubulin deglutamylase CCP1/ Nna1 which can modulate the velocity and localization of motor proteins (O'Hagan et al., 2011; Sirajuddin et al., 2014). Autophagic response to AdV entry has been shown to facilitate endosomal escape and accelerate trafficking of viral particles towards the nucleus (Montespan et al., 2017). Thus, CRM1 cargoes as the autophagy adaptor p62/SQSTM1, which interacts with the motor protein dynein and is necessary for its function (Calderilla-Barbosa et al., 2014) or the protein CIP2A, which negatively regulates autophagy (Puustinen et al., 2014) could be involved in modulating cytosolic trafficking of AdV to the NPC in a CRM1-dependent manner.

Alternatively, a disassembly gradient of CRM1-RanGTP-cargo complexes can be a regulating and localized trigger to mediate both, unloading of incoming capsids from MT and induce AdV capsid disassembly at the NPC. It is possible that a full assembly and disassembly cycle of CRM1-RanGTP-cargo complexes take place around the centrosome. A fraction of CRM1, RanGTP and RanBP1 but not RanGAP localize at the MTOC (reviewed in Lavia, 2016). Thus, soluble RanGAP in the surrounding centrosomal area could create a localized CRM1-RanGTP-cargo gradient similar to the one existing at the NE. The localized hydrolysis of GTP could destabilize incoming AdV capsid binding to dynein motors thereby locally triggering the unloading of the particle from MT. This system could favour first, unloading of AdV capsids from MTs near the MTOC and second, after a translocation step towards the NPC (e.g. through motor switch) a further disassembly of NPC-anchored AdV capsids, where successive events of GTP hydrolysis would destabilize the capsid, leading to complete capsid disassembly.

2.6.2. CRM1-dependent AdV genome delivery does not involve AdV protein pIX

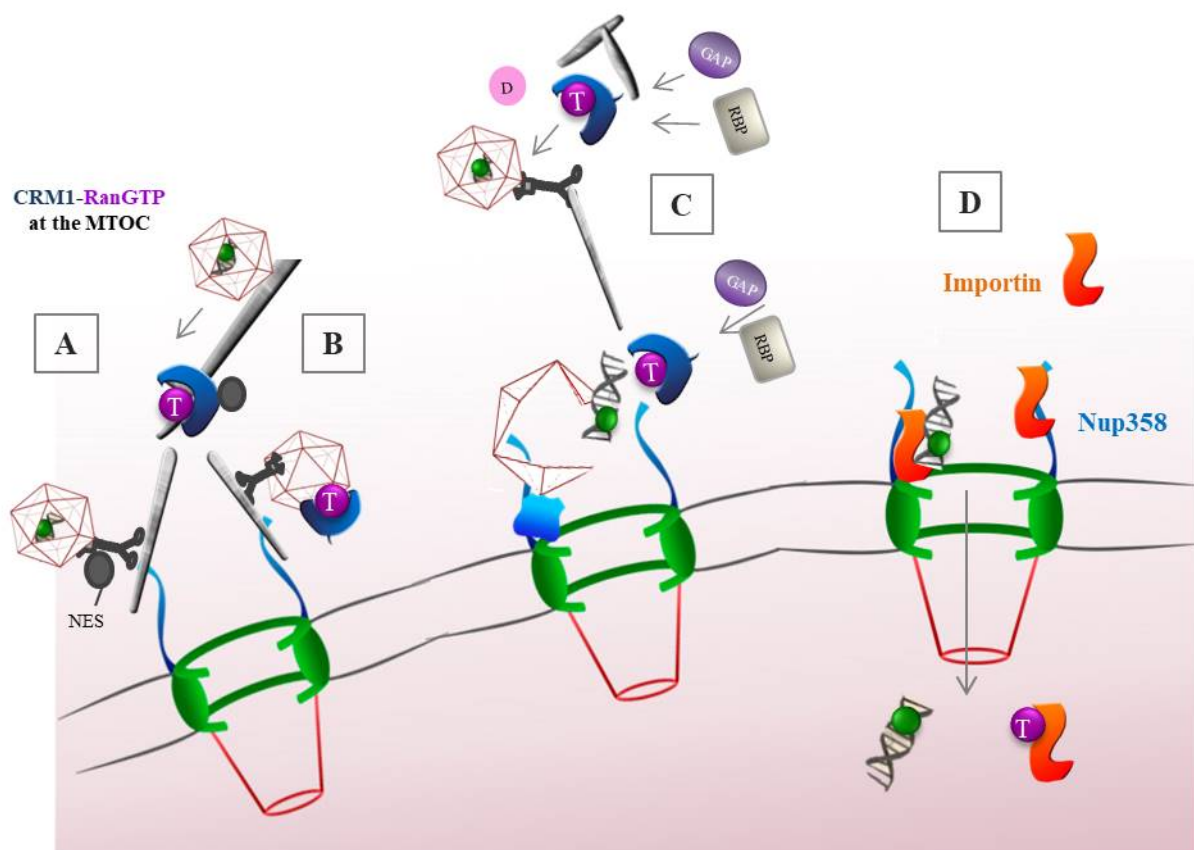
In a different study, protein IX has been related to kinesin-1 and Nup358-dependent disassembly of the AdV capsid at the NPC (Strunze et al., 2011). AdV lacking the protein IX showed a decreased infectivity suggested to be related to a deficient recruitment of kinesin-1 and thus, impaired capsid disassembly. We hypothesized that this protein could be involved in CRM1-dependent AdV genome delivery. Therefore, we first characterized the kinetic of genome delivery of Δ pIX Ad5 particles. Rather than an inefficient disassembly of the capsids, Δ pIX viral capsids were prematurely disintegrated, leading to cytosolic release of the AdV cores. A subpopulation of Δ pIX capsids seemed to be stable enough to reach the nucleus and deliver the genome. Specific inhibition of CRM1 by LMB treatment did not abrogate premature release of AdV cores, however it strongly induced accumulation of capsids at the MTOC, and prevented import of pVII-containing cores in the nucleus, similar than previous observations for wt capsids. Moreover this LMB-induced effect was reversed with the CRM1 mutant resistant to LMB. These results showed that a stable subpopulation of Δ pIX AdV capsids reach the NPC, and are able to deliver their genome into the nucleus in a CRM1-dependent but pIX-independent manner. On the other hand, results showed that prematurely released AdV cores are not functionally imported into the nucleus but probably detected and degraded in the cytoplasm. Thus, we can conclude that CRM1-dependent targeting of AdV capsids to the NPC does not involve the capsid protein IX and suggest that Δ pIX AdV capsids follow the same delivery route to the NPC as wt capsids, which excludes pIX as a major factor involved in subsequent steps. To further confirm this, infection of mitotic cells with Δ pIX Ad5 in presence of LMB should similarly impair AdV genome delivery; although premature disassembly of Δ pIX capsids might make it difficult to discriminate between spontaneously disassembled capsids and CRM1-dependent disassembled capsids. The potential role of the protein IX in capsid disassembly seemed an attractive model since its absence destabilizes the capsid, and thus, removal of pIX at the NPC would be an efficient trigger for capsid disassembly. However, since a considerable amount of Δ pIX viral particles reach the nucleus and normally disassemble their capsids at the NPC and deliver the genome, an additional step independently of viral pIX is more likely to take place at the NPC leading to complete disassembly of the capsid.

2.7. Conclusion

This work confirms the requirement of functional CRM1 for correct docking of AdV capsids at the NPC and revealed the involvement of C-terminal Nup358-associated factors at downstream steps of AdV genome delivery, during at least interphase. Successful AdV genome delivery in mitotic cells demonstrated that assembled NPC and nucleo-cytoplasmic transport are not necessary for AdV capsid disassembly and genome release. Instead, functional CRM1 is required in mitotic cells for correct capsid disassembly as well. Excess of CRM1 or soluble C-terminal CRM1-binding fragment of Nup358 enhanced efficiency of AdV genome delivery in mitosis. In contrast, a shorter C-terminal fragment of Nup358 unable to bind CRM1 and the C-terminal CRM1-binding region of Nup214 did not alter AdV genome delivery in mitotic conditions. This increment in AdV genome delivery efficiency did not correlate with an enhanced transport towards the chromatin, suggesting a role for CRM1, and probably the export machinery, specifically at the disassembly step of AdV genome delivery, independently of its nucleo-cytoplasmic function. Furthermore, we identified two point mutations at the N-terminal CRIME domain of CRM1 to be critical for restoring efficient AdV genome delivery in presence of LMB. Further studies are needed to clarify the exact mechanism through which CRM1 facilitates AdV capsid disassembly. It is also unclear how AdV particles interact with the transport machinery to be uncoated. Purified AdV particles were not able to bind with endogenous or transfected CRM1 *in vitro*, and IF analyses do not link the capsid protein pIX with CRM1-dependent delivery of AdV genomes, favouring the hypothesis of a role for CRM1 in the context of a CRM1-RanGTP-cargo in nuclear targeting and uncoating of AdV capsids.

3. GENERAL CONCLUSIONS

This work highlights the requirement of functional CRM1 at different steps of viral delivery. Our study uncovers a novel and unprecedented function for CRM1 in AdV capsid disassembly. This role is more likely linked to a CRM1-RanGTP-cargo complex rather than indirectly promoting transport of individual cargo, or interacting individually with incoming viral particles. Concentration of RanGTP at centrosomes could mediate targeting of a specific cargo locally to the centrosomes (A), where it would modulate the trafficking of incoming viral particles towards the nuclear periphery (e.g. through motor switch). Alternatively, CRM1 could bind the viral particle in complex with RanGTP and favour its translocation towards the nucleus (B). In a different scenario, concentration of RanGTP and CRM1 at centrosomes might create a local gradient of CRM1-RanGTP-cargo complex disassembly facilitated by soluble RanGAP and RanBP1 that would lead to the release of capsids from MT, favouring a motor switch towards the NPC (C). Once incoming viral particles dock at the NPC via binding to Nup214, successive events of CRM1-RanGTP-cargo complex disassembly could destabilize the capsid leading to complete AdV capsid disassembly. Optimal recruitment of transport receptors by Nup358 (D) would facilitate accessibility of the AdV core to the import machinery at the NPC, ensuring an efficient separation of AdV cores from capsids and import of the viral genome.



REFERENCES

- Adachi, Y., Yanagida, M., 1989. Higher order chromosome structure is affected by cold-sensitive mutations in a *Schizosaccharomyces pombe* gene *crm1+* which encodes a 115-kD protein preferentially localized in the nucleus and its periphery. *J. Cell Biol.* 108, 1195–1207.
- Anderson, C.W., Young, M.E., Flint, S.J., 1989. Characterization of the adenovirus 2 virion protein, mu. *Virology* 172, 506–512.
- Andersson, M., Pääbo, S., Nilsson, T., Peterson, P.A., 1985. Impaired intracellular transport of class I MHC antigens as a possible means for adenoviruses to evade immune surveillance. *Cell* 43, 215–222.
- Aramburu, I.V., Lemke, E.A., 2017. Floppy but not sloppy: Interaction mechanism of FG-nucleoporins and nuclear transport receptors. *Semin. Cell Dev. Biol., Nuclear pores* 68, 34–41.
doi:10.1016/j.semcdb.2017.06.026
- Armstrong, E.H., Goswami, D., Griffin, P.R., Noy, N., Ortlund, E.A., 2014. Structural basis for ligand regulation of the fatty acid-binding protein 5, peroxisome proliferator-activated receptor β/δ (FABP5-PPAR β/δ) signaling pathway. *J. Biol. Chem.* 289, 14941–14954. doi:10.1074/jbc.M113.514646
- Arnautov, A., Azuma, Y., Ribbeck, K., Joseph, J., Boyarchuk, Y., Karpova, T., McNally, J., Dasso, M., 2005. *Crm1* is a mitotic effector of Ran-GTP in somatic cells. *Nat. Cell Biol.* 7, 626–632.
doi:10.1038/ncb1263
- Aslanukov, A., Bhowmick, R., Guruju, M., Oswald, J., Raz, D., Bush, R.A., Sieving, P.A., Lu, X., Bock, C.B., Ferreira, P.A., 2006. RanBP2 Modulates Cox11 and Hexokinase I Activities and Haploinsufficiency of RanBP2 Causes Deficits in Glucose Metabolism. *PLoS Genet* 2, e177.
doi:10.1371/journal.pgen.0020177
- Astanina, K., Jacob, R., 2010. KIF5C, a kinesin motor involved in apical trafficking of MDCK cells. *Cell. Mol. Life Sci. CMLS* 67, 1331–1342. doi:10.1007/s00018-009-0253-6
- Bailey, C.J., Crystal, R.G., Leopold, P.L., 2003. Association of adenovirus with the microtubule organizing center. *J. Virol.* 77, 13275–13287.
- Baltimore, D., 1971. Expression of animal virus genomes. *Bacteriol. Rev.* 35, 235–241.
- Bayliss, R., Littlewood, T., Stewart, M., 2000. Structural Basis for the Interaction between FxFG Nucleoporin Repeats and Importin- β in Nuclear Trafficking. *Cell* 102, 99–108. doi:10.1016/S0092-8674(00)00014-3
- Beck, M., Förster, F., Ecke, M., Plitzko, J.M., Melchior, F., Gerisch, G., Baumeister, W., Medalia, O., 2004. Nuclear Pore Complex Structure and Dynamics Revealed by Cryoelectron Tomography. *Science* 306, 1387–1390. doi:10.1126/science.1104808
- Beck, M., Hurt, E., 2017. The nuclear pore complex: understanding its function through structural insight. *Nat. Rev. Mol. Cell Biol.* 18, 73–89. doi:10.1038/nrm.2016.147
- Belfield, J.L., Whittaker, C., Cader, M.Z., Chawla, S., 2006. Differential effects of Ca²⁺ and cAMP on transcription mediated by MEF2D and cAMP-response element-binding protein in hippocampal neurons. *J. Biol. Chem.* 281, 27724–27732. doi:10.1074/jbc.M601485200
- Ben-Efraim, I., Gerace, L., 2001. Gradient of Increasing Affinity of Importin β for Nucleoporins along the Pathway of Nuclear Import. *J. Cell Biol.* 152, 411–418. doi:10.1083/jcb.152.2.411
- Bergelson, J.M., Cunningham, J.A., Droguett, G., Kurt-Jones, E.A., Krithivas, A., Hong, J.S., Horwitz, M.S., Crowell, R.L., Finberg, R.W., 1997. Isolation of a Common Receptor for Coxsackie B Viruses and Adenoviruses 2 and 5. *Science* 275, 1320–1323. doi:10.1126/science.275.5304.1320

- Berget, S.M., Moore, C., Sharp, P.A., 1977. Spliced segments at the 5' terminus of adenovirus 2 late mRNA. *Proc. Natl. Acad. Sci. U. S. A.* 74, 3171–3175.
- Berk, A.J., 2016. Discovery of RNA splicing and genes in pieces. *Proc. Natl. Acad. Sci. U. S. A.* 113, 801–805. doi:10.1073/pnas.1525084113
- Bernad, R., Engelsma, D., Sanderson, H., Pickersgill, H., Fornerod, M., 2006. Nup214-Nup88 nucleoporin subcomplex is required for CRM1-mediated 60 S preribosomal nuclear export. *J. Biol. Chem.* 281, 19378–19386. doi:10.1074/jbc.M512585200
- Bernad, R., van der Velde, H., Fornerod, M., Pickersgill, H., 2004. Nup358/RanBP2 attaches to the nuclear pore complex via association with Nup88 and Nup214/CAN and plays a supporting role in CRM1-mediated nuclear protein export. *Mol. Cell. Biol.* 24, 2373–2384.
- Bernis, C., Swift-Taylor, B., Nord, M., Carmona, S., Chook, Y.M., Forbes, D.J., 2014. Transportin acts to regulate mitotic assembly events by target binding rather than Ran sequestration. *Mol. Biol. Cell* 25, 992–1009. doi:10.1091/mbc.E13-08-0506
- Bhattacharjya, S., Roy, K.S., Ganguly, A., Sarkar, S., Panda, C.K., Bhattacharyya, D., Bhattacharyya, N.P., Roychoudhury, S., 2015. Inhibition of nucleoporin member Nup214 expression by miR-133b perturbs mitotic timing and leads to cell death. *Mol. Cancer* 14, 42. doi:10.1186/s12943-015-0299-z
- Bischoff, F.R., Görlich, D., 1997. RanBP1 is crucial for the release of RanGTP from importin β -related nuclear transport factors. *FEBS Lett.* 419, 249–254. doi:10.1016/S0014-5793(97)01467-1
- Bischoff, F.R., Ponstingl, H., 1995. Catalysis of guanine nucleotide exchange of Ran by RCC1 and stimulation of hydrolysis of Ran-bound GTP by Ran-GAP1. *Methods Enzymol.* 257, 135–144.
- Bolhy, S., Bouhlel, I., Dultz, E., Nayak, T., Zuccolo, M., Gatti, X., Vallee, R., Ellenberg, J., Doye, V., 2011. A Nup133-dependent NPC-anchored network tethers centrosomes to the nuclear envelope in prophase. *J. Cell Biol.* 192, 855–871. doi:10.1083/jcb.201007118
- Bonifaci, N., Moroianu, J., Radu, A., Blobel, G., 1997. Karyopherin beta2 mediates nuclear import of a mRNA binding protein. *Proc. Natl. Acad. Sci. U. S. A.* 94, 5055–5060.
- Bremner, K.H., Scherer, J., Yi, J., Vershinin, M., Gross, S.P., Vallee, R.B., 2009. Adenovirus transport via direct interaction of cytoplasmic dynein with the viral capsid hexon subunit. *Cell Host Microbe* 6, 523–535. doi:10.1016/j.chom.2009.11.006
- Brohawn, S.G., Partridge, J.R., Whittle, J.R.R., Schwartz, T.U., 2009. The nuclear pore complex has entered the atomic age. *Struct. Lond. Engl.* 1993 17, 1156–1168. doi:10.1016/j.str.2009.07.014
- Brown, M., Weber, J., 1980. Virion core-like organization of intranuclear adenovirus chromatin late in infection. *Virology* 107, 306–310. doi:10.1016/0042-6822(80)90297-4
- Bui, K.H., von Appen, A., DiGiulio, A.L., Ori, A., Sparks, L., Mackmull, M.-T., Bock, T., Hagen, W., Andrés-Pons, A., Glavy, J.S., Beck, M., 2013. Integrated Structural Analysis of the Human Nuclear Pore Complex Scaffold. *Cell* 155, 1233–1243. doi:10.1016/j.cell.2013.10.055
- Burckhardt, C.J., Suomalainen, M., Schoenenberger, P., Boucke, K., Hemmi, S., Greber, U.F., 2011. Drifting Motions of the Adenovirus Receptor CAR and Immobile Integrins Initiate Virus Uncoating and Membrane Lytic Protein Exposure. *Cell Host Microbe* 10, 105–117. doi:10.1016/j.chom.2011.07.006
- Burgert, H.G., Kvist, S., 1985. An adenovirus type 2 glycoprotein blocks cell surface expression of human histocompatibility class I antigens. *Cell* 41, 987–997.

- Cai, Y., Singh, B.B., Aslanukov, A., Zhao, H., Ferreira, P.A., 2001. The Docking of Kinesins, KIF5B and KIF5C, to Ran-binding Protein 2 (RanBP2) Is Mediated via a Novel RanBP2 Domain. *J. Biol. Chem.* 276, 41594–41602. doi:10.1074/jbc.M104514200
- Calderilla-Barbosa, L., Seibenhener, M.L., Du, Y., Diaz-Meco, M.-T., Moscat, J., Yan, J., Wooten, M.W., Wooten, M.C., 2014. Interaction of SQSTM1 with the motor protein dynein – SQSTM1 is required for normal dynein function and trafficking. *J. Cell Sci.* 127, 4052–4063. doi:10.1242/jcs.152363
- Campbell, E.M., Hope, T.J., 2015. HIV-1 Capsid: The Multifaceted Key Player in HIV-1 infection. *Nat. Rev. Microbiol.* 13, 471–483. doi:10.1038/nrmicro3503
- Cansizoglu, A.E., Lee, B.J., Zhang, Z.C., Fontoura, B.M.A., Chook, Y.M., 2007. Structure-based design of a pathway-specific nuclear import inhibitor. *Nat. Struct. Mol. Biol.* 14, 452–454. doi:10.1038/nsmb1229
- Cassany, A., Ragues, J., Guan, T., Bégu, D., Wodrich, H., Kann, M., Nemerow, G.R., Gerace, L., 2015. Nuclear import of adenovirus DNA involves direct interaction of hexon with an N-terminal domain of the nucleoporin Nup214. *J. Virol.* JVI.02639-14. doi:10.1128/JVI.02639-14
- Cavazza, T., Vernos, I., 2016. The RanGTP Pathway: From Nucleo-Cytoplasmic Transport to Spindle Assembly and Beyond. *Front. Cell Dev. Biol.* 3. doi:10.3389/fcell.2015.00082
- Chatel, G., Fahrenkrog, B., 2011. Nucleoporins: Leaving the nuclear pore complex for a successful mitosis. *Cell. Signal.* 23, 1555–1562. doi:10.1016/j.cellsig.2011.05.023
- Chatterjee, P.K., Vayda, M.E., Flint, S.J., 1986. Adenoviral protein VII packages intracellular viral DNA throughout the early phase of infection. *EMBO J.* 5, 1633–1644.
- Chatterjee, P.K., Vayda, M.E., Flint, S.J., 1986. Identification of proteins and protein domains that contact DNA within adenovirus nucleoprotein cores by ultraviolet light crosslinking of oligonucleotides 32P-labelled in vivo. *J. Mol. Biol.* 188, 23–37.
- Chatterjee, P.K., Vayda, M.E., Flint, S.J., 1985. Interactions among the three adenovirus core proteins. *J. Virol.* 55, 379–386.
- Chen, J., Morral, N., Engel, D.A., 2007. Transcription releases protein VII from adenovirus chromatin. *Virology* 369, 411–422. doi:10.1016/j.virol.2007.08.012
- Chi, N.C., Adam, E.J., Adam, S.A., 1995. Sequence and characterization of cytoplasmic nuclear protein import factor p97. *J. Cell Biol.* 130, 265–274.
- Cho, K., Cai, Y., Yi, H., Yeh, A., Aslanukov, A., Ferreira, P.A., 2007. Association of the kinesin-binding domain of RanBP2 to KIF5B and KIF5C determines mitochondria localization and function. *Traffic Cph. Den.* 8, 1722–1735. doi:10.1111/j.1600-0854.2007.00647.x
- Cho, K., Yi, H., Desai, R., Hand, A.R., Haas, A.L., Ferreira, P.A., 2009. RANBP2 is an allosteric activator of the conventional kinesin-1 motor protein, KIF5B, in a minimal cell-free system. *EMBO Rep.* 10, 480–486. doi:10.1038/embor.2009.29
- Chook, Y.M., Jung, A., Rosen, M.K., Blobel, G., 2002. Uncoupling Kapbeta2 substrate dissociation and ran binding. *Biochemistry (Mosc.)* 41, 6955–6966.
- Chook, Y.M., Süel, K.E., 2011. Nuclear import by karyopherin-βs: Recognition and inhibition. *Biochim. Biophys. Acta BBA - Mol. Cell Res., Regulation of Signaling and Cellular Fate through Modulation of Nuclear Protein Import* 1813, 1593–1606. doi:10.1016/j.bbamcr.2010.10.014
- Chow, L.T., Gelinis, R.E., Broker, T.R., Roberts, R.J., 1977. An amazing sequence arrangement at the 5' ends of adenovirus 2 messenger RNA. *Cell* 12, 1–8.

- Christensen, J.B., Byrd, S.A., Walker, A.K., Strahler, J.R., Andrews, P.C., Imperiale, M.J., 2008. Presence of the Adenovirus IVa2 Protein at a Single Vertex of the Mature Virion. *J. Virol.* 82, 9086–9093. doi:10.1128/JVI.01024-08
- Christie, M., Chang, C.-W., Róna, G., Smith, K.M., Stewart, A.G., Takeda, A.A.S., Fontes, M.R.M., Stewart, M., Vértessy, B.G., Forwood, J.K., Kobe, B., 2016. Structural Biology and Regulation of Protein Import into the Nucleus. *J. Mol. Biol., Functional and Mechanistic Landscape of the Nuclear Pore Complex* 428, 2060–2090. doi:10.1016/j.jmb.2015.10.023
- Cingolani, G., Petosa, C., Weis, K., Müller, C.W., 1999. Structure of importin-beta bound to the IBB domain of importin-alpha. *Nature* 399, 221–229. doi:10.1038/20367
- Clemmons, N.S., McCormic, Z.D., Gaydos, J.C., Hawksworth, A.W., Jordan, N.N., 2017. Acute Respiratory Disease in US Army Trainees 3 Years after Reintroduction of Adenovirus Vaccine1. *Emerg. Infect. Dis.* 23, 95–98. doi:10.3201/eid2301.161297
- Colby, W.W., Shenk, T., 1981. Adenovirus type 5 virions can be assembled in vivo in the absence of detectable polypeptide IX. *J. Virol.* 39, 977–980.
- Condezo, G.N., San Martín, C., 2017. Localization of adenovirus morphogenesis players, together with visualization of assembly intermediates and failed products, favor a model where assembly and packaging occur concurrently at the periphery of the replication center. *PLoS Pathog.* 13. doi:10.1371/journal.ppat.1006320
- Cook, A., Bono, F., Jinek, M., Conti, E., 2007. Structural biology of nucleocytoplasmic transport. *Annu. Rev. Biochem.* 76, 647–671. doi:10.1146/annurev.biochem.76.052705.161529
- Copeland, A.M., Newcomb, W.W., Brown, J.C., 2009. Herpes Simplex Virus Replication: Roles of Viral Proteins and Nucleoporins in Capsid-Nucleus Attachment. *J. Virol.* 83, 1660–1668. doi:10.1128/JVI.01139-08
- Coyne, C.B., Bergelson, J.M., 2005. CAR: A virus receptor within the tight junction. *Adv. Drug Deliv. Rev., Adhesion Proteins in Cellular Tight Junctions: Critical Components in the Modulation of Paracellular Permeability* 57, 869–882. doi:10.1016/j.addr.2005.01.007
- Cronshaw, J.M., Krutchinsky, A.N., Zhang, W., Chait, B.T., Matunis, M.J., 2002. Proteomic analysis of the mammalian nuclear pore complex. *J. Cell Biol.* 158, 915–927. doi:10.1083/jcb.200206106
- Cros, J.F., García-Sastre, A., Palese, P., 2005. An unconventional NLS is critical for the nuclear import of the influenza A virus nucleoprotein and ribonucleoprotein. *Traffic Cph. Den.* 6, 205–213. doi:10.1111/j.1600-0854.2005.00263.x
- Cros, J.F., Palese, P., 2003. Trafficking of viral genomic RNA into and out of the nucleus: influenza, Thogoto and Borna disease viruses. *Virus Res., Nuclear Functions of RNA Virus Proteins* 95, 3–12. doi:10.1016/S0168-1702(03)00159-X
- Cupelli, K., Stehle, T., 2011. Viral attachment strategies: the many faces of adenoviruses. *Curr. Opin. Virol., Virus structure and function* 1, 84–91. doi:10.1016/j.coviro.2011.05.024
- Curiel, D.T., 2016. *Adenoviral Vectors for Gene Therapy*. Academic Press.
- Cusack, S., 2005. Adenovirus complex structures. *Curr. Opin. Struct. Biol.* 15, 237–243. doi:10.1016/j.sbi.2005.03.004
- Datta, S., Snow, C.J., Paschal, B.M., 2014. A pathway linking oxidative stress and the Ran GTPase system in progeria. *Mol. Biol. Cell* 25, 1202–1215. doi:10.1091/mbc.E13-07-0430

- Dawlaty, M.M., Malureanu, L., Jegathan, K.B., Kao, E., Sustmann, C., Tahk, S., Shuai, K., Grosschedl, R., van Deursen, J.M., 2008. Resolution of Sister Centromeres Requires RanBP2-Mediated SUMOylation of Topoisomerase II α . *Cell* 133, 103–115. doi:10.1016/j.cell.2008.01.045
- de Jong, R.N., Meijer, L.A.T., van der Vliet, P.C., 2003. DNA binding properties of the adenovirus DNA replication priming protein pTP. *Nucleic Acids Res.* 31, 3274–3286.
- Delphin, C., Guan, T., Melchior, F., Gerace, L., 1997. RanGTP targets p97 to RanBP2, a filamentous protein localized at the cytoplasmic periphery of the nuclear pore complex. *Mol. Biol. Cell* 8, 2379–2390.
- Dhanoya, A., Wang, T., Keshavarz-Moore, E., Fassati, A., Chain, B.M., 2013. Importin-7 Mediates Nuclear Trafficking of DNA in Mammalian Cells. *Traffic Cph. Den.* 14, 165–175. doi:10.1111/tra.12021
- Dingwall, C., Robbins, J., Dilworth, S.M., Roberts, B., Richardson, W.D., 1988. The nucleoplasmic nuclear location sequence is larger and more complex than that of SV-40 large T antigen. *J. Cell Biol.* 107, 841–849. doi:10.1083/jcb.107.3.841
- Dodding, M.P., Way, M., 2011. Coupling viruses to dynein and kinesin-1. *EMBO J.* 30, 3527–3539. doi:10.1038/emboj.2011.283
- Dultz, E., Zanin, E., Wurzenberger, C., Braun, M., Rabut, G., Sironi, L., Ellenberg, J., 2008. Systematic kinetic analysis of mitotic dis- and reassembly of the nuclear pore in living cells. *J. Cell Biol.* 180, 857–865. doi:10.1083/jcb.200707026
- Enders, J.F., Bell, J.A., Dingle, J.H., Francis, T., Hilleman, M.R., Huebner, R.J., Payne, A.M.-M., 1956. “Adenoviruses”: Group Name Proposed for New Respiratory-Tract Viruses. *Science* 124, 119–120.
- Engelsma, D., Bernad, R., Calafat, J., Fornerod, M., 2004. Supraphysiological nuclear export signals bind CRM1 independently of RanGTP and arrest at Nup358. *EMBO J.* 23, 3643–3652. doi:10.1038/sj.emboj.7600370
- Fay, N., Panté, N., 2015. Nuclear entry of DNA viruses. *Front. Microbiol.* 6, 467. doi:10.3389/fmicb.2015.00467
- Fischer, U., Huber, J., Boelens, W.C., Mattajt, L.W., Lührmann, R., 1995. The HIV-1 Rev Activation Domain is a nuclear export signal that accesses an export pathway used by specific cellular RNAs. *Cell* 82, 475–483. doi:10.1016/0092-8674(95)90436-0
- Flint, J., Nemerow, G.R., 2016. *Human Adenoviruses: From Villains to Vectors.* World Scientific.
- Forbes, D.J., Travesa, A., Nord, M.S., Bernis, C., 2015. Nuclear transport factors: global regulation of mitosis. *Curr. Opin. Cell Biol.* 35, 78–90. doi:10.1016/j.ceb.2015.04.012
- Forler, D., Rabut, G., Ciccarelli, F.D., Herold, A., Köcher, T., Niggeweg, R., Bork, P., Ellenberg, J., Izaurralde, E., 2004. RanBP2/Nup358 provides a major binding site for NXF1-p15 dimers at the nuclear pore complex and functions in nuclear mRNA export. *Mol. Cell. Biol.* 24, 1155–1167.
- Fornerod, M., Ohno, M., Yoshida, M., Mattaj, I.W., 1997a. CRM1 Is an Export Receptor for Leucine-Rich Nuclear Export Signals. *Cell* 90, 1051–1060. doi:10.1016/S0092-8674(00)80371-2
- Fornerod, M., van Deursen, J., van Baal, S., Reynolds, A., Davis, D., Murti, K.G., Fransen, J., Grosveld, G., 1997b. The human homologue of yeast CRM1 is in a dynamic subcomplex with CAN/Nup214 and a novel nuclear pore component Nup88. *EMBO J.* 16, 807–816. doi:10.1093/emboj/16.4.807
- Frey, S., Görlich, D., 2007. A saturated FG-repeat hydrogel can reproduce the permeability properties of nuclear pore complexes. *Cell* 130, 512–523. doi:10.1016/j.cell.2007.06.024

- Frohnert, C., Hutten, S., Wälde, S., Nath, A., Kehlenbach, R.H., 2014. Importin 7 and Nup358 promote nuclear import of the protein component of human telomerase. *PLoS One* 9, e88887.
doi:10.1371/journal.pone.0088887
- Fukuda, M., Asano, S., Nakamura, T., Adachi, M., Yoshida, M., Yanagida, M., Nishida, E., 1997. CRM1 is responsible for intracellular transport mediated by the nuclear export signal. *Nature* 390, 308–311.
doi:10.1038/36894
- Furcinitti, P.S., van Oostrum, J., Burnett, R.M., 1989. Adenovirus polypeptide IX revealed as capsid cement by difference images from electron microscopy and crystallography. *EMBO J.* 8, 3563–3570.
- Furuta, M., Kose, S., Koike, M., Shimi, T., Hiraoka, Y., Yoneda, Y., Haraguchi, T., Imamoto, N., 2004. Heat-shock induced nuclear retention and recycling inhibition of importin alpha. *Genes Cells Devoted Mol. Cell. Mech.* 9, 429–441. doi:10.1111/j.1356-9597.2004.00734.x
- Gabriel, G., Herwig, A., Klenk, H.-D., 2008. Interaction of polymerase subunit PB2 and NP with importin alpha is a determinant of host range of influenza A virus. *PLoS Pathog.* 4, e11.
doi:10.1371/journal.ppat.0040011
- Gallucci, L., Kann, M., 2017. Nuclear Import of Hepatitis B Virus Capsids and Genome. *Viruses* 9, 21.
- Geiss-Friedlander, R., Melchior, F., 2007. Concepts in sumoylation: a decade on. *Nat. Rev. Mol. Cell Biol.* 8, 947–956. doi:10.1038/nrm2293
- Ghebremedhin, B., 2014. Human adenovirus: Viral pathogen with increasing importance. *Eur. J. Microbiol. Immunol.* 4, 26–33. doi:10.1556/EuJMI.4.2014.1.2
- Ghosh, S.S., Gopinath, P., Ramesh, A., 2006. Adenoviral vectors: a promising tool for gene therapy. *Appl. Biochem. Biotechnol.* 133, 9–29.
- Giannakakou, P., Sackett, D.L., Ward, Y., Webster, K.R., Blagosklonny, M.V., Fojo, T., 2000. p53 is associated with cellular microtubules and is transported to the nucleus by dynein. *Nat. Cell Biol.* 2, 709–717.
doi:10.1038/35036335
- Gilistro, E., Turris, V. de, Damizia, M., Verrico, A., Moroni, S., Santis, R.D., Rosa, A., Lavia, P., 2017. Importin-β and CRM1 control a RANBP2 spatiotemporal switch essential for mitotic kinetochore function. *J Cell Sci* 130, 2564–2578. doi:10.1242/jcs.197905
- Glotzer, J.B., Michou, A.-I., Baker, A., Saltik, M., Cotten, M., 2001. Microtubule-Independent Motility and Nuclear Targeting of Adenoviruses with Fluorescently Labeled Genomes. *J. Virol.* 75, 2421–2434.
doi:10.1128/JVI.75.5.2421-2434.2001
- Gorman, J.J., Wallis, T.P., Whelan, D.A., Shaw, J., Both, G.W., 2005. LH3, a “homologue” of the mastadenoviral E1B 55-kDa protein is a structural protein of atadenoviruses. *Virology* 342, 159–166.
doi:10.1016/j.virol.2005.07.020
- Greber, U.F., Suomalainen, M., Stidwill, R.P., Boucke, K., Ebersold, M.W., Helenius, A., 1997. The role of the nuclear pore complex in adenovirus DNA entry. *EMBO J.* 16, 5998–6007.
doi:10.1093/emboj/16.19.5998
- Greber, U.F., Willetts, M., Webster, P., Helenius, A., 1993. Stepwise dismantling of adenovirus 2 during entry into cells. *Cell* 75, 477–486. doi:10.1016/0092-8674(93)90382-Z
- Green, M., Wold, W.S.M., Mackey, J.K., Rigden, P., 1979. Analysis of human tonsil and cancer DNAs and RNAs for DNA sequences of group C (serotypes 1, 2, 5, and 6) human adenoviruses. *Proc. Natl. Acad. Sci. U. S. A.* 76, 6606–6610.

- Güttinger, S., Laurell, E., Kutay, U., 2009. Orchestrating nuclear envelope disassembly and reassembly during mitosis. *Nat. Rev. Mol. Cell Biol.* 10, 178–191. doi:10.1038/nrm2641
- Hamada, M., Haeger, A., Jeganathan, K.B., van Ree, J.H., Malureanu, L., Wälde, S., Joseph, J., Kehlenbach, R.H., van Deursen, J.M., 2011. Ran-dependent docking of importin-beta to RanBP2/Nup358 filaments is essential for protein import and cell viability. *J. Cell Biol.* 194, 597–612. doi:10.1083/jcb.201102018
- Hamamoto, T., Gunji, S., Tsuji, H., Beppu, T., 1983. Leptomycins A and B, new antifungal antibiotics. I. Taxonomy of the producing strain and their fermentation, purification and characterization. *J. Antibiot. (Tokyo)* 36, 639–645.
- Hanz, S., Perlson, E., Willis, D., Zheng, J.-Q., Massarwa, R., Huerta, J.J., Koltzenburg, M., Kohler, M., van-Minnen, J., Twiss, J.L., Fainzilber, M., 2003. Axoplasmic Importins Enable Retrograde Injury Signaling in Lesioned Nerve. *Neuron* 40, 1095–1104. doi:10.1016/S0896-6273(03)00770-0
- Harel, A., Forbes, D.J., 2004. Importin beta: conducting a much larger cellular symphony. *Mol. Cell* 16, 319–330. doi:10.1016/j.molcel.2004.10.026
- Hashizume, C., Nakano, H., Yoshida, K., Wong, R.W., 2010. Characterization of the role of the tumor marker Nup88 in mitosis. *Mol. Cancer* 9, 119. doi:10.1186/1476-4598-9-119
- Hateboer, G., Hijmans, E.M., Nooij, J.B., Schlenker, S., Jentsch, S., Bernards, R., 1996. mUBC9, a novel adenovirus E1A-interacting protein that complements a yeast cell cycle defect. *J. Biol. Chem.* 271, 25906–25911.
- Hilleman, M.R., Werner, J.H., 1954. Recovery of new agent from patients with acute respiratory illness. *Proc. Soc. Exp. Biol. Med. Soc. Exp. Biol. Med. N. Y.* N 85, 183–188.
- Hindley, C.E., Lawrence, F.J., Matthews, D.A., 2007. A role for transportin in the nuclear import of adenovirus core proteins and DNA. *Traffic Cph. Den.* 8, 1313–1322. doi:10.1111/j.1600-0854.2007.00618.x
- Hoeben, R.C., Uil, T.G., 2013. Adenovirus DNA replication. *Cold Spring Harb. Perspect. Biol.* 5, a013003. doi:10.1101/cshperspect.a013003
- Hülsmann, B.B., Labokha, A.A., Görlich, D., 2012. The Permeability of Reconstituted Nuclear Pores Provides Direct Evidence for the Selective Phase Model. *Cell* 150, 738–751. doi:10.1016/j.cell.2012.07.019
- Hutten, S., Flotho, A., Melchior, F., Kehlenbach, R.H., 2008. The Nup358-RanGAP Complex Is Required for Efficient Importin α/β -dependent Nuclear Import. *Mol. Biol. Cell* 19, 2300–2310. doi:10.1091/mbc.E07-12-1279
- Hutten, S., Kehlenbach, R.H., 2007. CRM1-mediated nuclear export: to the pore and beyond. *Trends Cell Biol.* 17, 193–201. doi:10.1016/j.tcb.2007.02.003
- Hutten, S., Kehlenbach, R.H., 2006. Nup214 Is Required for CRM1-Dependent Nuclear Protein Export In Vivo. *Mol. Cell. Biol.* 26, 6772–6785. doi:10.1128/MCB.00342-06
- Hutten, S., Wälde, S., Spillner, C., Hauber, J., Kehlenbach, R.H., 2009. The nuclear pore component Nup358 promotes transportin-dependent nuclear import. *J. Cell Sci.* 122, 1100–1110. doi:10.1242/jcs.040154
- Ibarra, A., Hetzer, M.W., 2015. Nuclear pore proteins and the control of genome functions. *Genes Dev.* 29, 337–349. doi:10.1101/gad.256495.114
- Ishizawa, J., Kojima, K., Hail, N., Tabe, Y., Andreeff, M., 2015. Expression, function, and targeting of the nuclear exporter chromosome region maintenance 1 (CRM1) protein. *Pharmacol. Ther.* 153, 25–35. doi:10.1016/j.pharmthera.2015.06.001

- Jäkel, S., Albig, W., Kutay, U., Bischoff, F.R., Schwamborn, K., Doenecke, D., Görlich, D., 1999. The importin beta/importin 7 heterodimer is a functional nuclear import receptor for histone H1. *EMBO J.* 18, 2411–2423. doi:10.1093/emboj/18.9.2411
- Joseph, J., Dasso, M., 2008. The nucleoporin Nup358 associates with and regulates interphase microtubules. *FEBS Lett.* 582, 190–196. doi:10.1016/j.febslet.2007.11.087
- Joseph, J., Liu, S.-T., Jablonski, S.A., Yen, T.J., Dasso, M., 2004. The RanGAP1-RanBP2 complex is essential for microtubule-kinetochore interactions in vivo. *Curr. Biol. CB* 14, 611–617. doi:10.1016/j.cub.2004.03.031
- Joseph, J., Tan, S.-H., Karpova, T.S., McNally, J.G., Dasso, M., 2002. SUMO-1 targets RanGAP1 to kinetochores and mitotic spindles. *J. Cell Biol.* 156, 595–602. doi:10.1083/jcb.200110109
- Kanai, Y., Dohmae, N., Hirokawa, N., 2004. Kinesin Transports RNA: Isolation and Characterization of an RNA-Transporting Granule. *Neuron* 43, 513–525. doi:10.1016/j.neuron.2004.07.022
- Kanai, Y., Okada, Y., Tanaka, Y., Harada, A., Terada, S., Hirokawa, N., 2000. KIF5C, a Novel Neuronal Kinesin Enriched in Motor Neurons. *J. Neurosci.* 20, 6374–6384.
- Karen, K.A., Hearing, P., 2011. Adenovirus Core Protein VII Protects the Viral Genome from a DNA Damage Response at Early Times after Infection[∇]. *J. Virol.* 85, 4135–4142. doi:10.1128/JVI.02540-10
- Kassube, S.A., Stuwe, T., Lin, D.H., Antonuk, C.D., Napetschnig, J., Blobel, G., Hoelz, A., 2012. Crystal Structure of the N-Terminal Domain of Nup358/RanBP2. *J. Mol. Biol.* 423, 752–765. doi:10.1016/j.jmb.2012.08.026
- Kehlenbach, R.H., Dickmanns, A., Gerace, L., 1998. Nucleocytoplasmic shuttling factor including Ran and CRM1 mediate nuclear export of NFAT in vitro. *J Cell* 141–863.
- Kehlenbach, R.H., Dickmanns, A., Kehlenbach, A., Guan, T., Gerace, L., 1999. A role for RanBP1 in the release of CRM1 from the nuclear pore complex in a terminal step of nuclear export. *J. Cell Biol.* 145, 645–657.
- Keryer, G., Di Fiore, B., Celati, C., Lechtreck, K.F., Mogensen, M., Delouée, A., Lavia, P., Bornens, M., Tassin, A.-M., 2003. Part of Ran Is Associated with AKAP450 at the Centrosome: Involvement in Microtubule-organizing Activity. *Mol. Biol. Cell* 14, 4260–4271. doi:10.1091/mbc.E02-11-0773
- Kindsmüller, K., Groitl, P., Härtl, B., Blanchette, P., Hauber, J., Dobner, T., 2007. Intranuclear targeting and nuclear export of the adenovirus E1B-55K protein are regulated by SUMO1 conjugation. *Proc. Natl. Acad. Sci. U. S. A.* 104, 6684–6689. doi:10.1073/pnas.0702158104
- Kırlı, K., Karaca, S., Dehne, H.J., Samwer, M., Pan, K.T., Lenz, C., Urlaub, H., Görlich, D., 2015. A deep proteomics perspective on CRM1-mediated nuclear export and nucleocytoplasmic partitioning. *eLife* 4, e11466. doi:10.7554/eLife.11466
- Knockenbauer, K.E., Schwartz, T.U., 2016. The Nuclear Pore Complex as a Flexible and Dynamic Gate. *Cell* 164, 1162–1171. doi:10.1016/j.cell.2016.01.034
- Komatsu, T., Dacheux, D., Kreppel, F., Nagata, K., Wodrich, H., 2015. A Method for Visualization of Incoming Adenovirus Chromatin Complexes in Fixed and Living Cells. *PLoS ONE* 10. doi:10.1371/journal.pone.0137102
- Komatsu, T., Haruki, H., Nagata, K., 2011. Cellular and viral chromatin proteins are positive factors in the regulation of adenovirus gene expression. *Nucleic Acids Res.* 39, 889–901. doi:10.1093/nar/gkq783

- Komatsu, T., Nagata, K., 2012. Replication-Uncoupled Histone Deposition during Adenovirus DNA Replication. *J. Virol.* 86, 6701–6711. doi:10.1128/JVI.00380-12
- Kudo, N., Matsumori, N., Taoka, H., Fujiwara, D., Schreiner, E.P., Wolff, B., Yoshida, M., Horinouchi, S., 1999. Leptomycin B inactivates CRM1/exportin 1 by covalent modification at a cysteine residue in the central conserved region. *Proc. Natl. Acad. Sci. U. S. A.* 96, 9112–9117.
- Kutay, U., Güttinger, S., 2005. Leucine-rich nuclear-export signals: born to be weak. *Trends Cell Biol.* 15, 121–124. doi:10.1016/j.tcb.2005.01.005
- Kuusisto, H.V., Jans, D.A., 2015. Hyper-dependence of breast cancer cell types on the nuclear transporter Importin β 1. *Biochim. Biophys. Acta BBA - Mol. Cell Res.* 1853, 1870–1878. doi:10.1016/j.bbamcr.2015.05.002
- Lachish-Zalait, A., Lau, C.K., Fichtman, B., Zimmerman, E., Harel, A., Gaylord, M.R., Forbes, D.J., Elbaum, M., 2009. Transportin mediates nuclear entry of DNA in vertebrate systems. *Traffic Cph. Den.* 10, 1414–1428. doi:10.1111/j.1600-0854.2009.00968.x
- Lange, A., Mills, R.E., Lange, C.J., Stewart, M., Devine, S.E., Corbett, A.H., 2007. Classical Nuclear Localization Signals: Definition, Function, and Interaction with Importin α . *J. Biol. Chem.* 282, 5101–5105. doi:10.1074/jbc.R600026200
- Lau, C.K., Delmar, V.A., Chan, R.C., Phung, Q., Bernis, C., Fichtman, B., Rasala, B.A., Forbes, D.J., 2009. Transportin Regulates Major Mitotic Assembly Events: From Spindle to Nuclear Pore Assembly. *Mol. Biol. Cell* 20, 4043–4058. doi:10.1091/mbc.E09-02-0152
- Laurell, E., Beck, K., Krupina, K., Theerthagiri, G., Bodenmiller, B., Horvath, P., Aebersold, R., Antonin, W., Kutay, U., 2011. Phosphorylation of Nup98 by Multiple Kinases Is Crucial for NPC Disassembly during Mitotic Entry. *Cell* 144, 539–550. doi:10.1016/j.cell.2011.01.012
- Laurell, E., Kutay, U., 2011. Dismantling the NPC permeability barrier at the onset of mitosis. *Cell Cycle* 10, 2243–2245. doi:10.4161/cc.10.14.16195
- Lavia, P., 2016. The GTPase RAN regulates multiple steps of the centrosome life cycle. *Chromosome Res. Int. J. Mol. Supramol. Evol. Asp. Chromosome Biol.* 24, 53–65. doi:10.1007/s10577-015-9514-4
- Le Sage, V., Moulant, A.J., 2013. Viral Subversion of the Nuclear Pore Complex. *Viruses* 5, 2019–2042. doi:10.3390/v5082019
- Lee, B.J., Cansizoglu, A.E., Süel, K.E., Louis, T.H., Zhang, Z., Chook, Y.M., 2006. Rules for Nuclear Localization Sequence Recognition by Karyopherin β 2. *Cell* 126, 543–558. doi:10.1016/j.cell.2006.05.049
- Lee, C.M., 2014. Transport of c-MYC by Kinesin-1 for proteasomal degradation in the cytoplasm. *Biochim. Biophys. Acta* 1843, 2027–2036. doi:10.1016/j.bbamcr.2014.05.001
- Lee, K., Ambrose, Z., Martin, T.D., Oztop, I., Mulky, A., Julias, J.G., Vandegraaff, N., Baumann, J.G., Wang, R., Yuen, W., Takemura, T., Shelton, K., Taniuchi, I., Li, Y., Sodroski, J., Littman, D.R., Coffin, J.M., Hughes, S.H., Unutmaz, D., Engelman, A., KewalRamani, V.N., 2010. Flexible Use of Nuclear Import Pathways by HIV-1. *Cell Host Microbe* 7, 221–233. doi:10.1016/j.chom.2010.02.007
- Lee, T.W.R., Lawrence, F.J., Dauksaite, V., Akusjärvi, G., Blair, G.E., Matthews, D.A., 2004. Precursor of human adenovirus core polypeptide Mu targets the nucleolus and modulates the expression of E2 proteins. *J. Gen. Virol.* 85, 185–196. doi:10.1099/vir.0.19352-0

- Lenaerts, L., Naesens, L., 2006. Antiviral therapy for adenovirus infections. *Antiviral Res.*, Special Issue To Honour Professor Erik De Clercq 71, 172–180. doi:10.1016/j.antiviral.2006.04.007
- Lenman, A., Liaci, A.M., Liu, Y., Årdahl, C., Rajan, A., Nilsson, E., Bradford, W., Kaeshammer, L., Jones, M.S., Frängsmyr, L., Feizi, T., Stehle, T., Arnberg, N., 2015. Human Adenovirus 52 Uses Sialic Acid-containing Glycoproteins and the Coxsackie and Adenovirus Receptor for Binding to Target Cells. *PLOS Pathog.* 11, e1004657. doi:10.1371/journal.ppat.1004657
- Leopold, P.L., Kreitzer, G., Miyazawa, N., Rempel, S., Pfister, K.K., Rodriguez-Boulan, E., Crystal, R.G., 2000. Dynein- and microtubule-mediated translocation of adenovirus serotype 5 occurs after endosomal lysis. *Hum. Gene Ther.* 11, 151–165. doi:10.1089/10430340050016238
- Lever, M.B., Karpova, A., Kreutz, M.R., 2015. An Importin Code in neuronal transport from synapse-to-nucleus? *Front. Mol. Neurosci.* 8. doi:10.3389/fnmol.2015.00033
- Liashkovich, I., Hafezi, W., Kühn, J.M., Oberleithner, H., Shahin, V., 2011. Nuclear delivery mechanism of herpes simplex virus type 1 genome. *J. Mol. Recognit. JMR* 24, 414–421. doi:10.1002/jmr.1120
- Lindert, S., Silvestry, M., Mullen, T.-M., Nemerow, G.R., Stewart, P.L., 2009. Cryo-Electron Microscopy Structure of an Adenovirus-Integrin Complex Indicates Conformational Changes in both Penton Base and Integrin. *J. Virol.* 83, 11491–11501. doi:10.1128/JVI.01214-09
- Lion, T., 2014. Adenovirus Infections in Immunocompetent and Immunocompromised Patients. *Clin. Microbiol. Rev.* 27, 441–462. doi:10.1128/CMR.00116-13
- Liu, H., Jin, L., Koh, S.B.S., Atanasov, I., Schein, S., Wu, L., Zhou, Z.H., 2010. Atomic Structure of Human Adenovirus by Cryo-EM Reveals Interactions Among Protein Networks. *Science* 329, 1038–1043. doi:10.1126/science.1187433
- Liu, J., Prunuske, A.J., Fager, A.M., Ullman, K.S., 2003. The COPI Complex Functions in Nuclear Envelope Breakdown and Is Recruited by the Nucleoporin Nup153. *Dev. Cell* 5, 487–498. doi:10.1016/S1534-5807(03)00262-4
- Liu, Q., Jiang, Q., Zhang, C., 2009. A fraction of Crm1 locates at centrosomes by its CRIME domain and regulates the centrosomal localization of pericentrin. *Biochem. Biophys. Res. Commun.* 384, 383–388. doi:10.1016/j.bbrc.2009.04.154
- Lynch, J.P., Kajon, A.E., 2016. Adenovirus: Epidemiology, Global Spread of Novel Serotypes, and Advances in Treatment and Prevention. *Semin. Respir. Crit. Care Med.* 37, 586–602. doi:10.1055/s-0036-1584923
- Ma, H.-C., Hearing, P., 2011. Adenovirus structural protein IIIa is involved in the serotype specificity of viral DNA packaging. *J. Virol.* 85, 7849–7855. doi:10.1128/JVI.00467-11
- Ma, J., Goryaynov, A., Sarma, A., Yang, W., 2012. Self-regulated viscous channel in the nuclear pore complex. *Proc. Natl. Acad. Sci. U. S. A.* 109, 7326–7331. doi:10.1073/pnas.1201724109
- Mackey, J.K., Rigden, P.M., Green, M., 1976. Do highly oncogenic group A human adenoviruses cause human cancer? Analysis of human tumors for adenovirus 12 transforming DNA sequences. *Proc. Natl. Acad. Sci. U. S. A.* 73, 4657–4661.
- Maier, O., Galan, D.L., Wodrich, H., Wiethoff, C.M., 2010. An N-terminal Domain of Adenovirus Protein VI Fragments Membranes By Inducing Positive Membrane Curvature. *Virology* 402, 11–19. doi:10.1016/j.virol.2010.03.043

- Maier, O., Marvin, S.A., Wodrich, H., Campbell, E.M., Wiethoff, C.M., 2012. Spatiotemporal Dynamics of Adenovirus Membrane Rupture and Endosomal Escape. *J. Virol.* 86, 10821–10828. doi:10.1128/JVI.01428-12
- Maizel, J.V., White, D.O., Scharff, M.D., 1968. The polypeptides of adenovirus. I. Evidence for multiple protein components in the virion and a comparison of types 2, 7A, and 12. *Virology* 36, 115–125.
- Maler, M.D., Nielsen, P.J., Stichling, N., Cohen, I., Ruzsics, Z., Wood, C., Engelhard, P., Suomalainen, M., Gyory, I., Huber, M., Müller-Quernheim, J., Schamel, W.W.A., Gordon, S., Jakob, T., Martin, S.F., Jahnen-Dechent, W., Greber, U.F., Freudenberg, M.A., Fejer, G., 2017. Key Role of the Scavenger Receptor MARCO in Mediating Adenovirus Infection and Subsequent Innate Responses of Macrophages. *mBio* 8. doi:10.1128/mBio.00670-17
- Mangel, W.F., San Martín, C., 2014. Structure, function and dynamics in adenovirus maturation. *Viruses* 6, 4536–4570. doi:10.3390/v6114536
- Martinez, R., Schellenberger, P., Vasishtan, D., Akin, C., Austin, S., Dacheux, D., Rayne, F., Siebert, A., Ruzsics, Z., Gruenewald, K., Wodrich, H., 2015. The amphipathic helix of adenovirus capsid protein VI contributes to penton release and postentry sorting. *J. Virol.* 89, 2121–2135. doi:10.1128/JVI.02257-14
- Mohr, D., Frey, S., Fischer, T., Güttler, T., Görlich, D., 2009. Characterisation of the passive permeability barrier of nuclear pore complexes. *EMBO J.* 28, 2541–2553. doi:10.1038/emboj.2009.200
- Monecke, T., Dickmanns, A., Ficner, R., 2014. Allosteric control of the exportin CRM1 unraveled by crystal structure analysis. *Febs J.* 281, 4179–4194. doi:10.1111/febs.12842
- Monecke, T., Haselbach, D., Voß, B., Russek, A., Neumann, P., Thomson, E., Hurt, E., Zachariae, U., Stark, H., Grubmüller, H., Dickmanns, A., Ficner, R., 2013. Structural basis for cooperativity of CRM1 export complex formation. *Proc. Natl. Acad. Sci. U. S. A.* 110, 960–965. doi:10.1073/pnas.1215214110
- Montespan, C., Marvin, S.A., Austin, S., Burrage, A.M., Roger, B., Rayne, F., Faure, M., Campell, E.M., Schneider, C., Reimer, R., Grünewald, K., Wiethoff, C.M., Wodrich, H., 2017. Multi-layered control of Galectin-8 mediated autophagy during adenovirus cell entry through a conserved PPxY motif in the viral capsid. *PLoS Pathog.* 13. doi:10.1371/journal.ppat.1006217
- Moroianu, J., Hijikata, M., Blobel, G., Radu, A., 1995. Mammalian karyopherin alpha 1 beta and alpha 2 beta heterodimers: alpha 1 or alpha 2 subunit binds nuclear localization signal and beta subunit interacts with peptide repeat-containing nucleoporins. *Proc. Natl. Acad. Sci. U. S. A.* 92, 6532–6536.
- Mosammaparast, N., Jackson, K.R., Guo, Y., Brame, C.J., Shabanowitz, J., Hunt, D.F., Pemberton, L.F., 2001. Nuclear import of histone H2A and H2B is mediated by a network of karyopherins. *J. Cell Biol.* 153, 251–262.
- Mühlhäusser, P., Müller, E.-C., Otto, A., Kutay, U., 2001. Multiple pathways contribute to nuclear import of core histones. *EMBO Rep.* 2, 690–696. doi:10.1093/embo-reports/kve168
- Murawala, P., Tripathi, M.M., Vyas, P., Salunke, A., Joseph, J., 2009. Nup358 interacts with APC and plays a role in cell polarization. *J. Cell Sci.* 122, 3113–3122. doi:10.1242/jcs.037523
- Nemergut, M.E., Mizzen, C.A., Stukenberg, T., Allis, C.D., Macara, I.G., 2001. Chromatin docking and exchange activity enhancement of RCC1 by histones H2A and H2B. *Science* 292, 1540–1543. doi:10.1126/science.292.5521.1540

- O'Hagan, R., Piasecki, B.P., Silva, M., Phirke, P., Nguyen, K.C.Q., Hall, D.H., Swoboda, P., Barr, M.M., 2011. The Tubulin Deglutamylase CCPP-1 Regulates the Function and Stability of Sensory Cilia in *C. elegans*. *Curr. Biol. CB* 21, 1685–1694. doi:10.1016/j.cub.2011.08.049
- Ojala, P.M., Sodeik, B., Ebersold, M.W., Kutay, U., Helenius, A., 2000. Herpes simplex virus type 1 entry into host cells: reconstitution of capsid binding and uncoating at the nuclear pore complex in vitro. *Mol. Cell. Biol.* 20, 4922–4931.
- Ori, A., Banterle, N., Iskar, M., Andrés-Pons, A., Escher, C., Khanh Bui, H., Sparks, L., Solis-Mezarino, V., Rinner, O., Bork, P., Lemke, E.A., Beck, M., 2013. Cell type-specific nuclear pores: a case in point for context-dependent stoichiometry of molecular machines. *Mol. Syst. Biol.* 9, 648. doi:10.1038/msb.2013.4
- Ortega-Esteban, A., Pérez-Berná, A. J., Menéndez-Conejero, R., Flint, S. J., San Martín, C., de Pablo, P. J., 2013. Monitoring dynamics of human adenovirus disassembly induced by mechanical fatigue. *Scientific Reports.* 3, 1434. doi:10.1038/srep01434
- Panayotis, N., Karpova, A., Kreutz, M.R., Fainzilber, M., 2015. Macromolecular transport in synapse to nucleus communication. *Trends Neurosci.* 38, 108–116. doi:10.1016/j.tins.2014.12.001
- Panté, N., Kann, M., 2002. Nuclear pore complex is able to transport macromolecules with diameters of about 39 nm. *Mol. Biol. Cell* 13, 425–434. doi:10.1091/mbc.01-06-0308
- Pasdeloup, D., Blondel, D., Isidro, A.L., Rixon, F.J., 2009. Herpesvirus capsid association with the nuclear pore complex and viral DNA release involve the nucleoporin CAN/Nup214 and the capsid protein pUL25. *J. Virol.* 83, 6610–6623. doi:10.1128/JVI.02655-08
- Patil, H., Cho, K., Lee, J., Yang, Y., Orry, A., Ferreira, P.A., 2013. Kinesin-1 and mitochondrial motility control by discrimination of structurally equivalent but distinct subdomains in Ran-GTP-binding domains of Ran-binding protein 2. *Open Biol.* 3. doi:10.1098/rsob.120183
- Pérez-Berná, A.J., Mangel, W.F., McGrath, W.J., Graziano, V., Flint, J., San Martín, C., 2014. Processing of the 11 52/55k protein by the adenovirus protease: a new substrate and new insights into virion maturation. *J. Virol.* 88, 1513–1524. doi:10.1128/JVI.02884-13
- Pérez-Berná, A.J., Marabini, R., Scheres, S.H.W., Menéndez-Conejero, R., Dmitriev, I.P., Curiel, D.T., Mangel, W.F., Flint, S.J., San Martín, C., 2009. Structure and uncoating of immature adenovirus. *J. Mol. Biol.* 392, 547–557. doi:10.1016/j.jmb.2009.06.057
- Pérez-Berná, A.J., Ortega-Esteban, A., Menéndez-Conejero, R., Winkler, D.C., Menéndez, M., Steven, A.C., Flint, S.J., de Pablo, P.J., San Martín, C., 2012. The Role of Capsid Maturation on Adenovirus Priming for Sequential Uncoating. *J. Biol. Chem.* 287, 31582–31595. doi:10.1074/jbc.M112.389957
- Perez-Romero, P., Tyler, R.E., Abend, J.R., Dus, M., Imperiale, M.J., 2005. Analysis of the interaction of the adenovirus L1 52/55-kilodalton and IVa2 proteins with the packaging sequence in vivo and in vitro. *J. Virol.* 79, 2366–2374. doi:10.1128/JVI.79.4.2366-2374.2005
- Pérez-Vargas, J., Vaughan, R.C., Houser, C., Hastie, K.M., Kao, C.C., Nemerow, G.R., 2014. Isolation and Characterization of the DNA and Protein Binding Activities of Adenovirus Core Protein V. *J. Virol.* 88, 9287–9296. doi:10.1128/JVI.00935-14
- Perlson, E., Hanz, S., Ben-Yaakov, K., Segal-Ruder, Y., Seger, R., Fainzilber, M., 2005. Vimentin-Dependent Spatial Translocation of an Activated MAP Kinase in Injured Nerve. *Neuron* 45, 715–726. doi:10.1016/j.neuron.2005.01.023

- Peters, R., 2009. Translocation through the nuclear pore: Kaps pave the way. *BioEssays News Rev. Mol. Cell. Dev. Biol.* 31, 466–477. doi:10.1002/bies.200800159
- Petosa, C., Schoehn, G., Askjaer, P., Bauer, U., Moulin, M., Steuerwald, U., Soler-López, M., Baudin, F., Mattaj, I.W., Müller, C.W., 2004. Architecture of CRM1/Exportin1 Suggests How Cooperativity Is Achieved during Formation of a Nuclear Export Complex. *Mol. Cell* 16, 761–775. doi:10.1016/j.molcel.2004.11.018
- Pichler, A., Gast, A., Seeler, J.S., Dejean, A., Melchior, F., 2002. The nucleoporin RanBP2 has SUMO1 E3 ligase activity. *Cell* 108, 109–120.
- Pollard, V.W., Michael, W.M., Nakielny, S., Siomi, M.C., Wang, F., Dreyfuss, G., 1996. A novel receptor-mediated nuclear protein import pathway. *Cell* 86, 985–994.
- Port, S.A., Monecke, T., Dickmanns, A., Spillner, C., Hofele, R., Urlaub, H., Ficner, R., Kehlenbach, R.H., 2015. Structural and Functional Characterization of CRM1-Nup214 Interactions Reveals Multiple FG-Binding Sites Involved in Nuclear Export. *Cell Rep.* 13, 690–702. doi:10.1016/j.celrep.2015.09.042
- Prunuske, A.J., Liu, J., Elgort, S., Joseph, J., Dasso, M., Ullman, K.S., 2006. Nuclear envelope breakdown is coordinated by both Nup358/RanBP2 and Nup153, two nucleoporins with zinc finger modules. *Mol. Biol. Cell* 17, 760–769. doi:10.1091/mbc.E05-06-0485
- Pumroy, R.A., Cingolani, G., 2015. Diversification of importin- α isoforms in cellular trafficking and disease states. *Biochem. J.* 466, 13–28. doi:10.1042/BJ20141186
- Puntener, D., Engelke, M.F., Ruzsics, Z., Strunze, S., Wilhelm, C., Greber, U.F., 2011. Stepwise Loss of Fluorescent Core Protein V from Human Adenovirus during Entry into Cells. *J. Virol.* 85, 481–496. doi:10.1128/JVI.01571-10
- Puustinen, P., Rytter, A., Mortensen, M., Kohonen, P., Moreira, J.M., Jäättelä, M., 2014. CIP2A oncoprotein controls cell growth and autophagy through mTORC1 activation. *J. Cell Biol.* 204, 713–727. doi:10.1083/jcb.201304012
- Rabe, B., Vlachou, A., Panté, N., Helenius, A., Kann, M., 2003. Nuclear import of hepatitis B virus capsids and release of the viral genome. *Proc. Natl. Acad. Sci. U. S. A.* 100, 9849–9854. doi:10.1073/pnas.1730940100
- Rancourt, C., Keyvani-Amineh, H., Sircar, S., Labrecque, P., Weber, J.M., 1995. Proline 137 is critical for adenovirus protease encapsidation and activation but not enzyme activity. *Virology* 209, 167–173. doi:10.1006/viro.1995.1240
- Rathinam, V.A.K., Fitzgerald, K.A., 2011. Innate Immune sensing of DNA viruses. *Virology* 411, 153–162. doi:10.1016/j.virol.2011.02.003
- Reddy, V.S., Nemerow, G.R., 2014. Structures and organization of adenovirus cement proteins provide insights into the role of capsid maturation in virus entry and infection. *Proc. Natl. Acad. Sci. U. S. A.* 111, 11715–11720. doi:10.1073/pnas.1408462111
- Reid, S.P., Leung, L.W., Hartman, A.L., Martinez, O., Shaw, M.L., Carbonnelle, C., Volchkov, V.E., Nichol, S.T., Basler, C.F., 2006. Ebola Virus VP24 Binds Karyopherin $\alpha 1$ and Blocks STAT1 Nuclear Accumulation. *J. Virol.* 80, 5156–5167. doi:10.1128/JVI.02349-05
- Ribbeck, K., Lipowsky, G., Kent, H.M., Stewart, M., Görlich, D., 1998. NTF2 mediates nuclear import of Ran. *EMBO J.* 17, 6587–6598. doi:10.1093/emboj/17.22.6587

- Richards, S.A., Lounsbury, K.M., Carey, K.L., Macara, I.G., 1996. A nuclear export signal is essential for the cytosolic localization of the Ran binding protein, RanBP1. *J. Cell Biol.* 134, 1157–1168.
- Ritterhoff, T., Das, H., Hofhaus, G., Schröder, R.R., Flotho, A., Melchior, F., 2016. The RanBP2/RanGAP1*SUMO1/Ubc9 SUMO E3 ligase is a disassembly machine for Crm1-dependent nuclear export complexes. *Nat. Commun.* 7. doi:10.1038/ncomms11482
- Roelvink, P.W., Lizonova, A., Lee, J.G.M., Li, Y., Bergelson, J.M., Finberg, R.W., Brough, D.E., Kovesdi, I., Wickham, T.J., 1998. The Coxsackievirus-Adenovirus Receptor Protein Can Function as a Cellular Attachment Protein for Adenovirus Serotypes from Subgroups A, C, D, E, and F. *J. Virol.* 72, 7909–7915.
- Roloff, S., Spillner, C., Kehlenbach, R.H., 2013. Several Phenylalanine-Glycine Motives in the Nucleoporin Nup214 Are Essential for Binding of the Nuclear Export Receptor CRM1. *J. Biol. Chem.* 288, 3952–3963. doi:10.1074/jbc.M112.433243
- Roth, D.M., Moseley, G.W., Glover, D., Pouton, C.W., Jans, D.A., 2007. A microtubule-facilitated nuclear import pathway for cancer regulatory proteins. *Traffic Cph. Den.* 8, 673–686. doi:10.1111/j.1600-0854.2007.00564.x
- Roth, D.M., Moseley, G.W., Pouton, C.W., Jans, D.A., 2011. Mechanism of microtubule-facilitated “fast track” nuclear import. *J. Biol. Chem.* 286, 14335–14351. doi:10.1074/jbc.M110.210302
- Rout, M.P., Aitchison, J.D., Magnasco, M.O., Chait, B.T., 2003. Virtual gating and nuclear transport: the hole picture. *Trends Cell Biol.* 13, 622–628.
- Rowe, W.P., Huebner, R.J., Gilmore, L.K., Parrott, R.H., Ward, T.G., 1953. Isolation of a cytopathogenic agent from human adenoids undergoing spontaneous degeneration in tissue culture. *Proc. Soc. Exp. Biol. Med. Soc. Exp. Biol. Med. N. Y.* N 84, 570–573.
- Russell, W.C., 2009. Adenoviruses: update on structure and function. *J. Gen. Virol.* 90, 1–20. doi:10.1099/vir.0.003087-0
- Saitoh, H., Pizzi, M.D., Wang, J., 2002. Perturbation of SUMOylation Enzyme Ubc9 by Distinct Domain within Nucleoporin RanBP2/Nup358. *J. Biol. Chem.* 277, 4755–4763. doi:10.1074/jbc.M104453200
- Sakin, V., Richter, S.M., Hsiao, H.-H., Urlaub, H., Melchior, F., 2015. Sumoylation of the GTPase Ran by the RanBP2 SUMO E3 Ligase Complex. *J. Biol. Chem.* 290, 23589–23602. doi:10.1074/jbc.M115.660118
- Sakiyama, Y., Mazur, A., Kapinos, L.E., Lim, R.Y.H., 2016. Spatiotemporal dynamics of the nuclear pore complex transport barrier resolved by high-speed atomic force microscopy. *Nat. Nanotechnol.* 11, 719–723. doi:10.1038/nnano.2016.62
- Salina, D., Enarson, P., Rattner, J.B., Burke, B., 2003. Nup358 integrates nuclear envelope breakdown with kinetochore assembly. *J. Cell Biol.* 162, 991–1001. doi:10.1083/jcb.200304080
- San Martín, C., 2012. Latest Insights on Adenovirus Structure and Assembly. *Viruses* 4, 847–877. doi:10.3390/v4050847
- Sargent, K.L., Meulenbroek, R.A., Parks, R.J., 2004. Activation of adenoviral gene expression by protein IX is not required for efficient virus replication. *J. Virol.* 78, 5032–5037.
- Scherer, J., Vallee, R.B., 2014. Conformational Changes in the Adenovirus Hexon Subunit Responsible for Regulating Cytoplasmic Dynein Recruitment. *J. Virol.* 89, 1013–1023. doi:10.1128/JVI.02889-14
- Scherer, J., Yi, J., Vallee, R.B., 2014. PKA-dependent dynein switching from lysosomes to adenovirus: a novel form of host-virus competition. *J. Cell Biol.* 205, 163–177. doi:10.1083/jcb.201307116

- Schmid, M., Gonzalez, R.A., Dobner, T., 2012. CRM1-Dependent Transport Supports Cytoplasmic Accumulation of Adenoviral Early Transcripts. *J. Virol.* 86, 2282–2292. doi:10.1128/JVI.06275-11
- Schmitz, A., Schwarz, A., Foss, M., Zhou, L., Rabe, B., Hoellenriegel, J., Stoeber, M., Panté, N., Kann, M., 2010. Nucleoporin 153 arrests the nuclear import of hepatitis B virus capsids in the nuclear basket. *PLoS Pathog.* 6, e1000741. doi:10.1371/journal.ppat.1000741
- Shah, S., Forbes, D.J., 1998. Separate nuclear import pathways converge on the nucleoporin Nup153 and can be dissected with dominant-negative inhibitors. *Curr. Biol. CB* 8, 1376–1386.
- Singh, B.B., Patel, H.H., Roepman, R., Schick, D., Ferreira, P.A., 1999. The zinc finger cluster domain of RanBP2 is a specific docking site for the nuclear export factor, exportin-1. *J. Biol. Chem.* 274, 37370–37378.
- Singh-Naz, N., Rodriguez, W., 1996. Adenoviral infections in children. *Adv. Pediatr. Infect. Dis.* 11, 365–388.
- Sirajuddin, M., Rice, L.M., Vale, R.D., 2014. Regulation of microtubule motors by tubulin isotypes and posttranslational modifications. *Nat. Cell Biol.* 16, 335–344. doi:10.1038/ncb2920
- Smith, A., Brownawell, A., Macara, I.G., 1998. Nuclear import of Ran is mediated by the transport factor NTF2. *Curr. Biol. CB* 8, 1403–1406.
- Smith, J.G., Cassany, A., Gerace, L., Ralston, R., Nemerow, G.R., 2008. Neutralizing antibody blocks adenovirus infection by arresting microtubule-dependent cytoplasmic transport. *J. Virol.* 82, 6492–6500. doi:10.1128/JVI.00557-08
- Snijder, J., Reddy, V.S., May, E.R., Roos, W.H., Nemerow, G.R., Wuite, G.J.L., 2013. Integrin and defensin modulate the mechanical properties of adenovirus. *J. Virol.* 87, 2756–2766. doi:10.1128/JVI.02516-12
- Splinter, D., Tanenbaum, M.E., Lindqvist, A., Jaarsma, D., Flotho, A., Yu, K.L., Grigoriev, I., Engelsma, D., Haasdijk, E.D., Keijzer, N., Demmers, J., Fornerod, M., Melchior, F., Hoogenraad, C.C., Medema, R.H., Akhmanova, A., 2010. Bicaudal D2, Dynein, and Kinesin-1 Associate with Nuclear Pore Complexes and Regulate Centrosome and Nuclear Positioning during Mitotic Entry. *PLoS Biol* 8, e1000350. doi:10.1371/journal.pbio.1000350
- Strunze, S., Engelke, M.F., Wang, I.-H., Puntener, D., Boucke, K., Schleich, S., Way, M., Schoenenberger, P., Burckhardt, C.J., Greber, U.F., 2011. Kinesin-1-mediated capsid disassembly and disruption of the nuclear pore complex promote virus infection. *Cell Host Microbe* 10, 210–223. doi:10.1016/j.chom.2011.08.010
- Strunze, S., Trotman, L.C., Boucke, K., Greber, U.F., 2005. Nuclear targeting of adenovirus type 2 requires CRM1-mediated nuclear export. *Mol. Biol. Cell* 16, 2999–3009. doi:10.1091/mbc.E05-02-0121
- Sung, M.T., Cao, T.M., Coleman, R.T., Budelier, K.A., 1983. Gene and Protein Sequences of Adenovirus Protein VII, a Hybrid Basic Chromosomal Protein. *Proc. Natl. Acad. Sci. U. S. A.* 80, 2902–2906.
- Suomalainen, M., Luisoni, S., Boucke, K., Bianchi, S., Engel, D.A., Greber, U.F., 2013. A Direct and Versatile Assay Measuring Membrane Penetration of Adenovirus in Single Cells. *J. Virol.* 87, 12367–12379. doi:10.1128/JVI.01833-13
- Suomalainen, M., Nakano, M.Y., Boucke, K., Keller, S., Greber, U.F., 2001. Adenovirus-activated PKA and p38/MAPK pathways boost microtubule-mediated nuclear targeting of virus. *EMBO J.* 20, 1310–1319. doi:10.1093/emboj/20.6.1310

- Suomalainen, M., Nakano, M.Y., Keller, S., Boucke, K., Stidwill, R.P., Greber, U.F., 1999. Microtubule-dependent plus- and minus end-directed motilities are competing processes for nuclear targeting of adenovirus. *J. Cell Biol.* 144, 657–672.
- Swaminathan, S., Kiendl, F., Körner, R., Lupetti, R., Hengst, L., Melchior, F., 2004. RanGAP1*SUMO1 is phosphorylated at the onset of mitosis and remains associated with RanBP2 upon NPC disassembly. *J. Cell Biol.* 164, 965–971. doi:10.1083/jcb.200309126
- Symeonidis, N., Jakubowski, A., Pierre-Louis, S., Jaffe, D., Pamer, E., Sepkowitz, K., O'Reilly, R.J., Papanicolaou, G.A., 2007. Invasive adenoviral infections in T-cell-depleted allogeneic hematopoietic stem cell transplantation: high mortality in the era of cidofovir. *Transpl. Infect. Dis.* 9, 108–113. doi:10.1111/j.1399-3062.2006.00184.x
- Tatham, M.H., Kim, S., Jaffray, E., Song, J., Chen, Y., Hay, R.T., 2005. Unique binding interactions among Ubc9, SUMO and RanBP2 reveal a mechanism for SUMO paralogue selection. *Nat. Struct. Mol. Biol.* 12, 67–74. doi:10.1038/nsmb878
- Terry, L.J., Shows, E.B., Wentz, S.R., 2007. Crossing the nuclear envelope: hierarchical regulation of nucleocytoplasmic transport. *Science* 318, 1412–1416. doi:10.1126/science.1142204
- Thakar, K., Karaca, S., Port, S.A., Urlaub, H., Kehlenbach, R.H., 2013. Identification of CRM1-dependent Nuclear Export Cargos Using Quantitative Mass Spectrometry. *Mol. Cell. Proteomics MCP* 12, 664–678. doi:10.1074/mcp.M112.024877
- Timney, B.L., Tetenbaum-Novatt, J., Agate, D.S., Williams, R., Zhang, W., Chait, B.T., Rout, M.P., 2006. Simple kinetic relationships and nonspecific competition govern nuclear import rates in vivo. *J Cell Biol* 175, 579–593. doi:10.1083/jcb.200608141
- Tollefson, A.E., Ryerse, J.S., Scaria, A., Hermiston, T.W., Wold, W.S., 1996. The E3-11.6-kDa adenovirus death protein (ADP) is required for efficient cell death: characterization of cells infected with adp mutants. *Virology* 220, 152–162. doi:10.1006/viro.1996.0295
- Top, F.H., 1975. Control of adenovirus acute respiratory disease in U.S. Army trainees. *Yale J. Biol. Med.* 48, 185–195.
- Trentin, J.J., Yabe, Y., Taylor, G., 1962. The Quest for Human Cancer Viruses. *Science* 137, 835–841.
- Trotman, L.C., Mosberger, N., Fornerod, M., Stidwill, R.P., Greber, U.F., 2001. Import of adenovirus DNA involves the nuclear pore complex receptor CAN/Nup214 and histone H1. *Nat. Cell Biol.* 3, 1092–1100. doi:10.1038/ncb1201-1092
- Twyffels, L., Gueydan, C., Krays, V., 2014. Transportin-1 and Transportin-2: Protein nuclear import and beyond. *FEBS Lett.* 588, 1857–1868. doi:10.1016/j.febslet.2014.04.023
- Ugai, H., Borovjagin, A.V., Le, L.P., Wang, M., Curiel, D.T., 2007. Thermostability/infectivity defect caused by deletion of the core protein V gene in human adenovirus type 5 is rescued by thermo-selectable mutations in the core protein X precursor. *J. Mol. Biol.* 366, 1142–1160. doi:10.1016/j.jmb.2006.11.090
- Ugai, H., Dobbins, G.C., Wang, M., Le, L.P., Matthews, D.A., Curiel, D.T., The Gene Therapy Center, U. of A. at B., 2012. Adenoviral Protein V Promotes a Process of Viral Assembly Through Nucleophosmin 1. *Virology* 432. doi:10.1016/J.VIROL.2012.05.028
- van der Watt, P.J., Maske, C.P., Hendricks, D.T., Parker, M.I., Denny, L., Govender, D., Birrer, M.J., Leaner, V.D., 2009. The Karyopherin proteins, Crm1 and Karyopherin beta1, are overexpressed in cervical

- cancer and are critical for cancer cell survival and proliferation. *Int. J. Cancer* 124, 1829–1840.
doi:10.1002/ijc.24146
- van Deursen, J., Boer, J., Kasper, L., Grosveld, G., 1996. G2 arrest and impaired nucleocytoplasmic transport in mouse embryos lacking the proto-oncogene CAN/Nup214. *EMBO J.* 15, 5574–5583.
- Varadaraj, A., Mattoscio, D., Chiocca, S., 2014. SUMO Ubc9 enzyme as a viral target. *IUBMB Life* 66, 27–33.
doi:10.1002/iub.1240
- Vetter, I.R., Nowak, C., Nishimoto, T., Kuhlmann, J., Wittinghofer, A., 1999. Structure of a Ran-binding domain complexed with Ran bound to a GTP analogue: implications for nuclear transport. *Nature* 398, 39–46.
- von Appen, A., Kosinski, J., Sparks, L., Ori, A., DiGiulio, A.L., Vollmer, B., Mackmull, M.-T., Banterle, N., Parca, L., Kastiris, P., Buczak, K., Mosalaganti, S., Hagen, W., Andres-Pons, A., Lemke, E.A., Bork, P., Antonin, W., Glavy, J.S., Bui, K.H., Beck, M., 2015. In situ structural analysis of the human nuclear pore complex. *Nature* 526, 140–143. doi:10.1038/nature15381
- Wagstaff, K.M., Sivakumaran, H., Heaton, S.M., Harrich, D., Jans, D.A., 2012. Ivermectin is a specific inhibitor of importin α/β -mediated nuclear import able to inhibit replication of HIV-1 and dengue virus. *Biochem. J.* 443, 851–856. doi:10.1042/BJ20120150
- Wälde, S., Kehlenbach, R.H., 2010. The Part and the Whole: functions of nucleoporins in nucleocytoplasmic transport. *Trends Cell Biol.* 20, 461–469. doi:10.1016/j.tcb.2010.05.001
- Wälde, S., Thakar, K., Hutten, S., Spillner, C., Nath, A., Rothbauer, U., Wiemann, S., Kehlenbach, R.H., 2012. The nucleoporin Nup358/RanBP2 promotes nuclear import in a cargo- and transport receptor-specific manner. *Traffic Cph. Den.* 13, 218–233. doi:10.1111/j.1600-0854.2011.01302.x
- Walther, T.C., Pickersgill, H.S., Cordes, V.C., Goldberg, M.W., Allen, T.D., Mattaj, I.W., Fornerod, M., 2002. The cytoplasmic filaments of the nuclear pore complex are dispensable for selective nuclear protein import. *J. Cell Biol.* 158, 63–77. doi:10.1083/jcb.200202088
- Wang, I.-H., Burckhardt, C.J., Yakimovich, A., Morf, M.K., Greber, U.F., 2017a. The nuclear export factor CRM1 controls juxta-nuclear microtubule-dependent virus transport. *J. Cell Sci.* 130, 2185–2195. doi:10.1242/jcs.203794
- Wang, I.-H., Burckhardt, C.J., Yakimovich, A., Morf, M.K., Greber, U.F., 2017b. The nuclear export factor CRM1 controls juxta-nuclear microtubule-dependent virus transport. *J. Cell Sci.* 130, 2185–2195. doi:10.1242/jcs.203794
- Wang, I.-H., Suomalainen, M., Andriasyan, V., Kilcher, S., Mercer, J., Neef, A., Luedtke, N.W., Greber, U.F., 2013. Tracking Viral Genomes in Host Cells at Single-Molecule Resolution. *Cell Host Microbe* 14, 468–480. doi:10.1016/j.chom.2013.09.004
- Wang, K., Huang, S., Kapoor-Munshi, A., Nemerow, G., 1998. Adenovirus Internalization and Infection Require Dynamin. *J. Virol.* 72, 3455–3458.
- Weber, J.M., Déry, C.V., Mirza, M.A., Horvath, J., 1985. Adenovirus DNA synthesis is coupled to virus assembly. *Virology* 140, 351–359.
- Weberuss, M., Antonin, W., 2016. Perforating the nuclear boundary – how nuclear pore complexes assemble. *J. Cell Sci* 129, 4439–4447. doi:10.1242/jcs.194753
- Wen, W., Meinkoth, J.L., Tsien, R.Y., Taylor, S.S., 1995. Identification of a signal for rapid export of proteins from the nucleus. *Cell* 82, 463–473.

- Werner, A., Flotho, A., Melchior, F., 2012. The RanBP2/RanGAP1*SUMO1/Ubc9 complex is a multisubunit SUMO E3 ligase. *Mol. Cell* 46, 287–298. doi:10.1016/j.molcel.2012.02.017
- Wickham, T.J., Mathias, P., Cheresch, D.A., Nemerow, G.R., 1993. Integrins $\alpha\beta 3$ and $\alpha\beta 5$ promote adenovirus internalization but not virus attachment. *Cell* 73, 309–319. doi:10.1016/0092-8674(93)90231-E
- Wiethoff, C.M., Wodrich, H., Gerace, L., Nemerow, G.R., 2005. Adenovirus protein VI mediates membrane disruption following capsid disassembly. *J. Virol.* 79, 1992–2000. doi:10.1128/JVI.79.4.1992-2000.2005
- Wodrich, H., Cassany, A., D'Angelo, M.A., Guan, T., Nemerow, G., Gerace, L., 2006. Adenovirus core protein pVII is translocated into the nucleus by multiple import receptor pathways. *J. Virol.* 80, 9608–9618. doi:10.1128/JVI.00850-06
- Wodrich, H., Guan, T., Cingolani, G., Von Seggern, D., Nemerow, G., Gerace, L., 2003. Switch from capsid protein import to adenovirus assembly by cleavage of nuclear transport signals. *EMBO J.* 22, 6245–6255. doi:10.1093/emboj/cdg614
- Wodrich, H., Henaff, D., Jammart, B., Segura-Morales, C., Seelmeir, S., Coux, O., Ruzsics, Z., Wiethoff, C.M., Kremer, E.J., 2010. A capsid-encoded PPxY-motif facilitates adenovirus entry. *PLoS Pathog.* 6, e1000808. doi:10.1371/journal.ppat.1000808
- Wold, W.S., Mackey, J.K., Rigden, P., Green, M., 1979. Analysis of human cancer DNA's for DNA sequence of human adenovirus serotypes 3, 7, 11, 14, 16, and 21 in group B1. *Cancer Res.* 39, 3479–3484.
- Wu, J., Matunis, M.J., Kraemer, D., Blobel, G., Coutavas, E., 1995. Nup358, a Cytoplasmically Exposed Nucleoporin with Peptide Repeats, Ran-GTP Binding Sites, Zinc Fingers, a Cyclophilin A Homologous Domain, and a Leucine-rich Region. *J. Biol. Chem.* 270, 14209–14213. doi:10.1074/jbc.270.23.14209
- Wu, Z., Jiang, Q., Clarke, P.R., Zhang, C., 2013. Phosphorylation of Crm1 by CDK1-cyclin-B promotes Ran-dependent mitotic spindle assembly. *J. Cell Sci.* 126, 3417–3428. doi:10.1242/jcs.126854
- Xu, D., Farmer, A., Chook, Y.M., 2010. Recognition of nuclear targeting signals by Karyopherin- β proteins. *Curr. Opin. Struct. Biol.* 20, 782–790. doi:10.1016/j.sbi.2010.09.008
- Xu, W., Edwards, M.R., Borek, D.M., Feagins, A.R., Mittal, A., Alinger, J.B., Berry, K.N., Yen, B., Hamilton, J., Brett, T.J., Pappu, R.V., Leung, D.W., Basler, C.F., Amarasinghe, G.K., 2014. Ebola Virus VP24 Targets a Unique NLS Binding Site on Karyopherin Alpha 5 to Selectively Compete with Nuclear Import of Phosphorylated STAT1. *Cell Host Microbe* 16, 187–200. doi:10.1016/j.chom.2014.07.008
- Yabe, Y., Trentin, J.J., Taylor, G., 1962. Cancer induction in hamsters by human type 12 adenovirus. Effect of age and of virus dose. *Proc. Soc. Exp. Biol. Med. Soc. Exp. Biol. Med. N. Y.* N 111, 343–344.
- Yamada, J., Phillips, J.L., Patel, S., Goldfien, G., Calestagne-Morelli, A., Huang, H., Reza, R., Acheson, J., Krishnan, V.V., Newsam, S., Gopinathan, A., Lau, E.Y., Colvin, M.E., Uversky, V.N., Rexach, M.F., 2010. A bimodal distribution of two distinct categories of intrinsically disordered structures with separate functions in FG nucleoporins. *Mol. Cell. Proteomics MCP* 9, 2205–2224. doi:10.1074/mcp.M000035-MCP201
- Yaseen, N.R., Blobel, G., 1999. Two distinct classes of Ran-binding sites on the nucleoporin Nup-358. *Proc. Natl. Acad. Sci. U. S. A.* 96, 5516–5521.
- Yaseen, N.R., Blobel, G., 1997. Cloning and characterization of human karyopherin beta3. *Proc. Natl. Acad. Sci. U. S. A.* 94, 4451–4456.

- Yea, C., Dembowy, J., Pacione, L., Brown, M., 2007. Microtubule-Mediated and Microtubule-Independent Transport of Adenovirus Type 5 in HEK293 Cells. *J. Virol.* 81, 6899–6908. doi:10.1128/JVI.02330-05
- Yokoyama, N., Hayashi, N., Seki, T., Panté, N., Ohba, T., Nishii, K., Kuma, K., Hayashida, T., Miyata, T., Aebi, U., 1995. A giant nucleopore protein that binds Ran/TC4. *Nature* 376, 184–188. doi:10.1038/376184a0
- Zhang, H., Saitoh, H., Matunis, M.J., 2002. Enzymes of the SUMO Modification Pathway Localize to Filaments of the Nuclear Pore Complex. *Mol. Cell. Biol.* 22, 6498–6508. doi:10.1128/MCB.22.18.6498-6508.2002
- Zhang, W., Arcos, R., 2005. Interaction of the adenovirus major core protein precursor, pVII, with the viral DNA packaging machinery. *Virology* 334, 194–202. doi:10.1016/j.virol.2005.01.048
- Zhu, S., Zhang, H., Matunis, M.J., 2006. SUMO modification through rapamycin-mediated heterodimerization reveals a dual role for Ubc9 in targeting RanGAP1 to nuclear pore complexes. *Exp. Cell Res.* 312, 1042–1049. doi:10.1016/j.yexcr.2005.12.031
- Zieve, G.W., Turnbull, D., Mullins, J.M., McIntosh, J.R., 1980. Production of large numbers of mitotic mammalian cells by use of the reversible microtubule inhibitor Nocodazole: Nocodazole accumulated mitotic cells. *Exp. Cell Res.* 126, 397–405. doi:10.1016/0014-4827(80)90279-7

ABBREVIATIONS

A

ADP: Adenovirus death protein
AdV: Adenovirus
APC: Adenomatous polyposis coli
ATM: Atomic force microscopy
AVP: Adenoviral protease

C

cAPK: Cyclic AMP (Adenosine Monophosphate)-Dependent Protein Kinase
CAR: Coxackie and Adenovirus receptor
CAS: Cellular apoptosis susceptibility
CCP1: Cytosolic carboxypeptidase 1
CIP2A: Cancerous inhibitor of protein phosphatase 2A
cNLS: Classical NLS
Co-IP: Co-immunoprecipitation
COPI: Coat complex protein I
CPSF6: Cleavage and polyadenylation specific factor 6
CRIME: CRM1, importin β , etcetera
CRM1: Chromosome region of maintenance-1
CryoEM: Cryo-electron microscopy

D

Da: Dalton
DAPI: 4',6-diamidino-2-phenylindole
DBP: DNA-binding protein
dCMP: Deoxycytidine monophosphate
DMEM: Dulbecco's Modified Eagle's medium®
DMSO: Dimethyl sulfoxide
DNA: Deoxyribonucleic acid
dNTP: Deoxynucleotide

E

EdC: 5-ethynyl-2'-deoxycytidine

F

FABP5: Fatty acid binding protein 5
FCS: Fetal calf serum
FG: Phenylalanine-glycine
FISH: Fluorescence in situ hybridization

G

GAPDH: Glyceraldehyde-3-phosphate dehydrogenase
GDP: Guanosine diphosphate
GFP: Green fluorescent protein
GTP: Guanosine triphosphate

H

H: Histone
HA: Hemagglutinin
HAdV: Human adenovirus
HEAT: Huntingtin; Elongation factor 3; protein phosphatase 2A, PI3-kinase TOR1
HEK293: Human embryonic kidney 293 cells
HeLa: Henrietta Lacks cells
HIV-1: Human immunodeficiency virus 1
hnRNP: Heterogeneous nuclear ribonucleoprotein
hpi: Hours post infection
HSV: Herpes simplex virus I

I

IBB: Importin β -binding domain
IC: Intermediate chain
ICTV: International committee on taxonomy of viruses
IF: Immunofluorescence
IPTG: Isopropyl-1-thio- β -D-galactopyranoside
IR: Internal region
iRNA: interfering RNA

J

JX2: Kinesin binding domain

K

Kbp: Kilo base pair
KD: Knock-down
KLC: Kinesin light chain

L

LIC: Light intermediate chain
LMB: Leptomycin B

M

M: Middle region
MEF: Mouse embryonic fibroblast
MHC: Major histocompatibility complex
min pi: Minutes post infection
MLP: Major late promoter
MOI: Multiplicity of infection
mRNA: messenger ribonucleic acid
MT: microtubules
MTAS: MT association sequences
MTOC: Microtubule organizing center

N

NE: Nuclear envelope
NEBD: Nuclear envelope breakdown
NES: Nuclear export signal
NFAT: Nuclear factor of activated T-cells
NFI: Nuclear factor I

NLS: Nuclear localization signal
NMD3: Nonsense-mediated decay 3
NPC: Nuclear pore complex
NTF2: Nuclear transport factor 2
Nup: Nucleoporin
NXF1-p15: Nuclear RNA Export Factor 1-p15 heterodimer

O

Oct-1: Octamer-binding protein I

P

PCR: Polymerase chain reaction
PKA: Protein kinase A
PKC: Protein kinase C
PMSF: Phenylmethylsulfonyl fluoride
PPXY: Proline-Proline-X-Tyrosine (where x = any amino acid)
PTHrP: Parathyroid hormone-related protein
PY: proline and tyrosine rich NLS

R

RanBP: Ran binding protein
RanGAP: Ran GTP-ase activating protein
Rb: Retinoblastoma protein
RFP: Red fluorescent protein
RGD: Arginine, glycine, aspartic acid

S

SAF: Spindle assembly factors
SDS: Sodium dodecyl sulfate
shRNA: small hairpin RNA
SIM: SUMO-interaction motif
siRNA: small-interfering RNA
SQSTM: Sequestosome-1
STAT1: Signal transducer and activator of transcription 1
SUMO: Small Ubiquitin-like Modifier
SV40: Simian virus 40

T

TAF-1: Template activating factor-1

TNPO-1: Transportin-1

TP: Terminal protein

TPR: Tetratricopeptide repeats

TRF1: Telomere repeat-binding factor

Ts1: Thermosensitive 1

TuRC: Tubulin ring complex

U

U2OS: Human osteosarcoma derived cells

Ubc9: Ubiquitin carrier protein 9

V

vDNA: viral DNA

VP35: Viral protein 35

vRNP: viral ribonucleoprotein

W

WB: Western blot

WT: Wild type

Z

ZnF: Zinc fingers

LIST OF FIGURES

Figure 1: Capsid structure and composition of HAdV.....	5
Figure 2: Schematic representation of the adenoviral genome organization	8
Figure 3: Adenovirus infection cycle.....	10
Figure 4: The RanGTP gradient.....	16
Figure 5: Bidirectional active transport across the NPC.....	18
Figure 6: Structure and components of the nuclear pore complex.....	21
Figure 7: Role of cytoplasmic Nup214 and Nup358 in CRM1-mediated nuclear protein export.....	24
Figure 8: Structure and interacting partners of Nup358.....	26
Figure 9: Role of the nucleo-cytoplasmic machinery in mitosis.....	34
Figure 10: AdV genome delivery.....	37
Figure 11: Quantification of fluorescence intensity.....	56
Figure 12: Quantification of single signal.....	57
Figure 13: Quantification of co-localization.....	58
Figure 14: Nup358 depletion delays AdV genome import.....	64
Figure 15: Nup358 depletion does not affect AdV entry.....	68
Figure 16: The N-terminal half of Nup358 is sufficient for promoting efficient AdV genome import.....	70
Figure 17: Transport receptors compensate the lack of Nup358.....	73
Figure 18: Depletion of transportin-1 does not impact AdV genome import.....	74
Figure 19: Specific inhibition of transportin-1 does not affect AdV genome import efficiency.....	75
Figure 20: The N-terminal soluble fragment of Nup358 (aa 806-1306) mislocalizes transportin-1.....	77
Figure 21: The N-terminal FG-repeats of Nup358 mislocalizes both transportin-1 and importin- β	79
Figure 22: The N-terminal soluble fragment of Nup358 (aa 806-1306) binds endogenous importin- β	81
Figure 23: The N-terminal half of Nup358 is not sufficient to target CRM1 to the NPC.....	83
Figure 24: The C-terminal CRM1-binding fragment of Nup214 competes with AdV genome delivery.....	86

Figure 25: Soluble fragments of Nup358 impair AdV genome delivery.....	89
Figure 26: Soluble CRM1-binding fragments of Nup358 induce accumulation of AdV capsids at the MTOC.....	91
Figure 27: CRM1-binding fragments of Nup358 disrupt CRM1 export function.....	93
Figure 28: The C-terminal fragments of Nup358 impair nuclear accumulation of AdV cores in a CRM1-dependent and -independent manner.....	95
Figure 29: The C-terminal CRM1-binding fragment of Nup358 impairs nuclear targeting of AdV capsids in a CRM1-dependent manner.....	96
Figure 30: Infection protocol for mitotic cells to study AdV genome delivery.....	98
Figure 31: Mitotic spindles are reconstituted in infected cells upon release from colcemid-treatment.....	99
Figure 32: AdV deliver their genome in mitotic cells.....	101
Figure 33: LMB treatment does not impair AdV entry in mitosis.....	102
Figure 34: Disassembly of AdV capsids depends on functional CRM1.....	104
Figure 35: Exposure of AdV core accelerates AdV capsid targeting to the chromatin.....	106
Figure 36: Disassembled capsids are targeted to the chromatin in mitotic cells.....	110
Figure 37: NPC-non-anchored fragments of Nups affect AdV genome delivery differently in mitosis.....	112
Figure 38: The C-terminal CRM1 binding fragment of Nup358 increases separation of AdV cores from disassembled capsids.....	114
Figure 39: Point mutations in residues W142A and P143A of CRM1 impair AdV genome delivery in mitosis.....	117
Figure 40: Point mutations in residues W142A and P143A of CRM1 impair AdV genome delivery in interphase.....	119
Figure 41: CRM1 mutant W142A P143A conserves the ability to export RanBP1.....	121
Figure 42: CRM1 mutant W142A P143A is able to bind soluble fragments of Nup214 and Nup358.....	123
Figure 43: CRM1 does not interact with purified Ad5 particles.....	125
Figure 44: The Δ pIX AdV mutant shows premature disassembly of the capsid.....	127
Figure 45: Δ pIX AdV genome delivery requires CRM1.....	130

LIST OF TABLES

Table 1: Classification of human AdV's.....	2
Table 2: Human karyopherin- β family.....	15
Table 3: List of primers.....	42
Table 4: Reaction mix for PCR.....	42
Table 5: PCR programme.....	42
Table 6: Available plasmids for mammalian cell expression.....	43
Table 7: Generated plasmids.....	45
Table 8: Mammalian cell lines.....	46
Table 9: Scheme for DNA transfection.....	47
Table 10: Sequences of oligonucleotides used for RNAi.....	48
Table 11: Scheme for siRNA transfection.....	48
Table 12: List of primary antibodies used for IF and WB analyses.....	54

